Characterization of evolutionarily conserved and divergent features of plant membrane trafficking

By
Dana Amira Dahhan

A dissertation submitted in partial fulfillment of

the requirements for the degree of

Doctor of Philosophy

(Biochemistry)

at the

UNIVERSITY OF WISCONSIN-MADISON

2022

Date of final oral examination: 8/24/2022

The dissertation is approved by the following members of the Final Oral Committee:

Sebastian Y. Bednarek, Professor, Biochemistry
Richard M. Amasino, Professor, Biochemistry
Simon Gilroy, Professor, Botany
Christina M. Hull, Professor, Biomolecular Chemistry
Marisa S. Otegui, Professor, Botany

Abstract

The sub-compartmentalization of plant cells has necessitated the development of transport mechanisms which deliver protein and membrane cargos in a spatially and temporally controlled fashion between the various endomembrane compartments within the cell as well as the cell periphery. These transport pathways are essential to several subcellular processes and organismal responses including cell growth and expansion, the construction of *de novo* plasma membrane and cell wall during cytokinesis, construction of the cell wall, and the delivery and recycling of transporters and receptors located at the interface between the plant cell and its environment. Consequently, disruption of the proteins or lipid homeostasis facilitating these transport pathways results in a range of developmental defects, including seedling lethality.

Many of the key principles of endomembrane transport (cargo recognition and recruitment of vesicle coat proteins through adaptors, membrane deformation, vesicle scission, vesicle transport, and vesicle docking and fusion) are evolutionarily conserved across Eukaryotes and specifically between land plants and members of the Opisthokont supergroup, which includes yeast and animals. Yet, since the evolution of plants, yeast, and animals from the last eukaryotic common ancestor, proteins facilitating membrane trafficking have expanded, diverged in function, or become lost in specific lineages, resulting in evolutionarily divergent vesicle transport mechanisms. The work described in this thesis characterizes evolutionarily conserved membrane trafficking pathways in plants and identifies key points of evolutionarily divergence between plants and Opisthokonts.

First, the proteomic and biochemical characterization of a heterogenous mixture of clathrin coated vesicles (CCVs) from undifferentiated, suspension cultured Arabidopsis cells yields the surprising enrichment of the vesicle adaptor, AP-4, with plant CCVs and the low abundance and depletion from purified CCVs of the known clathrin-mediated endocytosis adaptor, TPLATE complex. Secondly, I include biochemical data supporting the peripheral association of the TPLATE subunit of the Jotnarlog and endocytic adaptor, TPLATE complex, with enriched clathrin coated vesicles relative to the evolutionarily conserved endocytic adaptor, AP-2, which is more tightly associated. Additional data describing the assembly and interaction network of the Stomatal Cytokinesis Defective complex, an evolutionarily divergent regulator of an evolutionarily conserved small GTPase, RabE1, which functions in post-Golgi trafficking.

Acknowledgments

This thesis is first dedicated to all the teachers and mentors (Brennan, Westfall, Kanzok, Liu, Olsen, Becker, Webster, Hull, Otegui, Bednarek) in my life who encouraged me to pursue my education at all levels and who continuously challenged me to become a more rigorous thinker, a clear communicator, and a self-assured scientist. I am particularly indebted to Sebastian who supported my journey from an enthusiastic and reserved graduate student into an independent scientist confident enough to recognize herself among her peers and capable enough to ask and answer difficult questions. Thank you especially to my thesis committee (Christina, Marisa, Simon, and Rick) who challenged me to think through my research questions, who guided me through difficult transitions in my thesis work, and who ensured I never lost sight of my personal and research goals.

I am thankful to all members of the Bednarek Lab who taught me valuable lab skills and made completing the experiments of my thesis possible and who guided me through the logistic and existential challenges of graduate school. To Jon, Jessica, and Greg – thank you for your patience, your time, and your endless support. To Ashley, Julie, Rui, and Eddie – thank you for your company and your warm hearts. I was fortunate to have a huge network of supportive plant and endomembrane scientists who guided me through data analysis and new techniques – thanks to Stacy, Stephanie, Sydney, Masaki, Giulia, and Rob. I would also like to express a special thank you to Alex for extending so many opportunities to join productive & fun collaborations, championing my work, and humoring my endless requests for cool CCV pictures. To my undergraduate mentees, Morgan, Kate, and Fang – thank you for your patience while I learned how to be a better mentor & for all you taught me along the way. It has been a joy to know you! Thanks especially

to Kate Ryan for shepherding all of the graduate students through the program & for your genuine care and infinite well of support.

Thanks to my friends in and out of Madison who saw me through difficult times and never let me forget that I actually could be (and in fact was) a good scientist: Harriet, for being my creative & pastry soulmate (and your endless votes of confidence!); Megan L., for getting me through prelims & for sharing my love of Chicago; Delia, for the lovely drawings and notes, which are still stashed in my desk for when I need a boost; Bassie, for tea and tennis; Dylan, for books and challenging conversations; Christine, for great music, better food, and being my honorary older sister; Sophie, for making me laugh & encouraging me to have fun; Brian, for working alongside me and the best cocktails; Sydney and Nathan, for being my concert and opera partners for several lovely seasons. Thanks to Eddie, Hridindu, Rachel, and Megan D. for working so hard to make IPiB a better place and for becoming my friend in the process.

Thanks to Molly, Mary, and Jenny for your practical, emotional, writing, illustrative, and culinary support since my earliest lab days. Love and miss you every day. To my partner Camden – without your wisdom, your kindness, your concern & care, I would not be standing at the successful end of such a challenging journey. I love you. To my brother Zach, for always challenging me/spurring me to be the best scientist in the Dahhan family (at least until you get there, too).

Finally, to my parents – this thesis is for you. You were my first STEM role models, and I am so lucky and grateful to have had your support since my earliest days in school. I recognize the lengths you went to so that my schooling could always come first, and I love you for that practical support, as well as for your constant encouragement to work

hard while taking care of myself. You have been first in my head and heart since I can remember. I love you, too.

Preface

This thesis is organized into 5 chapters and one appendix. Chapter 1 contains a review of clathrin-mediated and clathrin-independent plant endocytosis and is modestly adapted from a version published in *FEBS Letters*. Chapter 2 details the proteome and biochemical characterization of the plant CCV as published in *Plant Cell*. Chapter 3 contains additional biochemical analyses of plant CCVs and reflects small projects and experiments studying plant CCVs which contributed to a publication in *PNAS* as well as an additional manuscript under review at *Molecular Plant*. Chapter 4 contains preliminary results from a study of SCD complex assembly *in vivo* as well as a lengthy introduction which reviews features of endomembrane trafficking pathways not covered in the review in Chapter 1. Chapter 5 is a summary of the conclusions presented throughout the previous chapters and of the future directions inspired by the results presented. The discussion in this chapter is informed by a publication in *Plant Cell* describing the interplay between the endocytic and post-Golgi trafficking pathways intersecting at the trans-Golgi network/early endosome compartment in plant cells. An additional appendix describes tools generated for the comparative study of SCD complex function using the moss, *Physcomitrium patens.*

Table of Contents

List of figures and tables

Common Abbreviations

AP	Adaptor Protein
ANTH	AP-180 N-terminal Homology
CME	Clathrin-mediated endocytosis
CIE	Clathrin-independent endocytosis
CCV	Clathrin-coated vesicle
CCP	Clathrin-coated pit
CLC	Clathrin light chain
CHC	Clathrin heavy chain
DRP	Dynamin-related protein
EAPs	Endocytic accessory proteins
ENTH	Epsin N-terminal homology
ESCRT	Endosomal sorting complex required for transport
LECA	Last eukaryotic common ancestor
TGN/EE	trans-Golgi network/early endosome
TIRF	Total internal reflection fluorescence
TPC	TPLATE complex
VHS	Vps-27, Hrs, STAM

Chapter 1: Introduction

This chapter is adapted from published work:

Dahhan DA and Bednarek SY (2022) Advances in structural, spatial, and temporal mechanics of plant endocytosis. FEBS Letters doi:10.1002/1873-3468.14420

Dahhan DA and Bednarek SY (2022) A contextualized catalog: proteomic analyses of plant CCVs. The Plant Cell: In a Nutshell.

DAD reviewed literature and wrote the paper.

Reuse permission:

The re-use of Figure 9 from Bonnett and Newcomb *Protoplasma* 1966 in Figure 1.3 of this chapter has been granted by license from Springer Nature. Alexander Johnson and Jiri Friml of IST Austria have generously provided EM images for use in Figure 1.3.

Endocytosis is an evolutionarily conserved process by which organisms internalize membrane, proteins, and small molecules from the plasma membrane. Complex regulation over the endocytic process is exerted by a host of proteins, hormones, and small molecules that selectively determine what cargo is internalized when and, ultimately, to what fate. In plants, the internalization of membrane and protein cargo from the plasma membrane regulates the abundance of proteins critical to numerous cellular processes including nutrient uptake (Barberon et al., 2011; Wang et al., 2013b; Barberon et al., 2014; Wang et al., 2017b; Martiniere et al., 2019; Wang et al., 2019a), hormone signaling (Dhonukshe et al., 2007; Irani et al., 2012; Liu et al., 2020; Marhava, 2021), pathogen perception and stress responses (Robatzek et al., 2006; Lu et al., 2011), signal transduction (Yu et al., 2020), gravitropism (Men et al., 2008), and cell wall biogenesis (Bashline et al., 2013; Sanchez-Rodriguez et al., 2018). The endocytosis of membrane and proteins also occurs at the division plane of plant cells thereby facilitating *de novo* plasma membrane synthesis during formation of the cell plate (Otegui et al., 2001; Boutte et al., 2010; Fujimoto et al., 2020).

Membrane and proteins internalized from the plasma membrane and newly forming cell plate are delivered to the trans-Golgi network/early endosome (TGN/EE), the nexus for multiple endomembrane trafficking pathways (Figure 1.1). Within the TGN/EE, endocytic proteins internalized from the plasma membrane are sorted and either targeted to the vacuole for degradation or recycled back to the plasma membrane via exocytosis. Endocytosed membrane proteins that undergo trafficking from the TGN/EE to the vacuole are marked by ubiquitination which serves to aid in their recognition and packaging into

intraluminal vesicles within the multivesicular bodies by the endosomal sorting complex required for transport (ESCRT) machinery prior to the subsequent fusion of the latter with the vacuole, culminating in their degradation (Paez Valencia et al., 2016; Schwihla and Korbei, 2020; Aniento et al., 2021).

The mechanisms underlying endocytosis are generally classified by their involvement of the vesicle coat protein complex, clathrin (clathrin-mediated endocytosis; CME) or by lack of clathrin proteins (clathrin-independent endocytosis; CIE). In the former, the formation and release of clathrin-coated vesicles (CCV) from the plasma membrane require the recognition of endocytic cargo together with the recruitment of clathrin and endocytic accessory proteins (EAPs). Recent advances in temporal and structural resolution have clarified details about the stages and timeline of plant CME. Clathrin-independent endocytosis is comparatively less well understood and is often distinguished from CME by monitoring the internalization of endocytic cargo under conditions that block CME and/or the involvement of a limited set of CIE markers.

While endocytosis is a process conserved among eukaryotes, a number of evolutionary divergences since the last eukaryotic common ancestor (LECA) have diversified the complement of proteins facilitating endocytosis resulting in key departures between the molecular machinery involved in CME and CIE in plant and primarily yeast and metazoan systems. Clarifying instances of evolutionary conservation and divergence consequently requires the identification in plants of the protein machinery underlying CME and CIE and of the functions, regulation, and requirements of these machinery for plant growth and development. Efforts to establish the mechanistic details of CME and CIE, as

well as the interaction and redundancy of clathrin-independent endocytic mechanisms with clathrin-mediated mechanisms are an ongoing area of research.

The functions of non-conserved, as well as evolutionarily conserved proteins in plant CME and CIE; the intersection and compensatory nature of clathrin-independent and -dependent transport pathways in plant endocytosis; and the influence of non-endocytic transport pathways (e.g. post-Golgi trafficking) and other organelles on CME are summarized in this review. Recent progress which have advanced our knowledge of the structural, spatial, and temporal characteristics of plant endocytosis, as well as the methodologies which have facilitated these discoveries, are also discussed.

Clathrin-mediated endocytosis

Clathrin coat proteins

The process of CME can be divided into the following stages: initiation and maturation of a clathrin-coated pit (CCP) into which cargo is clustered; release of a CCV from the plasma membrane, followed by vesicle uncoating; and tethering and fusion of the vesicle with the TGN/EE (Figure 1.2A and Figure 1.3) (Cocucci et al., 2012; Aniento et al., 2021).

The formation of an endocytic clathrin-coated pit requires the recruitment of clathrin triskelia by EAPs to specific sites at the plasma membrane and cell plate. Subsequent polymerization of clathrin triskelia generates the characteristic lattice-like coat of CCVs (Figure 1.1). The Arabidopsis genome encodes multiple isoforms of clathrin light chain (CLC) and clathrin heavy chain (CHC) which together form the clathrin triskelia. While CCV formation at the plasma membrane and cell plate underlies CME, CLCs and

CHCs also colocalize at and form CCVs from the TGN/EE which facilitate post-Golgi trafficking (Yan et al., 2021). Consistent with this, the 3 CLC and 2 CHC isoforms have been identified in a predominantly 1:1 ratio in enriched post-Golgi trafficking-derived and endocytic CCVs from Arabidopsis cells (Dahhan et al., 2022).

Interference with clathrin function results in aberrant cytokinesis (Tahara et al., 2007); agravitropism and defective seedling growth and development (Kitakura et al., 2011); and shorter siliques, longer hypocotyls, and fewer trichomes (Wang et al., 2013a). Phenotypic analysis of *chc1* and *chc2* mutants indicate a functional redundancy between the two isoforms (Kitakura et al., 2011). Likewise, developmental defects in single *clc* Arabidopsis backgrounds demonstrate functional redundancy among CLC isoforms (Wang et al., 2013a). While CLC and CHC function in tandem in endocytosis and post-Golgi trafficking, they are differentially affected by auxin treatment, which is an inhibitor of clathrin-mediated endocytosis (Wang et al., 2013a). To circumvent the pleiotropic defects of clathrin loss-of-function mutants that complicate the study of mechanisms of CME, a chemical inhibitor, ES9-17, was recently developed that reversibly inhibits CME by disrupting CHC function but lacks undesirable, off-target effects observed with other small molecule inhibitors of CME (Reynolds et al., 2018; Dejonghe et al., 2019).

To measure temporal parameters of plant CME such as the order of EAP recruitment to the plasma membrane relative to clathrin and the dwell times of CME machinery at the plasma membrane, live-cell imaging methods have been applied to study the dynamics of clathrin, cargo, EAPs, and other CME machinery in root and shoot cells. These studies quantitatively assess the dynamics of fluorescently-tagged cargos

and EAPs, noting their arrival and departures at the PM relative to clathrin to understand whether a protein of interest might recruit clathrin to sites of endocytosis and whether newly identified, putative EAPs function in CME by comparing their dynamics to clathrin at the PM. The combination of total internal reflection fluorescence (TIRF) microscopy with automated single-particle detection and tracking software packages has enabled the study of endocytic trafficking at a high spatial and temporal resolution. These methodologies have been recently reviewed alongside a demonstration of single- and dual-channel TIRF microscopy employed to study CME, as well as an in depth discussion of the current advantages and limitations of commonly used endocytic tracers and genetic and small molecule-based perturbation of CME and endomembrane trafficking (Johnson et al., 2020).

Parsing high-resolution population data into distinct subpopulations enables the identification of non-productive and productive CME events based on the lifetime of clathrin at the plasma membrane. Single particle tracking of the dynamics of CLC2-positive foci indicated that non-productive CME events exhibited CLC2 lifetimes of 2 and 9 seconds, while bona fide (positive for presence of clathrin and EAPs) CME events showed CLC2 lifetimes of 42 seconds in root cells and 33 seconds in hypocotyl cells (Narasimhan et al., 2020). The dwell time of CLC2 in bona fide CME events in these experiments is longer than previously shown CLC lifetimes that were averages of all CLC-positive foci likely due to the inclusion of abortive CME events in the quantitative analyses in previous studies (Konopka et al., 2008; Johnson and Vert, 2017).

AP-2 adaptor complex

Initiation of endocytosis and formation of the clathrin-coated pit is facilitated by monomeric and oligomeric adaptors that collectively bridge clathrin with endocytic cargo, recruit additional EAPs, and generate membrane curvature. One such adaptor is the heterotetramer, Adaptor Protein 2 (AP-2), which is evolutionarily conserved and related to other oligomeric endomembrane trafficking complexes that organize and contribute to the formation of a vesicle coat including other adaptor protein complexes, AP-1 through AP-5, the TSET/TPLATE Complex (TPC), and the COPI coatamer complex (Gu et al., 2013; Robinson, 2015; Dacks and Robinson, 2017; Kovtun et al., 2020). The AP-2 complex contains two large subunits (β and α), a medium subunit (μ), and small subunit (σ). Genetic and proteomic analyses identify two isoforms of AP2β, two isoforms of AP2α, AP2μ, and AP2σ as members of the AP-2 complex in Arabidopsis (Bashline et al., 2013; Di Rubbo et al., 2013; Yamaoka et al., 2013).

Structural studies of metazoan AP-2 delineate the major functional domains of the individual subunits of the complex including the regions within AP-2 that bind phospholipids, cargo, and the N-terminus of CHC (Smith et al., 2021). The recognition by endocytic adaptors of plasma membrane-localized anionic phosphatidylinositol phospholipids (PIP) such as $PI(4,5)P_2$, a regulatory feature which is evolutionarily conserved, contributes to the initiation of a clathrin-coated pit at the plasma membrane (Ischebeck et al., 2013; Kelly et al., 2014; Li and Pan, 2017; Liu et al., 2020; Doumane et al., 2021). Mammalian cytosolic AP-2 exists in a closed, cargo-inaccessible formation until a conformational change induced by binding of membrane-bound $PI(4,5)P_2$ exposes

the AP-2α binding sites that recognize endocytic motifs of plasma membrane-localized cargo (Schmid and McMahon, 2007; Kelly et al., 2008; Kelly et al., 2014; Kovtun et al., 2020). The μ and σ subunits of metazoan AP-2 recognize tyrosine-based and dileucine motifs within endocytic cargo, respectively (Arora and Damme, 2021). While the μ subunit of plant AP-2 has been shown to interact directly with a canonical tyrosine-based recognition motif of the CME cargo, BRI1 (Liu et al., 2020), there is no evidence yet *in planta* for interaction between AP2σ with dileucine recognition motifs. However, this interaction has been demonstrated between the dileucine motifs of protein cargo and the σ subunit of other AP complexes indicating that the recognition of these linear motifs by clathrin adaptors is evolutionarily conserved (Arora and Damme, 2021). Recent cryo-EM data show that animal AP2β2 binds and crosslinks clathrin triskelia, thereby promoting the formation of a clathrin coated-pit (Smith et al., 2021). Mammalian AP2α contributes to $PI(4,5)P_2$ interaction at the plasma membrane and is capable of binding to EAPs such as auxilin and epsin which mediate vesicle uncoating and membrane curvature, respectively, though the interactions between AP2α and other EAPs may be partially redundant with interactions between EAPs and other subunits of AP-2 (Motley et al., 2006). Further studies are necessary to evaluate whether the mechanisms of mammalian AP-2 are conserved in plant AP-2s.

Fluorescence microscopy in plant cells demonstrate that AP-2 and clathrin exhibit similar transient dynamics at the plasma membrane with average lifetimes of fluorescent AP2μ and CLC foci at the plasma membrane of 24 ± 8 and 19 ± 7 seconds, respectively,

and that this endocytic adaptor precedes clathrin in their arrival at the plasma membrane (Bashline et al., 2013; Johnson and Vert, 2017).

The disruption of AP-2 function by genetic means or the expression of a dominant negative *ap2μ* variant demonstrates that AP-2 functions in the internalization of membrane using the endocytic/plasma membrane lipid marker, FM4-64, and mediates the internalization of protein cargos BRI1, PIN2, and the cellulose synthase complex proteins, CESA3 and CESA6 (Bashline et al., 2013; Di Rubbo et al., 2013; Kim et al., 2013). Although AP-2 is thought to function as a heterotetramer, the continued association of AP-2 subunits with the plasma membrane, albeit at a reduced level, in single *ap-2* subunit loss-of-function mutants suggests that partial hemicomplexes of AP-2 exist *in vivo* and may explain the viability of single *ap-2* mutants (Kim et al., 2013; Yamaoka et al., 2013; Wang et al., 2016).

TPLATE complex

Plant CME is dependent on an additional heterooligomeric adaptor, the TPLATE/TSET complex, which descended from the LECA but is lost in some eukaryotic lineages such as metazoans and fungi (Hirst et al., 2014; Zhang et al., 2015; More et al., 2020). Early support for the role of the TPLATE complex (TPC) in CME is based on identification of the protein, TPLATE and its co-localization with clathrin to the cell plate with similar dynamics (Van Damme et al., 2006; Van Damme et al., 2011). Tandem affinity purification (TAP) in Arabidopsis has identified seven associated proteins (TASH3, EH1, EH2, LOLITA, TML, TWD40-1, and TWD40-2) which in addition to TPLATE form the octameric,

918 kDa TPLATE complex (TPC) that is recruited en masse to the plasma membrane (Gadeyne et al., 2014; Wang et al., 2020).

Within the growing pollen tube, TPC subunits accumulate in the subapical region of the pollen tube and not the tip, supporting specifically a role in endocytic trafficking (Gadeyne et al., 2014). The TML subunit of the TPC is postulated to be required for assembly, stability and recruitment of the complex to the plasma membrane through its μ homology domain (HD), which appears to be structurally related to the μ subunit of the adaptin, AP-2. Clathrin and AP-2 subunits, as well as other CME machinery, are also identified as interactors of the TPC suggesting that this endocytic adaptor function in CME. Similarly to AP-2, live cell imaging of CME events by fluorescence microscopy shows TPC recruitment preceding clathrin at TML-positive foci at the plasma membrane (Figure 1.2B), indicating that these endocytic adaptors recruited clathrin to sites of endocytosis (Gadeyne et al., 2014). Both TML and TPLATE are capable of direct interaction with endocytic cargo (Sanchez-Rodriguez et al., 2018). Presumably the μ homology domain of TML mediates interaction with endocytic cargo, similarly to AP-2μ, but further interaction studies are needed to confirm this.

While TPLATE and the remainder of the TPC were initially thought to be plant-specific CME factors, bioinformatic analyses found that six core TPC subunits collectively known as TSET, lacking the EH1 and EH2 subunits of the orthologous TPC, are more widely evolutionarily conserved, including in the protist, *D. discoideum*. Yet, while TSET function in endocytosis in *D. discoideum* is evolutionarily conserved, this complex is not required for viability, in sharp contrast to the requirement for TPC in Arabidopsis (Hirst et

al., 2014; More et al., 2020). Loss-of-function mutations and/or knockdown of the expression of genes encoding individual TPC subunits in Arabidopsis cause severe phenotypic defects including male sterility caused by pollen developmental defects, seedling lethality, endocytic defects, and decreases in hypocotyl length and rosette size (Gadeyne et al., 2014; Bashline et al., 2015).

The lethality of individual TPLATE complex subunits has led to the creative development of protocols for conditional and/or partial disruption of TPC function in CME. A heat-shock inducible TPLATE allele, “TPLATE-WDXM2” with mutations in an evolutionary conserved motif within the trunk domain of the TPLATE subunit reduces CME of the aquaporin, PIP2;7 by destabilizing TPC protein levels while rescuing seedling lethality (Wang et al., 2021). An alternative approach that inhibits TPLATE complex function utilizes constitutive expression of nanobodies targeting GFP in epidermis, cortex, and lateral root cap cells in *tml* loss-of-function lines complemented with *TML:GFP-TML*. Fusion of the expressed nanobodies to a mitochondrial targeting signal largely re-localizes TML, as well as AP2α, from the plasma membrane and cell plate of Arabidopsis root cells into cytosolic puncta with a consequential decrease in the internalization of FM4-64 (Winkler et al., 2021).

AP-2 and TPLATE function in tandem, though not exclusively, in the early stages of CME (Bashline et al., 2013; Bashline et al., 2015; Sanchez-Rodriguez et al., 2018). The occurrence of endocytic recognition motifs and post-translational modifications (e.g. ubiquitylation) of cargo and their experimentally validated interactions with endocytic adaptors, AP2 and TPLATE complex, as well as the functional consequences of

mutations of these recognition motifs has been recently and comprehensively reviewed (Schwihla and Korbei, 2020; Arora and Damme, 2021).

TPC- and AP-2-positive foci at the plasma membrane contain both adaptors, and representative AP-2 and TPC subunits display similar lifetime distributions (Figure 1.2B) and lack of lateral mobility (Gadeyne et al., 2014). Silencing of the expression of the gene encoding the TPC subunit, TML, results in reduced AP2α protein levels at the plasma membrane and cell plate (Gadeyne et al., 2014). Both endocytic adaptor complexes are required for the recruitment of clathrin to the plasma membrane (Wang et al., 2016). However, TPC and AP-2 do not always co-localize at the plasma membrane (Gadeyne et al., 2014), and the plasma membrane associations of AP-2 and TPC display differential sensitivity to inhibitors of endocytosis (Wang et al., 2016). Considering the difference between the severity of mutations of *tpc* and *ap-2* subunits, the circumstances in which these endocytic adaptors function independently of each other remain an intriguing gap in our knowledge.

Interestingly, while the TPC is, in contrast to AP-2, essential for endocytosis in plants (Winkler et al., 2021), TPLATE complex subunits are found to not co-purify with enriched CCVs to the same extent as AP-2 subunits (Dahhan et al., 2022). The associations of AP-2 and TPLATE with the plant CCV, as assessed by quantitative mass spectrometry and immunoblotting to measure the enrichment and depletion of EAPs co-purifying with plant CCVs, corroborate data showing that AP-2 is more abundant than TPC in the CCV proteome (Dahhan et al., 2022) (Figure 1.4). The apparent discrepancy between data showing a reduced association of the TPC with the enriched CCVs relative

to AP-2 and the requirement of the TPC for CME and plant viability, in contrast to AP-2, suggests that these EAPs may have differential affinities for the CCV and/or different spatial organization on the CCV. Consistent with this hypothesis, recent proteomic and super-resolution microscopy localization analyses of TPLATE relative to clathrin on the endocytic vesicle (Johnson et al., 2021) indicate that the TPC is located on the exterior of the CCV, unlike the adaptor, AP-2, which bridges cargo with clathrin and is contained within the coat on the endocytic vesicle.

To increase the temporal resolution of CME, Wang et al. developed a methodology to slow down endocytic events by lowering the temperature of a slide-mounted Arabidopsis seedling from 25 °C to 12 °C which decreases the rate at which FM4-64 and proteins were internalized. As a result, differences in recruitment of TPLATE complex subunits and clathrin are enhanced, and the simultaneous recruitment of all members of the TPLATE complex to the plasma membrane has been established with confidence. TPLATE is also observed to be recruited to the plasma membrane before clathrin (Wang et al., 2020) (Figure 1.2B), and lifetime of a bona fide CME event and recruitment of TPLATE to the plasma membrane of Arabidopsis root cells prior to clathrin is supported by dual-channel TIRF microscopy (Johnson et al., 2020). However, the arrival of TPLATE at the plasma membrane is also observed to be concurrent with that of clathrin in hypocotyl cells, where the timeline of CME is shorter than in root cells, suggesting that the mechanism of CME may differ slightly in different cell types in plants (Narasimhan et al., 2020) (Figure 1.2B).

ANTH/ENTH/VHS domain-containing, monomeric adapters

In addition to AP-2 and TPC, plant CME is dependent on monomeric accessory proteins containing Epsin N-Terminal Homology (ENTH), AP180 N-Terminal Homology (ANTH), or Vps-27, Hrs, STAM (VHS) domains that interact with clathrin, TPLATE, and AP-2 (Zouhar and Sauer, 2014; Ekanayake et al., 2019). The Arabidopsis genome encodes 43 ENTH/ANTH/VHS domain-containing proteins, more than a third of which are identified by proteomic analyses of CCVs enriched from Arabidopsis suspension cultured cells (Zouhar and Sauer, 2014; Dahhan et al., 2022). The majority of ENTH/ANTH/VHS domain-containing proteins are involved in vesicle formation at various sites within the endomembrane system based on their putative or demonstrated interactions with phospholipids (such as $PI(4,5)P_2$), clathrin and endocytic adaptor proteins, and specific plasma membrane-localized cargo (Zouhar and Sauer, 2014; de Jong and Munnik, 2021). The function of ANTH/ENTH/VHS domain-containing proteins in membrane trafficking pathways has been comprehensively reviewed in this issue (Feng et al., 2022), and thus further discussion of these monomeric adaptors will be limited to those that function in endocytosis.

The Arabidopsis ENTH/ANTH proteins, ECA1, ECA2, and ECA4 co-fractionate with enriched CCVs, localize to the plasma membrane, and accumulate at the subapical region of the growing pollen tube, suggesting that these accessory proteins function in CME, relative to other transport pathways (Song et al., 2012; Kaneda et al., 2019; Dahhan et al., 2022). AtECA4 in particular localizes also to the TGN/EE and has been further implicated in the recycling of endocytic cargo from the TGN/EE to the plasma membrane

(Nguyen et al., 2018; Lee et al., 2022). Recombinant ECA2 and AP180 associate with liposomes enriched for either PA and PI(4,5)P_2, phospholipid species enriched at the cell plate and plasma membrane, supporting a role for clathrin and EAP recruitment and/or cargo recognition in CME (Kaneda et al., 2019). The ENTH/ANTH protein, AtCAP1, is also identified as an interactor of CLC and TPLATE complex, as well as of other CME machinery (Gadeyne et al., 2014; Adamowski et al., 2018). ENTH/ANTH proteins are likely adaptors for the internalization of specific cargo as the ANTH-domain containing proteins, PICALM1a/1b, are required for the recognition and retrieval of the secretory SNARE, VAMP72, but are dispensable for the internalization of other endocytic cargo, such as cellulose synthase (CESA) complexes, and bulk plasma membrane markers (i.e. FM4-64) (Fujimoto et al., 2020). PICALM1a is recruited to the plasma membrane in a phosphatidic acid (PA)-dependent manner in response to salt stress and has been shown *in vitro* to specifically bind liposomes bearing PA in a pH-dependent manner, as well as to PI(4,5)P_2 (Putta et al., 2020).

AP180 is shown to not only interact with AP2α and CHC, but is also sufficient to induce the formation of clathrin cages *in vitro* raising the possibility that this ENTH/ANTH species could facilitate CME at a structural level and not solely through the recruitment of clathrin and its EAPs to sites of endocytosis (Barth and Holstein, 2004). The metazoan ENTH-domain containing protein, Epsin, binds curved membranes and, *in vitro*, is sufficient to drive bending of PI(4,5)P_2-enriched liposomes, supporting a role *in vivo* for plasma membrane deformation and CCV maturation (Ford et al., 2002). However, further

studies of plant ENTH/ANTH proteins are required to determine if they similarly function in CME membrane dynamics.

Dynamin-related proteins

Plants express six protein families (DRP1-6) related to mammalian dynamin, a GTPase and phosphatidylinositol phospholipid (PIP) binding-protein that functions in CME (Fujimoto and Tsutsumi, 2014). Mammalian dynamin oligomerizes around the neck of budding endocytic vesicle undergoing conformational changes upon GTP hydrolysis, thereby releasing CCVs from the plasma membrane (Fujimoto and Tsutsumi, 2014). Of the six DRP families in plants, DYNAMIN-RELATED PROTEIN 1 and 2 (DRP1 and DRP2) function in CME and contain a N-terminal GTPase domain, a linker with structural homology to the domain mediating oligomerization of mammalian dynamin, and C-terminal, regulatory GTPase effector domains (GED). In addition, similarly to mammalian dynamin, DRP2s contain pleckstrin homology and proline rich domains that putatively bind PIPs and EAPs via Src-homology (SH3) domains, respectively (Schmid and Frolov, 2011).

Members of the Arabidopsis DRP1 family (DRP1a-e) function in cell division and CME (Bednarek and Backues, 2010; Fujimoto and Tsutsumi, 2014). DRP1c and its related isoform, DRP1a, show similar (but not identical) behaviors at the plasma membrane including differential lifetimes, mobilities, dependence on plasma membrane lipid composition, and changes in these properties in response to cytoskeletal inhibitors, all of which reflect their functions in CME (Konopka and Bednarek, 2008). The over-

expression of *DRP1C* is additionally insufficient to rescue some of the phenotypic defects of *drp1a* mutants supporting limited functional redundancy between these two isoforms (Kang et al., 2003a; Kang et al., 2003b; Konopka and Bednarek, 2008). Loss-of-function *drp1a* mutants exhibit abnormal cell division and endocytosis and reduced cell expansion (Kang et al., 2003a; Collings et al., 2008). *drp1c* mutants similarly display phenotypic defects with aberrant pollen grains featuring abnormal plasma membrane morphology (Kang et al., 2003b). DRP1C also localizes to the subapical region of the expanding root hair and possesses similar dynamics at the plasma membrane as CLC (Konopka et al., 2008). Recombinant AtDRP1A is capable of self-polymerizing and binding plasma membrane mimetic liposomes *in vitro*, and spirals of DRP1A have been observed in ring-like structures around cell plate membrane tubules during cytokinesis, supporting the function of plant DRP proteins specifically as membrane constriction factors (Otegui et al., 2001; Backues and Bednarek, 2010).

The two Arabidopsis DRP2 isoforms bear the most similarity in terms of domain organization (including the presence of a PIP-binding pleckstrin homology domain) to mammalian dynamin and localize to the cell plate, plasma membrane, and TGN/EE (Fujimoto et al., 2008; Bednarek and Backues, 2010). DRP2A and DRP2B are themselves functionally redundant and required for gametophyte development (Backues et al., 2010). Both DRP1A and DRP2B predominantly colocalize with clathrin at the plasma membrane as well as with each other, indicating that both plant DRP1 and DRP2 proteins function in tandem in CME (Fujimoto et al., 2010).

Representative members DRP1A and DRP2B jointly appear together at endocytic sites on the plasma membrane after the recruitment of clathrin by EAPs and disappear simultaneously with clathrin from the plasma membrane, supporting their role in the cleavage of mature CCV from the plasma membrane (Figure 1.2B) (Fujimoto et al., 2010). Considering the known roles of DRP1 and DRP2 in CME, the low abundances of DRP1 and DRP2 proteins relative to clathrin and other CME machinery in the proteome of purified plant CCVs likely reflect the dynamic association of DRP1 and DRP2 during the release of mature CCVs from the plasma membrane in contrast to other EAPs, such as AP-2, which remain associated with PIPs, cargo and clathrin prior to uncoating of the CCVs and consequently are more abundant in the CCV proteome and exhibit stronger co-enrichment with purified CCVs (Dahhan et al., 2022). Live-cell imaging at lower temperatures enabled the visualization of plant CME at high temporal resolution showing that DRP1A is recruited to the plasma membrane after the simultaneous recruitment of all TPC subunits and the recruitment of clathrin (Wang et al., 2020) (Figure 1.2B).

DRP1A and DRP2B function in tandem as *drp1a/drp2b* double mutants display a degree of stunted growth of roots and cotyledons, defective pavement cell shape, and aberrant cytokinesis beyond those of individual *drp1a* or *drp2b* mutants (Ekanayake et al., 2021). DRP1 and DRP2 have been documented to function in CME facilitating nutrient sensing, immune responses, and callose transport (Smith et al., 2014; Chaparro-Garcia et al., 2015; Leslie et al., 2016; Yoshinari et al., 2016; Pizarro et al., 2019; Ekanayake et al., 2021).

CCV scission and transport, and CCV-uncoating factors

Following their release from the plasma membrane, plant CCVs are trafficked to the TGN/EE. The simultaneous disappearance of CLC2-positive endocytic structures and appearance of actin filaments observed by TIRF microscopy complements evidence that actin is likely dispensable for the formation and/or release of CCVs in plants (Konopka et al., 2008; Narasimhan et al., 2020). The lack of actin involvement in the initiation and maturation is unexpected as actin polymerization drives membrane invagination and CCV scission in yeast (Goode et al., 2015) and in mammalian cells under stress (Lopez-Hernandez et al., 2020). Consequently, other factors could compensate for the lack of actin in CCV maturation and drive membrane bending against the high turgor pressor in plants. In fact, functional TPLATE complex is required to produce curved membrane and spherical CCVs, and recombinant EH1, a peripheral subunit of the TPC, was shown to tubulate liposomes *in vitro*, suggesting that this TPC subunit could facilitate membrane remodeling *in vivo* (Johnson et al., 2021).

In plant cells, the movement and trafficking of Golgi stacks and TGN/EE occurs along actin filaments (Hawes, 2005). Consequently, observations by Narasimhan et al. of the simultaneous appearance of actin filaments and the disappearance of CCVs from the plasma membrane provides evidence that, in plants, actin could guide CCV transport and facilitate their capture by the TGN/EE through the coordination of TGN/EE movement along actin filaments (Narasimhan et al., 2020).

The canonical model of CME derived from mammalian data holds that CCV uncoating occurs immediately after cleavage of the endocytic vesicle (Kirchhausen et al.,

2014), but recent data from plant model systems indicate that uncoating of the CCV in plants may not occur immediately after scissioning. Endocytic vesicles still retaining their clathrin coats are observed to reach the TGN/EE at which point, or immediately prior, they shed their clathrin coats and associated EAPs. Observations by electron microscopy of partially coated CCVs near the plasma membrane of plant cells suggest that uncoating happens sequentially, gradually shedding clathrin triskelia and adaptor complexes (Narasimhan et al., 2020). Notably, the TPLATE adaptor is observed to be shed from the endocytic CCV *before* the loss of clathrin (Narasimhan et al., 2020; Johnson et al., 2021).

What protein factors facilitate the uncoating of plant CCVs? In mammalian systems, this is accomplished by the coordinated action of the chaperone, Hsc70, and its J domain co-factor, auxilin1 or its homolog, auxilin 2 (also known as cyclin-G-associated kinase) (Ungewickell et al., 1995; Eisenberg and Greene, 2007). Domains within mammalian auxilins confer binding to $PI(4,5)P_2$ as well as to clathrin, AP2, and dynamin (Scheele et al., 2001; Eisenberg and Greene, 2007). The Arabidopsis genome encodes two auxilin-like proteins, AUXILIN-LIKE 1 and AUXILIN-LIKE 2, that interact with clathrin as well as other endocytic accessory proteins such as CAP1 (Adamowski et al., 2018). AUXILIN-LIKE 1/2 localize to the plasma membrane and cell plate of Arabidopsis root cells and can be visualized at or near the plasma membrane as highly dynamic foci which localize to the ends of clathrin lifetimes at the plasma membrane (Adamowski et al., 2018). The association of only a small subset of CCPs with auxilin and AUXILIN-LIKE1/2 at the plasma membrane is a feature of both animal and plant CME, as is the recruitment

of this uncoating factor to the CCP during the latest stage of clathrin association with the plasma membrane (Massol et al., 2006; Adamowski et al., 2018).

Similar to mammalian auxillins, plant auxilin-like proteins stimulate the release of membrane-associated clathrin *in vitro* (Lam et al., 2001). The overexpression of *AUXILIN-LIKE 1/2* results in severe developmental defects, inhibition of CME based on quantitative assay of the internalization of cell plate cargo, KNOLLE, and depletion of clathrin and DRP1C from the plasma membrane (Adamowski et al., 2018). These *in vitro* and over-expression data suggest that the function of AUXILIN-LIKE proteins in plants must be essential to plant CME yet curiously, loss-of-function of both *AUXILIN-LIKE 1/2* results in no discernable plant growth and development phenotype or change in the internalization of FM4-64 (Adamowski et al., 2018). Thus, the mechanistic function of plant auxillin as well as the overall mechanism of CCV uncoating, docking and fusion with the TGN/EE remain important areas of further research.

Clathrin-independent endocytosis

Similar to CME, the disruption of CIE pathway(s) by genetic and/or pharmacological treatment causes severe growth and developmental defects (Li et al., 2012). CIE transport plays a role in mediating plant defense and abiotic stress response (Baral et al., 2015; Lo Presti and Kahmann, 2017; Cui et al., 2018), gravitropic responses (Men et al., 2008), solute transport in trees (Slupianek et al., 2019), fertilization and plant development (Yu et al., 2020), and boron transport (Yoshinari et al., 2019).

The existence of plant CIE pathway(s) has been primarily established by demonstrating the internalization of impermeable markers such as the fluorescent, non-metabolizable glucose derivative, 2-NBDG (Bandmann and Homann, 2012), charged gold nanoparticles (Onelli et al., 2008; Bandmann and Homann, 2012), and fluorescent nano beads of varying diameter size (Bandmann et al., 2012) into various cell types including tobacco BY-2 protoplasts (Bandmann and Homann, 2012; Bandmann et al., 2012), tobacco pollen tubes (Moscatelli et al., 2007), and Arabidopsis epidermal root cells (Li et al., 2011; Li et al., 2012) under conditions that inhibit CME.

Unlike CCVs, vesicles originating through CIE have a broad size distribution and lack a distinctive coat that permit their morphological identification. Vesicles internalizing a fluorescent, non-metabolizable glucose derivative, 2-NBDG, in tobacco BY-2 cells are found to be between 80-220 nm in diameter as determined by membrane capacitance measurements (Bandmann and Homann, 2012). This range of CIE-derived vesicles is comparable to endocytic vesicles internalizing fluorescent, hydrophilic Alexa 488 small molecules from the fluid surrounding plant guard cells (Gall et al., 2010) but larger than those of isolated CCVs purified from Arabidopsis suspension-cultured cells, carrot suspension-cultured cells, and pea cotyledons (Depta and Robinson, 1986; Harley and Beevers, 1989; Reynolds et al., 2014; Dahhan et al., 2022). The broad range in sizes of CIE vesicles suggests the existence of multiple independent CIE pathways, but delineating multiple different pathways is hampered by a relative lack of knowledge of the mechanisms of CIE in comparison to CME.

One partially characterized clathrin-independent endocytic pathway is mediated through a type of membrane microdomain enriched in sterols and sphingolipids that is marked by the presence of the protein, Flotillin1 (Flot1) (Sharma et al., 2002; Li et al., 2012; Ott, 2017). In mammalian cells, Flot1 is found to be sufficient for the induction of membrane curvature independent of another protein involved in mammalian CIE, caveolin (Kurzchalia and Parton, 1999; Morrow et al., 2002; Frick et al., 2007). Plant homologs of Flot1 are identified in a proteomic study of detergent-resistant membrane fractions prepared from Arabidopsis (Borner et al., 2005), and AtFlotillin1 (Flot1) is shown to localize to the plasma membrane and undergo internalization with dynamics distinct from those of clathrin light chain (Li et al., 2012).

The small molecule methyl-β-cyclodextrin (MβCD), a reversible sterol depleting reagent, has been used to perturb membrane microdomains and assess the involvement of CIE in the internalization of specific cargo (Li et al., 2011). Disruption of membrane microdomain formation using MβCD and/or silencing of *Flot1* using artificial microRNA are each sufficient to inhibit the internalization of plasma membrane-localized endocytic cargo like ammonium transporter AMT1;3 (Wang et al., 2013b). However, caution is warranted in the use of MβCD as a selective reagent for inhibition of CIE, as MβCD is known in mammalian cells to interfere with CCP maturation and internalization of CCVs containing the cargo proteins transferrin and epidermal growth factor (Rodal et al., 1999). Recent work investigating the mechanism by which the quorum sensing molecule, diffusible signal factor (DSF), inhibits plant pathogen triggered immunity pathways demonstrated that changes in plant sterol levels induced by DSF modulated endocytosis,

including CME (Tran et al., 2020). A MβCD-reversible increase in sterol levels resulting from DSF treatment increased the lifetimes of CLC2 and FLS2, a cargo internalized likely by both CME and CIE (Cui et al., 2018), at the plasma membrane and concomitantly caused a modest inhibition of FM4-64 internalization (Tran et al., 2020). Consequently, modulating of sterol levels affects both CME and CIE, and further efforts are required to develop additional tools that selectively perturb CIE but do not affect CME.

Cargo proteins internalized by both CIE and CME

The identification of plasma membrane proteins that are internalized by both CIE and CME pathways is important for our understanding of the mechanisms underlying each endocytic pathway. Whether CIE and CME function in tandem or whether one pathway predominates under certain (i.e. environmental- or cell type-dependent) conditions is an active area of research.

The plasma membrane receptor kinase, FERONIA (FER), is transported by CIE, as well as CME. FER colocalizes with Flot1 at the plasma membrane and MβCD treatment inhibits the level of FER internalization, suggesting that membrane microdomains and CIE are involved in the trafficking of FER from the plasma membrane. However, in the presence of the rapid alkalinization factor 1 peptide, which binds to the extracellular domain of FER, FER-RALF1 uptake into plant cells is primarily dependent on CME (Yu et al., 2020).

Environmental conditions may also determine the mode of internalization of plasma membrane proteins. Although the aquaporin, AtPIP2;1 co-localizes with AtFlot1

at the plasma membrane it appears to undergo internalization via CME. However under elevated (100 mM) NaCl conditions, uptake of AtPIP2;1 is inhibited by MβCD (but not under low salt conditions) (Li et al., 2011; Luu et al., 2012) indicating that abiotic stress could influence the selection of cargo through CIE and CME pathways. Similarly, the Arabidopsis borate efflux transporter, BOR1 undergoes CME and CIE. Under low and high boron conditions, the endocytosis of the Arabidopsis borate efflux transporter, BOR1 is AP2-dependent and AP-2-independent, respectively (Yoshinari et al., 2019). Whether the internalization of AtBOR1 under high boron conditions occurs through a CME mechanism in which AP-2 is not essential (reflecting the viability of *ap2* mutants), or whether the internalization of AtBOR1 in these circumstances is solely through CIE is not apparent. However, studies in rice suggest that CIE may be the prevalent mode of internalization of BOR1 under low- and high-boron conditions indicating that species differences may also dictate the mode of endocytosis of plasma membrane proteins (Huang et al., 2021).

The production of superoxide species is also regulated by a combination of CIE and CME transport pathways. Respiratory burst oxidase homolog protein D (RbohD), which generates reactive oxygen species critical for a variety of cellular responses (Waszczak et al., 2018), localizes to plasma membrane microdomains, and its internalization is affected both in *chc2* mutants and by downregulation of *Flot1* expression suggesting that both CIE and CME contribute to RbohD uptake (Hao et al., 2014). The study of RbohD transport is notable for its use of genetic tools to explore the

internalization of RbohD, rather than sole reliance on small molecule perturbation of CIE and CME.

The prevalence of CIE vs CME pathways appears to also be tissue context-dependent. Using three probes for CME, CIE, and bulk endocytosis, Baral et al. show that while CME constitutively operates in all layers of the root, constitutive CIE is restricted primarily to the epidermal root cells. However, salt stress leads to an increase in the sterol content of internal root cells, which is postulated to be the basis for the expansion of CIE pathways into the interior layers of the Arabidopsis root under these specific environmental conditions (Baral et al., 2015).

Coordination of phospholipid metabolism and endocytosis

Anionic phospholipids, including phosphatidic acid (PA), phosphatidylserine (PS), and the phosphatidylinositol phospholipids (PIPs) represent only a small percentage of the total lipid content of the plant cell membranes. Nevertheless, they contribute significantly to the electrostatic signature of the plasma membrane and cell plate and serve as major regulators of many fundamental cellular processes, including cell signaling and membrane trafficking (Platre et al., 2018; Noack and Jaillais, 2020).

In particular, use of the recently developed iDePP (inducible depletion of $PI(4,5)P_2$ in plants) system demonstrates that $PI(4,5)P_2$ is critical for CME (Doumane et al., 2021). Interestingly, the inducible depletion of plasma membrane $PI(4,5)P_2$ levels affects the plasma membrane localization of the AP2μ2 subunit but not of clathrin, suggesting that in addition to AP2, other EAPs and lipids, beside $PI(4,5)P_2$, may function coordinately for

clathrin recruitment to plasma membrane CCPs. Indeed, the Eps15 homology (EH) domains of AtEH1, a subunit of the TPC that exhibits membrane bending activity (Johnson et al 2021), preferentially and differentially bind PI(4,5)P_2 as well as PA (Yperman et al., 2021a). In addition, multiple subunits of the TPC display interactions with a range of anionic phospholipids, including PI(4,5)P_2 and PI(4)P, the latter of which accumulates at the plasma membrane of plants in contrast to animal and yeast systems (Simon et al., 2016; Yperman et al., 2021b). Disruption of PI(4)P levels by small molecule-induced inhibition of the production of PI(4)P entirely abrogates the plasma membrane localization of an over-expressed GFP-tagged μ homology domain (μHD) of the TPC subunit, TML (Yperman et al., 2021b). This finding suggests that PI(4)P contributes to the recruitment of this CME adaptor to the plasma membrane.

Mirroring the requirement of PI(4,5)P_2 for CME at the plasma membrane, the dynamics and functions of kinases producing PI(4,5)P_2 also regulate plant CME (Zhao et al., 2010; Ischebeck et al., 2013). Clustering of the CME cargo, PIN2, at the plasma membrane is inhibited in the double *pip5k1/pip5k2* mutants in which the functions of PIP5K1 and PIP5K2 kinases converting PI4P into PI(4,5)P_2 are disrupted, further emphasizing the role of this phospholipid in regulating CME at early stages of clathrin recruitment to the plasma membrane (Tejos et al., 2014; Li et al., 2021), and the putative PI(4,5)P_2 phosphatase, SAC9, is notably abundant in the proteome of enriched plant CCVs (Dahhan et al., 2022).

Despite its role in CME at the plasma membrane, the early cell plate lacks PI(4,5)P_2 suggesting that other lipids may function in the recycling of proteins and

membrane from the cell plate during cytokinesis. The phosphoinositide kinase, PI4Kβ1 localizes to the cell plate and converts phosphatidylinositol into PI(4)P, and double mutants of *pi4kβ1/pi4kβ2* demonstrate reduced clathrin light chain recruitment to the cell plate and reduced internalization of the endocytic cargo, KNOLLE, from the cell plate. However, clathrin lifetime at the plasma membrane was increased in *pi4kβ1/pi4kβ2* lines, suggesting that regulation of the function of PI(4)P in facilitating clathrin recruitment to sites of endocytosis may differ between cells undergoing cytokinesis and interphase (Lin et al., 2019).

Relationships of CME with the TGN/EE and the ER

Recent studies indicate that regulation of CME is coordinated with endoplasmic reticulum (ER) and TGN/EE activities that are critical for the synthesis and trafficking of lipids and proteins to the plasma membrane.

The plant cortical ER network and plasma membrane are associated through contact sites (EPCSs) defined as ribosome-excluding areas where the ER and plasma membrane are less than 10 nanometers apart. Plant EPCSs are characterized by ER-anchored protein tethers, Vesicle-Associated Membrane Protein (VAMP)-Associated Proteins, VAPs, including VAP27 and synaptotagmin1; plasma membrane-associated proteins such as NET3c; and microtubules and actin that together serve to bridge the gap between membranes (Wang et al., 2017a; Zaman et al., 2020). The precise functions of plant EPCSs are still being established; however given the conserved nature of EPCSs across systems, it is likely that plant EPCSs function in lipid biosynthesis and transfer, the

formation of autophagosomes, and endocytosis (Wang and Hussey, 2019; Zaman et al., 2020).

The Arabidopsis VAP27 isoforms, VAP27-1 and VAP27-3, interact with CLC and CHC and broadly with multiple PIP species (Stefano et al., 2018). In addition, the TPC subunit, EH1 binds to VAP27-1 and recruits other components of the CME machinery including the TPC subunits, CHC, and AP-2 subunits to autophagosomes associated with EPCSs (Wang et al., 2019b). The degradation of TPLATE in response to carbon starvation indicates that EPCSs function to regulate endocytosis through an autophagy-dependent mechanism that leads to the degradation of essential components of CME machinery (Wang et al., 2019b). In addition to their role in the autophagy of CME machinery, VAP27 proteins are implicated in endocytosis, as *vap27-1/-3* loss-of-function double mutants display altered clathrin dynamics at the plasma membrane and impaired endocytosis of FM4-64 (Stefano et al., 2018).

Endocytosis in plants is also modulated by the coordination of CME and clathrin-dependent post-Golgi trafficking. Studies in yeast, metazoans, and *Trypanosoma brucei* have suggested links between CME and the exocytic machinery involved in the delivery of secretory proteins and the recycling of endocytosed proteins to the plasma membrane (Gurunathan et al., 2000; Sommer et al., 2005; Jose et al., 2015; Boehm et al., 2017). Similarly, CME is inhibited in mutant plants that display defects in exocytosis, such as the secretory SNARE mutant, *syp121* (Larson et al., 2017) and mutants defective for subunits of the SCD complex, which functions in the activation of post-Golgi vesicle-associated RabE1 GTPases and interacts with the exocyst tethering complex (McMichael and

Bednarek, 2013; Mayers et al., 2017; Wang et al., 2022). These data demonstrate the intersection of post-Golgi trafficking with CME in plants.

In addition, the association of clathrin and its accessory factors with the TGN/EE (AP-1 and clathrin) and plasma membrane (AP-2, TPC, DRP, and clathrin) appears to be coordinately regulated (Larson et al., 2017; Yan et al., 2021). Specifically, disruption of post-Golgi trafficking in loss-of-function *ap-1* mutants inhibits the recruitment of components of the CME machinery (clathrin and subunits of AP-2 and TPC), consequentially causing defects in the internalization of FM4-64 and the plasma membrane protein, PIN2. In turn, disruption of multiple subunits of AP-2 and TPC causes a depletion of AP-1 subunits and clathrin from the TGN/EE, consequentially impairing secretion and recycling of endocytosed cargo from the TGN/EE (Yan et al., 2021). These data demonstrate that CME and post-Golgi trafficking are coordinately regulated at the TGN/EE. The concomitant mislocalization of TGN/EE markers in *ap-1* mutants suggests that TGN/EE identity is critical to CME, and indeed, the origin of *vap27-1/-3* defects may also be related to the altered TGN/EE morphology observed in *vap27-1/-3* loss-of-function plants (Stefano et al., 2015). Here, too, the relationship between the structural integrities of the ER and TGN/EE and their effect on CME are also demonstrated in *root hair defective 3* (*rhd3)* in which disruptions of ER morphology and partially aggregated TGN/EE are simultaneously observed (Stefano et al., 2015).

Conclusions and Outstanding Questions

Great leaps have been made in the last ten years in the field of plant endocytosis, in terms of rapidly identifying the existence of multiple endocytic pathways, characterizing the stages of CCV formation at high structural and temporal resolution, and identifying the protein machinery and interactions that facilitate the internalization of membrane and proteins in constitutive and conserved or environmental-, cell-, and/or species-dependent manners. While the continued characterization of individual components of plant endocytosis is essential, future research should particularly explore the intersections between facets of plant endocytosis at a micro- (e.g., the functional redundancies between EAPs), intermediate- (e.g. the overlap between CIE and CME), and macro-scale (e.g. the degree to which endocytic pathways regulate, and are regulated by, other protein transport pathways and organelles of the endomembrane system). Some outstanding questions that will hopefully soon be addressed include:

1. Considering the severe phenotypic consequences resulting from loss of TPC function in plants in comparison to the relatively benign phenotypes observed in the absence of AP-2, to what degree does AP-2 promote CME? In what biological contexts does AP-2 compensate for TPC function, and to what extent do both endocytic adaptor complexes function together?
2. As the loss of AUXILIN-LIKE 1/2 proteins in Arabidopsis appears to have no significant phenotypic defects, what other factors in plants could mediate CCV uncoating? And, to what extent is uncoating of the CCV required at all for trafficking of the endocytosed vesicle to the TGN/EE?

3. How many distinct pathways facilitate CIE in plants? Future research will further characterize the endocytic structures formed in these pathways and identify any variations.
4. To what extent are there similarities between the regions of plasma membrane internalized by CIE and CME in terms of phospholipid composition and clustering of protein cargos?
5. What are the molecular signaling events that coordinately regulate clathrin dependent post-Golgi trafficking and CME, and how do they influence TGN/EE identity and/or integrity?

Acknowledgments

We thank Laura Vanderploeg for graphic design assistance and apologize to those colleagues whose work we were unable to cover due space restrictions. Work on clathrin-mediated trafficking in the Bednarek lab is supported by an award from the National Science Foundation (NSF-MCB Award No. 1614915) to S.Y.B.

Figures

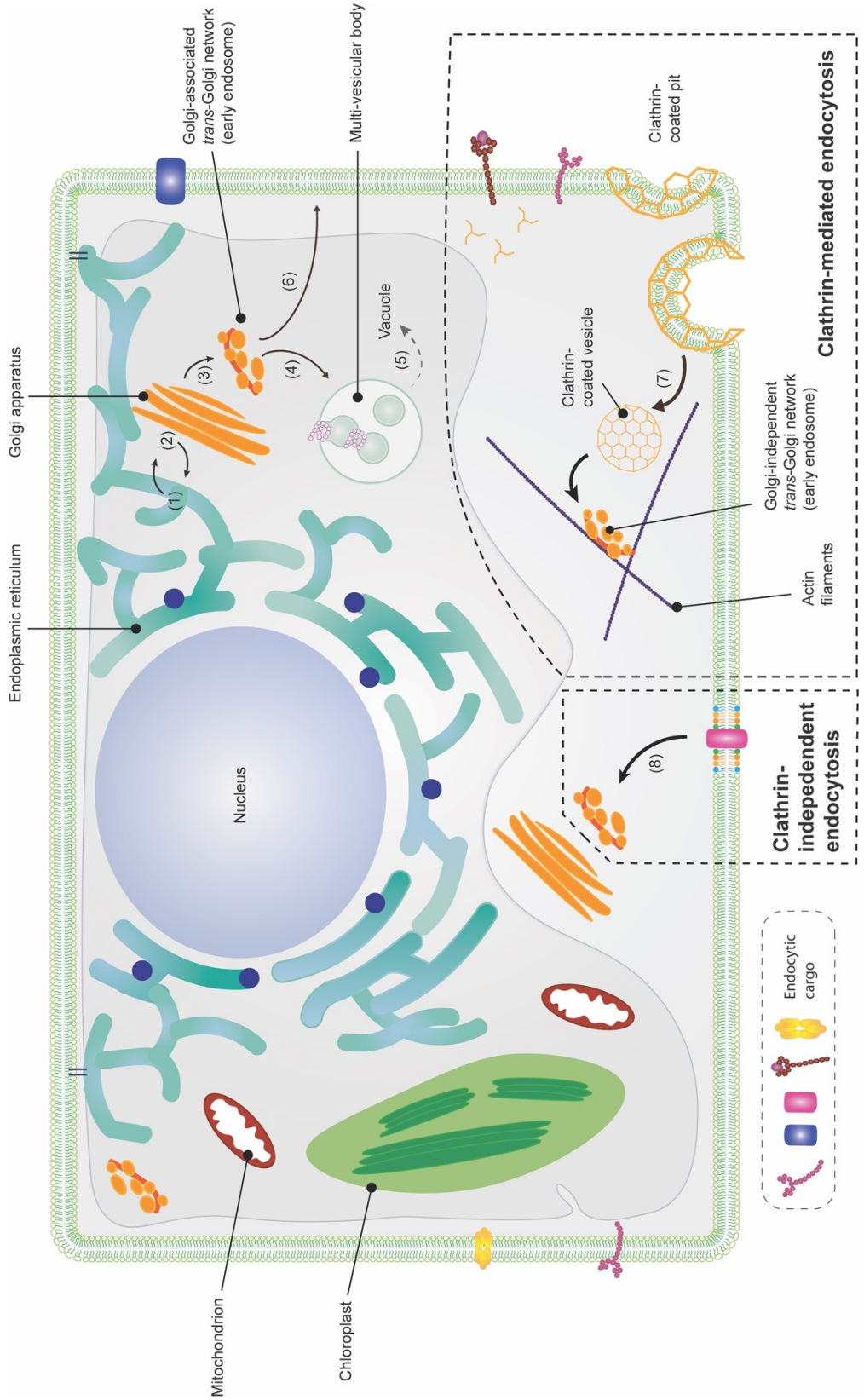

Figure 1.1: Schematic of plant endomembrane trafficking pathways

Figure 1.1: Schematic of plant endomembrane trafficking pathways.

Stylized illustration of plant cell with annotated organelles and endocytic cargo (e.g. plasma membrane (PM)-localized receptors, transporters, and cellulose synthase rosettes). Biosynthetic secretory trafficking pathways are numbered in the upper right hand. Soluble and membrane secretory proteins are synthesized in the endoplasmic reticulum (ER) and transported via COPII vesicles (1) to the Golgi apparatus. COPI vesicles (2) mediate retrograde trafficking of proteins from the Golgi to the ER and between Golgi cisternae. Within the trans-Golgi network/early endosome (TGN/EE) (3) newly synthesized secretory and endocytosed proteins are sorted and trafficked through the late endosome/multi-vesicular body (4) which upon fusion with the tonoplast delivers its cargo contents to the vacuole (5). Alternatively, exocytic transport (6) from the TGN/EE facilitates the secretion of newly synthesized proteins destined for the PM and recycles endocytosed PM-resident proteins including transporters, receptors, kinases, and biosynthetic enzymes. Endocytosis of plasma membrane and extracellular material is accomplished through clathrin-mediated (7) or clathrin-independent (8) endocytic pathways (designated within dashed lines). The former pathway requires the initiation, maturation, and release of clathrin-coated vesicles into the cytosol which traffic to the TGN/EE. The cargo are subsequently targeted for vacuolar degradation or recycling to the plasma membrane. In addition, clathrin-independent endocytic pathways mediate the internalization of a partially overlapping set of plasma membrane-resident proteins through mechanisms involving the formation of membrane microdomains and are marked by the protein, Flotillin1.

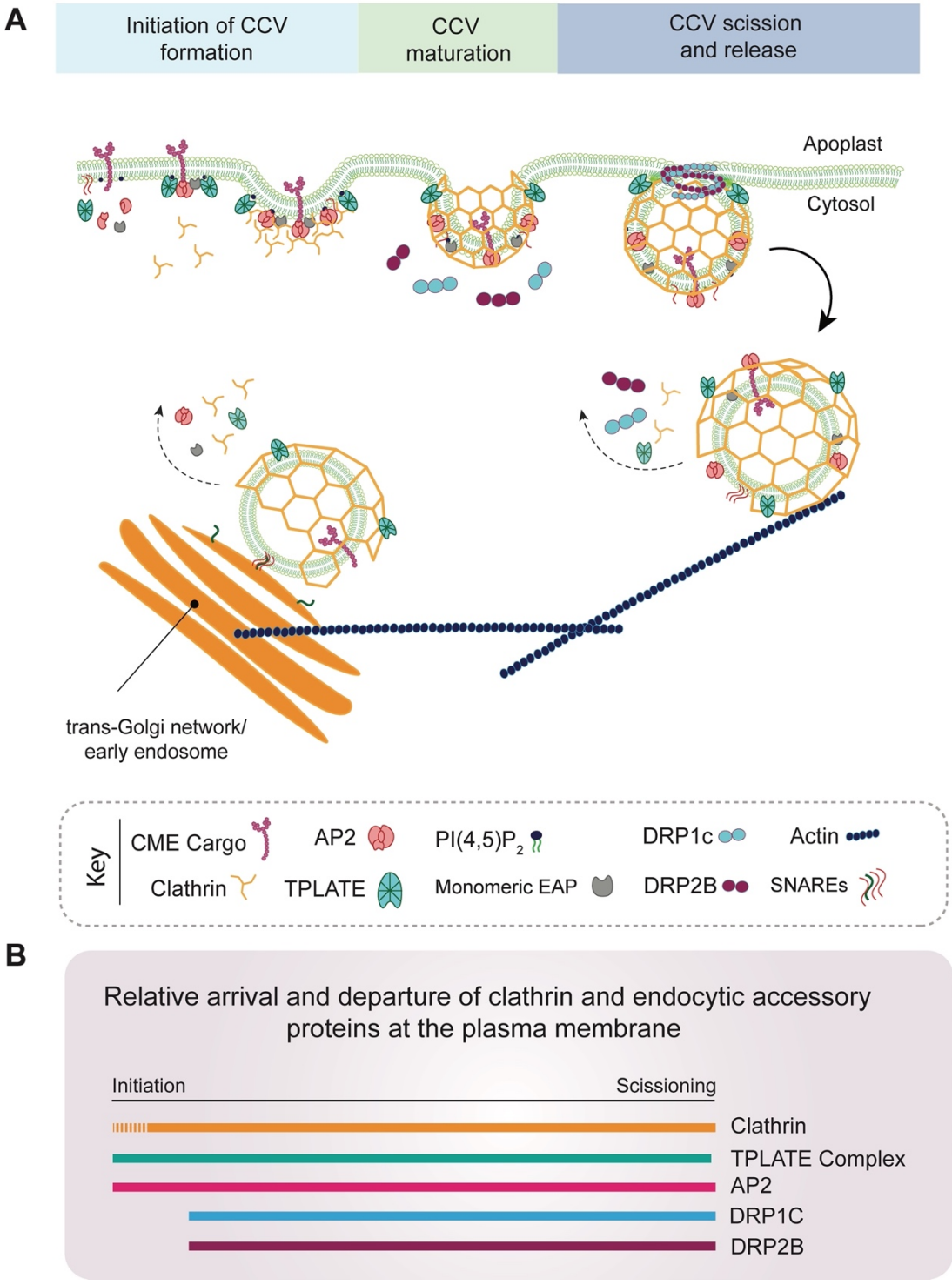

Figure 1.2: Stages of clathrin-coated vesicle formation

Figure 1.2: Stages of clathrin-coated vesicle formation.

(A) Three stages of clathrin-coated vesicle formation are depicted. Initiation of clathrin-coated vesicle (CCV) formation is mediated through recognition of plasma membrane-associated endocytic cargo and phosphatidylinositol phospholipids by oligomeric adaptors, AP-2 and TPLATE complex, that consequently recruit clathrin triskelia to the plasma membrane, as well as through monomeric EAPs (e.g. PICALM1a/1b). In the second phase, polymerization of clathrin triskelia at the plasma membrane, as well as potential action of additional EAPs, e.g. the TPLATE complex, drive membrane deformation and generate a clathrin-coated pit which matures into a clathrin-coated vesicle. In the final stage of CCV formation, the action of Dynamin-Related Proteins 1 and 2 severs the budding endocytic vesicle from the membrane, releasing the CCV into the cytosol whereupon it is trafficked to the TGN/EE along actin microfilaments. Sequential uncoating of the CCV indicated by dashed arrows occurs after cleavage and possibly up to the point when the endocytic CCV tethers to and fuses with the TGN/EE by the action of SNARE proteins.

(B) Illustration of the arrival and departure of machinery relative to clathrin at productive CME events on the plasma membrane. A dashed line indicates ambiguity in presence based on the literature.

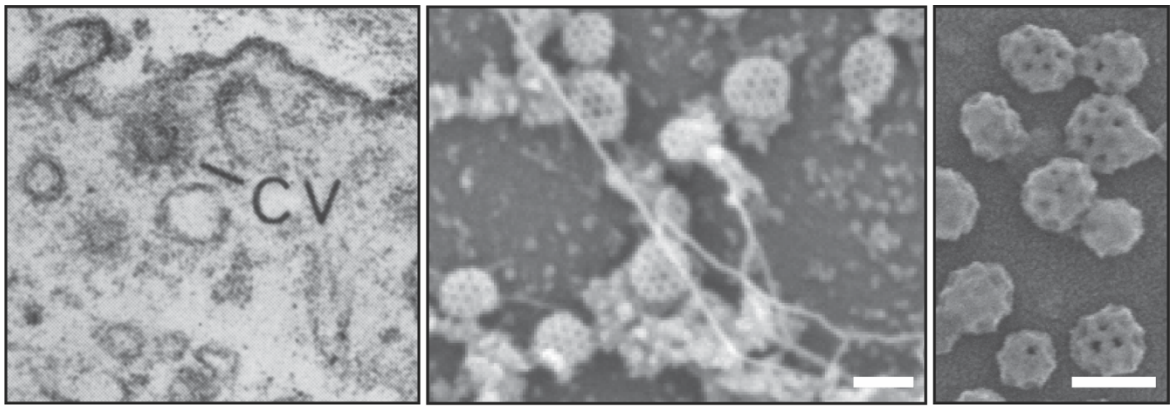

Figure 1.3 Historical perspective of plant clathrin-mediated trafficking

Figure 1.3 Historical perspective of plant clathrin-mediated trafficking

Major advances in our understanding of the molecular mechanisms of plant endocytosis have occurred in the last 20 years, including the appreciation of its essential function in plant growth and development despite the hypothesis that it was not physically possible in plants. Yet as far back as 1966, coated vesicles were observed at the plasma membrane in electron micrographs of radish root hair cells (Bonnett Jr. and Newcomb, 1966) even though it would take another 10 years for the molecular identification of clathrin by Barbara Pearse (Pearse, 1976). Today, high resolution imaging of the dynamics of clathrin-coated vesicle formation and transport, the identifications in plants of evolutionarily conserved factors mediating endocytosis as well as of those which are absent from metazoan CME (such as the TPLATE complex and dynamin-related proteins), and the development of tools like conditional mutants and small molecule inhibitors that specifically perturb endocytic pathways have together unequivocally validated the fact that CME occurs in plant cells.

(Left) Electron micrograph of coated vesicle (CV) at the plasma membrane of a radish root hair. Magnification: 61,000x. Figure adapted from Bonnett Jr. and Newcomb with permission from Wiley.

(Middle) SEM image of clathrin-coated structures of Arabidopsis root protoplasts. Scale bar: 100 nm. Image used with permission of A. Johnson and J. Friml (IST Austria).

(Right) SEM image of clathrin-coated vesicles enriched from Arabidopsis suspension cultured-cells. Scale bar: 100 nm. Image used with permission of A. Johnson and J. Friml (IST Austria).

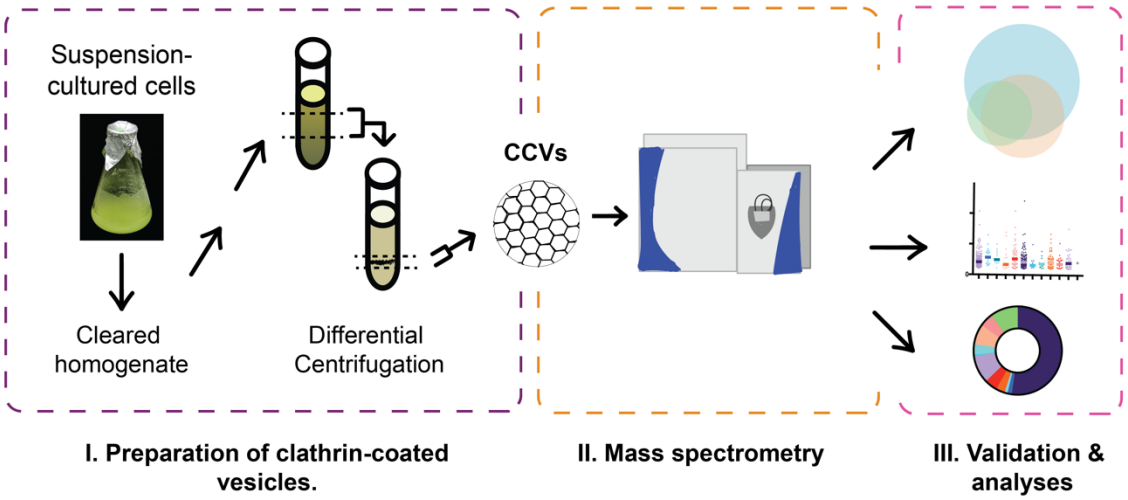

Figure 1.4 Proteomic analyses of plant CCVs and compartments of the endomembrane network.

Figure 1.4 Proteomic analyses of plant CCVs and compartments of the endomembrane network.

Our knowledge of proteins trafficked by and facilitating CME in plants was expanded by the proteomic characterization of a pool of endocytic and post-Golgi trafficking-derived CCVs purified from Arabidopsis suspension cultured cells (Dahhan et al., 2022). Two unlabeled mass spectrometry workflows identifying a core CCV proteome were supported by a third proteomic workflow incorporating stable isotope labeling that enabled the quantitation of the fold enrichment and depletion of CCV-associated proteins throughout the vesicle purification process. Quantitative immunoblotting of CCV-associated proteins and markers of unassociated organelles validate these enrichment and depletion values. Manual annotation of the proteome describe the abundances and fold enrichments of a subset of proteins involved in the production, regulation, and tethering of CCVs, as well as known endocytic cargo. Besides resolving mechanistic details of CME, the integrated proteomic datasets serve as a reference for researchers interested in gauging whether their proteins of interest are associated with CCV-mediated trafficking. Follow-up experiments are essential to confirming the association of a protein of interest with CCV-mediated trafficking and particularly with CME, as the proteomic resource describes a heterogeneous pool of plant CCVs. The absence of a protein from the proteomic datasets is also not necessarily indicative of its non-involvement with CCV-mediated transport, as the proteins DRP1 and DRP2, which are known to be involved in CME, are of low abundance and do not co-enrich with the CCVs, which is likely due to the temporal nature of their association (Collings et al., 2008; Konopka et al., 2008; Gadeyne et al., 2014;

Ekanayake et al., 2021). Integration of earlier proteomic explorations of functionally distinct, yet intersecting domains of the endomembrane network in plants using markers of subcellular compartments and mass spectrometry with the CCV proteome will also help to measure the extent to which endocytic trafficking contributes to the protein content of those domains (Heard et al., 2015). Where the plant CCV proteome is obtained from vesicles purified through a differential centrifugation-based scheme using undifferentiated, suspension-cultured Arabidopsis cells as source material (Reynolds et al., 2014), Mosesso et al. recently described a protocol for the purification of CCVs from whole seedlings thus conferring the advantage of studying CCV populations in seedlings where CME is genetically, conditionally, or inducible perturbed (Mosesso et al., 2018).

References

Adamowski, M., Narasimhan, M., Kania, U., Glanc, M., De Jaeger, G., and Friml, J. (2018). A Functional Study of AUXILIN-LIKE1 and 2, Two Putative Clathrin Uncoating Factors in Arabidopsis. Plant Cell **30,** 700-716.

Aniento, F., de Medina Hernandez, V.S., Dagdas, Y., Rojas-Pierce, M., and Russinova, E. (2021). Molecular mechanisms of endomembrane trafficking in plants. Plant Cell.

Arora, D., and Damme, D.V. (2021). Motif-based endomembrane trafficking. Plant Physiol **186,** 221-238.

Backues, S.K., and Bednarek, S.Y. (2010). Arabidopsis dynamin-related protein 1A polymers bind, but do not tubulate, liposomes. Biochem Biophys Res Commun **393,** 734-739.

Backues, S.K., Korasick, D.A., Heese, A., and Bednarek, S.Y. (2010). The Arabidopsis dynamin-related protein2 family is essential for gametophyte development. Plant Cell **22,** 3218-3231.

Bandmann, V., and Homann, U. (2012). Clathrin-independent endocytosis contributes to uptake of glucose into BY-2 protoplasts. Plant J **70,** 578-584.

Bandmann, V., Muller, J.D., Kohler, T., and Homann, U. (2012). Uptake of fluorescent nano beads into BY2-cells involves clathrin-dependent and clathrin-independent endocytosis. FEBS Lett **586,** 3626-3632.

Baral, A., Irani, N.G., Fujimoto, M., Nakano, A., Mayor, S., and Mathew, M.K. (2015). Salt-induced remodeling of spatially restricted clathrin-independent endocytic pathways in Arabidopsis root. Plant Cell **27,** 1297-1315.

Barberon, M., Dubeaux, G., Kolb, C., Isono, E., Zelazny, E., and Vert, G. (2014). Polarization of IRON-REGULATED TRANSPORTER 1 (IRT1) to the plant-soil interface plays crucial role in metal homeostasis. Proc Natl Acad Sci U S A **111,** 8293-8298.

Barberon, M., Zelazny, E., Robert, S., Conejero, G., Curie, C., Friml, J., and Vert, G. (2011). Monoubiquitin-dependent endocytosis of the iron-regulated transporter 1 (IRT1) transporter controls iron uptake in plants. Proc Natl Acad Sci U S A **108,** E450-458.

Barth, M., and Holstein, S.E. (2004). Identification and functional characterization of Arabidopsis AP180, a binding partner of plant alphaC-adaptin. J Cell Sci **117,** 2051-2062.

Bashline, L., Li, S., Zhu, X., and Gu, Y. (2015). The TWD40-2 protein and the AP2 complex cooperate in the clathrin-mediated endocytosis of cellulose synthase to regulate cellulose biosynthesis. Proc Natl Acad Sci U S A **112,** 12870-12875.

Bashline, L., Li, S., Anderson, C.T., Lei, L., and Gu, Y. (2013). The endocytosis of cellulose synthase in Arabidopsis is dependent on mu2, a clathrin-mediated endocytosis adaptin. Plant Physiol **163,** 150-160.

Bednarek, S.Y., and Backues, S.K. (2010). Plant dynamin-related protein families DRP1 and DRP2 in plant development. Biochem Soc Trans **38,** 797-806.

Boehm, C.M., Obado, S., Gadelha, C., Kaupisch, A., Manna, P.T., Gould, G.W., Munson, M., Chait, B.T., Rout, M.P., and Field, M.C. (2017). The Trypanosome

Exocyst: A Conserved Structure Revealing a New Role in Endocytosis. PLoS Pathog **13,** e1006063.

Bonnett Jr., H.T., and Newcomb, E.H. (1966). Coated Vesicles and Other Cytoplasmic Components of Growing Root Hairs of Radish. Protoplasma **62,** 59-75.

Borner, G.H., Sherrier, D.J., Weimar, T., Michaelson, L.V., Hawkins, N.D., Macaskill, A., Napier, J.A., Beale, M.H., Lilley, K.S., and Dupree, P. (2005). Analysis of detergent-resistant membranes in Arabidopsis. Evidence for plasma membrane lipid rafts. Plant Physiol **137,** 104-116.

Boutte, Y., Frescatada-Rosa, M., Men, S., Chow, C.M., Ebine, K., Gustavsson, A., Johansson, L., Ueda, T., Moore, I., Jurgens, G., and Grebe, M. (2010). Endocytosis restricts Arabidopsis KNOLLE syntaxin to the cell division plane during late cytokinesis. EMBO J **29,** 546-558.

Chaparro-Garcia, A., Schwizer, S., Sklenar, J., Yoshida, K., Petre, B., Bos, J.I., Schornack, S., Jones, A.M., Bozkurt, T.O., and Kamoun, S. (2015). Phytophthora infestans RXLR-WY Effector AVR3a Associates with Dynamin-Related Protein 2 Required for Endocytosis of the Plant Pattern Recognition Receptor FLS2. PLoS One **10,** e0137071.

Cocucci, E., Aguet, F., Boulant, S., and Kirchhausen, T. (2012). The first five seconds in the life of a clathrin-coated pit. Cell **150,** 495-507.

Collings, D.A., Gebbie, L.K., Howles, P.A., Hurley, U.A., Birch, R.J., Cork, A.H., Hocart, C.H., Arioli, T., and Williamson, R.E. (2008). Arabidopsis dynamin-like protein DRP1A: a null mutant with widespread defects in endocytosis, cellulose synthesis, cytokinesis, and cell expansion. J Exp Bot **59,** 361-376.

Cui, Y., Li, X., Yu, M., Li, R., Fan, L., Zhu, Y., and Lin, J. (2018). Sterols regulate endocytic pathways during flg22-induced defense responses in Arabidopsis. Development **145**.

Dacks, J.B., and Robinson, M.S. (2017). Outerwear through the ages: evolutionary cell biology of vesicle coats. Curr Opin Cell Biol **47,** 108-116.

Dahhan, D.A., Reynolds, G.D., Cardenas, J.J., Eeckhout, D., Johnson, A., Yperman, K., Kaufmann, W.A., Vang, N., Yan, X., Hwang, I., Heese, A., De Jaeger, G., Friml, J., Van Damme, D., Pan, J., and Bednarek, S.Y. (2022). Proteomic characterization of isolated Arabidopsis clathrin-coated vesicles reveals evolutionarily conserved and plant-specific components. Plant Cell.

de Jong, F., and Munnik, T. (2021). Attracted to membranes: lipid-binding domains in plants. Plant Physiol **185,** 707-723.

Dejonghe, W., Sharma, I., Denoo, B., De Munck, S., Lu, Q., Mishev, K., Bulut, H., Mylle, E., De Rycke, R., Vasileva, M., Savatin, D.V., Nerinckx, W., Staes, A., Drozdzecki, A., Audenaert, D., Yperman, K., Madder, A., Friml, J., Van Damme, D., Gevaert, K., Haucke, V., Savvides, S.N., Winne, J., and Russinova, E. (2019). Disruption of endocytosis through chemical inhibition of clathrin heavy chain function. Nat Chem Biol **15,** 641-649.

Depta, H., and Robinson, D.G. (1986). The isolation and enrichment of coated vesicles from suspension-cultured carrot cells. Protoplasma **130,** 162-170.

Dhonukshe, P., Aniento, F., Hwang, I., Robinson, D.G., Mravec, J., Stierhof, Y.D., and Friml, J. (2007). Clathrin-mediated constitutive endocytosis of PIN auxin efflux carriers in Arabidopsis. Curr Biol **17,** 520-527.

Di Rubbo, S., Irani, N.G., Kim, S.Y., Xu, Z.Y., Gadeyne, A., Dejonghe, W., Vanhoutte, I., Persiau, G., Eeckhout, D., Simon, S., Song, K., Kleine-Vehn, J., Friml, J., De Jaeger, G., Van Damme, D., Hwang, I., and Russinova, E. (2013). The clathrin adaptor complex AP-2 mediates endocytosis of brassinosteroid insensitive1 in Arabidopsis. Plant Cell **25,** 2986-2997.

Doumane, M., Lebecq, A., Colin, L., Fangain, A., Stevens, F.D., Bareille, J., Hamant, O., Belkhadir, Y., Munnik, T., Jaillais, Y., and Caillaud, M.C. (2021). Inducible depletion of PI(4,5)P2 by the synthetic iDePP system in Arabidopsis. Nat Plants **7,** 587-597.

Eisenberg, E., and Greene, L.E. (2007). Multiple roles of auxilin and hsc70 in clathrin-mediated endocytosis. Traffic **8,** 640-646.

Ekanayake, G., LaMontagne, E.D., and Heese, A. (2019). Never Walk Alone: Clathrin-Coated Vesicle (CCV) Components in Plant Immunity. Annu Rev Phytopathol **57,** 387-409.

Ekanayake, G., Smith, J.M., Jones, K.B., Stiers, H.M., Robinson, S.J., LaMontagne, E.D., Kostos, P.H., Cornish, P.V., Bednarek, S.Y., and Heese, A. (2021). DYNAMIN-RELATED PROTEIN DRP1A functions with DRP2B in plant growth, flg22-immune responses, and endocytosis. Plant Physiol **185,** 1986-2002.

Ford, M.G., Mills, I.G., Peter, B.J., Vallis, Y., Praefcke, G.J., Evans, P.R., and McMahon, H.T. (2002). Curvature of clathrin-coated pits driven by epsin. Nature **419,** 361-366.

Frick, M., Bright, N.A., Riento, K., Bray, A., Merrified, C., and Nichols, B.J. (2007). Coassembly of flotillins induces formation of membrane microdomains, membrane curvature, and vesicle budding. Curr Biol **17,** 1151-1156.

Fujimoto, M., and Tsutsumi, N. (2014). Dynamin-related proteins in plant post-Golgi traffic. Front Plant Sci **5,** 408.

Fujimoto, M., Arimura, S., Nakazono, M., and Tsutsumi, N. (2008). Arabidopsis dynamin-related protein DRP2B is co-localized with DRP1A on the leading edge of the forming cell plate. Plant Cell Rep **27,** 1581-1586.

Fujimoto, M., Ebine, K., Nishimura, K., Tsutsumi, N., and Ueda, T. (2020). Longin R-SNARE is retrieved from the plasma membrane by ANTH domain-containing proteins in Arabidopsis. Proc Natl Acad Sci U S A **117,** 25150-25158.

Fujimoto, M., Arimura, S., Ueda, T., Takanashi, H., Hayashi, Y., Nakano, A., and Tsutsumi, N. (2010). Arabidopsis dynamin-related proteins DRP2B and DRP1A participate together in clathrin-coated vesicle formation during endocytosis. Proc Natl Acad Sci U S A **107,** 6094-6099.

Gadeyne, A., Sanchez-Rodriguez, C., Vanneste, S., Di Rubbo, S., Zauber, H., Vanneste, K., Van Leene, J., De Winne, N., Eeckhout, D., Persiau, G., Van De Slijke, E., Cannoot, B., Vercruysse, L., Mayers, J.R., Adamowski, M., Kania, U., Ehrlich, M., Schweighofer, A., Ketelaar, T., Maere, S., Bednarek, S.Y., Friml, J., Gevaert, K., Witters, E., Russinova, E., Persson, S., De Jaeger, G.,

and Van Damme, D. (2014). The TPLATE adaptor complex drives clathrin-mediated endocytosis in plants. Cell **156,** 691-704.

Gall, L., Stan, R.C., Kress, A., Hertel, B., Thiel, G., and Meckel, T. (2010). Fluorescent detection of fluid phase endocytosis allows for in vivo estimation of endocytic vesicle sizes in plant cells with sub-diffraction accuracy. Traffic **11,** 548-559.

Goode, B.L., Eskin, J.A., and Wendland, B. (2015). Actin and endocytosis in budding yeast. Genetics **199,** 315-358.

Gu, M., Liu, Q., Watanabe, S., Sun, L., Hollopeter, G., Grant, B.D., and Jorgensen, E.M. (2013). AP2 hemicomplexes contribute independently to synaptic vesicle endocytosis. Elife **2,** e00190.

Gurunathan, S., Chapman-Shimshoni, D., Trajkovic, S., and Gerst, J.E. (2000). Yeast exocytic v-SNAREs confer endocytosis. Mol Biol Cell **11,** 3629-3643.

Hao, H., Fan, L., Chen, T., Li, R., Li, X., He, Q., Botella, M.A., and Lin, J. (2014). Clathrin and Membrane Microdomains Cooperatively Regulate RbohD Dynamics and Activity in Arabidopsis. Plant Cell **26,** 1729-1745.

Harley, S.M., and Beevers, L. (1989). Isolation and partial characterization of clathrin-coated vesicles from pea (Pisum sativum L.) cotyledons. Protoplasma **150,** 103-109.

Hawes, C. (2005). Cell biology of the plant Golgi apparatus. New Phytol **165,** 29-44.

Hirst, J., Schlacht, A., Norcott, J.P., Traynor, D., Bloomfield, G., Antrobus, R., Kay, R.R., Dacks, J.B., and Robinson, M.S. (2014). Characterization of TSET, an ancient and widespread membrane trafficking complex. Elife **3,** e02866.

Huang, S., Konishi, N., Yamaji, N., Shao, J.F., Mitani-Ueno, N., and Ma, J.F. (2021). Boron uptake in rice is regulated posttranslationally via a clathrin-independent pathway. Plant Physiology.

Irani, N.G., Di Rubbo, S., Mylle, E., Van den Begin, J., Schneider-Pizon, J., Hnilikova, J., Sisa, M., Buyst, D., Vilarrasa-Blasi, J., Szatmari, A.M., Van Damme, D., Mishev, K., Codreanu, M.C., Kohout, L., Strnad, M., Cano-Delgado, A.I., Friml, J., Madder, A., and Russinova, E. (2012). Fluorescent castasterone reveals BRI1 signaling from the plasma membrane. Nat Chem Biol **8,** 583-589.

Ischebeck, T., Werner, S., Krishnamoorthy, P., Lerche, J., Meijon, M., Stenzel, I., Lofke, C., Wiessner, T., Im, Y.J., Perera, I.Y., Iven, T., Feussner, I., Busch, W., Boss, W.F., Teichmann, T., Hause, B., Persson, S., and Heilmann, I. (2013). Phosphatidylinositol 4,5-bisphosphate influences PIN polarization by controlling clathrin-mediated membrane trafficking in Arabidopsis. Plant Cell **25,** 4894-4911.

Johnson, A., and Vert, G. (2017). Single Event Resolution of Plant Plasma Membrane Protein Endocytosis by TIRF Microscopy. Front Plant Sci **8,** 612.

Johnson, A., Gnyliukh, N., Kaufmann, W.A., Narasimhan, M., Vert, G., Bednarek, S.Y., and Friml, J. (2020). Experimental toolbox for quantitative evaluation of clathrin-mediated endocytosis in the plant model Arabidopsis. J Cell Sci **133**.

Johnson, A., Dahhan, D.A., Gnyliukh, N., Kaufmann, W.A., Zheden, V., Costanzo, T., Mahou, P., Hrtyan, M., Wang, J., Aguilera-Servin, J., van Damme, D., Beaurepaire, E., Loose, M., Bednarek, S.Y., and Friml, J. (2021). The TPLATE complex mediates membrane bending during plant clathrin-mediated endocytosis. Proc Natl Acad Sci U S A **118**.

Jose, M., Tollis, S., Nair, D., Mitteau, R., Velours, C., Massoni-Laporte, A., Royou, A., Sibarita, J.B., and McCusker, D. (2015). A quantitative imaging-based screen reveals the exocyst as a network hub connecting endocytosis and exocytosis. Mol Biol Cell **26,** 2519-2534.

Kaneda, M., van Oostende-Triplet, C., Chebli, Y., Testerink, C., Bednarek, S.Y., and Geitmann, A. (2019). Plant AP180 N-Terminal Homolog Proteins Are Involved in Clathrin-Dependent Endocytosis during Pollen Tube Growth in Arabidopsis thaliana. Plant Cell Physiol **60,** 1316-1330.

Kang, B.H., Rancour, D.M., and Bednarek, S.Y. (2003a). The dynamin-like protein ADL1C is essential for plasma membrane maintenance during pollen maturation. Plant J **35,** 1-15.

Kang, B.H., Busse, J.S., and Bednarek, S.Y. (2003b). Members of the Arabidopsis dynamin-like gene family, ADL1, are essential for plant cytokinesis and polarized cell growth. Plant Cell **15,** 899-913.

Kelly, B.T., McCoy, A.J., Spate, K., Miller, S.E., Evans, P.R., Honing, S., and Owen, D.J. (2008). A structural explanation for the binding of endocytic dileucine motifs by the AP2 complex. Nature **456,** 976-979.

Kelly, B.T., Graham, S.C., Liska, N., Dannhauser, P.N., Honing, S., Ungewickell, E.J., and Owen, D.J. (2014). Clathrin adaptors. AP2 controls clathrin polymerization with a membrane-activated switch. Science **345,** 459-463.

Kim, S.Y., Xu, Z.Y., Song, K., Kim, D.H., Kang, H., Reichardt, I., Sohn, E.J., Friml, J., Juergens, G., and Hwang, I. (2013). Adaptor protein complex 2-mediated endocytosis is crucial for male reproductive organ development in Arabidopsis. Plant Cell **25,** 2970-2985.

Kirchhausen, T., Owen, D., and Harrison, S.C. (2014). Molecular structure, function, and dynamics of clathrin-mediated membrane traffic. Cold Spring Harb Perspect Biol **6,** a016725.

Kitakura, S., Vanneste, S., Robert, S., Lofke, C., Teichmann, T., Tanaka, H., and Friml, J. (2011). Clathrin mediates endocytosis and polar distribution of PIN auxin transporters in Arabidopsis. Plant Cell **23,** 1920-1931.

Konopka, C.A., and Bednarek, S.Y. (2008). Comparison of the dynamics and functional redundancy of the Arabidopsis dynamin-related isoforms DRP1A and DRP1C during plant development. Plant Physiol **147,** 1590-1602.

Konopka, C.A., Backues, S.K., and Bednarek, S.Y. (2008). Dynamics of Arabidopsis dynamin-related protein 1C and a clathrin light chain at the plasma membrane. Plant Cell **20,** 1363-1380.

Kovtun, O., Dickson, V.K., Kelly, B.T., Owen, D.J., and Briggs, J.A.G. (2020). Architecture of the AP2/clathrin coat on the membranes of clathrin-coated vesicles. Sci Adv **6,** eaba8381.

Kurzchalia, T.V., and Parton, R.G. (1999). Membrane microdomains and caveolae. Curr Opin Cell Biol **11,** 424-431.

Larson, E.R., Van Zelm, E., Roux, C., Marion-Poll, A., and Blatt, M.R. (2017). Clathrin Heavy Chain Subunits Coordinate Endo- and Exocytic Traffic and Affect Stomatal Movement. Plant Physiol **175,** 708-720.

Leslie, M.E., Rogers, S.W., and Heese, A. (2016). Increased callose deposition in plants lacking DYNAMIN-RELATED PROTEIN 2B is dependent upon POWDERY MILDEW RESISTANT 4. Plant Signal Behav **11,** e1244594.

Li, H., von Wangenheim, D., Zhang, X., Tan, S., Darwish-Miranda, N., Naramoto, S., Wabnik, K., De Rycke, R., Kaufmann, W.A., Gutl, D., Tejos, R., Grones, P., Ke, M., Chen, X., Dettmer, J., and Friml, J. (2021). Cellular requirements for PIN polar cargo clustering in Arabidopsis thaliana. New Phytol **229,** 351-369.

Li, R., Liu, P., Wan, Y., Chen, T., Wang, Q., Mettbach, U., Baluska, F., Samaj, J., Fang, X., Lucas, W.J., and Lin, J. (2012). A membrane microdomain-associated protein, Arabidopsis Flot1, is involved in a clathrin-independent endocytic pathway and is required for seedling development. Plant Cell **24,** 2105-2122.

Li, X., and Pan, S.Q. (2017). Agrobacterium delivers VirE2 protein into host cells via clathrin-mediated endocytosis. Sci Adv **3,** e1601528.

Li, X., Wang, X., Yang, Y., Li, R., He, Q., Fang, X., Luu, D.T., Maurel, C., and Lin, J. (2011). Single-molecule analysis of PIP2;1 dynamics and partitioning reveals multiple modes of Arabidopsis plasma membrane aquaporin regulation. Plant Cell **23,** 3780-3797.

Lin, F., Krishnamoorthy, P., Schubert, V., Hause, G., Heilmann, M., and Heilmann, I. (2019). A dual role for cell plate-associated PI4Kbeta in endocytosis and phragmoplast dynamics during plant somatic cytokinesis. EMBO J **38**.

Liu, D., Kumar, R., Claus, L.A.N., Johnson, A.J., Siao, W., Vanhoutte, I., Wang, P., Bender, K.W., Yperman, K., Martins, S., Zhao, X., Vert, G., Van Damme, D., Friml, J., and Russinova, E. (2020). Endocytosis of BRASSINOSTEROID INSENSITIVE1 Is Partly Driven by a Canonical Tyr-Based Motif. Plant Cell **32,** 3598-3612.

Lo Presti, L., and Kahmann, R. (2017). How filamentous plant pathogen effectors are translocated to host cells. Curr Opin Plant Biol **38,** 19-24.

Lopez-Hernandez, T., Haucke, V., and Maritzen, T. (2020). Endocytosis in the adaptation to cellular stress. Cell Stress **4,** 230-247.

Lu, D., Lin, W., Gao, X., Wu, S., Cheng, C., Avila, J., Heese, A., Devarenne, T.P., He, P., and Shan, L. (2011). Direct ubiquitination of pattern recognition receptor FLS2 attenuates plant innate immunity. Science **332,** 1439-1442.

Luu, D.T., Martiniere, A., Sorieul, M., Runions, J., and Maurel, C. (2012). Fluorescence recovery after photobleaching reveals high cycling dynamics of plasma membrane aquaporins in Arabidopsis roots under salt stress. Plant J **69,** 894-905.

Marhava, P. (2021). Recent developments in the understanding of PIN polarity. New Phytol.

Martiniere, A., Fiche, J.B., Smokvarska, M., Mari, S., Alcon, C., Dumont, X., Hematy, K., Jaillais, Y., Nollmann, M., and Maurel, C. (2019). Osmotic Stress Activates Two Reactive Oxygen Species Pathways with Distinct Effects on Protein Nanodomains and Diffusion. Plant Physiol **179,** 1581-1593.

Massol, R.H., Boll, W., Griffin, A.M., and Kirchhausen, T. (2006). A burst of auxilin recruitment determines the onset of clathrin-coated vesicle uncoating. Proc Natl Acad Sci U S A **103,** 10265-10270.

Mayers, J.R., Hu, T., Wang, C., Cardenas, J.J., Tan, Y., Pan, J., and Bednarek, S.Y. (2017). SCD1 and SCD2 Form a Complex That Functions with the Exocyst and RabE1 in Exocytosis and Cytokinesis. Plant Cell **29,** 2610-2625.

McMichael, C.M., and Bednarek, S.Y. (2013). Cytoskeletal and membrane dynamics during higher plant cytokinesis. New Phytol **197,** 1039-1057.

Men, S., Boutte, Y., Ikeda, Y., Li, X., Palme, K., Stierhof, Y.D., Hartmann, M.A., Moritz, T., and Grebe, M. (2008). Sterol-dependent endocytosis mediates post-cytokinetic acquisition of PIN2 auxin efflux carrier polarity. Nat Cell Biol **10,** 237-244.

More, K., Klinger, C.M., Barlow, L.D., and Dacks, J.B. (2020). Evolution and Natural History of Membrane Trafficking in Eukaryotes. Curr Biol **30,** R553-R564.

Morrow, I.C., Rea, S., Martin, S., Prior, I.A., Prohaska, R., Hancock, J.F., James, D.E., and Parton, R.G. (2002). Flotillin-1/reggie-2 traffics to surface raft domains via a novel golgi-independent pathway. Identification of a novel membrane targeting domain and a role for palmitoylation. J Biol Chem **277,** 48834-48841.

Moscatelli, A., Ciampolini, F., Rodighiero, S., Onelli, E., Cresti, M., Santo, N., and Idilli, A. (2007). Distinct endocytic pathways identified in tobacco pollen tubes using charged nanogold. J Cell Sci **120,** 3804-3819.

Motley, A.M., Berg, N., Taylor, M.J., Sahlender, D.A., Hirst, J., Owen, D.J., and Robinson, M.S. (2006). Functional analysis of AP-2 alpha and mu2 subunits. Mol Biol Cell **17,** 5298-5308.

Narasimhan, M., Johnson, A., Prizak, R., Kaufmann, W.A., Tan, S., Casillas-Perez, B., and Friml, J. (2020). Evolutionarily unique mechanistic framework of clathrin-mediated endocytosis in plants. Elife **9**.

Noack, L.C., and Jaillais, Y. (2020). Functions of Anionic Lipids in Plants. Annu Rev Plant Biol **71,** 71-102.

Onelli, E., Prescianotto-Baschong, C., Caccianiga, M., and Moscatelli, A. (2008). Clathrin-dependent and independent endocytic pathways in tobacco protoplasts revealed by labelling with charged nanogold. J Exp Bot **59,** 3051-3068.

Otegui, M.S., Mastronarde, D.N., Kang, B.H., Bednarek, S.Y., and Staehelin, L.A. (2001). Three-dimensional analysis of syncytial-type cell plates during endosperm cellularization visualized by high resolution electron tomography. Plant Cell **13,** 2033-2051.

Ott, T. (2017). Membrane nanodomains and microdomains in plant-microbe interactions. Curr Opin Plant Biol **40,** 82-88.

Paez Valencia, J., Goodman, K., and Otegui, M.S. (2016). Endocytosis and Endosomal Trafficking in Plants. Annu Rev Plant Biol **67,** 309-335.

Pearse, B.M. (1976). Clathrin: a unique protein associated with intracellular transfer of membrane by coated vesicles. Proc Natl Acad Sci U S A **73,** 1255-1259.

Pizarro, L., Leibman-Markus, M., Schuster, S., Bar, M., and Avni, A. (2019). Tomato Dynamin Related Protein 2A Associates With LeEIX2 and Enhances PRR Mediated Defense by Modulating Receptor Trafficking. Front Plant Sci **10,** 936.

Platre, M.P., Noack, L.C., Doumane, M., Bayle, V., Simon, M.L.A., Maneta-Peyret, L., Fouillen, L., Stanislas, T., Armengot, L., Pejchar, P., Caillaud, M.C., Potocky, M., Copic, A., Moreau, P., and Jaillais, Y. (2018). A Combinatorial Lipid Code

Shapes the Electrostatic Landscape of Plant Endomembranes. Dev Cell **45,** 465-480 e411.

Putta, P., Creque, E., Piontkivska, H., and Kooijman, E.E. (2020). Lipid-protein interactions for ECA1 an N-ANTH domain protein involved in stress signaling in plants. Chem Phys Lipids **231,** 104919.

Reynolds, G.D., August, B., and Bednarek, S.Y. (2014). Preparation of enriched plant clathrin-coated vesicles by differential and density gradient centrifugation. Methods Mol Biol **1209,** 163-177.

Reynolds, G.D., Wang, C., Pan, J., and Bednarek, S.Y. (2018). Inroads into Internalization: Five Years of Endocytic Exploration. Plant Physiol **176,** 208-218.

Robatzek, S., Chinchilla, D., and Boller, T. (2006). Ligand-induced endocytosis of the pattern recognition receptor FLS2 in Arabidopsis. Genes Dev **20,** 537-542.

Robinson, M.S. (2015). Forty Years of Clathrin-coated Vesicles. Traffic **16,** 1210-1238.

Rodal, S.K., Skretting, G., Garred, Ø., Vilhardt, F., Deurs, B.v., and Sandvig, K. (1999). Extraction of Cholesterol with Methyl-β-Cyclodextrin Perturbs Formation of Clathrin-coated Endocytic Vesicles. Molecular Biology of the Cell **10,** 961-974.

Sanchez-Rodriguez, C., Shi, Y., Kesten, C., Zhang, D., Sancho-Andres, G., Ivakov, A., Lampugnani, E.R., Sklodowski, K., Fujimoto, M., Nakano, A., Bacic, A., Wallace, I.S., Ueda, T., Van Damme, D., Zhou, Y., and Persson, S. (2018). The Cellulose Synthases Are Cargo of the TPLATE Adaptor Complex. Mol Plant **11,** 346-349.

Scheele, U., Kalthoff, C., and Ungewickell, E. (2001). Multiple interactions of auxilin 1 with clathrin and the AP-2 adaptor complex. J Biol Chem **276,** 36131-36138.

Schmid, E.M., and McMahon, H.T. (2007). Integrating molecular and network biology to decode endocytosis. Nature **448,** 883-888.

Schmid, S.L., and Frolov, V.A. (2011). Dynamin: functional design of a membrane fission catalyst. Annu Rev Cell Dev Biol **27,** 79-105.

Schwihla, M., and Korbei, B. (2020). The Beginning of the End: Initial Steps in the Degradation of Plasma Membrane Proteins. Front Plant Sci **11,** 680.

Sharma, P., Sabharanjak, S., and Mayor, S. (2002). Endocytosis of lipid rafts: an identity crisis. Semin Cell Dev Biol **13,** 205-214.

Slupianek, A., Kasprowicz-Maluski, A., Myskow, E., Turzanska, M., and Sokolowska, K. (2019). Endocytosis acts as transport pathway in wood. New Phytol **222,** 1846-1861.

Smith, J.M., Leslie, M.E., Robinson, S.J., Korasick, D.A., Zhang, T., Backues, S.K., Cornish, P.V., Koo, A.J., Bednarek, S.Y., and Heese, A. (2014). Loss of Arabidopsis thaliana Dynamin-Related Protein 2B reveals separation of innate immune signaling pathways. PLoS Pathog **10,** e1004578.

Smith, S.M., Larocque, G., Wood, K.M., Morris, K.L., Roseman, A.M., Sessions, R.B., Royle, S.J., and Smith, C.J. (2021). Multi-modal adaptor-clathrin contacts drive coated vesicle assembly. EMBO J **40,** e108795.

Sommer, B., Oprins, A., Rabouille, C., and Munro, S. (2005). The exocyst component Sec5 is present on endocytic vesicles in the oocyte of Drosophila melanogaster. J Cell Biol **169,** 953-963.

Song, K., Jang, M., Kim, S.Y., Lee, G., Lee, G.J., Kim, D.H., Lee, Y., Cho, W., and Hwang, I. (2012). An A/ENTH domain-containing protein functions as an adaptor for clathrin-coated vesicles on the growing cell plate in Arabidopsis root cells. Plant Physiol **159,** 1013-1025.

Stefano, G., Renna, L., Wormsbaecher, C., Gamble, J., Zienkiewicz, K., and Brandizzi, F. (2018). Plant Endocytosis Requires the ER Membrane-Anchored Proteins VAP27-1 and VAP27-3. Cell Rep **23,** 2299-2307.

Stefano, G., Renna, L., Lai, Y., Slabaugh, E., Mannino, N., Buono, R.A., Otegui, M.S., and Brandizzi, F. (2015). ER network homeostasis is critical for plant endosome streaming and endocytosis. Cell Discov **1,** 15033.

Tahara, H., Yokota, E., Igarashi, H., Orii, H., Yao, M., Sonobe, S., Hashimoto, T., Hussey, P.J., and Shimmen, T. (2007). Clathrin is involved in organization of mitotic spindle and phragmoplast as well as in endocytosis in tobacco cell cultures. Protoplasma **230,** 1-11.

Tejos, R., Sauer, M., Vanneste, S., Palacios-Gomez, M., Li, H., Heilmann, M., van Wijk, R., Vermeer, J.E., Heilmann, I., Munnik, T., and Friml, J. (2014). Bipolar Plasma Membrane Distribution of Phosphoinositides and Their Requirement for Auxin-Mediated Cell Polarity and Patterning in Arabidopsis. Plant Cell **26,** 2114-2128.

Ungewickell, E., Ungewickell, H., Holstein, S.E., Lindner, R., Prasad, K., Barouch, W., Martin, B., Greene, L.E., and Eisenberg, E. (1995). Role of auxilin in uncoating clathrin-coated vesicles. Nature **378,** 632-635.

Van Damme, D., Coutuer, S., De Rycke, R., Bouget, F.Y., Inze, D., and Geelen, D. (2006). Somatic cytokinesis and pollen maturation in Arabidopsis depend on TPLATE, which has domains similar to coat proteins. Plant Cell **18,** 3502-3518.

Van Damme, D., Gadeyne, A., Vanstraelen, M., Inze, D., Van Montagu, M.C., De Jaeger, G., Russinova, E., and Geelen, D. (2011). Adaptin-like protein TPLATE and clathrin recruitment during plant somatic cytokinesis occurs via two distinct pathways. Proc Natl Acad Sci U S A **108,** 615-620.

Wang, C., Yan, X., Chen, Q., Jiang, N., Fu, W., Ma, B., Liu, J., Li, C., Bednarek, S.Y., and Pan, J. (2013a). Clathrin light chains regulate clathrin-mediated trafficking, auxin signaling, and development in Arabidopsis. Plant Cell **25,** 499-516.

Wang, C., Hu, T., Yan, X., Meng, T., Wang, Y., Wang, Q., Zhang, X., Gu, Y., Sanchez-Rodriguez, C., Gadeyne, A., Lin, J., Persson, S., Van Damme, D., Li, C., Bednarek, S.Y., and Pan, J. (2016). Differential Regulation of Clathrin and Its Adaptor Proteins during Membrane Recruitment for Endocytosis. Plant Physiol **171,** 215-229.

Wang, F., Cheng, Z., Wang, J., Zhang, F., Zhang, B., Luo, S., Lei, C., Pan, T., Wang, Y., Zhu, Y., Wang, M., Chen, W., Lin, Q., Zhu, S., Zhou, Y., Zhao, Z., Wang, J., Guo, X., Zhang, X., Jiang, L., Bao, Y., Ren, Y., and Wan, J. (2022). Rice STOMATAL CYTOKINESIS DEFECTIVE2 regulates cell expansion by affecting vesicular trafficking in rice. Plant Physiol.

Wang, J., Mylle, E., Johnson, A., Besbrugge, N., De Jaeger, G., Friml, J., Pleskot, R., and Van Damme, D. (2020). High Temporal Resolution Reveals Simultaneous

Plasma Membrane Recruitment of TPLATE Complex Subunits. Plant Physiol **183,** 986-997.

Wang, J., Yperman, K., Grones, P., Jiang, Q., Dragwidge, J., Mylle, E., Mor, E., Nolf, J., Eeckhout, D., De Jaeger, G., De Rybel, B., Pleskot, R., and Van Damme, D. (2021). Conditional destabilization of the TPLATE complex impairs endocytic internalization. Proc Natl Acad Sci U S A **118**.

Wang, L., Cheng, M., Yang, Q., Li, J., Wang, X., Zhou, Q., Nagawa, S., Xia, B., Xu, T., Huang, R., He, J., Li, C., Fu, Y., Liu, Y., Bao, J., Wei, H., Li, H., Tan, L., Gu, Z., Xia, A., Huang, X., Yang, Z., and Deng, X.W. (2019a). Arabinogalactan protein-rare earth element complexes activate plant endocytosis. Proc Natl Acad Sci U S A **116,** 14349-14357.

Wang, P., and Hussey, P.J. (2019). Plant ER-PM Contact Sites in Endocytosis and Autophagy: Does the Local Composition of Membrane Phospholipid Play a Role? Front Plant Sci **10,** 23.

Wang, P., Hawes, C., and Hussey, P.J. (2017a). Plant Endoplasmic Reticulum-Plasma Membrane Contact Sites. Trends Plant Sci **22,** 289-297.

Wang, P., Pleskot, R., Zang, J., Winkler, J., Wang, J., Yperman, K., Zhang, T., Wang, K., Gong, J., Guan, Y., Richardson, C., Duckney, P., Vandorpe, M., Mylle, E., Fiserova, J., Van Damme, D., and Hussey, P.J. (2019b). Plant AtEH/Pan1 proteins drive autophagosome formation at ER-PM contact sites with actin and endocytic machinery. Nat Commun **10,** 5132.

Wang, Q., Zhao, Y., Luo, W., Li, R., He, Q., Fang, X., Michele, R.D., Ast, C., von Wiren, N., and Lin, J. (2013b). Single-particle analysis reveals shutoff control of the Arabidopsis ammonium transporter AMT1;3 by clustering and internalization. Proc Natl Acad Sci U S A **110,** 13204-13209.

Wang, S., Yoshinari, A., Shimada, T., Hara-Nishimura, I., Mitani-Ueno, N., Feng Ma, J., Naito, S., and Takano, J. (2017b). Polar Localization of the NIP5;1 Boric Acid Channel Is Maintained by Endocytosis and Facilitates Boron Transport in Arabidopsis Roots. Plant Cell **29,** 824-842.

Waszczak, C., Carmody, M., and Kangasjarvi, J. (2018). Reactive Oxygen Species in Plant Signaling. Annu Rev Plant Biol **69,** 209-236.

Winkler, J., De Meyer, A., Mylle, E., Storme, V., Grones, P., and Van Damme, D. (2021). Nanobody-Dependent Delocalization of Endocytic Machinery in Arabidopsis Root Cells Dampens Their Internalization Capacity. Front Plant Sci **12,** 538580.

Yamaoka, S., Shimono, Y., Shirakawa, M., Fukao, Y., Kawase, T., Hatsugai, N., Tamura, K., Shimada, T., and Hara-Nishimura, I. (2013). Identification and dynamics of Arabidopsis adaptor protein-2 complex and its involvement in floral organ development. Plant Cell **25,** 2958-2969.

Yan, X., Wang, Y., Xu, M., Dahhan, D.A., Liu, C., Zhang, Y., Lin, J., Bednarek, S.Y., and Pan, J. (2021). Cross-talk between clathrin-dependent post-Golgi trafficking and clathrin-mediated endocytosis in Arabidopsis root cells. Plant Cell **33,** 3057-3075.

Yoshinari, A., Fujimoto, M., Ueda, T., Inada, N., Naito, S., and Takano, J. (2016). DRP1-Dependent Endocytosis is Essential for Polar Localization and Boron-

Induced Degradation of the Borate Transporter BOR1 in Arabidopsis thaliana. Plant Cell Physiol **57,** 1985-2000.

Yoshinari, A., Hosokawa, T., Amano, T., Beier, M.P., Kunieda, T., Shimada, T., Hara-Nishimura, I., Naito, S., and Takano, J. (2019). Polar Localization of the Borate Exporter BOR1 Requires AP2-Dependent Endocytosis. Plant Physiol **179,** 1569-1580.

Yperman, K., Wang, J., Eeckhout, D., Winkler, J., Vu, L.D., Vandorpe, M., Grones, P., Mylle, E., Kraus, M., Merceron, R., Nolf, J., Mor, E., De Bruyn, P., Loris, R., Potocky, M., Savvides, S.N., De Rybel, B., De Jaeger, G., Van Damme, D., and Pleskot, R. (2021a). Molecular architecture of the endocytic TPLATE complex. Sci Adv **7**.

Yperman, K., Papageorgiou, A.C., Merceron, R., De Munck, S., Bloch, Y., Eeckhout, D., Jiang, Q., Tack, P., Grigoryan, R., Evangelidis, T., Van Leene, J., Vincze, L., Vandenabeele, P., Vanhaecke, F., Potocky, M., De Jaeger, G., Savvides, S.N., Tripsianes, K., Pleskot, R., and Van Damme, D. (2021b). Distinct EH domains of the endocytic TPLATE complex confer lipid and protein binding. Nat Commun **12,** 3050.

Yu, M., Li, R., Cui, Y., Chen, W., Li, B., Zhang, X., Bu, Y., Cao, Y., Xing, J., Jewaria, P.K., Li, X., Bhalerao, R.P., Yu, F., and Lin, J. (2020). The RALF1-FERONIA interaction modulates endocytosis to mediate control of root growth in Arabidopsis. Development **147**.

Zaman, M.F., Nenadic, A., Radojicic, A., Rosado, A., and Beh, C.T. (2020). Sticking With It: ER-PM Membrane Contact Sites as a Coordinating Nexus for Regulating Lipids and Proteins at the Cell Cortex. Front Cell Dev Biol **8,** 675.

Zhang, Y., Persson, S., Hirst, J., Robinson, M.S., van Damme, D., and Sanchez-Rodriguez, C. (2015). Change your TPLATE, change your fate: plant CME and beyond. Trends Plant Sci **20,** 41-48.

Zhao, Y., Yan, A., Feijo, J.A., Furutani, M., Takenawa, T., Hwang, I., Fu, Y., and Yang, Z. (2010). Phosphoinositides regulate clathrin-dependent endocytosis at the tip of pollen tubes in Arabidopsis and tobacco. Plant Cell **22,** 4031-4044.

Zouhar, J., and Sauer, M. (2014). Helping hands for budding prospects: ENTH/ANTH/VHS accessory proteins in endocytosis, vacuolar transport, and secretion. Plant Cell **26,** 4232-4244.

Chapter 2: Proteomic characterization of isolated Arabidopsis clathrin-coated vesicles reveals evolutionarily conserved and plant-specific components

This chapter is adapted from published work:

Dahhan DA, Reynolds GD, Cárdenas JJ, Eeckhout D, Johnson A, Yperman K, Kaufmann WA, Vang N, Yan X, Hwang I, Heese A, De Jaeger G, Friml J, Van Damme D, Pan J, Bednarek SY (2022) *Plant Cell* 34: 2150-2173

DAD and GDR contributed equally to this work. DAD performed experiments and analyzed data relating to Figures 2.1 B and 2.1 C, 2.2 A – 2.2 C, 2.3, 2.4, and 2.5; Table 2.1; Supplemental Datasets 2S1, 2S2, 2S4, and 2S5; Supplemental Figures 2S1 and 2S2; Supplemental Table 2S1. GDR performed experiments and analyzed data relating to Figures 2.1 A, 2.2 A, 2.3, 2.4 A and 2.4 B, 2.5, and 2.6; Table 2.1; Supplemental Datasets 2S1, 2S3, 2S4, and 2S5; Supplemental Figures 2S2, 2S3, and 2S4; and Supplemental Table 2S1. AJ contributed 2.1B, 2.1C, and 2S1. DAD and GDR co-wrote the manuscript.

Abstract

In eukaryotes, clathrin-coated vesicles (CCVs) facilitate the internalization of material from the cell surface as well as the movement of cargo in post-Golgi trafficking pathways. This diversity of functions is partially provided by multiple monomeric and multimeric clathrin adaptor complexes that provide compartment and cargo selectivity. The adaptor-protein AP-1 complex operates as part of the secretory pathway at the *trans*-Golgi network, while the AP-2 complex and the TPLATE complex (TPC) jointly operate at the plasma membrane to execute clathrin-mediated endocytosis. Key to our further understanding of clathrin-mediated trafficking in plants will be the comprehensive identification and characterization of the network of evolutionarily conserved and plant-specific core and accessory machinery involved in the formation and targeting of CCVs. To facilitate these studies, we have analyzed the proteome of enriched *trans*-Golgi network/early endosome-derived and endocytic CCVs isolated from dividing and expanding suspension-cultured Arabidopsis cells. Tandem mass spectrometry analysis results were validated by differential chemical labeling experiments to identify proteins co-enriching with CCVs. Proteins enriched in CCVs included previously characterized CCV components and cargos such as the vacuolar sorting receptors in addition to conserved and plant-specific components whose function in clathrin-mediated trafficking has not been previously defined. Notably, in addition to AP-1 and AP-2, all subunits of the AP-4 complex, but not AP-3 or AP-5, were found to be in high abundance in the CCV proteome. The association of AP-4 with suspension-cultured Arabidopsis CCVs is further supported via additional biochemical data.

Introduction

Vesicle trafficking is critical for the exchange of materials between the various biochemically and functionally distinct compartments of the biosynthetic/secretory and endocytic pathways. In particular, the trafficking of vacuolar proteins and the polar localization of plasma membrane proteins is critical for nutrient uptake, pathogen response, and organismal homeostasis.

Fundamental to the process of vesicle trafficking is the assembly of cytosolic coat protein complexes, which cluster cargo and generate the membrane curvature necessary for a budding vesicle (Bonifacino and Glick, 2004; Robinson, 2015). The distinctive geometric lattice that surrounds clathrin-coated vesicles (CCVs) is composed of clathrin triskelia, which in turn are composed of clathrin heavy chain (CHC) and clathrin light chain (CLC) subunits.

Since their initial discovery in metazoans and plants (Gray, 1961; Roth and Porter, 1964; Bonnett and Newcomb, 1966), CCVs have been demonstrated to function in endocytosis (Robinson, 2015; Reynolds et al., 2018) and post-Golgi trafficking (Orci et al., 1985; Hirst et al., 2012). The highly choreographed multi-step process of clathrin-mediated endocytosis (CME) requires clathrin and a large number of endocytic accessory proteins (EAPs) that function at specific sites on the plasma membrane (PM) (i.e., clathrin-coated pits) to mediate cargo recruitment, membrane invagination, scission/severing of the nascent clathrin-coated vesicle from the PM and their uncoating prior to fusion with endosomes (Taylor et al., 2011; Kaksonen and Roux, 2018; Wu and Wu, 2021). Our current understanding of the complex network of proteins and lipids required for post-Golgi trafficking and endocytosis in plants largely comes from yeast and

mammalian systems and the use of various biochemical, proteomic, genetic, and advanced quantitative live-cell imaging approaches. By comparison, mechanistic insight into clathrin-dependent membrane trafficking in plants remains limited.

CCVs facilitate multiple intracellular trafficking pathways via the action of adaptor protein complexes that are tasked with pathway-specific cargo recognition and clathrin recruitment at the PM and endomembrane compartments. The first clathrin adaptors to be identified were the assembly polypeptide (AP)-2 and AP-1 heterotetrameric complexes (Pearse and Robinson, 1984; Keen, 1987) that interact with protein cargo and specific phospholipids residing at the plasma membrane and the trans-Golgi Network (TGN), respectively (Robinson, 2015). These functions are largely conserved in plants, including the central role of AP-2 in endocytosis (Bashline et al., 2013; Di Rubbo et al., 2013; Fan et al., 2013; Kim et al., 2013) and of AP-1 in trafficking at TGN / early endosomes (TGN/EE) (Song et al., 2006; Park et al., 2013; Teh et al., 2013). The latter's function is somewhat more complex as the plant TGN/EE appears to comprise numerous distinct sub-compartments with varying morphologies and functions in contrast to its metazoan counterpart (Dettmer et al., 2006; Viotti et al., 2010; Kang et al., 2011; Rosquete et al., 2018; Heinze et al., 2020; Shimizu et al., 2021). Moreover, an increasing number of studies have demonstrated that these core CCV trafficking proteins have evolved to accommodate processes critical for plant growth and development against the differing biophysical properties of plant cells, including cell wall formation, cytokinesis, and pathogen response (McMichael and Bednarek, 2013; Zhang et al., 2015; Gu et al., 2017; Ekanayake et al., 2019).

In addition to AP-2 and AP-1, three additional AP complexes, AP-3 (Dell'Angelica et al., 1997; Simpson et al., 1997; Zwiewka et al., 2011), AP-4 (Dell'Angelica et al., 1999; Hirst et al., 1999), and AP-5 (Hirst et al., 2013), mediate post-Golgi endomembrane trafficking in multicellular eukaryotes. However, relative to AP-1 and AP-2, their interaction with the clathrin machinery in mammalian and other systems is less defined. Proteomic analyses of mammalian CCVs suggest that of the five evolutionarily conserved adaptor complexes, only AP-1 and AP-2 were found to be associated with the clathrin coat (Blondeau et al., 2004; Borner et al., 2012). Recent super-resolution microscopy of plant cells showed a lack of colocalization between AP4 and clathrin (Shimizu et al., 2021). Lastly, the association of AP-5 with clathrin in metazoans and plants remains undetermined (Sanger et al., 2019).

Plants have shown evolutionary divergence in their key EAPs compared to other model systems including, for example, the TPLATE complex (TPC), which likely evolved in early eukaryotes but is notably absent from yeast and metazoans and which is essential for plant clathrin-mediated endocytosis (Gadeyne et al., 2014; Hirst et al., 2014; Bashline et al., 2015; Wang et al., 2021). Similar to AP-2, TPC functions exclusively at the PM and acts as a central interaction hub required for the formation of endocytic CCVs (Gadeyne et al., 2014; Zhang et al., 2015; Wang et al., 2016; Yperman et al., 2021). Additional conserved accessory proteins have been demonstrated to be required for CCV maturation including monomeric cargo adaptor families such as the ENTH/ANTH/VHS domain containing proteins, which aid in cargo recognition and membrane deformation (Zouhar and Sauer, 2014; Fujimoto, 2020). In addition, CCV formation requires members of the Arabidopsis dynamin related protein families DRP1s and DRP2s, which are

necessary for scission of the budding vesicle from the plasma membrane (Bednarek and Backues, 2010). DRP1 and DRP2 protein assembly into clathrin-coated pits (CCPs) is critical for efficient CME and cell plate biogenesis but the precise mechanistic details of their function(s) in these processes are not fully established (Konopka et al., 2008; Backues et al., 2010; Fujimoto et al., 2010; Mravec et al., 2011; Narasimhan et al., 2020; Ekanayake et al., 2021). Various plant uncoating factors have been identified, and the mechanistic details are under investigation (Robinson, 2015; Adamowski et al., 2018). Trafficking factors including Rab and ARF-related small GTPases (Jürgens et al., 2015; Lipatova et al., 2015; Takemoto et al., 2018), vesicle tethering complexes (Jürgens et al., 2015; Takemoto et al., 2018), and soluble N-ethylmaleimide-sensitive factor adaptor protein receptors (SNARE) proteins (Yun and Kwon, 2017) add complexity to the regulation of clathrin-mediated trafficking pathways.

Defining the protein complement of post-Golgi and endocytic CCVs will further enhance our understanding of the evolutionarily conserved and plant-specific core and accessory machinery involved in the formation and targeting of plant clathrin-coated vesicles. Organelle proteomics is a useful tool for such studies as it can provide a global view of the protein content of a particular organelle, thereby placing known and un-annotated gene products in a functional context. Several studies have employed mass spectrometry (MS) to answer questions of mammalian CCV content including analyses of rat brain CCVs to examine their role in synaptic vesicle recycling (Blondeau et al., 2004; Takamori et al., 2006) and of those isolated from HeLa cells (Borner et al., 2006; Borner et al., 2012). In addition to the identification of previously unknown CCV components, the relative abundance of proteins across CCVs isolated from rat brain and liver has been

examined to interrogate pathway-specific proteins such as AP-1 and AP-2 subunits (functioning in secretion and endocytosis, respectively) and the proportion of CCVs involved in post-Golgi and endocytic trafficking in different cell types (Girard et al., 2005). In plants, subcellular fractionation coupled with tandem MS has also been utilized to elucidate the protein content of endomembrane compartments including Arabidopsis Golgi cisternae (Parsons et al., 2012; Okekeogbu et al., 2019; Parsons et al., 2019), vacuoles (Carter et al., 2004), syntaxin of plants 61 (SYP61)-positive TGN compartments (Drakakaki et al., 2012), and multiple compartments of the Arabidopsis endomembrane system (Heard et al., 2015). Here, we report the proteomic assessment of CCVs isolated from undifferentiated Arabidopsis suspension cultured cells using tandem mass spectrometry and quantitative immunoblotting to elucidate the ensemble of proteins underlying clathrin-mediated trafficking in plants and to better understand the similarities and differences among trafficking protein pathways within eukaryotes.

Results and Discussion

CCV Isolation

In plants, CCVs mediate trafficking of secretory and endocytic cargo necessary for cell expansion, cytokinesis, nutrient uptake, and pathogen immunity pathways underlying growth, morphogenesis, and defense in a variety of developmentally distinct cell types (Reynolds et al., 2018; Ekanayake et al., 2019). Undifferentiated suspension-cultured plant cells offer, however, several benefits as a biological sample source for proteomic analysis of plant CCVs as they: 1) display high levels of division and expansion, processes that require a large flux of vesicular trafficking; 2) are easily scaled to provide

large amounts of material; and 3) when grown under constant conditions, provide a population of cells uniform in cell type and development between biological replicates. With these features in mind, the CCVs used for proteomic analysis in this study were isolated from 3- to 4 day-old T87 suspension-cultured Arabidopsis cells (Axelos et al., 1992). In addition, the availability of the Arabidopsis genome sequence and *in silico* proteome (Arabidopsis Genome, 2000; Berardini et al., 2015) as well as the T87 transcriptome datasets (Stolc et al., 2005) facilitate the assessment of the enrichment or depletion of proteins of interest in the CCV proteome.

For proteomic analyses, plant CCVs were isolated under pH conditions that inhibit clathrin cage disassembly using a fractionation scheme that includes differential, rate-zonal centrifugation, and a final equilibrium deuterium/Ficoll gradient as described previously (Reynolds et al., 2014). Prior to mass spectrometry analysis, the composition and quality of CCV preparations were assessed by morphological analysis using transmission electron microscopy (TEM) and immunoblotting for protein markers of the secretory and endocytic pathways. TEM analysis (Figure 2.1A) of the enriched clathrin-coated vesicle samples revealed that 80% ± 7.6% of the vesicles from four independent CCV preparations used for mass spectrometry analysis displayed the characteristic geometry of clathrin coats with an average diameter of 75 nm ± 5.3 nm. Transmission electron micrographs of enriched CCVs at higher resolution show striking symmetry of the coat (Figures 2.1B and 2.1C, Supplemental Figure 2S1).

CCV MS/MS Sample Preparation & Analysis

To establish a comprehensive understanding of the protein composition of plant CCVs, two independent, parallel proteomic workflows were performed on enriched CCV protein samples (Supplemental Figure 2S2). In the first methodology, CCVs isolated from four independent preparations were resolved via one-dimensional SDS-PAGE before in-gel digestion of proteins by trypsin and subjection to LC/MS-MS. To account for differences in protein sampling related to 1D SDS-PAGE sample fractionation and the use of detergents, we used a second methodology in which three independent CCV preparations were denatured in a urea buffer prior to trypsin digestion in-solution and separation of recovered peptides by LC/MS-MS.

Coomassie staining of a representative enriched CCV fraction separated by 1D SDS-PAGE is shown in Figure 2.2A. Gel slices 2, 6, and 8 contain bands of high protein abundance (intense Coomassie staining), which migrate at rates corresponding to the molecular weights of the clathrin coat proteins. To confirm the identity of the specific heavy or light chain clathrin isoforms in each polyacrylamide gel slice, we plotted the unique spectral counts as a percentage of unique spectral counts for that isoform across the entire SDS-PAGE gel and showed that the protein abundances in gel slices 2, 6, and 8 in Figure 2.2A corresponded to the presence of clathrin subunits (Figure 2.2B). Arabidopsis encodes two CHC isoforms, CHC1 and CHC2, of approximately the same mass (193kD) which share >90% sequence identity (Kitakura et al., 2011) and are transcribed at comparable levels in T87 suspension cultured cells (Stolc et al., 2005). In contrast to CHC, the three Arabidopsis CLC isoforms share only ~55% sequence identity (Wang et al., 2013) and vary in predicted mass (37.2, 28.8, and 29.1 kD, CLC1-3, respectively). The spectral count and SDS-PAGE data confirmed that clathrin heavy chain

contributes to the high protein abundance of gel slice 2 (predicted molecular weight of CHC1 and CHC2, 193 kDa), and that clathrin light chain contribute to the protein abundance of gel slices 6 and 8 (predicted molecular weight of CLC1, 37 kDa; of CLC2 and CLC3, 29 kDa). The identities of the other CCV-associated proteins in Figure 2.2A with abundances below the limits of detection by Coomassie staining were determined by proteomic and immunoblot analyses addressed below.

To define the CCV proteome, protein or protein group assignments were considered true if at least two unique peptides denoting the protein or protein group were found in at least two biological replicates based on a 1% false discovery rate protein and peptide threshold (Supplemental Figures 2S2B and 2S2C). Processed spectra from the first methodology were matched against the Arabidopsis protein sequence database using the Mascot searching algorithm (Perkins et al., 1999), while in the second methodology, MS/MS spectra were analyzed with the MaxQuant software package.

Following these criteria, protein assignments from the four independent CCV preparations analyzed by the first methodology (in which CCVs were separated by 1D SDS-PAGE) comprised a list of 3,745 proteins (Supplemental Dataset S1), the vast majority of which (~70%) were in relatively low abundance (< 50 spectral counts across four replicates). Total spectral counts have previously been used as an approximation of overall protein abundance in biological samples for those proteins with a reasonably high (>10–20) total number of counts (Lundgren et al., 2010). Accordingly, we compared total counts over four independent CCV preparations without normalization as an approximation of overall protein abundance within CCVs and focused our analysis on those proteins with the highest associated spectral count totals. The proteomic data from

CCVs fractionated by 1D SDS-PAGE and analyzed by tandem MS is presented in Supplemental Datasets S1, S4, and S5. Protein assignments obtained from the second CCV methodology resulted in a list of 1,981 protein groups (Supplemental Dataset S2). Intensity based absolute quantitation (iBAQ) values were used to sort protein groups within this dataset, as this method of label-free quantification has been previously judged to be a metric for protein abundances within biological samples and enables comparison of these abundances (Nagaraj et al., 2011; Schwanhäusser et al., 2011; Arike et al., 2012). The data from this second methodology are presented in Supplemental Datasets S2 and S4.

Previous proteomic studies of CCVs purified from mammalian tissue have found that clathrin light and heavy chains predominantly exist in a stoichiometric 1:1 ratio. However, clathrin subunits were also found in non-stoichiometric ratios depending on the tissue and species source of the CCV sample (Blondeau et al., 2004; Girard et al., 2005; Borner et al., 2012). We used iBAQ levels to analyze the abundances of clathrin heavy and light chain subunits and determine the ratio of subunits within the triskelion independently of immunoblotting based methods. We summed the iBAQ values for CHC and CLC subunits from each of three independent CCV preparations and calculated the ratio between these values as the measure of CLC:CHC per replicate of 1.24, 2.05, and 1.07 (Figure 2.2C; Supplemental Dataset S2). These values generally support a 1:1 ratio but suggest that, in some CCV preparations from plant cells, clathrin light chain subunits are in excess.

The numbers of proteins comprising each proteomic dataset and shared between both sample preparations described above are illustrated in Figure 2.3. Cross-referencing

the datasets derived from these independent, parallel workflows established an overlapping CCV proteome comprising 1,683 proteins (Figure 2.3).

Assessment of Protein Enrichment and Depletion in CCV Fraction

To further refine the CCV proteome, we quantitatively compared the abundance of peptides in pre- and post- deuterium/Ficoll gradient samples, termed Deuterium Ficoll Gradient Load (DFGL) and CCV samples, respectively. To do so, we assessed the relative enrichment or depletion of proteins identified by mass spectrometry in an unbiased manner through a differential labeling strategy with stable isotope dimethyl moieties (Boersema et al., 2009). This methodology involves the reaction of peptide primary amines with either formaldehyde or deuterated formaldehyde to form methylated peptides, which results in identical peptides treated in this way differing by 4 Daltons. Accordingly, a quantitative ratio of an individual peptide's abundance in the DFGL relative to the final enriched CCV preparation, as represented by spectral counts, can be derived.

DFGL and CCV fractions from two independent CCV preparations were separated by 1D SDS-PAGE prior to gel sectioning and in-gel digestion with trypsin. Peptides from both fractions were recovered and treated with dimethyl reagents as previously described (Boersema et al., 2009). In the second replicate, heavy (deuterated) and light labels applied to CCV and DFGL samples were swapped to control for potential discrepancies resulting in the identification of proteins that were enriched in (CCV:DFGL spectral count ratio ≥ 2.0) or depleted from (DFGL:CCV spectral count ratio ≥ 2.0) the purified clathrin-coated vesicles (Figure 2.3, Supplemental Dataset S3). Cross-referencing these datasets yielded a core set of 781 proteins in the enriched CCV purification sample as detected by

all three proteomic workflows, 213 (27%) of which had a CCV:DFGL spectral count ratio ≥ 2.0, i.e. were enriched more than two-fold in the final preparatory step resulting in purified clathrin-coated vesicles (Figure 2.3, Supplemental Dataset S3).

In previous studies, immunoblotting has been used to validate differential centrifugation as a means to purify clathrin-coated vesicles from plant cells by confirming the depletion of markers of the endoplasmic reticulum (ER) and Golgi, as well as of other organelles including plastids, peroxisomes, and mitochondria, in addition to confirming the enrichment of CCV associated proteins (McMichael et al., 2013; Reynolds et al., 2014). However, the fold enrichment or depletion of these proteins relative to their initial abundance in the lysate (S0.1) fraction has not been quantified. Here, we performed quantitative immunoblotting of equal amounts of protein from steps throughout the CCV purification process, including the DFGL and CCV fractions, to establish the fold enrichment and depletion of CCV mediated trafficking-associated and unassociated proteins, respectively, relative to the lysate (Figure 2.4). We then used the average fold enrichments between the DFGL and CCV fractions from quantitative immunoblotting of three independent CCV preparations (apart from immunoblotting for DRP2, where n = 2) to corroborate the values obtained by the dimethyl labeling proteomic workflow (Table 2.1).

The expected enrichment of CCV associated proteins, such as clathrin coat proteins CHC and CLC2 and subunits of AP-1 and AP-2 complexes, as well as the cell plate, TGN, and putative CCV cargo marker, KNOLLE (Dhonukshe et al., 2006; Reichardt et al., 2007; Boutte et al., 2010), is shown in Figure 2.4A. To demonstrate the removal of non-CCV trafficking associated proteins from the purified CCVs, the depletion of cFBPase

and SEC12 proteins, markers for the cytosol and ER, respectively, between the S0.1 fraction and final CCV sample, is shown in Figure 2.4B. We also quantitated the intensity of the proteins in Figures 2.4A and 2.4B at the DFGL and CCV steps of the CCV purification scheme and compared these values to those obtained in the dimethyl labeling experiment (Table 2.1). The average fold enrichment values between the CCV and DFGL samples for the proteins in Figures 2.4A and 2.4B as determined by immunoblotting or dimethyl labeling are compared in Table 2.1, which shows that the general trends of enrichment of CCV associated proteins and depletion of markers of subcellular compartments not associated with CCV-mediated trafficking away from the final CCV sample are consistent across both methods. These quantitative immunoblotting data support the use of the dimethyl labeling proteomic dataset (Supplemental Dataset S3) as a tool for researchers investigating proteins of interest and the strength of potential connections to CCV mediated trafficking processes.

To assess the contributions of subcellular organelles to the complement of the 546 proteins detected by the first methodology that were depleted at least 2-fold during the final CCV purification step, their predicted subcellular localizations were determined using the SUBAcon (SUBcellular Arabidopsis consensus) bioinformatics tool, an algorithm that integrates experimental fluorescent and proteomic data, as well as computational prediction algorithms to identify a likely protein location (Hooper et al., 2014) (Supplemental Dataset S5). The average fold depletion of each of the 546 proteins sorted by subcellular localization as identified by SUBAcon is shown in Figure 2.5A, and the contribution of each organelle to the abundance of spectral counts represented in the 546 protein depletion-dataset is depicted in Figure 2.5B. Approximately 49% of depleted

spectra were attributed to proteins associated with the cytoplasm and other organelles likely not directly participating in clathrin-mediated trafficking, such as the ER (Figure 2.5B). Demonstrating the effectiveness of the deuterium/Ficoll gradient, approximately 24% and 4% of all spectra corresponding to peptides more abundant in the DFGL relative to the final post centrifugation CCV fraction (i.e. peptides indicating the 546 depleted proteins) were attributed to components of the ribosome and 26S proteasome, respectively.

Manual annotation of the 257 proteins that were enriched at least 2-fold in the final CCV fraction relative to the deuterium/Ficoll gradient load is depicted in Figure 2.5C. The fold enrichment and total spectral count are plotted for the enriched proteins sorted by manually assigned category relating to their roles in CCV trafficking. The fold enrichment and abundance of specific categories of CCV associated proteins will be discussed further below.

VALIDATION OF CCV-ASSOCIATED PROTEINS

Clathrin

Morphological and SDS-PAGE analyses demonstrated that clathrin heavy chain (CHC) and light chain (CLC) subunits were highly enriched in the CCV preparations (Figures 2.1A and 2.2A). Consistent with this, 41% of all spectra assigned to peptides corresponding to the 257 proteins that were enriched in the CCV fraction corresponded to the core clathrin coat components, namely CHC and CLC (Figure 2.5C). CHC1 and CHC2 were enriched 6- and 5-fold, respectively, in CCVs compared to the DFGL (Table 2.1, Supplemental Dataset S4), which is comparable to their 3-fold DFGL to CCV

enrichment observed via quantitative immunoblotting (Figures 2.4A and 4C). CLC1-3 were 8-, 18-, and 9-fold enriched in CCVs relative to the DFGL in dimethyl labeling experiments (Supplemental Dataset S4), while quantitative immunoblotting with αCLC2 antibody supported an enrichment for the CLC2 isoform in the final CCV fraction (Table 2.1, Figures 2.4A and 4C).

The AP-1, AP-2, and TPC Hetero-oligomeric Adaptor Protein Complexes

Subunits of the previously characterized multimeric adaptor protein complexes AP-2, TPC, and AP-1 underlying endocytic and post-Golgi clathrin-dependent trafficking, respectively, were also identified in the suspension-cultured cell CCV proteome. All subunits, including large (A, B, G), medium (M), and small (S) proteins, of the canonical, conserved heterotetrameric adaptin AP-1 and AP-2 complexes were detected in our datasets in high abundance, accounting for 16% of all spectra assigned to peptides enriched in CCVs in dimethyl labeling experiments (Supplemental Dataset S4). AP1G and AP2A were 6- and 3-fold more abundant in CCVs relative to the DFGL as observed by dimethyl labeling (Table 2.1 and Supplemental Dataset S4). Consistent with this, AP1G was found to be enriched 2-fold, and AP2A was found to be present in the final CCV fraction as determined by quantitative immunoblotting (Table 2.1, Figures 2.4A and 2.4C), indicating that the enriched CCV preparations are a mixed population of post-Golgi and PM-derived CCVs. While both AP1G1 and AP1G2 homologs were detected in the dimethyl labeling replicates at an enrichment of about 5-fold, only one of two AP2A homologs, AP2A2, was detected in the labeling studies at an enrichment of 2.6-fold, suggesting that AP2A1 is less abundant in the suspension cultured cell CCV fraction. The

medium and small subunits of the AP-1 and AP-2 complexes were enriched 3-fold or greater as were the AP-1/2 B1 and B2 large subunits (6- and 4- fold enrichment; Supplemental Dataset 4), which, similar to the case in Dictyostelium (Sosa et al., 2012) have been postulated to be interchangeably associated with AP-1 and AP-2 complexes in plants (Bassham et al., 2008). Efforts in recent years have established that the role of AP-1 in the trafficking of vacuolar cargo and clathrin recruitment in plant cells resembles that observed in yeast and mammalian systems. AP1M isoform mutants (*ap1m1* and *ap1m2*) both show defects in trafficking of the soluble vacuolar protease precursor proaleurain (Song et al., 2006; Park et al., 2013). In addition, the AP-1 complex is critical for proper targeting of membrane-bound cargo to the tonoplast, at least partially via cytoplasmic sorting signals such as the N-terminal dileucine motif found in VACUOLAR ION TRANSPORTER1 (VIT1), which is mislocalized to the PM in *ap1g* mutants (Wang et al., 2014). TGN/EE integrity is however compromised in *ap1* mutants, which manifests not only in defects in vacuolar protein transport but also in exocytic trafficking to the plasma membrane and cell plate, as well as clathrin-mediated endocytosis (Park et al., 2013; Yan et al., 2021).

Recent characterization of the plant-specific TPC has revealed that the complex functions in endocytosis in concert with clathrin and AP-2 (Gadeyne et al., 2014; Bashline et al., 2015; Zhang et al., 2015; Wang et al., 2016). The two adapter complexes likely have overlapping as well as distinct functions (Gadeyne et al., 2014; Narasimhan et al., 2020; Johnson et al., 2021). Consistent with the former, both AP-2 and TPC bind clathrin and have been shown to interact with a common endocytic cargo protein, CESA6 (Bashline et al., 2013; Sánchez-Rodríguez et al., 2018), one of three CESAs identified in

the CCV proteome (Supplemental Dataset S4). However, compared to *ap2* mutants, loss-of-function TPC subunit mutants display more severe biological phenotypic defects including pollen lethality (Van Damme et al., 2006; Gadeyne et al., 2014). Thus, given the essential nature of TPC in plant CME and the absence of homologs of most TPC subunits in yeast and metazoans, TPC is critical for functions unique to plants (Zhang et al., 2015). In our studies, mass spectrometry analysis identified all eight core TPC subunits in the proteome derived from 1D SDS-PAGE separated CCVs (Supplemental Dataset S4). However, unlike the subunits of the heterotetrameric AP-1 and AP-2 complexes, which are all enriched in the CCV relative to DFGL fraction, the enrichment of the core TPC subunits was generally lower. Although the enrichment values of TPC subunits, TML and TASH3, were somewhat higher than those of the other subunits of TPC (e.g. TPLATE), no TPC subunit was strongly enriched in the last CCV purification step as detected by immunoblotting or dimethyl labeling (Table 2.1 and Supplemental Dataset S4). Consistent with recent data from Johnson et al. showing that TPC is structurally more external to endocytic CCVs than AP-2, localizing around clathrin and AP2, and that TPC is loosely associated with purified CCV (Johnson et al., 2021), the EH domain-containing proteins EH1 and EH2 were present in the CCV proteome and similarly neither enriched alongside the vesicles as measured by the dimethyl labeling experiments (Supplemental Dataset S4). However, two ENTH-domain-containing TPC accessory components (AtECA4 and CAP1) were found in comparatively high abundance in CCVs (Supplemental Dataset S4). Given that ENTH proteins directly interact with membranes (Zouhar and Sauer, 2014), AtECA4 and CAP1 may be retained on CCVs to a larger extent than the core TPC. These data may explain why TPC components do not enrich to the degree of AP-2 subunits

between the DFGL and CCV steps as measured by dimethyl labeling or immunoblotting, in that TPC subunits may have dissociated from the purified CCV. The abundance of TPC core and accessory proteins identified did not differ based on CCV sample preparation, including a similar enrichment of AtECA4 and CAP1 in CCVs relative to TPC core subunits (Supplemental Dataset S4).

The AP-4 adapter complex, but not AP-3 and AP-5, is associated with CCVs

In addition to the known clathrin associated heterooligomeric adapter complexes, AP-1, AP-2 and TPC, the detection of all subunits of the less-studied AP-4 complex (AP4E, B, M, S) and the abundance thereof at levels comparable to that of AP-1 and AP-2 are notable in the CCV proteome (Supplemental Dataset S4). The enrichment of the AP4E large subunit in CCV preparations was similar to that of AP2A and AP1G subunits (4.6-, 2.6-, and 5.6-fold CCV:DFGL ratios, respectively) as was the medium AP4M subunit relative to those corresponding to AP-2 and AP-1 (3.2-, 2.9-, and 5.9-fold, respectively) as determined by differential labeling experiments (Supplemental Dataset S4). In mammals, AP4M was not detected by immunoblotting in purified CCVs and the AP-4 complex was revealed to associate with non-clathrin-coated vesicles near the TGN via immunogold electron microscopy (Hirst et al., 1999), suggesting AP-4 is not associated with clathrin in these organisms.

In plants, the four AP-4 subunits function together in a complex critical in trafficking to the protein storage vacuole (PSV). Similar to vacuolar sorting receptor (VSR) mutants *vsr1*, *vsr3*, and *vsr4* (Zouhar et al., 2010), GREEN FLUORESCENT SEED (GFS) loss-of-function AP-4 mutants *gfs4, gfs5, gfs6, ap4e-1* corresponding to AP4B, AP4M, AP4S,

and AP4E, respectively, mislocalize the PSV-targeted 12S globulin seed storage protein to the extracellular space (Fuji et al., 2016). Binding studies have demonstrated that the Arabidopsis AP4M subunit interacts with the cytoplasmic tail of VSR2 (Gershlick et al., 2014). Recently, evidence for interaction between AP4 subunits with DRPs and clathrin was shown via several independent approaches, including coimmunoprecipitations and yeast two-hybrid experiments (Fuji et al., 2016; Shimizu et al., 2021).

To further investigate the association of AP-4 subunits with plant CCVs, we generated a recombinant antibody against the C-terminal 22 amino acids of the AP4-E large subunit. The specificity of this antibody was confirmed by immunoblotting of total protein extracts prepared from wild-type, *ap4e*, and complemented *ap4e* plants, which showed the presence, absence, and presence, respectively, of a band corresponding to the molecular weight of AP4E (Supplemental Figure S3). AP4E co-enriched with *bona fide* CCV proteins and was approximately 90-fold more abundant in the CCV fraction compared with lysate and 3-fold more abundant in the CCV fraction compared to the DFGL (Table 2.1 and Figures 2.4A and 2.4C).

Previous studies have indicated AP-4 functions at the TGN/EE (Hirst et al., 1999; Fuji et al., 2016; Shimizu et al., 2021). Consistent with this, functional GFP-tagged AP4M colocalizes with the TGN-resident SNARE mRFP-SYP43 and the endocytic tracer FM4-64 in Arabidopsis root tip cells (Fuji et al., 2016). Recently, GFP-tagged AP4M was shown to localize to the TGN/EE at sites distinct from AP1M2 (Shimizu et al., 2021). To further investigate the subcellular distribution of AP-4 and to determine whether it colocalizes with clathrin at the TGN/EE, we constructed lines that stably expressed N-terminal and C-terminal GFP- and RFP-tagged AP4E fusion proteins under control of the ubiquitin-10

promoter (Grefen et al., 2010). These constructs are functional *in vivo* as demonstrated by the rescue of the overall dwarf and abnormal growth phenotype observed in homozygous *ap4e-1* and *ap4e-2* plants (Figure 2S4). Consistent with visualization of GFP-tagged AP4M (Fuji et al., 2016), *ap4e-2* lines that expressed GFP-AP4E primarily displayed cytosolic and endomembrane subcellular localization with signal notably absent from the plasma membrane and tonoplast (Figure 2.6A).

We corroborated the subcellular localization of RFP-AP4E by pulse labeling, co-localization studies with the endocytic tracer dye, FM4-64. This dye has been used to distinguish plant endosomal compartments based on their spatial and temporal distribution of the dye upon internalization, for example, by labeling the TGN/EE within 2–6 min of internalization (Dettmer et al., 2006; Viotti et al., 2010). We observed co-localization between RFP-AP4E and FM4-64 (Pearson's correlation coefficient [PCC] = 0.705 utilizing a Costes' automated threshold, Costes P = 1.00) on a similar timescale (Figure 2.6B), which confirmed that AP4E, like AP4M and AP4S, localized to the TGN/EE (Fuji et al., 2016; Shimizu et al., 2021). Clathrin distribution within the cell is divided into soluble (cytosolic) and membrane associated pools, the latter of which includes the plasma membrane, TGN/EE and cell plate. Root epidermal cells expressing *CLC2-GFP* under control of the native CLC2 promoter (Konopka et al., 2008) and *ProUB10:RFP-AP4E* showed occasional colocalization of these fluorophores (PCC = 0.37 utilizing a Costes' automated threshold, Costes P = 1.00) in endosomal structures, but not at the PM nor at the cell plate (Figure 2.6D). Taken together with the presence of AP-4 in the CCV proteome, these data suggest AP-4 is incorporated into CCVs, likely at the TGN as part of a trafficking pathway to the PSV.

In contrast to AP-1, AP-2, and AP-4, subunits of the AP-3 and AP-5 complexes were absent or were detected in only trace amounts in our CCV proteomes (Supplemental Dataset S4). Mammalian AP-3 is involved in trafficking between recycling and late endosomes (LE) with mixed evidence of a clathrin association (Hirst et al., 1999). In plants, AP-3 has been found to localize to compartments distinct from the TGN/EE, recycling endosome, and Golgi (Feraru et al., 2010). The Arabidopsis AP3B and AP3D mutants, *protein affected trafficking2* (*pat2*) and *pat4*, display defects in a vacuole biogenesis pathway apparently independent of the canonical PVC / MVB maturation sequence, though both mutants display overall normal growth and development, suggesting AP-3 mediates trafficking of some but not all tonoplast proteins (Feraru et al., 2010; Zwiewka et al., 2011; Wolfenstetter et al., 2012; Feng et al., 2017). Furthermore, while Zwiewka et al. observed that clathrin heavy chain was identified as a potential interactor of AP3 by immunoprecipitation (IP) of AP3B subunit and subsequent mass spectrometry (MS), this was not supported by IP of AP3D or in the CCV proteomic datasets presented herein (Supplemental Dataset S4, Zwiewka et al., 2011). Little is known of the AP-5 complex, though recent studies in mammalian cells have suggested that it functions in late endosome to Golgi protein retrieval in a clathrin independent fashion (Hirst et al., 2011; Hirst et al., 2018). The AP-5 complex is essentially uncharacterized in plants, though its absence in the CCV proteome (Supplemental Dataset S4) suggests its function(s) are also clathrin independent.

Clathrin Accessory Factors

In addition to hetero-oligomeric protein complexes, monomeric adapters, including members of the ENTH/ANTH/VHS domain-containing protein family and the Golgi-localized, gamma-ear-containing, ARF (ADP-ribosylation factor)-binding (GGA) family, facilitate cargo recognition and vesicle formation at various points in the late endomembrane system. GGA proteins, which function in CCV formation at the TGN in yeast and mammals (Bonifacino, 2004), are absent from plants (Zouhar and Sauer, 2014). Arabidopsis contains 35 ENTH/ANTH/VHS domain-containing genes, 24 of which are putatively expressed in T87 suspension-cultured cells (Stolc et al., 2005). In addition to the TPC accessory proteins AtECA4 and CAP1 (see above), 13 other ENTH/ANTH/VHS-domain containing proteins were identified in the suspension-cultured cell CCV proteome (Supplemental Dataset S4) including the ENTH domain-containing monomeric clathrin adaptors EPSIN1 (EPS1) and EPS2 (Song et al., 2006; Lee et al., 2007; Collins et al., 2020) and the TGN-localized MODIFIED TRANSPORT TO THE VACUOLE 1 (MTV1) (Sauer et al., 2013; Heinze et al., 2020).

EPS1 and MTV1 have previously been implicated in clathrin-mediated trafficking to the vacuole (Song et al., 2006; Sauer et al., 2013; Heinze et al., 2020). Consistent with additional roles in cargo trafficking to the PM, EPS1 modulates the plasma membrane abundance of the immune receptor FLAGELLIN SENSING2 and its co-receptor, BRI1-ASSOCIATED KINASE (BAK1) for effective defense responses (Collins et al., 2020). In our study, EPS1, EPS2, and MTV1 were enriched in CCVs relative to the DFGL in labeling experiments 5-, 5-, and 7-fold, respectively (Supplemental Dataset S4), consistent with data demonstrating their incorporation into CCVs (Sauer et al., 2013), biochemical interaction with clathrin and AP-1 (Song et al., 2006), and similar defects in the trafficking

of the soluble vacuolar protease precursor proaleurain in *epsin1* and *ap1m* lines (Song et al., 2006; Park et al., 2013).

Mammalian and plant clathrin-mediated endocytosis are also regulated by Eps15 homology domain-containing proteins, which function as membrane and/or protein adaptors (Chen et al., 1998; Bar et al., 2008; Schwihla et al., 2020; Yperman et al., 2021). The Arabidopsis Eps15 homology domain-containing proteins, EHD1 and EHD2, were also found in the CCV proteome derived from both methodologies (Supplemental Dataset S4).

Several other proteins putatively functioning as trafficking adaptors were identified in the CCV proteome datasets including the sorting nexin homologs SNX1 and SNX2b (Supplemental Dataset S4). Mammalian sorting nexins interact with subunits of the endosomal retromer coat protein complex in a clathrin-independent fashion (McGough and Cullen, 2013) to mediate protein export from the early endosome to the TGN and PM by retrieving sorting receptors (e.g. the mannose-6-phosphate receptor) from the lysosome (Burd and Cullen, 2014). However, an interaction between the Arabidopsis retromer (VPS26a, 26b, 29, 35a, 35b, 35c) and the three sorting nexin homologs (SNX1, 2a, 2b) has yet to be shown, and conflicting evidence in the literature regarding SNX and retromer localization in plant cells at the TGN and MVB (reviewed in (Heucken and Ivanov, 2018; Robinson, 2018)) suggest multiple, independent roles for these complexes. Intriguingly, 12S globulin trafficking to the PSV is disrupted in *snx* mutants while that of 2S globulin remains apparently normal (Pourcher et al., 2010), a phenotype also observed in *ap4* mutants (Fuji et al., 2016). Moreover, a YFP fusion with the *Pisum sativum* (pea) homolog of Arabidopsis VSR1 (BP80) colocalizes with AtSNX1 (Jaillais et

al., 2008) and trafficking of a similar BP80 reporter depends on SNX1 and SNX2 function (Niemes et al., 2010). In contrast to SNX1 and SNX2b, components of the retromer core (VPS26A, VPS26B, VPS29, VPS35A, VPS35B, and VPS35C) were identified in the CCV proteome in low abundance (Supplemental Dataset S4), suggesting a possible role for SNX proteins in CCVs independent of retromer. Further studies are required to investigate the role of SNX proteins and a possible association with CCVs as an evolutionary divergence from the clathrin-independent nature of mammalian retromer / SNX function.

Several SH3Ps (SH3 domain-containing proteins) implicated in CCV trafficking were present in the suspension-cultured cell CCV proteome including the TASH3 subunit of the TPC, as well as SH3P1 and SH3P2, the latter of which is in high abundance and enriched in CCVs relative to DFGL fractions as measured by quantitative dimethyl labeling (8-fold CCV:DFGL, Supplemental Dataset S4) and by immunoblotting (Nagel et al., 2017). Ubiquitylation of PM proteins serves as a post-translational modification signaling for internalization and vacuolar degradation (Martins et al., 2015). SH3P2 localizes to the PM and functions as a ubiquitin-binding protein that may facilitate ESCRT recognition of ubiquitylated cargo for subsequent degradation (Nagel et al., 2017). However, SH3P2 also localizes to the cell plate and to other clathrin-positive foci, suggesting this and other ubiquitin adaptors may function at other membranes beyond the PM.

Another set of clathrin accessory factors identified in the CCV proteome are Arabidopsis homologs of animal SCY1-LIKE2 proteins (SCYL2A and SCYL2B); SCYL2B is in high abundance and was found to co-enrich with CCVs by quantitative dimethyl

labeling MS/MS experiments (15-fold CCV:DFGL ratio, Supplemental Dataset S4). In animals, SCYL2 binds clathrin (Duwel and Ungewickell, 2006), localizes to the Golgi, TGN, and other endosomes, and is incorporated into CCVs (Conner and Schmid, 2005; Borner et al., 2007). Although less is known about SCY1-LIKE2 protein function in plants, SCYL2B was recently shown to localize to the TGN and interact with CHC as well as two related but functionally distinct TGN-associated SNAREs, VTI11 and VTI12, both of which were also identified in the CCV proteome (Supplemental Dataset 4; Jung et al., 2017). Taken together, these data suggest SCYL2A and SCYL2B function may reflect that of mammalian SCYL2 by mediating TGN CCV formation in Arabidopsis.

Dynamin Related Proteins

Following cargo recognition and clathrin recruitment, the maturing CCV must separate from the plasma membrane prior to internalization. In metazoans, this is accomplished by the action of the dynamin GTPases, which oligomerize around the vesicle neck and utilize GTP hydrolysis to exert a constricting, twisting force, achieving scission (Antonny et al., 2016; Cheng et al., 2021). In plants, members of the DYNAMIN RELATED PROTEIN 2 (DRP2) protein family, DRP2A and DRP2B, which are most closely related to mammalian dynamin (Backues et al., 2010; Smith et al., 2014), and the plant-specific DRP1 family members DRP1A and DRP1C (Collings et al., 2008; Mravec et al., 2011; Smith et al., 2014; Ekanayake et al., 2021) function together in cargo trafficking via CME (Ekanayake et al., 2021). DRP2 and DRP1 family members also biochemically interact with TPC and AP-2 (Gadeyne et al., 2014) and localize to PM CCPs (Konopka et al., 2008; Fujimoto et al., 2010; Wang et al., 2020).

Despite their clear association with PM CCPs (Konopka et al., 2008; Konopka and Bednarek, 2008; Fujimoto et al., 2010), DRP proteins were only detected at low levels in the total CCV proteome datasets (Table 2.1, Supplemental Dataset S4). Consistent with this, DRP1A and DRP1C show significant depletion in the CCV fraction relative to the DFGL as determined via quantitative immunoblotting (Figures 2.4B and 2.4C, Table 2.1). This apparent discrepancy may reflect a short residency of DRP proteins at the PM wherein DRPs are recruited, accomplish their function(s), and dissociate from the newly formed CCV. The former hypothesis is supported by high-temporal-resolution imaging data showing recruitment of DRP2B, DRP1C, and DRP1A to endocytic foci at the PM simultaneously with or shortly after clathrin before their simultaneous disappearance, potentially reflecting a function in CCV maturation and/or scission (Konopka et al., 2008; Konopka and Bednarek, 2008; Fujimoto et al., 2010). The brief tenure of DRPs at nascent CCVs may also be reflected in the putative interaction between DRPs and the TASH3 subunits of the TPC (Gadeyne et al., 2014), which, along with other core TPC components, were likewise detected at relatively low abundance in the suspension-cultured cell CCV proteome (Supplemental Dataset S4). This parallel may reflect a functional coordination of recruitment and dissociation between DRPs and TPC in endocytic CCV formation. Alternatively, we cannot rule out the low abundance of DRP peptides in our dataset may be due to poor retention of the DRPs during the CCV isolation. In contrast, the DnaJ related AUXILIN-LIKE1 and AUXILIN-LIKE2 proteins, which are postulated to function in uncoating of CCVs (Lam et al., 2001; Adamowski et al., 2018), were readily identified in the suspension-cell cultured CCV proteome (Figure 2.5C; Supplemental Dataset S4), possibly due to the conditions used in vesicle

preparation (pH 6.4) that block clathrin coat disassembly but permit association of the AUXILIN-LIKE proteins with CCVs (Reynolds et al., 2014). Furthermore, recent data suggest that uncoating of CCVs in plants may not occur immediately after scission but as the CCV is trafficked away from the plasma membrane (Narasimhan et al., 2021).

Our results appear consistent with those observed in mammalian and yeast systems including the apparent uncertainty of dynamin association with isolated mammalian CCVs, with the protein being alternatively undetected (Blondeau et al., 2004) or observed with high confidence (Borner et al., 2006) in different preparations. However, the precise role(s) of members of the DRP2 and DRP1 protein families in CCV maturation and/or scission remains to be determined.

Vacuolar Protein Trafficking

Plant Vacuolar Sorting Receptors (VSRs) bind soluble vacuolar proteins including hydrolytic enzymes and vacuolar storage proteins (e.g. 12S globulin and 2S albumin) in the lumen of the secretory pathway through recognition of sorting motifs of vacuolar ligands, sequestering these cargo from others that are secreted or targeted towards the plasma membrane (Shimada et al., 2003). The primary mode of VSR function in plants had been postulated to reflect that of the mammalian mannose 6-phosphate receptor (MPR), which binds and traffics soluble lysosomal hydrolases via CCVs to the late endosome. The increasingly acidic nature of the maturing endosome triggers pH-dependent dissociation of its ligand, resulting in MPR recycling back to the TGN via retromer-mediated trafficking (Braulke and Bonifacino, 2009), at which the pH falls within the pH range for optimal MPR-ligand binding established by *in vitro* experiments (Tong et

al., 1989). However, increasing evidence indicates that VSR-mediated vacuolar protein trafficking is distinct in plants (Robinson and Neuhaus, 2016). In one instance of divergence from the mammalian MPR sorting model, plant VSR–ligand interaction appears to be initiated in the ER and cis-Golgi rather than the TGN/EE (daSilva et al., 2005; Gershlick et al., 2014; Künzl et al., 2016). Furthermore, the pH of the plant TGN (5.5) is lower than that of other compartments involved in VSR trafficking (Luo et al., 2015), ostensibly marking it as the site of ligand dissociation. Thus, the newly liberated VSRs must be recycled from the TGN back to the ER. In line with this hypothesis, a recent study has demonstrated the retrograde movement of nano-body tagged VSR from the TGN/EE to the early secretory pathway in tobacco (*Nicotiana tabacum*) protoplasts (Früholz et al., 2018). Therefore, in addition to the AP/CCV-mediated anterograde trafficking of VSRs, alternative proposals have questioned whether VSR-laden CCVs carry soluble vacuolar cargo directly or are instead part of a recycling mechanism responsible for bringing VSRs back to the early secretory pathway after cargo dissociation in the TGN (reviewed in (Kang and Hwang, 2014; Robinson and Neuhaus, 2016).

Previous analyses of isolated plant CCVs have identified abundant VSR proteins, consistent with a role for CCVs as VSR carriers (Masclaux et al., 2005; De Marcos Lousa et al., 2012). Indeed, the first plant VSR to be discovered (BP80) was initially detected in CCVs isolated from pea (*P. sativum*) cotyledons (Kirsch et al., 1994), and VSRs have been shown to co-fractionate with clathrin and vacuolar cargos during CCV preparations (Jolliffe et al., 2004). Consistent with this, five VSR proteins were identified in the suspension-cultured cell CCV proteome, of which three (VSR1, 3, and 4) were in highest abundance (Figure 2.5C, Supplemental Dataset S4).

Adaptor protein 1 and 4 complexes mediate the interaction of clathrin with VSR-ligand complexes, facilitating clustering of vacuolar cargo and vesicular formation necessary for vacuolar protein trafficking. The function of the AP-1 complex as an adaptor of vacuolar trafficking in plants reflects that of its mammalian/yeast counterparts in lysosomal/vacuolar trafficking. Recent work in *S. cerevisiae* has demonstrated AP-1 is critical for retrograde recycling of cargo from mature to earlier Golgi cisternae (Papanikou et al., 2015; Day et al., 2018; Casler et al., 2019), suggesting that retrograde trafficking of VSRs and other cargo from the TGN and/or late Golgi to the early secretory pathway in plants may be mediated by AP-dependent CCVs. Moreover, binding of plant VSRs to AP1M is dependent on a cytoplasmic motif and is required for proper trafficking and maturation of the 12S globulin precursor seed storage protein (Gershlick et al., 2014; Fuji et al., 2016). Another member of the Arabidopsis VSR family, VSR4, interacts with AP1M2 partly through a complex cargo-recognition sequence. Mutations of this AP1M2 interaction motif result in VSR4 mislocalization to the PM and increased residency at the tonoplast, suggesting that this motif mediates both anterograde and retrograde VSR4 transport (Nishimura et al., 2016).

As noted above, mutants of AP-4 subunits mislocalize PSV cargo, a phenotype also observed in *vsr* and AP-1 subunit mutants (Zouhar et al., 2010; Park et al., 2013; Fuji et al., 2016), raising questions regarding the cargo and destination specificity of AP-1 and AP-4 dependent vacuolar trafficking. Pathway specific accessory proteins may aid in differentiating AP-1 and AP-4 function, such as the Arabidopsis homolog of the mammalian AP-4 accessory protein tepsin, MTV1, which has been shown to both bind clathrin and co-enrich with isolated CCVs as measured by immunoblotting and electron

microscopy techniques (Borner et al., 2012; Sauer et al., 2013; Heinze et al., 2020). We have also found the AP4 interactor, MTV1, to be highly abundant in the Arabidopsis suspension-cultured cell CCV proteome and enriched in CCV pools relative to DFGL (7-fold enrichment, Supplemental Dataset S4). Recent studies present a genetic interaction between *AP4* and *MTV1* and demonstrate that MTV1 functions in vacuolar trafficking (Heinze et al., 2020). Furthermore, the presence of EPS1, AP-1, AP-4, VTI11, and VSR1, 3, and 4 in the CCV dataset (Figure 2.5C, Supplemental Dataset S4) considered alongside available data regarding the vacuolar trafficking defects of *ap1, ap4,* and *vsr* mutants suggest that AP-1 and AP-4 facilitate anterograde, and possibly retrograde, CCV-mediated trafficking of VSRs to some degree.

Regulators of Clathrin-Mediated Trafficking

Phospholipid Metabolism

Intriguingly, one of the most abundant CCV proteome components identified was the phosphoinositide phosphatase SAC9, which is thought to regulate levels of phosphatidylinositol 4,5-bisphosphate [PI(4,5)P_2] (Williams et al., 2005; Vollmer et al., 2011). In mammals, PI(4,5)P_2 in the inner leaflet of the PM mediates CCP formation (Antonescu et al., 2011) through interactions with clathrin adaptor and accessory proteins including subunits of the AP-2 complex (AP2A, AP2B, AP2M) (Jackson et al., 2010), epsin (Itoh et al., 2001), and dynamin (Vallis et al., 1999). The importance of these interactions in plant CME remains to be demonstrated, though PI(4,5)P_2 accumulates at sites of high membrane flux, like the growing pollen tube tip (Kost et al., 1999; Yao et al., 1999) and at the apex of expanding root hairs (Braun et al., 1999) and is incorporated

into CCVs (Zhao et al., 2010). Moreover, mutants lacking the CCV-associated enzymes involved in the synthesis of PI(4,5)P_2, phosphatidylinositol 4-phosphate 5-kinases PIP5K1 and PIP5K, show fewer CCPs at the PM of root epidermal cells (Ischebeck et al., 2013). Studies in plants have demonstrated that PI(4,5)P_2 recruits the endocytic accessory factor AP2M to the plasma membrane and interacts with the EH1 subunit of the TPLATE complex, suggesting that this phospholipid plays a role in the regulation of clathrin mediated endocytosis (Doumane et al., 2021a; Yperman et al., 2021). Furthermore, recent data demonstrate that disruption of PI(4,5)P_2 levels at the plasma membrane is caused by loss of SAC9 function and consequently results in impaired endocytic trafficking (Doumane et al., 2021b). The presence of SAC9 in the CCV proteome (Figure 2.5C; Supplemental Dataset S4), taken together with the numerous defects in membrane morphology including vesicle accumulation observed in Arabidopsis *sac9* mutants (Vollmer et al., 2011), suggests that PI(4,5)P_2 turnover in mature CCVs may play an important role in the regulation of CCV trafficking.

Small GTPases

Rabs and ARF GTPases regulate vesicle trafficking by modulating between GTP and GDP (active and inactive) bound states, which govern interactions with downstream effector proteins. Arabidopsis maintains 57 Rabs and 27 ARFs, of which the former can be grouped into eight distinct clades corresponding to mammalian Rab groups mediating different trafficking pathways (Rutherford and Moore, 2002). Of the numerous Rabs identified in our study, members of the RabA1, D2, and E1 families were most abundant (Figure 2.5C; Supplemental Dataset S4). RabA proteins are most closely related to

mammalian Rab11, which regulates endosomal trafficking and mediates TGN-PM trafficking in plants (Nielsen et al., 2008; Li et al., 2017; Zhou et al., 2020). In addition, members of the RabE family, which are orthologs of the Sec4p/Rab8 GTPase family, mediate exocytosis in yeast and mammalian cells (Rutherford and Moore, 2002) and regulate post-Golgi trafficking to the PM and to the cell plate during cytokinesis (Speth et al., 2009; Ahn et al., 2013; Orr et al., 2021). RabD2 proteins are related to mammalian Rab1s, which participate in the early secretory pathway. In plants, however, RabD2 proteins localize to the Golgi / TGN (Pinheiro et al., 2009) and mediate post-Golgi trafficking at certain endosomes (Drakakaki et al., 2012).

Guanine nucleotide exchange factors (GEFs) activate GTPases by catalyzing the exchange of GDP for GTP. Evidence has shown STOMATAL CYTOKINESIS DEFECTIVE1 (SCD1) and SCD2 proteins participate in a complex that interacts with RabE1s in a nucleotide-dependent matter as well as subunits of the exocyst (Mayers et al., 2017), suggesting the SCD complex may function as a RabGEF in exocytosis. Both SCD1 and SCD2 enrich with the purification of CCVs by immunoblot analysis (McMichael et al., 2013) and were detected, albeit at low levels, in both unlabeled CCV proteomic datasets (Supplemental Dataset S4). Despite the presence of SCD1 and SCD2 in enriched CCVs and impaired internalization and post-Golgi trafficking defects of *scd* mutants, it is not clear whether the SCD complex directly functions in endocytosis or functions in recycling endocytic machinery to the plasma membrane.

The Arabidopsis suspension-cultured cell CCV proteome contains several additional structural and regulatory components of the exocyst tethering complex including SEC6, SEC15b, SEC10, EXO84B, and EXO70A1 (Figure 2.5C; Supplemental

Dataset S4). Mammalian SEC15, SEC10, and EXO84 interact with vesicle-bound small GTPases to facilitate secretory trafficking from the TGN while EXO70 localizes to target membranes (Wu and Guo, 2015). Exocyst function in Arabidopsis appears to be conserved, including putative subcellular localizations at sites with high rates of vesicle fusion, e.g. EXO70A1 and EXO84b at the CP (Fendrych et al., 2010).

In addition to GEFs, which initiate GTPase activation, GTPase activating proteins (GAPs) promoting Rab GTP hydrolysis to terminate GTPase signaling are likewise critical for controlling vesicle trafficking. The ARF-GAP NEVERSHED/AGD5/MTV4, which is required for vacuolar protein trafficking (Sauer et al., 2013), was previously demonstrated to co-enrich with CCVs using immunoblotting and immunoEM techniques. In agreement, this ARF-GAP is well represented in the CCV proteome (Supplemental Dataset S4).

SNAREs

In this study, we identified PM- and endosome-localized SNAREs in the CCV proteome (da Silva Conceicao et al., 1997; Bassham et al., 2000; Suwastika et al., 2008; Ebine et al., 2011; Eisenach et al., 2012; Uemura et al., 2012; Ichikawa et al., 2014). SNAREs that localized to the PM, such as SYP121, VAMP722, SYP132, and SYP71, were enriched 7-, 5-, 8-, and 6-fold, respectively, in the CCV fraction. Endosomal SNAREs, SYP61, SYP41, VTI12, VAMP727, SYP21, and SYP43, were enriched 6-, 13-, 7-, 5-, 2-, and 9-fold, respectively (Figure 2.5C; Supplemental Dataset S4). The cell plate/cytokinesis-specific syntaxin and putative CCV cargo KNOLLE (KN) (Lauber et al., 1997; Boutté et al., 2010) was notably enriched in CCVs in dimethyl labeling (6-fold) and modestly enriched in quantitative immunoblotting (1.3-fold) experiments (Figure 2.4, Table 2.1,

Supplemental Dataset S4). In contrast, SNAREs localized to compartments likely not engaged in CCV trafficking, such as the tonoplast protein VAMP713 (Takemoto et al., 2018) and the Golgi-localized VAMP714 (Uemura et al., 2005), were depleted in CCVs 5- and 3-fold relative to the DFGL, respectively (Supplemental Dataset S4).

We also identified several homologs of mammalian trafficking regulators involved in vesicle fusion in the CCV proteome, including PROTON ATPASE TRANSLOCATION CONTROL 1 (PATROL1), which contains the Munc13 MUN domain (Figure 2.4C; Supplemental Dataset S4). While the mammalian Munc13 interacts with the SNARE syntaxin-1 to prime synaptic vesicles for fusion with the PM (Ma et al., 2011), less is known of MUN-domain containing protein function in plants. PATROL1 appears to modulate the delivery of the PM H^+-ATPase AHA1 to the PM possibly through interactions with the exocyst complex and localizes to endosomes and dynamic foci at the cell cortex (Hashimoto-Sugimoto et al., 2013; Higaki et al., 2014; Zhu et al., 2018). The presence of both PATROL1 and AHA1 in the CCV proteome (Figure 2.5C; Supplemental Dataset S4) suggests PATROL may regulate the trafficking of CCVs containing AHA1 through interactions with its MUN domain. Another SNARE interacting protein, VPS45, was detected in abundance in the CCV proteome and found to enrich in CCVs in differential labeling experiments (5-fold CCV:DFGL enrichment, Supplemental Dataset S4). VPS45 is a Munc18 protein that binds and regulates the TGN SNARE complex composed of SYP41, SYP61, YKT61, and VTI12, potentially to mediate fusion of PVC-derived vesicles at the TGN (Bassham et al., 2000; Zouhar et al., 2009). Given the presence of VPS45 and its cognate SNAREs (SYP41, SYP61, VTI12, YKT61) in the CCV proteome (Figure 2.5C; Supplemental Dataset S4), clathrin-mediated trafficking may play a role in the

regulation / function of the complex, possibly by recycling individual SNAREs for subsequent fusion events.

Conclusion

Space constraints prohibit a full discussion of all protein groups identified in the suspension-cultured cell CCV proteome; instead, we have reported on a subset of actively discussed protein groups and provided the complete CCV proteome as a rich data reference and resource for future investigations of proteins putatively involved in clathrin-mediated trafficking. An important caveat to interpreting the biological significance of the suspension cultured CCV proteome is that CCV composition reflects the tissue/cell type and developmental stage of the biological source material from which they are isolated. The data reported here reflect the content of CCVs isolated from undifferentiated, rapidly dividing and expanding Arabidopsis suspension cultured cells under conditions amenable to tissue culture. Future experiments probing CCV content in other cell and tissue types under varying conditions or in different genetic backgrounds might apply our isolation methodology (Reynolds et al., 2014) using seedlings as a sample source as recently described (Nagel et al., 2017; Mosesso et al., 2019).

Our proteomic data demonstrate that, in addition to the canonical clathrin coat adapters AP-1 and AP-2, the AP-4 complex is incorporated into plant CCVs in an apparent contrast to its function in metazoans (Mattera et al., 2015; Robinson, 2015). This result inspires numerous questions regarding the evolutionary divergence of plant trafficking proteins relative to other eukaryotes, as well as the identity of which pathway(s) might be mediated by AP-4 and clathrin. Current biochemical and genetic studies in the

literature suggest AP-4 mediates the trafficking of specific cargos to the PSV (Gershlick et al., 2014; Fuji et al., 2016), though whether AP-4 function in CCVs directly facilitates the anterograde trafficking of soluble cargos and their cognate receptors (i.e. VSRs) or instead participates in the recycling thereof remains to be determined. Additional studies identifying the composition of AP-2, AP-1, and AP-4-positive CCVs are needed to better understand cargo specificity and identify the regulators governing formation, trafficking, and fusion of these vesicles. Nevertheless, the identification of AP-4 as a CCV-associated protein complex presented here, together with recent genetic and biochemical evidence, will contribute to future experiments focused on elucidating the mechanisms of AP-4-dependent post-Golgi trafficking to the PSV. The question remains: is the interaction between AP-4 and clathrin direct as is the case for AP-1 and AP-2? Coimmunoprecipitation experiments (Fuji et al., 2016; Shimizu et al., 2021) and AP-4 abundance in the CCV proteome suggest that it might be, but a conclusive demonstration of a direct biochemical interaction remains to be determined. Determining the role of clathrin in VSR sorting, given the recent evidence of an ER/cis-Golgi to TGN/EE VSR-dependent, vacuolar trafficking pathway, will be essential as plant endomembrane dynamics become better understood (Robinson and Pimpl, 2014; Robinson and Neuhaus, 2016).

In contrast to the evolutionarily conserved endocytic adaptor AP-2, subunits of the TPLATE complex, which is essential for CME, were not significantly enriched in the final enrichment step towards purified CCVs, suggesting that the TPLATE complex may dissociate more readily from CCVs following their budding from the plasma membrane relative to AP-2. This observation may be resolved by a recent study in which TPLATE

dissociated from CCVs earlier than clathrin and which positioned the TPLATE complex on the periphery of a clathrin coated structure at the plasma membrane (Johnson et al., 2021). The positioning of the TPLATE complex to the periphery of the budding vesicle will be of significant biological interest.

As discussed above, the enriched CCV proteomic datasets contain numerous proteins that are unlikely to be associated with CCVs (e.g. ribosomal subunits). The presence of a protein in a shotgun MS/MS dataset, especially those of low abundance, must be taken as a preliminary indication only of its presence and therefore requires subsequent confirmation. Conversely, the absence or low abundance of proteins of interest might also be explained by low intracellular concentrations, such as in the case of regulatory proteins like the SCD1 and SCD2 subunits of the SCD complex which, while in low abundance in the MS/MS dataset, are shown to coenrich with isolated CCVs via immunoblotting and other techniques. Nevertheless, our CCV proteomics data expand our understanding of the plant endomembrane compartments for subsequent efforts to investigate the plant endomembrane network and their physiological function.

Materials & Methods

Plant Materials and Growth Conditions

Seed stocks of Col-0 (CS70000) and Col-3 (CS708) were obtained from the Arabidopsis Biological Research Center (ABRC). Seed stocks of the *ap4e-1* and *ap4e-2* T-DNA insertion mutants (Fuji et al., 2016) were graciously provided by T. Shimada of Kyoto University. CLC2-GFP transgenic plant lines were generated as previously described (Konopka et al., 2008). Seeds were sterilized in 70% (v/v) ethanol with 0.1% (v/v) Triton

X-10 for 5 min and in 90% (v/v) ethanol for 1 min prior to plating on 0.5X strength MS media (Murashige and Skoog, 1962) containing 0.6% (w/v) agar. Seeds were stratified without light at 4°C for 3 days prior to growing under continuous light at 22°C (T8 fluorescent bulb of 120 $\mu mol^{-2} s^{-1}$). Plants grown on soil were transferred from plates after 7 to 14 days to Metro-Mix 360 (SunGro Horticulture) and grown at 22°C long days (16 hours of light exposure using T12 fluorescent bulb of 160 $\mu mol^{-2} s^{-1}$). *ap4e-1* and *ap4e-2* mutants were genotyped using primers GR1, 2, & 5 and GR3, 4, & 5, respectively (sequences listed in next section).

Undifferentiated Arabidopsis T87 cells (Axelos et al., 1992) were maintained in MS media supplemented with 0.2 mg/L 2,4-Dichlorophenoxyacetic (2,4-D) acid and 1.32 mM KH_2PO_4 under continuous light (T12 fluorescent bulb of 160 $\mu mol^{-2} s^{-1}$) at 22°C on an orbital shaker at 140 RPM. Cells were passaged weekly by a 1:10 dilution of a 7-day-old suspension-culture into fresh MS 0.2mg/L 2,4-D media.

Primers

GR1 – SAIL866C01_LP – 5'-CATGGGTATTGATGGTCTTGG-3'

GR2 – SAIL866C01_RP – AGACCAGAACAGCTAAGCACG

GR3 – SAIL60E03_LP – ATAGGCTTCGAATCGAAGAGC

GR4 – SAIL60E03_RP – ATGCAGGTGGAATCGTACTTG

GR5 – SAIL_LB3 – TAGCATCTGAATTTCATAACCAATCTCGATA

GR6 – SB1859STOPsense – CAAAGATCTCCTCGGCTGAGCACCTCTCTTCTTCA

GR7 – SB1859STOPanti - TGAAGAAGAGAGGTGCTCAGCCGAGGAGATCTTTG

GR8 – SB1859del673sense - CAAAAAAGCAGGCTTCGCAAGAAGGTCCATGGA

GR9 – SB1859del673anti – CTCCATGGACCTTCTTGCGAAGCCTGCTTTTTTG

Plasmid Construction and Plant Transformation

All oligonucleotide primers used in this study were synthesized by Integrated DNA Technologies. Transgenic plants were generated using the floral dip method (Clough and Bent, 1998) with the *Agrobacterium tumefaciens* strain EHA105. N-terminal and C-terminal GFP and RFP fusions with AP4E under control of the UBQ10 promoter were created in pUBN-Dest and pUBC-Dest vectors (Grefen et al., 2010) using Gateway™ cloning (Invitrogen). The AP4E CDS in pLIC6, obtained from ABRC clone DKLAT1G31730, was moved into pDONR221 (Invitrogen) using the BP Clonase kit. Stop codon insertion and frame correction for pUBN constructs was accomplished with primer pairs GR6&7 and GR8&9, respectively, before using the LR Clonase kit (Invitrogen) to move respective AP4E constructs into pUBN and pUBC destination vectors.

T1 seedlings from pUBN/pUBC transformed plants were sown on soil and selected by spray application of a 120 µg/ml Glufosinate (Liberty Herbicide, Bayer Crop Sciences) water solution containing 0.05% (v/v) Silwet-77 surfactant 7, 9, 12, and 14 days after germination.

CCV Enrichment and Analysis

CCVs were isolated from undifferentiated Arabidopsis T87 cells as described (Reynolds et al., 2014). Total protein yield in the enriched CCV fraction was approximately 300–500 µg per biological replicate. Protein concentrations of individual fractions for subsequent

immunoblotting analysis and total CCV yield were obtained using the Pierce® 660nm Protein Assay (Thermo Scientific).

Immunoblotting was performed as described (McMichael et al., 2013). Information about generation of antibodies and concentrations used is described in Supplemental Table S1.

Anti-AP4E Antibody Generation

The C-terminal 22 amino acids of the Arabidopsis AP4 Epsilon subunit were cloned from the ABRC stock DKLAT1G31730 into the pAN4GST GST-expression vector and the resulting construct used for phage display as described (Blanc et al., 2014) by the Geneva Antibody Facility at the Université de Genève, Switzerland. Antibody specificity was tested by probing the total protein content of wild-type, *ap4e-1*, *ap4e-2*, and various transgenic plants expressing GFP and RFP fusions with AP4E (Supplemental Figure S3). Seedlings grown on plates as described for 7-14 days were flash frozen and homogenized via mortar and pestle under liquid nitrogen. Tissue was resuspended in 2X Laemmli buffer, quantified using the Pierce® 660nm Protein Assay (Thermo Scientific). 23.5 µg of each sample were fractionated on a 11% Tris-HCl SDS-PAGE gel and analyzed via immunoblotting.

Light Microscopy

All confocal imaging experiments were conducted on a Nikon A1R-Si+ microscope. Colocalization and localization observations were made in root tip epidermal cells of 5 to 7-day old T3 generation seedlings grown on plates as described above. Seedlings were

mounted for imaging in 0.5X MS media. FM4-64 treated samples were incubated in 0.5X MS containing 4μM FM4-64 for 3 min and mounted in the same solution before imaging after 6 min total incubation.

Colocalization analysis was performed using the JACoP plugin (Bolte and Cordelieres, 2006) in the Fiji (Schindelin et al., 2012) distribution of ImageJ2 (Rueden et al., 2017). Images were processed to remove background (Rolling ball 50-pixel diameter) and cropped to relevant ROIs before analysis with JACoP utilizing 1000 Costes randomizations with a point spread function of two pixels and Costes' automated thresholding.

STEM Imaging of Purified CCVs

4 μl of purified CCV preparation (0.33 mg/μl) was applied to carbon-coated and glow discharged (2 min at 7x10-1 mbar) 300-mesh copper EM grids (Electron Microscopy Sciences; CF300-CU) and incubated for 4 min at room temperature. Excess solution was removed with blotting paper and samples immediately fixed by a 20 min incubation at room temperature with 2% glutaraldehyde (v/v) in PEM buffer (100 mM PIPES, 1 mM MgCl2, 1 mM EGTA, pH 6.9). Samples were then washed with phosphate buffer (0.1 M, pH 7.4) and distilled water, followed by a 20 min incubation with 0.1% tannic acid (w/v) in MilliQ water. After three washes in water, the samples were incubated with 0.2% aqueous uranyl acetate for 30 min at room temperature and then washed three times with water before being dehydrated in a series of graded ethanol (10%, 20%, 40%, 60%, 80%, 96% and 100% for 2 min each) and two washes with hexamethyldisilane (99%). Dried samples were then coated with 3 nm platinum and 4 nm carbon using an ACE600 coating device

(Leica Microsystems). The sample grids were imaged using a JEOL JEM2800 scanning/transmission electron microscope at 200 kV.

LC/MS/MS of CCVs separated by 1D SDS-PAGE

Enriched CCV fractions were resolved via 1D SDS-PAGE on a 4–15% Tris-HCl gradient gel (BioRad cat# 161-1158) at a constant 200V for ~90 min. Gels were stained with Coomassie R250 and cut into ~10 bands. Gel bands were digested in-gel as described (Shevchenko et al., 1996) with modifications. Briefly, gel bands were dehydrated using 100% acetonitrile and incubated with 10mM dithiothreitol in 100mM ammonium bicarbonate, pH~8, at 56 ℃ for 45min, dehydrated again and incubated in the dark with 50mM iodoacetamide in 100mM ammonium bicarbonate for 20 min. Gel bands were then washed with ammonium bicarbonate and dehydrated again. Sequencing grade modified trypsin was prepared to 0.01µg/µl in 50mM ammonium bicarbonate and ~50µl of this was added to each gel band so that the gel was completely submerged. Bands were then incubated at 37°C overnight. Peptides were extracted from the gel by water bath sonication in a solution of 60% acetonitrile/1.0% trifluoroacetic acid and vacuum dried to ~2µl.

Enriched DFGL or CCV fractions for dimethyl labeling experiments were prepared in the same manner as the other CCV samples up to peptide extraction and vacuum drying except that a 12.5% Tris-HCl SDS polyacrylamide gel was used. Each peptide sample was then re-suspended in 100mM Triethylammonium and labeled in solution with dimethyl reagents (light label – C2H6, medium label – C2H2D4) according to (Boersema et al., 2009). Aliquots of DFGL and CCV samples labeled with light and heavy

formaldehyde were analyzed by mass spectrometry to measure the labeling efficiency, which was found to be greater than 95% for each replicate. After labeling, peptides were purified using solid phase extraction tips (OMIX, www.varian.com). Same slice samples from each condition were combined and dried to ~2µl. Peptides were then re-suspended in 2% acetonitrile/0.1%TFA to 25µl. From this, 10µl was automatically injected by a Waters nanoAcquity Sample Manager (www.waters.com) and loaded for 5 min onto a Waters Symmetry C18 peptide trap (5µm, 180µm x 20mm) at 4µl/min in 5% acetonitrile /0.1%Formic Acid. The bound peptides were then eluted onto a MICHROM Bioresources (www.michrom.com) 0.1 x 150mm column packed with 3µm, 200A Magic C18AQ material over 90min with a gradient of 5% B to 35% B in 77min, ramping to 90%B at 79min, holding for 1min and returning to 5%B at 80.1min for the remainder of the analysis using a Waters nanoAcquity UPLC (Solvent A = 99.9% Water/0.1% Formic Acid, Solvent B = 99.9% Acetonitrile/0.1% Formic Acid) with an initial flow rate of 1µl/min.

Peptides were then re-suspended in 2% acetonitrile/0.1%TFA to 20µl. From this, 10µl was automatically injected by a Thermo (www.thermo.com) EASYnLC onto a Thermo Acclaim PepMap RSLC 0.075mm x 150mm C18 column and eluted at 250nL over 90min with a gradient of 5%B to 30%B in 79min, ramping to 100%B at 80min and held at 100%B for the duration of the run (Solvent A = 99.9% Water/0.1% Formic Acid, Solvent B = 99.9% Acetonitrile/0.1% Formic Acid). Eluted peptides were analyzed as follows: **CCV I**: peptides were sprayed into a hybrid ThermoFisher LTQ FT-ICR Ultra mass spectrometer with both ion cyclotron resonance (ICR) and LTQ linear ion trap mass analyzers and a Michrom ADVANCE nanospray source with survey scans taken in the FT (25000 resolution determined at m/z 400) and the top five ions in each survey scan

then subjected to automatic low energy collision induced dissociation (CID) in the LTQ; **CCV II:** peptides were sprayed into a ThermoFisher LTQ Linear Ion trap mass spectrometer using a Michrom ADVANCE nanospray source with the top eight ions in each survey scan are then subjected to low energy CID in a data dependent manner; **CCV III & CCV IV**: peptides were sprayed into a ThermoFisher Q-Exactive mass spectrometer using a FlexSpray spray ion source with survey scans taken in the Orbi trap (70,000 resolution, determined at m/z 200) and the top twelve ions in each survey scan then subjected to automatic higher energy collision induced dissociation (HCD at 25%) with fragment spectra acquired at 17,500 resolution; **Dimethyl Labeling Samples:** peptides were sprayed into ThermoFisher LTQ FT-ICR Ultra mass spectrometer using a Michrom ADVANCE nanospray source with intensity measurements of the two diMe forms made in the FT-ICR portion of the instrument and peptide fragmentation performed in the linear ion trap. The resulting MS/MS spectra from CCV replicates were converted to peak lists using Mascot Distiller, v2.4.3.3 (www.matrixscience.com) and searched against a custom database that included all entries in the TAIR10 protein sequence database (downloaded from www.arabidopsis.org), appended with common laboratory contaminants (downloaded from www.thegpm.org, cRAP project), using the Mascot searching algorithm, v2.4, with the following parameters: 2 allowed missed tryptic cleavages, fixed modification of carbamidomethyl cysteine, variable modification of oxidation of methionine, peptide tolerance ±5ppm, MS/MS tolerance 0.50 Da (Replicates I, II) and 0.015 Da (Replicates III and IV). False Discovery Rates (FDR) were calculated against a randomized database search. The Mascot output was then analyzed using Scaffold, v4.8.4 (Proteome Software Inc., Portland, OR) to probabilistically validate

protein identifications. Assignments validated using the Scaffold 1% FDR protein threshold, containing 2 unique peptides, meeting the 1% FDR peptide threshold were considered true. Assignments matching these criteria from four distinct biological replicates (CCV enrichments) were cross-referenced to eliminate duplicates and filtered to exclude proteins not present in at least two biological replicates, generating a list of 3,745 protein assignments.

Quantitation of labeled MS peaks from dimethyl labeling samples and processing of the resulting MS/MS spectra to peak lists was done using MaxQuant3, v1.2.2.5 (Cox and Mann, 2008). Peak lists were searched against the TAIR10 protein sequence database, downloaded from www.arabidopsis.org and appended with common laboratory contaminants using the Andromeda search algorithm within MaxQuant with the following parameters: two allowed missed tryptic cleavages, fixed modification of carbamidomethyl cysteine, variable modification of oxidation of methionine and acetylation of protein N-termini, DimethLys0, DimethNter0; DimethLys4, DimethNter4, peptide tolerance ±6ppm, MS/MS tolerance 20ppm, protein and peptide FDR filter set to 1% (Cox et al., 2011). A total of 1,109 unique proteins were identified between both replicates, 957 of which were identified in the LC/MS-MS dataset corresponding to CCVs digested in gel across two or more biological replicates.

Overlaps between proteomic datasets were identified by matching accession numbers between the 3,745 accession numbers in column 1 of Supplemental Dataset S1, the accession numbers of the 1,109 proteins identified in at least one of two dimethyl replicates (Supplemental Dataset S3), and the first accession number (corresponding to iBAQ values listed) of the majority accession numbers (identifiers of all sequences

containing at least half of the peptides of the leading sequence) within each protein group (n = 1,981) in the alternative methodology CCV LC/MS-MS dataset (Supplemental Dataset S4). Overlaps between proteomic datasets were visualized using the application BioVenn (Hulsen et al., 2008).

Protein localization of the 546 more than two-fold depleted proteins between the DFGL and CCV purification steps (Supplemental Dataset S3) was determined by submission of the corresponding accession numbers (Supplemental Dataset S5) to the SUBcellular Arabidopsis (SUBA) consensus algorithm (Hooper et al., 2014).

LC/MS-MS of CCVs digested in solution

5µg of 1 µg/µl isolated CCVs was lysed in a urea lysis buffer containing 8 M urea, 20 mM HEPES pH 8.0, by repeatedly pipetting up and down. Proteins in each sample were reduced by adding 15 mM dithiothreitol and incubating the samples for 30 min at 55˚C. Proteins were alkylated by addition of 30 mM iodoacetamide for 15 min at room temperature in the dark. The samples were diluted with 20 mM HEPES pH 8.0 to a urea concentration of 2 M and the proteins were digested with 4 µl Trypsin/LysC (Promega V5073: 20µg + 80µl 50mM acetic acid) for 4 hours at 37˚C and boosted with an extra 2µl Trypsin/LysC (Promega V5073: 20µg + 80µl 50mM acetic acid) overnight at 37˚C. Peptides were then purified on a OMIX C18 pipette tip (Agilent).

Purified peptides were re-dissolved in 25 µl loading solvent A (0.1% trifluoroacetic acid in water/acetonitrile (98:2, v/v)) and 5 µl was injected for LC-MS/MS analysis on an Ultimate 3000 RSLCnano ProFLow system in-line connected to a Q Exactive HF mass spectrometer (Thermo). Trapping was performed at 10 µl/min for 4 min in loading solvent

A on a 20 mm trapping column (made in-house, 100 µm internal diameter (I.D.), 5 µm beads, C18 Reprosil-HD, Dr. Maisch, Germany) and the sample was loaded on a 200 mm analytical column (made in-house, 75 µm I.D., 1.9 µm beads C18 Reprosil-HD, Dr. Maisch). Peptides were eluted by a non-linear gradient from 2 to 55% MS solvent B (0.1% FA in water/acetonitrile (2:8, v/v)) over 175 min at a constant flow rate of 250 nl/min, reaching 99% MS solvent B after 200 min, followed by a 10 min wash with 99% MS solvent B and re-equilibration with MS solvent A (0.1% FA in water). The column temperature was kept constant at 50°C in a column oven (Butterfly, Phoenix S&T). The mass spectrometer was operated in data-dependent mode, automatically switching between MS and MS/MS acquisition for the 16 most abundant ion peaks per MS spectrum. Full-scan MS spectra (375-1500 m/z) were acquired at a resolution of 60,000 in the orbitrap analyzer after accumulation to a target value of 3E6. The 16 most intense ions above a threshold value of 1.3E4 were isolated for fragmentation at a normalized collision energy of 28% after filling the trap at a target value of 1E5 for a maximum of 80 ms. MS/MS spectra (200-2000 m/z) were acquired at a resolution of 15,000 in the orbitrap analyzer.

Data were analyzed with MaxQuant (version 1.6.10.43) using the built in Andromeda search engine with default settings, including a false discovery rate set at 1% on both the peptide and protein level. Spectra were searched against the Araport11plus database, consisting of the Araport11_genes.2016.06.pep.fasta downloaded from www.arabidopsis.org, extended with sequences of all types of possible contaminants in proteomics experiments in general. These contaminants include the cRAP protein sequences, a list of proteins commonly found in proteomics experiments, which are

present either by accident or by unavoidable contamination of protein samples (The Global Proteome Machine, http://www.thegpm.org/crap/). In addition, commonly used tag sequences and typical contaminants, such as sequences from frequently used resins and proteases, were added. The Araport11plus database contains in total 49,057 sequence entries. The mass tolerance for precursor and fragment ions was set to 4.5 and 20 ppm, respectively, including matching between runs and false discovery rate set at 1% on PSM, peptide and protein level. Enzyme specificity was set as C-terminal to arginine and lysine (trypsin), also allowing cleavage at arginine/lysine-proline bonds with a maximum of two missed cleavages. Variable modifications were set to oxidation of methionine residues and acetylation of protein N-termini. Proteins were quantified by the MaxLFQ algorithm integrated in the MaxQuant software. Only protein groups with at least one unique peptide and with peptides identified in at least two of three biological replicates were retained, yielding a list of 1,981 protein groups (Supplemental Dataset S4).

Accession Numbers

Accession numbers corresponding to proteins identified in this study can be found in Supplemental Datasets S1-3. Files corresponding to raw proteomics data, as well as results, search, and peak list files can be accessed at the MassIVE data repository (MassIVE, University of California at San Diego) using the identifiers, PXD026180 or at doi:10.25345/C50F9D, or at the following URL: ftp://massive.ucsd.edu/MSV000087472/ . A summary of the methods & protocols used, as well as gel images and supplementary files, can also be accessed here.

Acknowledgments

We would like to express our gratitude to the VIB Proteomics Core Facility (VIB-UGent Center for Medical Biotechnology in Ghent, Belgium) and the Research Technology Support Facility Proteomics Core (Michigan State University in East Lansing, Michigan) for help and expertise with sample analysis, as well as the University of Wisconsin Biotechnology Center Mass Spectrometry Core Facility (Madison, WI) for help with data processing. Additionally, we are grateful to Drs. Sue Weintraub and Sydney Thomas for assistance with data analysis. This research was supported by grants to S.Y.B. from the National Science Foundation (Nos. 1121998 and 1614915) and a Vilas Associate Award (University of Wisconsin, Madison, Graduate School); to J.P. from the National Natural Science Foundation of China (Nos. 91754104, 31820103008, and 31670283); and to I.H. from the National Research Foundation of Korea (No. 2019R1A2B5B03099982). This research was also supported by the Scientific Service Units (SSU) of IST Austria through resources provided by the Electron microscopy Facility (EMF). A.J. is supported by funding from the Austrian Science Fund (FWF): I3630B25 to J.F. A.H. is supported by funding from the National Science Foundation (NSF IOS Nos. 1147032 and 1758843). D.V.D is supported by a grant from the European Research Council T-Rex Project No. 682436.

Author Contributions

D.A.D., G.D.R., S.Y.B., J.J.C., D.V.D., A.J., and J.P. conceived the study and designed the experiments. D.A.D., G.D.R., S.Y.B., J.J.C., D.V.D., A.J., J.P, K.Y., D.E., Y.X., W.K., and N.V. carried out experiments and conducted data analysis. G.D.R., D.A.D., and

S.Y.B. wrote the manuscript. D.A.D., G.D.R., S.Y.B., J.J.C., A.H., D.V.D., A.J., K.Y., G.D., and D.E. edited the manuscript.

Figures

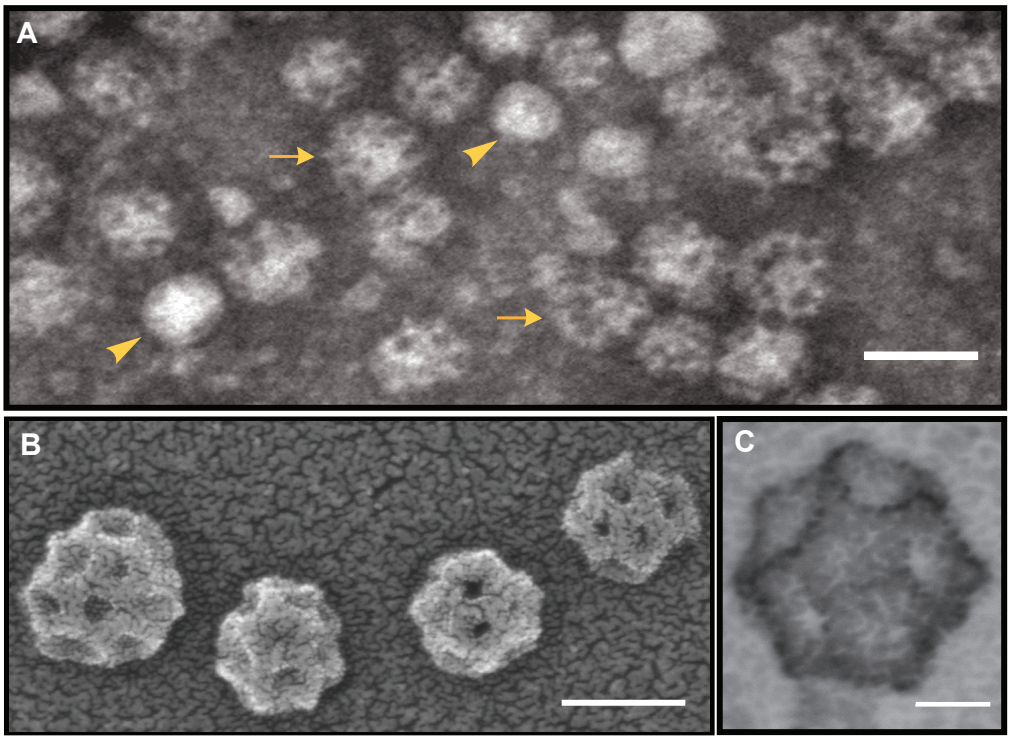

Figure 2.1 TEM of purified plant CCVs

Figure 2.1 Transmission electron microscopy of purified plant clathrin-coated vesicles.

(A) Negative stain transmission electron micrographs of a typical CCV preparation. Uncoated vesicles are indicated by arrowheads and coated vesicles by arrows.

(B) and **(C)**, Positive stain scanning transmission electron micrographs of CCVs. Scale bars (clockwise, starting top): 100, 20, and 50 nm.

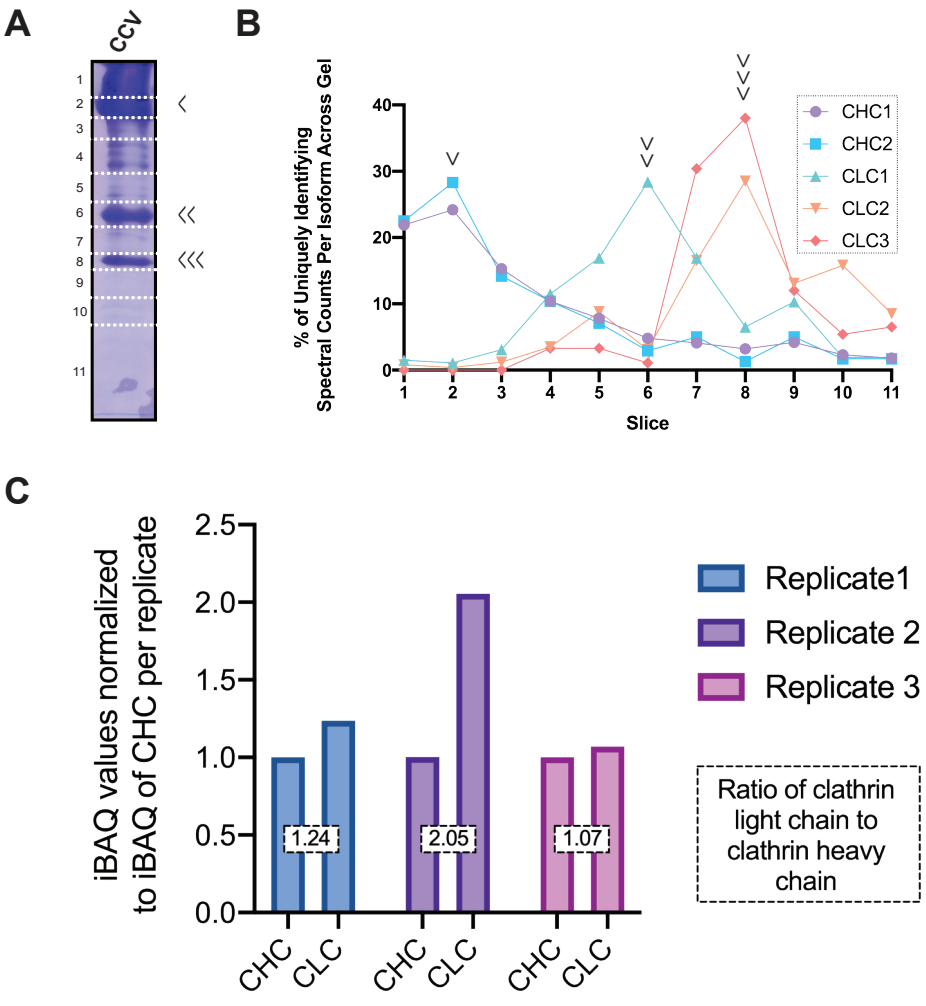

Figure 2.2 Distinction of clathrin isoforms by MS and stoichiometry of clathrin subunits

Figure 2.2 Distinction of clathrin isoforms by MS and stoichiometry of clathrin subunits

(A) Representative Coomassie stained SDS–PAGE analysis of 1 mg of clathrin-coated vesicles purified by differential centrifugation from Arabidopsis T87 suspension cultured cells. After separation by SDS– PAGE, gels were sliced along the indicated dotted lines before in-gel trypsin digest and analysis of each fragment by LC/MS–MS. The identity of abundant CCV associated proteins marked by arrowheads to the right of the gel were found to be clathrin heavy (single arrow head) and light chain isoforms (CLC1, double arrowhead; CLC2 and CLC3, triple arrowheads) based on MS and analysis in Figure 2.2B.

(B) Spectral counts attributed to a specific clathrin heavy or light chain isoform from the unlabeled LC/MS–MS analysis of the CCV purifications separated by 1D SDS-PAGE and visualized by Coomassie staining in Figure 2.2A. Peaks in the line graphs were used to assign particular clathrin heavy and light chain isoforms to the indicated bands in Figure 2.2A.

(C) Ratio of clathrin heavy chain to clathrin light chain subunits for three independent CCV purifications analyzed by LC/MS–MS without separation by one dimensional SDS–PAGE. The iBAQ value plotted on the y-axis is derived from the sums of the iBAQ intensity values assigned to clathrin light or heavy chain isoforms from the indicated replicate normalized to the sum of the iBAQ intensity value assigned to CHC for each replicate. The boxed number overlaid on the columns is the ratio of CLC:CHC for each replicate.

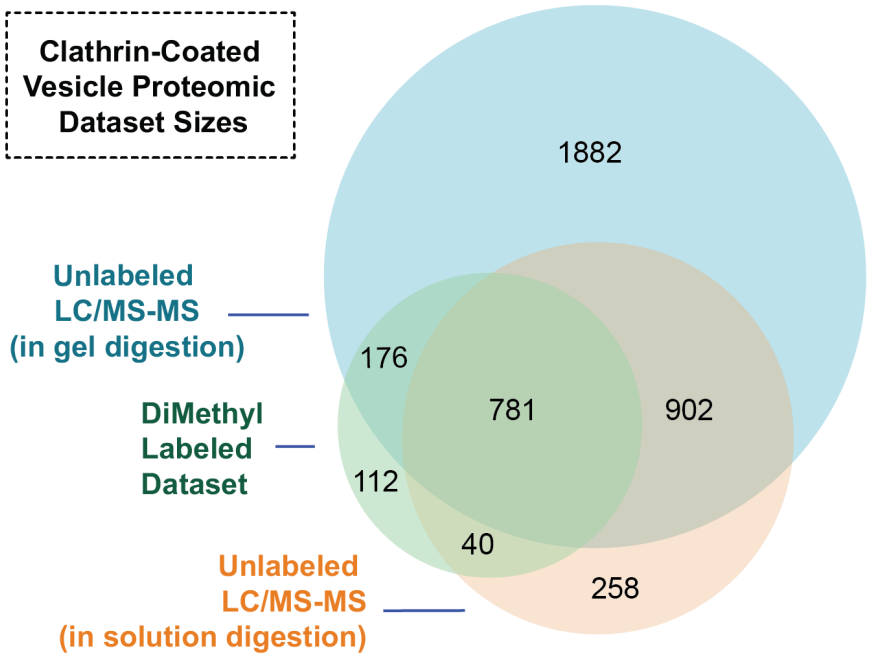

Figure 2.3 Sizes of and overlaps in proteomic datasets defining proteins associated with CCVs purified from Arabidopsis cells

Figure 2.3 Sizes of and overlaps in proteomic datasets defining proteins associated with CCVs purified from Arabidopsis cells

Four independent CCV preparations were separated by 1D SDS–PAGE before LC/MS–MS. Proteins or proteins representative of protein groups were incorporated into the unlabeled LC/MS–MS dataset (circle with largest area) if total spectral counts for the protein/protein group were present in ≥ 2 replicates (3,745 proteins). Three independent CCV preparations were not separated by SDS–PAGE but treated with urea before trypsin digest and subsequent LC/MS–MS. Protein groups were incorporated into in-solution digest, unlabeled LC/MS–MS dataset (circle with intermediate area) if they were identified in ≥ 2 replicates (1,981 protein groups); overlap with this dataset was determined using the first protein within the protein groups identified. Deuterium ficoll gradient load (DFGL) and CCV fractions from two independent preparations were reciprocally labeled with light and heavy formaldehyde before separation with SDS–PAGE and subjection to LC/MS–MS. Proteins identified in at least one replicate as increased or decreased in abundance between CCV and DFGL fractions were included in the dimethyl labeling LC/MS–MS dataset (1,109 proteins; circle with smallest area). The sizes of circles and overlaps are proportional to the number of proteins or protein groups contained within.

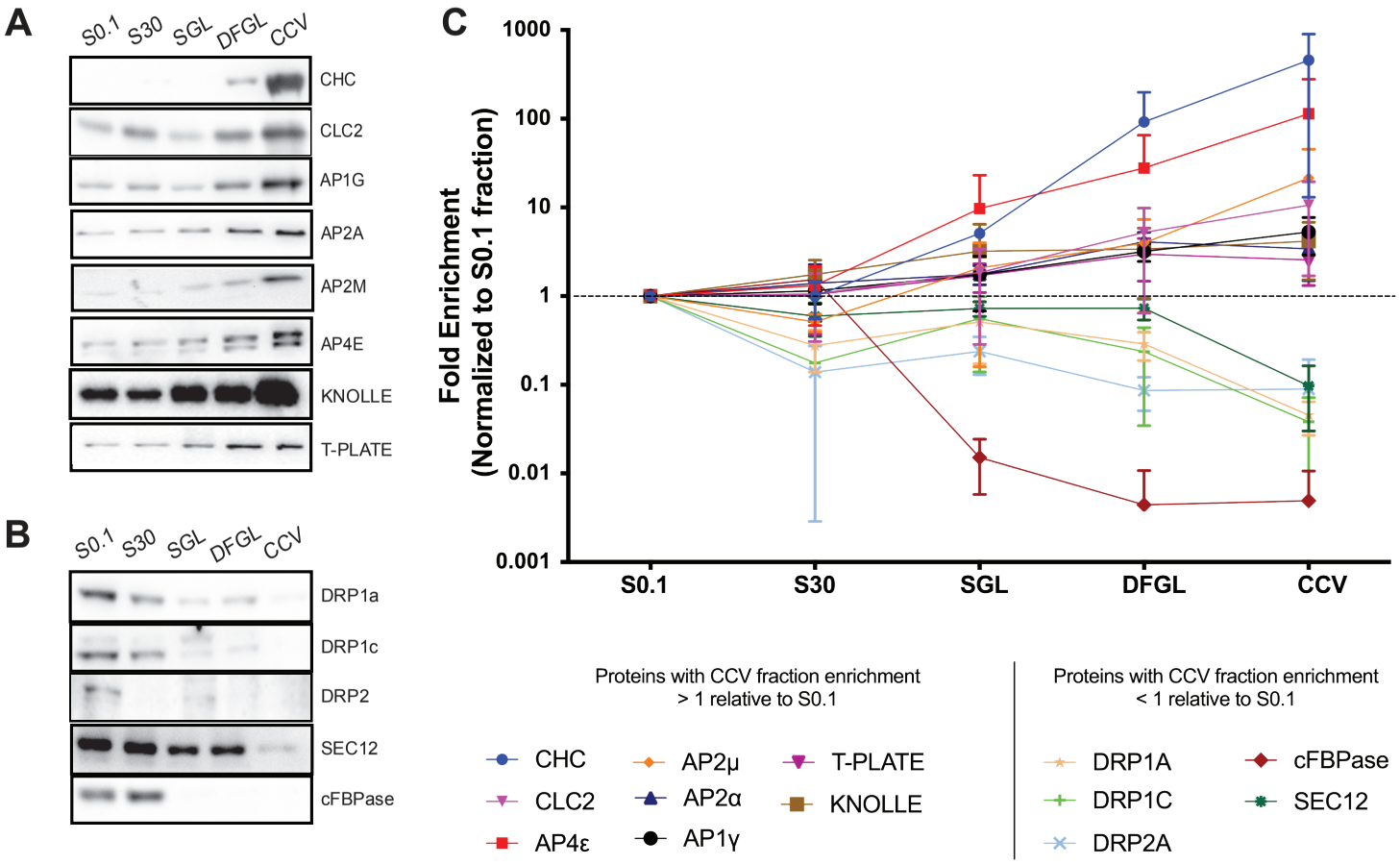

Figure 2.4 Stepwise enrichment and depletions of AP4 and trafficking and marker proteins throughout the CCV purification process

Figure 2.4 Stepwise enrichments and depletions of AP4 and trafficking and marker proteins throughout the CCV purification process

(A) Equal amounts of protein from S0.1 (lysate), S30, sucrose step-gradient load (SGL), DFGL, and CCV fractions were immunoblotted with antibodies against known CCV associated proteins (CHC, CLC2, AP1G, AP2A, AP2M, and T-PLATE) as well as AP4E and the cell plate marker, KNOLLE. These proteins were found to be enriched in the final CCV fraction relative to the lysate.

(B) Equal amounts of protein from S0.1, S30, SGL, DFGL, and CCV fractions were immunoblotted with antibodies for proteins known to be transiently associated with the CCV formation process (DRP1c, DRP1a, and DRP2) as well as for organellar markers, cFBPase (cytosol) and SEC12 (endoplasmic reticulum). These proteins were found to be depleted in the final CCV fraction relative to the lysate.

(C) Quantitation of the enrichment of proteins in (A) and (B) from three independent CCV preparations (apart from DRP2, where n = 2). The mean signal intensity of each step relative to that of the mean signal intensity in the lysate for each protein was plotted on a logarithmic scale with error bars indicating standard deviation about the mean. S0.1, lysate; S30, 30,000 x g supernatant.

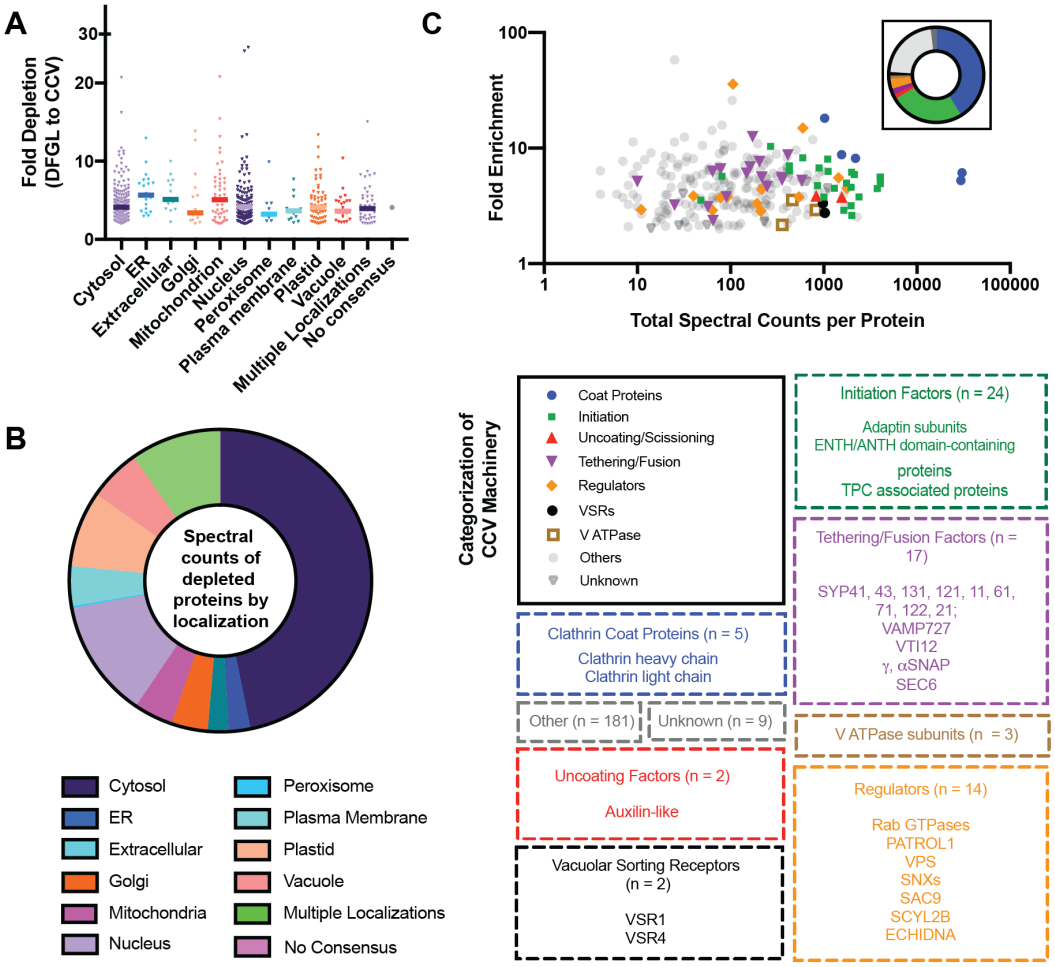

Figure 2.5: Annotations of proteins identified by shotgun CCV proteomics that were more than two-fold depleted or enriched in the last stage of the CCV purification process

Figure 2.5: Annotations of proteins identified by shotgun CCV proteomics that were more than two-fold depleted or enriched in the last stage of the CCV purification process

(A) The average fold depletions of the 546 proteins that were more than two-fold depleted between the DFGL and CCV fractions and which overlapped with the CCV LC/MS–MS dataset deriving from 1D SDS–PAGE separation were plotted against the consensus subcellular localizations of the corresponding accession numbers predicted by the SUBA algorithm based on experimental and computational data.

(B) Proportion of total spectral counts across four independent CCV preparations for each ≥ 2-fold depleted protein also present in the CCV LC/MS–MS dataset deriving from 1D SDS–PAGE separation as categorized by SUBA annotated subcellular localization.

(C) The average fold enrichments of the 257 proteins that were ≥ 2-fold enriched between the DFGL and CCV fractions and that overlapped with the CCV LC/ MS–MS dataset deriving from 1D SDS–PAGE separation were plotted against the sum of the total spectral counts of each corresponding protein across four independent CCV preparations. Functional categorization of these proteins was manually annotated; the size and composition of each functional category are indicated below. The inset depicts the relative abundance of each functional category by summing and graphing the total spectral counts assigned to proteins within that functional category.

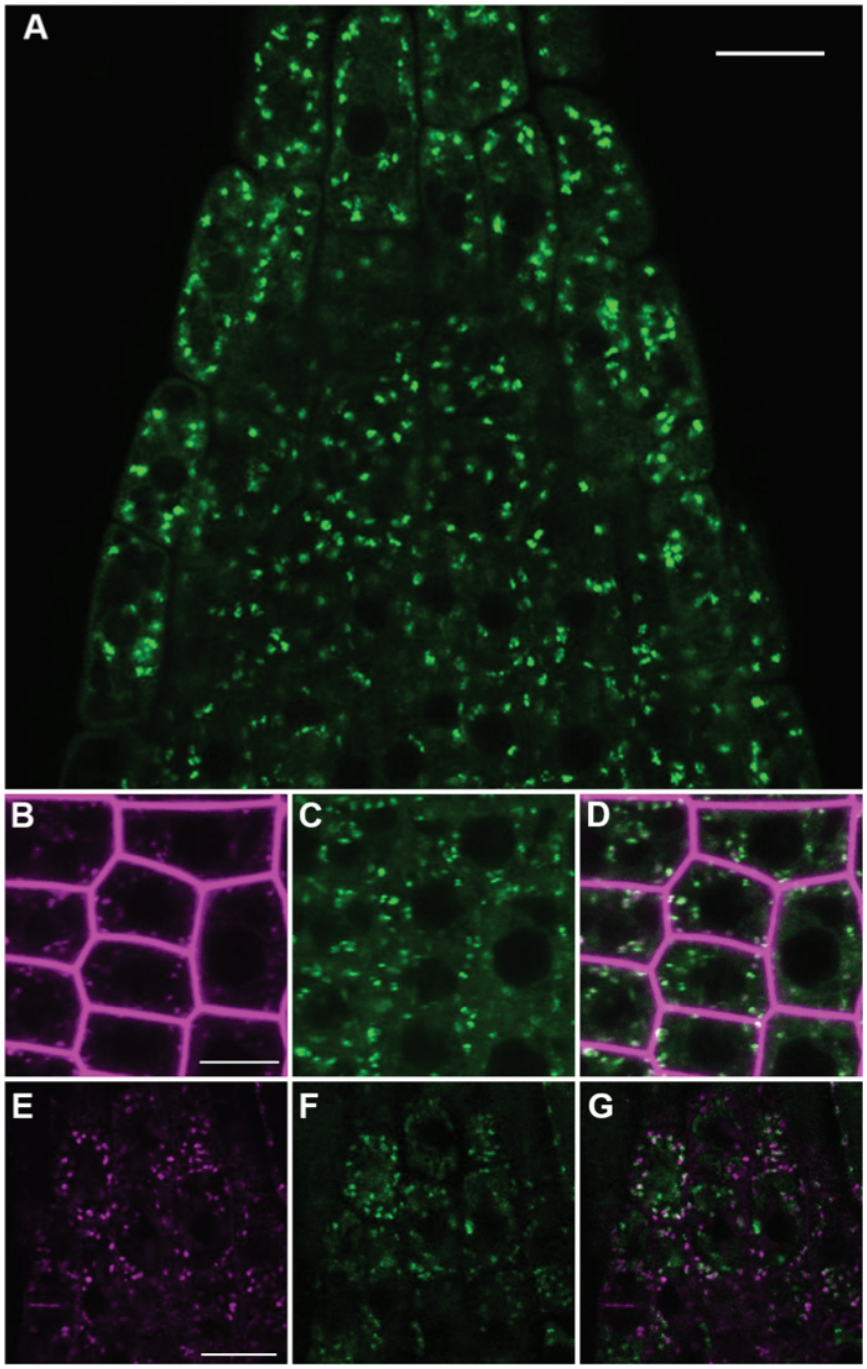

Figure 2.6 AP4E colocalizes with FM4-64 and clathrin at the TGN

Figure 2.6 AP4E colocalizes with FM4-64 and clathrin at the TGN

(A) ProUB10:GFP-AP4E expressed in homozygous *ap4e-2* knockout lines has a primarily cytosolic and endomembrane localization in epidermal cells of root tips.

(B) TGN/EE labeled with FM4-64 after 6 min incubation colocalizes with ProUB10:RFP-AP4E in homozygous *ap4e-2* knockouts **(C)**; **(D)** Merge (Costes P-value, 1.00; Pearson's correlation coefficient, 0.705).

(E) ProCLC2:CLC2-GFP and ProUB10:RFP-AP4E **(F)** colocalize at the TGN but not at the PM nor cell plate; **(G)** Merge (Costes P-value, 1.00; Pearson's correlation coefficient, 0.37). Scale bars = 10 μm.

Protein Name	Average Fold Enrichment of CCV Relative to DFGL	
	Immunoblot	Dimethyl Labeling
CHC	5.15 ± 2.37	5.68 ± 1.48
AP4E	3.14 ± 1.10	3.18 ± 0.60
CLC2	2.07 ± 0.14	18.17 ± 13.70
AP2M	4.33 ± 1.91	2.89
AP1G	1.69 ± 0.53	5.28 ± 0.72
KNOLLE	1.29 ± 0.15	6.28 ± 4.87
T-PLATE	0.88 ± 0.28	0.53
AP2A	0.84 ± 0.30	2.62 ± 1.06
cFBPase	0.77 ± 0.43	-
SEC12	0.13 ± 0.06	-
DRP1A	0.16 ± 0.02	-
DRP1C	0.32 ± 0.34	-
DRP2A	0.87 ± 0.59	-

Table 2.1 Enrichment and depletion profiles of CCV-associated proteins and organellar markers

Table 2.1 Enrichment and depletion profiles of CCV associated proteins and organellar markers.

The ratio of protein levels in the CCV fraction relative to levels in the DFGL fraction (without normalizing to levels in the S0.1 fraction) are presented alongside standard deviation about the mean. For average ratios derived by immunoblotting, n = 3 biological replicates, except for DRP2 (n = 2). For dimethyl labeling values, a dash in the right-hand column indicates the protein was not detected in the labeling datasets. An absence of standard deviation about the mean in the right-hand column indicates the protein was present in only one of two replicates.

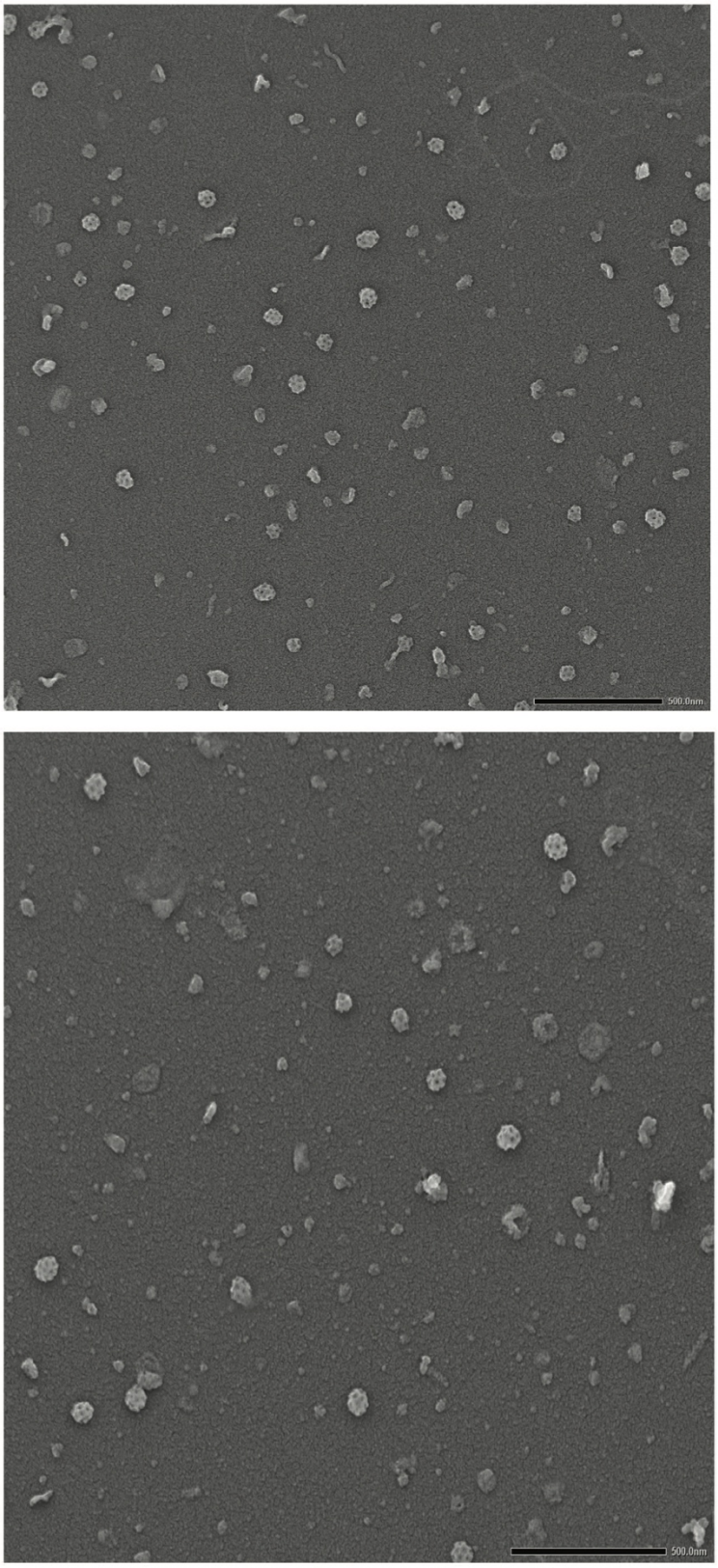

Figure 2S1: Transmission Electron Microscopy of CCVs

Figure 2S1: Transmission Electron Microscopy of CCVs

Representative images collected by scanning transmission electron microscopy of CCVs purified by differential centrifugation from T87 suspension cultured Arabidopsis cells. Scale bar: 500 nm.

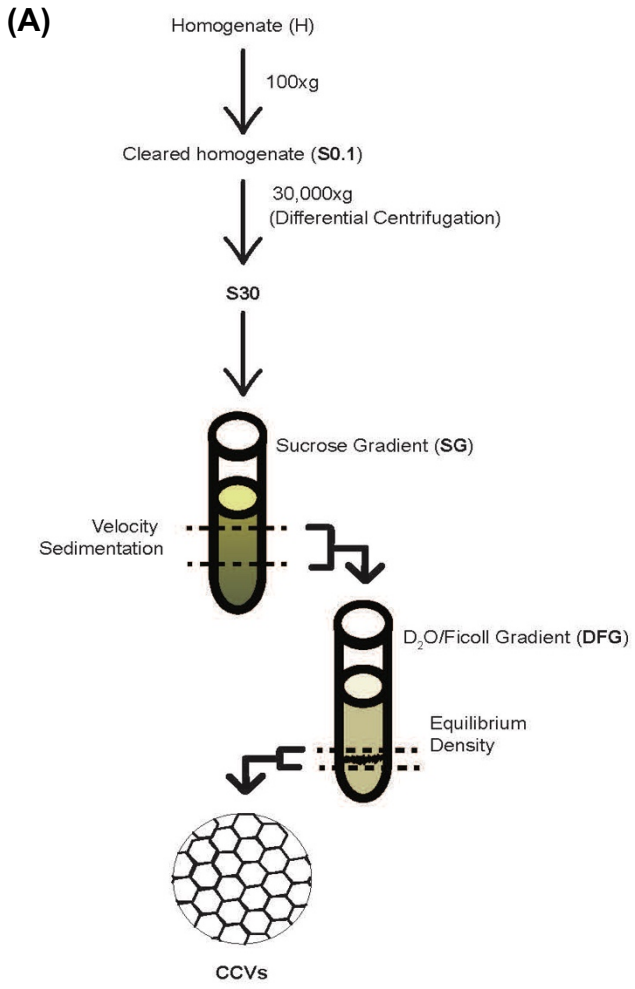

Figure 2S2: Schematics illustrating protocol for clathrin coated vesicle purification and workflows detailing the CCV proteome

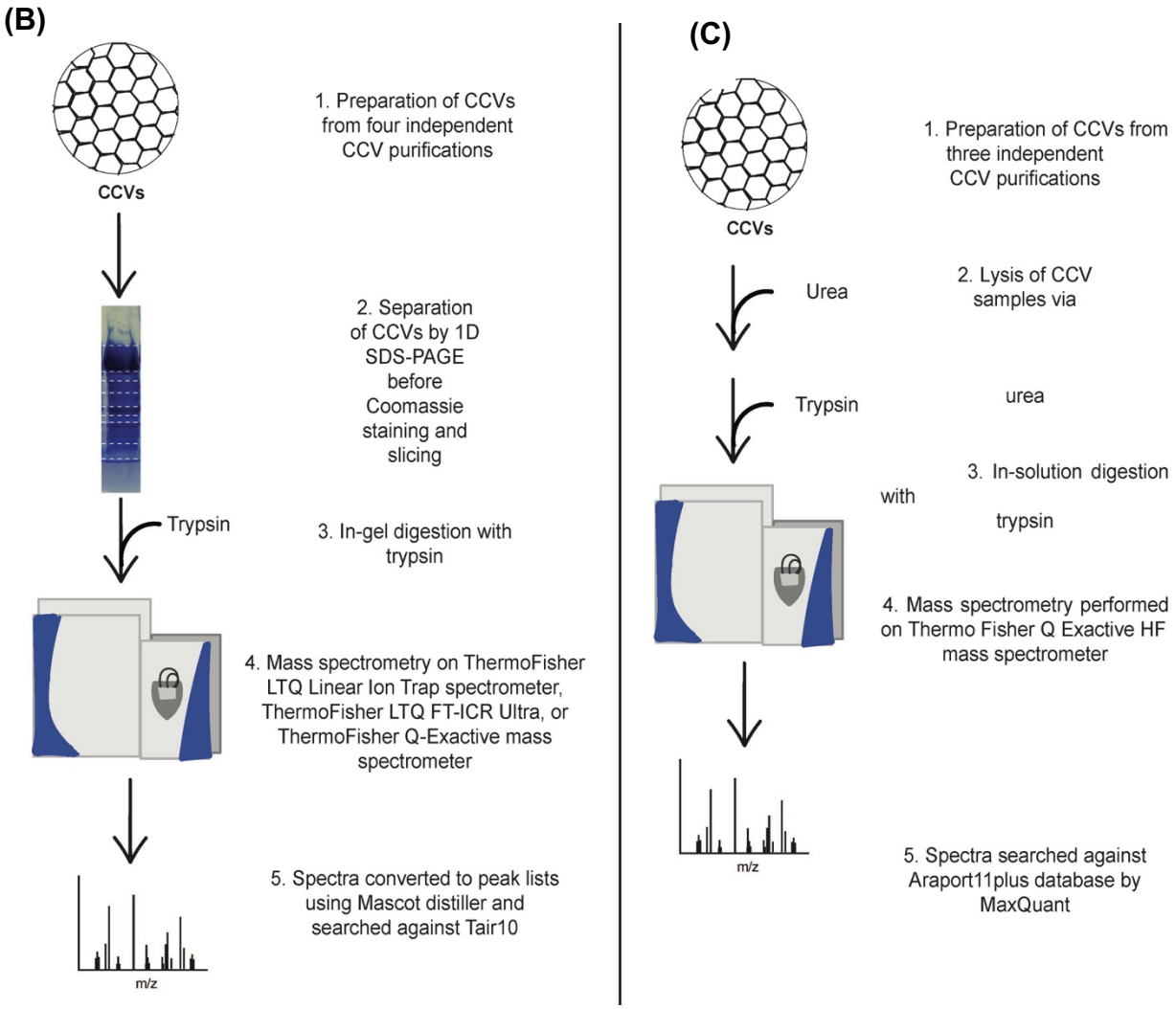

Figure 2S2: Schematics illustrating protocol for clathrin coated vesicle purification and workflows detailing the CCV proteome

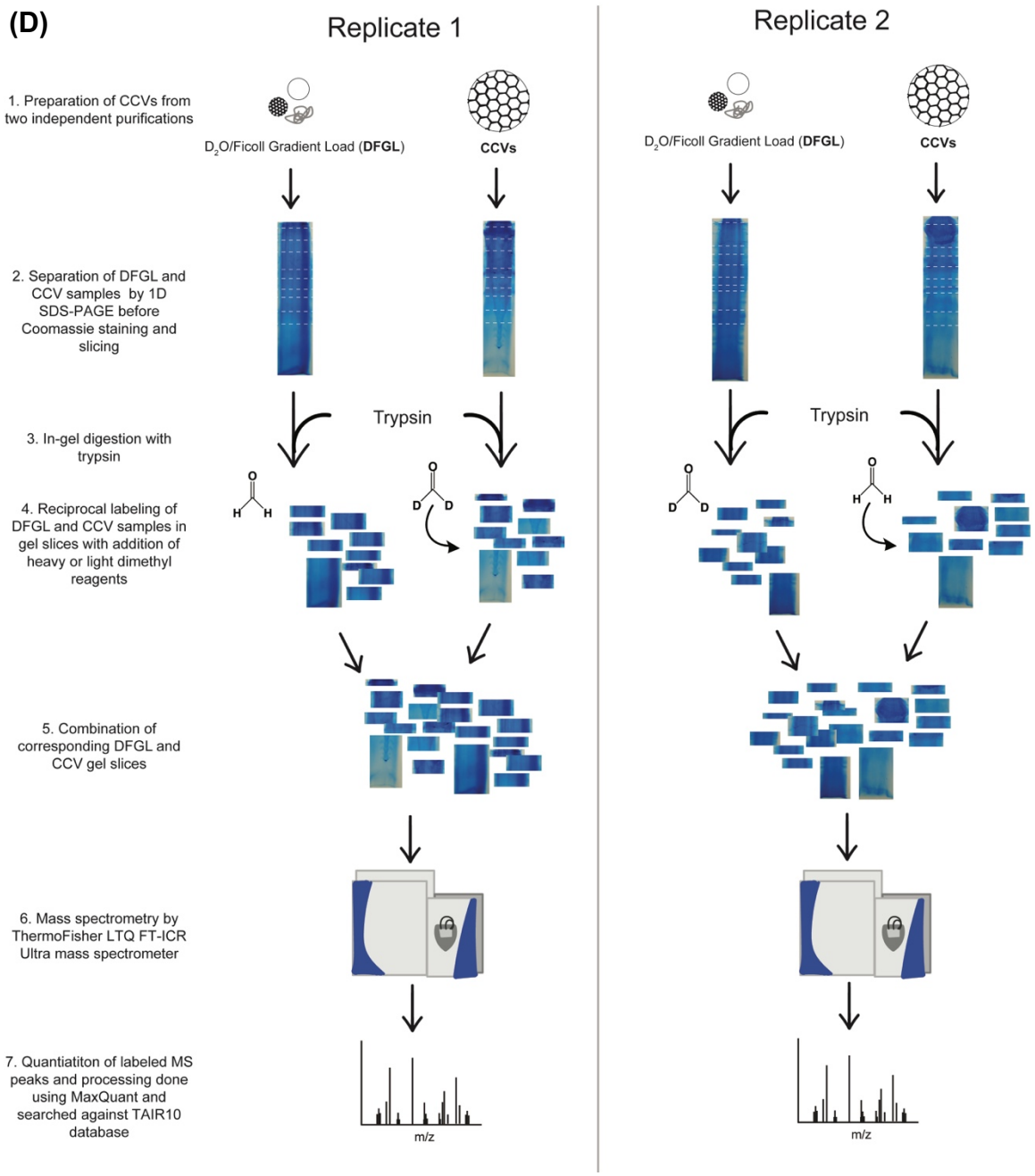

Figure 2S2: Schematics illustrating protocol for clathrin coated vesicle purification and workflows detailing the CCV proteome

Figure 2S2: Schematics illustrating protocol for clathrin coated vesicle purification and workflows detailing the CCV proteome.

(A) Abbreviated protocol for purification of clathrin coated vesicles from Arabidopsis T87 suspension cultured cells (adapted from Reynolds, et al. *MMB*. 2014). Steps in the purification process which were immunoblotted are highlighted in bold.

(B) Proteomic workflow leading to collection of CCV proteomic dataset shown in Supplemental Dataset 1 and described in Materials & Methods.

(C) Proteomic workflow leading to collection of CCV proteomic dataset shown in Supplemental Dataset 2 and described in Materials & Methods.

(D) Proteomic workflow leading to collection of enrichment/depletion CCV proteomic dataset shown in Supplemental Dataset 3 and described in Materials & Methods.

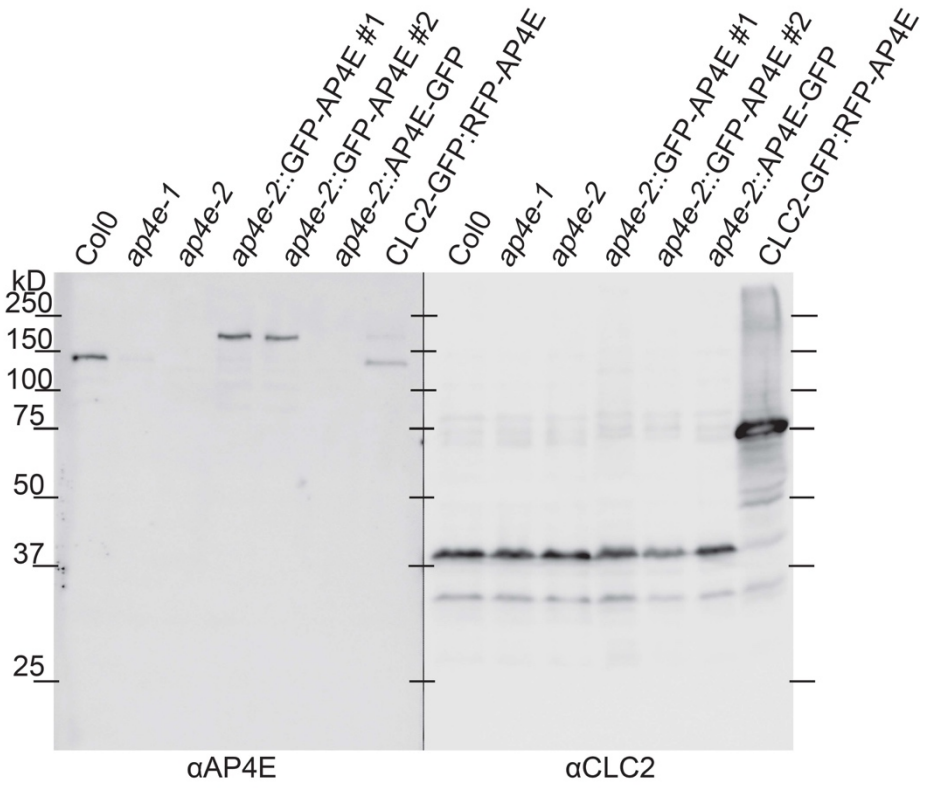

Figure 2S3: AP4E antibody is specific for the AP4E subunit

Figure 2S3: AP4E antibody is specific for the AP4E subunit

Equal amounts of total protein extract from Arabidopsis seedlings were probed with αAP4E to demonstrate specificity and αCLC2 as a loading control. αAP4E recognizes the AP4E large subunit in wild type (Col0) and wild-type plants transformed with *proUB10:RFP-AP4E* and *proCLC2:CLC2-GFP* (CLC2-GFP:RFP-AP4E), but not in plants homozygous for either the *ap4e-1* or *ap4e-2* t-DNA alleles (*ap4e-1*, *ap4e-2*, *ap4e- 2:GFP-AP4E #1*, *ap4e-2:GFP-AP4E #2*, *ap4e-2:AP4E-GFP*). The larger GFP RFP fusion proteins were detected by αAP4E in plants transformed with *pUBN:GFP-AP4E* (two independent transformants, *ap4e-2:GFP-AP4E #1, ap4e-2:GFP-AP4E #2*) or *proUB10:AP4e-GFP (ap4e-2:AP4E-GFP).*

Figure 2S4: *proUB10:GFP-AP4E* is functional *in vivo*

Figure 2S4: *proUB10:GFP-AP4E* is functional *in vivo*

(A) *ap4e-2* homozygotes display abnormal growth defects including stunted/aborted siliques.

(B) *ap4e-2* homozygotes transformed with *proUB10:GFP-AP4E* display phenotypically wild-type inflorescences.

(C) *ap4e-2* homozygotes are overall dwarfed.

(D) *proUB10:GFP-AP4E* rescues the dwarf phenotype of *ap4e-2* homozygotes. Each plant in **D** derives from an independent transformant.

Antibodies	Clonality	Primary Dilution for Immunoblot	Secondary	Secondary Dilution	Citation in Manuscript
anti-CLC2	polyclonal	1:10000	Rabbit	1:5000	Backues. Dissertation, University of Wisconsin-Madison. 2010
anti-CHC	monoclonal	1:1000	Mouse	1:5000	Santa Cruz Biotechnology, sc-57684
anti-AP2A	polyclonal	1:500	Rabbit	1:5000	Song et al. *Plant Physiology* 2012
anti-AP1G	polyclonal	1:2000	Rabbit	1:5000	Park et al. *PNAS.* 2013
anti-AP2M	polyclonal	1:250	Rabbit	1:5000	Wang et al. *Plant Physiol.* 2016
anti-KNOLLE	polyclonal	1:1000	Rabbit	1:5000	Rancour et al. *Plant Physiol.* 2002
anti-TPLATE	polyclonal	1:1000	Rabbit	1:5000	Dejonghe et al. *Nature Chem Biol.* 2019
anti-SEC12	polyclonal	1:1000	Rabbit	1:5000	Bar-Peled and Raikhel. *Plant Physiol.* 1997
anti-DRP1A	polyclonal	1:500	Rabbit	1:5000	Kang et al. *Plant Physiol.* 2001
anti-DRP1C	polyclonal	1:500	Rabbit	1:5000	Kang et al. *Plant Journal* 2003
anti-DRP2	polyclonal	1:5000	Rabbit	1:5000	Backues et al. *Plant Cell.* 2010.
anti-cFBPase	polyclonal	1:5000	Rabbit	1:5000	Agrisera, AS04 043
anti-AP4E	recombinant	1:100	Mouse	1:5000	This manuscript

Table 2S1: Antibodies used in this study

Table 2S1: Antibodies used in this study

Information describing the antibodies used in this study are presented (clonality, dilution factor of the primary antibody, secondary antibody information, and citation).

			Total Spectral Counts					Fold Enrichment (CCV:DFGL)			iBAQ Values			
Accession	Label	MW	Rep 1	Rep 2	Rep 3	Rep 4	Sum	Rep 1	Rep 2	Average	Rep 1	Rep 2	Rep 3	Sum
Clathrin														
AT3G11130	CHC1	193	2341	3684	13959	10441	30,425	7.34	4.88	6.11	6.7E+08	6.8E+08	2.6E+08	1.6E+09
AT3G08530	CHC2	193	2288	3430	13683	10174	29,575	6.82	3.67	5.25	6.7E+08	6.6E+08	2.4E+08	1.6E+09
AT2G20760	CLC1	37	175	239	918	857	2,189	3.57	12.77	8.17	8.9E+08	1.6E+09	2.5E+08	2.7E+09
AT2G40060	CLC2	29	36	95	533	358	1,022	4.47	31.87	18.17	6.2E+08	1.0E+09	2.6E+08	1.9E+09
AT3G51890	CLC3	29	16	7	895	635	1,553	11.07	6.49	8.78	1.4E+08	1.8E+08	2.0E+07	3.4E+08
Adaptins														
AT4G11380	AP1/2B1	99	181	355	2061	1444	4,041	3.53	7.65	5.59	7.1E+07	5.9E+07	1.8E+07	1.5E+08
AT4G23460	AP1/2B2	99	124	242	1981	1410	3,757	4.13	4.81	4.47	1.9E+07	1.7E+07	1.1E+07	4.7E+07
AT1G60070	AP1G1	95	222	224	1784	1792	4,022	5.06	6.20	5.63	9.5E+07	1.2E+08	2.9E+07	2.5E+08
AT1G23900	AP1G2	96	223	411	1949	1462	4,045	4.25	5.61	4.93	3.4E+07	4.5E+07	2.4E+07	1.0E+08
AT1G10730	AP1M1	49	91	83	498	431	1,103		8.02	8.02	3.8E+05	5.4E+05	6.2E+04	9.8E+05
AT1G60780	AP1M2	49	161	505	999	726	2,391	3.07	4.50	3.78	5.0E+07	6.6E+07	2.2E+07	1.4E+08
AT2G17380	AP1S1	19	35	59	189	145	428		7.01	7.01	5.0E+07	7.9E+07	1.0E+07	1.4E+08
AT4G35410	AP1S2	19	6	11	152	99	268	10.33		10.33	2.8E+06	6.9E+06	1.3E+06	1.1E+07
AT5G22770	AP2A1	112	61	123	1022	837	2,043				1.5E+06	1.2E+06	5.4E+05	3.3E+06
AT5G22780	AP2A2	112	88	84	1071	759	2,002	1.56	3.68	2.62	3.4E+06	2.7E+06	3.3E+05	6.4E+06
AT5G46630	AP2M	49	102	399	568	579	1,648		2.89	2.89	2.0E+07	2.1E+07	3.9E+06	4.4E+07
AT1G47830	AP2S	17	1	4	39	37	81		5.71	5.71	2.8E+07	2.7E+07	2.9E+06	5.7E+07
AT1G48760	AP3D	97	5	0	68	56	129							
AT1G56590	AP3M	46	3	0	15	11	29							
AT5G11490	AP4B	93	73	232	412	399	1,116		6.27	6.27	4.5E+07	6.4E+07	9.0E+06	1.2E+08
AT1G31730	AP4E	104	89	612	613	654	1,968	3.30	5.86	4.58	6.4E+07	8.7E+07	1.3E+07	1.6E+08
AT4G24550	AP4M	51	104	493	649	714	1,960	3.47	2.88	3.17	2.9E+07	4.1E+07	6.6E+06	7.7E+07
AT2G19790	AP4S	17	0	58	58	250	366				5.6E+07	8.7E+07	2.6E+06	1.5E+08
AT3G19870	AP5B	122	0	0	8	5	13							
AT2G20790	AP5M	67	0	0	8	2	10							
TPC														
AT3G01780	TPLATE	131	1	1	147	83	232		0.53	0.53	6.1E+06	5.3E+06	1.3E+06	1.3E+07
AT1G20760	AthEH1	110	3	2	65	65	135				3.4E+05	7.9E+05	1.2E+05	1.3E+06
AT1G21630	AtEH2	132	0	10	75	31	116				2.7E+06	3.0E+06	9.3E+05	6.6E+06
AT2G07360	TASH3	130	0	25	125	78	228		1.29	1.29	6.6E+06	8.1E+06	2.2E+06	1.7E+07
AT5G57460	TML	71	38	58	81	45	222		1.38	1.38	3.4E+06	4.3E+06	9.5E+05	8.7E+06
AT3G50590	TWD40-1	176	10	15	129	59	213		0.20	0.20	4.4E+06	4.2E+06	7.3E+05	9.4E+06
AT5G24710	TWD40-2	148	60	93	173	228	554		0.25	0.25	8.2E+06	9.0E+06	2.7E+06	2.0E+07
AT1G15370	LOLITA	17	0	0	1	2	3							
DRPs														
AT5G42080	DRP1A	68	0	1	13	10	24				7.2E+05	7.5E+05	0.0E+00	1.5E+06
AT1G14830	DRP1C	69	0	0	23	13	36							
AT3G60190	DRP1E	70	0	0	16	20	36							
AT1G10290	DRP2A	99	0	0	12	5	17							
AT1G59610	DRP2B	100	0	0	12	9	21							
ENTH/ANTH														
AT2G01600	AtECA1	64	2	21	440	393	856	2.66	6.79	4.72	1.9E+07	2.3E+07	2.3E+06	4.5E+07
AT1G03050	AtECA2	67	0	0	22	24	46							
AT2G25430	AtECA4	72	124	333	928	611	1,996	3.78	8.61	6.19	2.0E+07	3.0E+07	1.5E+06	5.2E+07
AT4G32285	CAP1	71	168	271	930	757	2,126	6.04	5.78	5.91	3.3E+07	4.9E+07	4.4E+06	8.6E+07
AT2G38410	TOL6	72	62	328	327	288	1,005	3.52	4.03	3.78	3.7E+06	4.7E+06	7.4E+05	9.1E+06
AT4G32760	TOL9	73	21	69	213	124	427	8.88	3.86	6.37	1.4E+07	1.4E+07	8.7E+06	3.7E+07
AT3G59290	EPSIN3	110	35	33	228	170	466				6.0E+05	9.8E+05	3.1E+05	1.9E+06
AT5G35200	PICALM3	61	4	6	40	29	79				2.1E+05	6.3E+05	0.0E+00	8.4E+05
AT1G14910	PICALM1B	76	26	72	150	91	339				1.3E+06	1.4E+06	2.9E+05	2.9E+06
AT5G63640	TOL5	49	0	0	22	16	38							
AT5G01760	TOL7	60	0	0	21	21	42							
AT4G25940	PICALM2B	68	4	6	43	32	85							
AT5G11710	EpsinR1	61	113	159	745	733	1,750	3.31	6.66	4.98	1.1E+08	1.7E+08	3.3E+07	3.2E+08

Table 2S2: LC/MS-MS data corresponding to discussed proteins.

			Total Spectral Counts					Fold Enrichment (CCV:DFGL)			iBAQ Values			
Accession	Label	MW	Rep 1	Rep 2	Rep 3	Rep 4	Sum	Rep 1	Rep 2	Average	Rep 1	Rep 2	Rep 3	Sum
AT2G43160	EpsinR2	95	104	304	461	428	1,297	4.32	4.68	4.50	3.0E+07	4.0E+07	1.0E+07	8.1E+07
AT3G16270	MTV1	75	51	45	516	277	889		6.74	6.74	1.7E+07	2.6E+07	9.6E+06	5.3E+07
SNAREs														
AT1G77140	VPS45	65	32	76	274	200	582		5.25	5.25	5.9E+06	3.2E+06	2.1E+06	1.1E+07
AT1G28490	SYP61	28	3	3	128	83	217	3.65	7.54	5.60	5.3E+06	8.8E+06	2.5E+06	1.7E+07
AT3G09740	SYP71	30	20	63	163	110	356	2.66	8.43	5.55	4.2E+07	4.0E+07	1.6E+06	8.3E+07
AT3G54300	VAMP727	27	0	15	201	141	357	2.54	8.06	5.30	5.4E+07	7.4E+07	6.3E+06	1.3E+08
AT2G33120	VAMP722	26	1	13	130	102	246	2.06	7.20	4.63	2.7E+06	2.3E+06	3.6E+05	5.4E+06
AT5G08080	SYP132	34	0	1	128	76	205		7.63	7.63	1.4E+08	1.1E+08	3.7E+06	2.6E+08
AT3G05710	SYP43	37	33	73	161	145	412		8.72	8.72		9.5E+05	5.3E+04	1.0E+06
AT3G11820	SYP121	38	4	10	66	82	162		6.86	6.86	2.4E+06	2.2E+06	8.1E+04	4.8E+06
AT5G11150	VAMP713	25	15	26	53	79	173	0.23	0.18	0.21	1.6E+07	5.8E+06	2.0E+06	2.4E+07
AT4G02195	SYP42	36	4	9	153	140	306				9.3E+05	6.1E+05	1.4E+05	1.7E+06
AT5G46860	SYP22	29	0	3	72	66	141				1.9E+07	1.5E+07	9.7E+05	3.5E+07
AT1G48240	NPSN12	30	0	2	13	17	32				8.4E+06	1.2E+07	0.0E+00	2.0E+07
AT1G08560	KNOLLE	35	2	6	30	26	64	1.41	11.15	6.28				
AT5G26980	SYP41	36	0	5	94	73	172		12.55	12.55		9.6E+05		9.6E+05
AT5G22360	VAMP714	25	0	10	13	9	32		0.31	0.31	2.1E+06		2.3E+05	2.4E+06
AT4G15780	VAMP724	25	0	1	7	3	11							
AT1G26670	VTI12	25	0	0	43	35	78	6.59		6.59				
AT5G39510	VTI11	25	1	4	18	16	39	0.39	1.60	1.00	4.0E+06	2.8E+06	9.9E+05	7.7E+06
AT3G52400	SYP122	38	0	1	7	2	10		5.15	5.15	2.4E+07	1.5E+07	2.9E+04	3.9E+07
AT1G04750	VAMP721	25									2.1E+06	2.1E+06	0.0E+00	4.2E+06
AT5G16830	SYP21	31	0	0	41	24	65		2.36	2.36				
AT4G32150	VAMP711	25	0	1	6	0	7							
AT1G16240	SYP51	26	0	0	28	19	47							
AT3G17440	NPSN13	30	0	0	87	62	149		6.05	6.05	1.2E+07	1.4E+07	0.0E+00	2.6E+07
AT1G79590	SYP52	26	0	0	23	18	41							
AT5G61210	SNAP33	34	2	0	22	15	39							
AT2G35190	NPSN11	30	0	0	23	75	98				1.8E+06	7.2E+05	0.0E+00	2.5E+06
AT1G04760	VAMP726	25	7	2	44	35	88							
AT1G80500	TRAPPC2	15	0	0	12	12	24		0.39	0.39				
VSRs														
AT3G52850	VSR1	69	60	93	428	401	982	3.68	2.99	3.33	4.2E+07	5.5E+07	7.4E+06	1.0E+08
AT2G14740	VSR3	70	58	146	442	218	864				8.4E+05	8.2E+05	8.6E+05	2.5E+06
AT2G14720	VSR4	70	83	73	469	403	1,028	1.47	4.03	2.75	6.0E+06	8.0E+06	2.2E+06	1.6E+07
AT1G30900	VSR6	70	0	1	2	2	5							
AT4G20110	VSR7	70	8	0	105	59	172							
LRRK-RLKs														
AT5G46330	FLS2	129	0	0	41	60	101							
AT4G33430	BAK1	74	1	1	11	17	30				4.0E+06	2.6E+06	0.0E+00	6.6E+06
AT2G01820		102	98	401	593	590	1,682	2.93	3.51	3.22	9.5E+07	7.4E+07	1.3E+07	1.8E+08
AT3G49490		105	32	77	274	207	590		5.08	5.08	2.5E+06	4.0E+06	5.6E+06	1.2E+07
AT3G02880	KIN7	68	69	117	277	404	867	2.49	5.94	4.22	2.5E+07	1.9E+07	6.2E+05	4.5E+07
AT4G08850	MIK2	115	33	98	268	148	547	2.67	4.82	3.74	4.8E+07	4.2E+07	3.0E+06	9.3E+07
AT1G11130		84	11	15	106	73	205		5.32	5.32	1.2E+07	8.9E+06	7.6E+04	2.1E+07
AT5G16590		67	3	1	179	184	367		2.98	2.98	3.4E+06	3.2E+06	0.0E+00	6.6E+06
AT5G49760		105	0	2	5	1	8				1.9E+05	1.3E+05	0.0E+00	3.3E+05
AT5G58150		87	0	0	27	17	44							
AT3G23750		100	18	28	127	139	312				7.0E+06	3.0E+06	4.4E+04	1.0E+07
AT1G33590		52	0	48	123	178	349	0.08	0.24	0.16	6.4E+07	3.7E+07	7.0E+06	1.1E+08
AT1G27190		65	27	68	51	39	185		0.74	0.74	3.1E+06	3.8E+05	0.0E+00	3.4E+06
AT2G37050		104	9	2	76	67	154				4.6E+06	3.7E+06	0.0E+00	8.3E+06
AT5G05160		71	25	10	83	45	163				2.4E+06	1.6E+06	0.0E+00	3.9E+06
AT1G56140		114	0	1	53	15	69				1.2E+06	9.7E+05	0.0E+00	2.1E+06
AT2G26730		72	60	27	56	64	207				1.2E+06	4.6E+05	0.0E+00	1.6E+06
AT5G10290		69	0	11	31	34	76				6.1E+05	4.0E+05	0.0E+00	1.0E+06
AT3G28450		67	4	9	29	32	74		2.23	2.23	9.1E+06	4.7E+06	0.0E+00	1.4E+07
AT1G06840		106	0	6	27	29	62		1.81	1.81	8.9E+05	3.3E+05	2.7E+04	1.2E+06
AT5G65700		109	10	6	29	18	63				1.2E+06	4.1E+05	5.4E+04	1.6E+06
AT2G36570		74	0	1	36	28	65				6.0E+06	2.7E+06	0.0E+00	8.7E+06

Table 2S2: LC/MS-MS data corresponding to discussed proteins.

			Total Spectral Counts					Fold Enrichment (CCV:DFGL)			iBAQ Values			
Accession	Label	MW	Rep 1	Rep 2	Rep 3	Rep 4	Sum	Rep 1	Rep 2	Average	Rep 1	Rep 2	Rep 3	Sum
AT2G16250		100	5	9	20	16	50				1.8E+06	1.2E+06	0.0E+00	3.0E+06
AT5G10020		115	3	1	27	14	45				1.1E+06	8.0E+05	0.0E+00	1.9E+06
AT4G22730		76	9	16	22	24	71				9.7E+05	4.0E+05	0.0E+00	1.4E+06
AT2G41820		97	4	1	14	10	29				2.1E+06	1.9E+07	0.0E+00	2.1E+07
AT1G51850		96	2	0	69	44	115							
AT5G07910			0	0	31	28	59		6.76	6.76				
AT3G14350		78	0	1	11	8	20				1.5E+06	1.6E+06	0.0E+00	3.0E+06
AT3G14840		112	0	14	38	65	117							
AT4G20940		105	0	3	10	5	18							
AT5G62710		67	0	2	3	4	9							
AT4G34220		83	8	0	57	9	74							
AT5G67200		74	0	1	9	4	14							
AT3G08680		69	0	1	1	2	4							
AT3G47570		111	0	2	2	8	12							
AT1G63430		74	0	0	70	71	141							
AT5G65240		68	1	18	23	7	49							
AT1G53430		114	0	5	19	6	30							
AT1G31420		65	0	0	28	34	62							
AT5G21090		24	4	0	11	10	25							
AT5G14210		86	0	0	14	9	23							
AT1G67720		104	0	0	7	21	28							
AT2G24230		94	0	2	10	19	31							
AT1G68400		74	0	0	36	26	62							
AT5G01890		104	0	0	21	24	45							
AT1G09970		107	0	0	12	5	17							
AT1G10850		73	0	0	9	11	20							
AT4G23740		71	0	0	17	6	23							
AT4G36180		124	4	0	14	4	22							
AT2G25790		106	0	0	19	15	34							
AT2G31880		71	0	6	9	6	21							
AT1G56145		112	0	2	17	10	29							
AT2G35620		64	1	0	19	52	72							
AT5G58300		72	0	0	33	39	72							
AT2G27060		110	0	0	6	1	7				3.5E+05	1.1E+05	0.0E+00	4.7E+05
AT5G53320		67	0	0	2	1	3							
AT1G53440		115	0	2	12	11	25							
AT1G25320		76	0	0	9	17	26							
AT1G15740		64	0	0	3	5	8							
CDPKs														
AT4G04720	CPK21	60	54	54	389	326	823	3.90	6.80	5.35	3.6E+07	2.1E+07	1.8E+06	5.9E+07
AT4G23650	CPK3	59	54	130	205	280	669		2.64	2.64	2.2E+07	8.2E+06	1.1E+05	3.0E+07
AT3G57530	CPK32	61	0	1	67	37	105				2.7E+06	2.0E+06	0.0E+00	4.6E+06
AT4G04700	CPK27	55	0	7	45	40	92		3.20	3.20				
AT5G24430	CPK	67	0	2	25	27	54		3.13	3.13				
AT3G49370	CPK	66	0	1	4	3	8							
AT1G49580	CPK	68	0	0	36	20	56							
AT5G19450	CDPK19	60	4	11	40	26	81				2.4E+06	1.8E+06	0.0E+00	4.2E+06
AT5G04870	CPK1	68	0	0	4	10	14							
AT3G51850	CPK13	59	4	8	7	1	20				6.1E+06	3.4E+06	0.0E+00	9.5E+06
AT4G21940	CPK15	63	34	11	179	133	357							
AT4G04740	CPK23	59	0	1	80	65	146							
AT5G66210	CPK29	59	6	0	34	16	56							
AT1G76040	CPK29	64	3	14	94	76	187							
AT1G74740	CPK30	61	6	2	12	12	32							
AT4G04695	CPK31	55	0	1	7	2	10							
AT1G50700	CPK33	59	0	2	39	49	90							
AT2G17290	CPK6	61	0	0	8	1	9							
AT5G12480	CPK7	60	4	3	18	10	35				2.1E+06	1.1E+06	0.0E+00	3.2E+06
CrRLK1Ls														
AT5G24010		92	26	67	218	122	433	7.60	4.49	6.05	2.1E+07	1.3E+07	2.2E+05	3.3E+07
AT3G51550	FER	98	2	4	131	134	271	3.29	5.63	4.46	9.1E+06	8.5E+06	8.4E+04	1.8E+07
AT3G46290	HERK1	91	15	48	125	79	267		3.16	3.16	9.4E+06	6.1E+06	0.0E+00	1.5E+07

Table 2S2: LC/MS-MS data corresponding to discussed proteins.

			Total Spectral Counts					Fold Enrichment (CCV:DFGL)			iBAQ Values			
Accession	Label	MW	Rep 1	Rep 2	Rep 3	Rep 4	Sum	Rep 1	Rep 2	Average	Rep 1	Rep 2	Rep 3	Sum
AT2G39360	CrRLK1L	91	0	5	8	4	17							
AT5G38990	CrRLK1L	98	0	0	17	31	48							
AT5G59700	CrRLK1L	92	2	6	19	25	52							
AT5G54380	THE1	93	0	1	20	30	51				9.3E+05	8.8E+05	0.0E+00	1.8E+06
AT1G30570	HERK2	94	0	1	27	47	75				3.9E+05	4.3E+05	0.0E+00	8.2E+05
Cargo														
AT4G32410	CESA1	122	0	1	10	6	17							
AT5G05170	CESA3	120	0	4	11	18	33							
AT5G64740	CESA6	123	0	0	14	32	46							
AT3G53420	PIP2;1	30	1	4	8	6	19				1.5E+06	9.2E+05	0.0E+00	2.4E+06
AT5G47910	RBOHD	104	19	4	31	55	109				1.1E+06	1.2E+06	0.0E+00	2.3E+06
AT1G73590	PIN1	67	2	5	34	48	89							
AT1G70940	PIN3	69	5	4	20	14	43							
AT1G77110	PIN6	62	14	0	46	22	82							
AT1G69840	AtHIR1	31	15	12	105	56	188	1.36	4.20	2.78	2.3E+07	1.2E+07	9.2E+05	3.6E+07
AT3G01290	AtHIR2	31	2	10	51	47	110		5.83	5.83				
AT5G51570	AtHIR3	32	41	40	184	183	448	0.47	4.42	2.45	5.9E+06	1.9E+06	6.2E+06	1.4E+07
AT5G62740	AtHIR4	31	25	24	203	155	407	1.02	5.27	3.15	3.5E+07	2.8E+07	3.4E+06	6.6E+07
AT2G18960	AHA1	104	75	324	538	502	1,439	1.61	0.44	1.03	4.5E+07	2.8E+07	3.9E+06	7.6E+07
AT5G57350	AHA3	104	62	47	328	274	711				1.7E+06	4.9E+05	0.0E+00	2.2E+06
AT4G30190	AHA2	104	68	66	499	397	1,030		0.16	0.16	2.5E+07	2.0E+07	1.6E+06	4.7E+07
AT3G28710	V0-C/D	41	0	104	254	0	358	0.52	3.82	2.17	3.4E+06	3.3E+06	4.3E+05	7.1E+06
AT3G28715	V0-C/D	41	27	34	259	139	459		3.57	3.57	1.0E+07	3.3E+06	1.2E+05	1.4E+07
AT1G78900	V1-A	69	60	131	937	619	1,747	0.12	0.46	0.29	1.8E+08	1.1E+08	2.0E+07	3.2E+08
AT2G28520	V1-A1	93	60	82	260	422	824	3.92	1.91	2.91	7.0E+06	8.3E+06	4.0E+06	1.9E+07
AT2G21410	V1-A2	93	28	77	106	84	295	0.67	0.21	0.44	9.0E+05	4.8E+05	0.0E+00	1.4E+06
AT4G39080	V1-A3	93	15	38	197	119	369	0.39	0.21	0.30	1.8E+07	1.0E+07	8.9E+06	3.7E+07
AT1G76030	V1-B	54	100	27	786	490	1,403				3.4E+07	2.3E+07	3.0E+06	6.0E+07
AT1G12840	V1-C	43	54	49	186	149	438	0.22	2.00	1.11	5.2E+07	2.9E+07	4.3E+06	8.6E+07
AT3G58730	V1-D	29	9	21	69	33	132	0.31	2.26	1.29	3.6E+07	2.0E+07	3.9E+06	6.0E+07
AT4G11150	V1-E1	26	9	4	184	122	319	0.33	1.67	1.00	9.7E+07	6.0E+07	3.3E+06	1.6E+08
AT1G64200	V1-E3	27	25	59	146	116	346		1.48	1.48	4.4E+06	7.4E+05	2.1E+06	7.2E+06
AT4G23710	V1-G2	12	0	0	6	7	13	0.37	0.69	0.53	7.7E+07	4.3E+07	4.1E+06	1.2E+08
Tethering														
AT5G03540	EXO70A1	72	0	2	30	11	43							
AT5G58430	EXO70B1	71	0	1	26	16	43							
AT1G72470	EXO70D1	71	0	0	5	7	12							
AT1G54090	EXO70D2	71	0	0	7	12	19							
AT3G14090	EXO70D3	71	0	0	6	4	10							
AT3G29400	EXO70E1	75	0	0	2	6	8							
AT5G50380	EXO70F1	77	0	2	6	4	12				1.2E+05	8.1E+05	0.0E+00	9.3E+05
AT4G31540	EXO70G1	78	0	0	6	9	15							
AT5G59730	EXO70H7	71	0	0	7	4	11							
AT5G49830	EXO84B	90	2	2	25	39	68							
AT5G12370	SEC10	90	0	7	30	14	51				2.9E+05	5.7E+05	0.0E+00	8.6E+05
AT3G56640	SEC15A	90	1	0	11	2	14							
AT4G02350	SEC15B	88	5	10	34	23	72							
AT1G47550	SEC3A	100	2	5	13	13	33				1.9E+05	2.1E+05	0.0E+00	4.0E+05
AT1G76850	SEC5A	122	0	0	29	17	46							
AT1G21170	SEC5B	123	0	0	64	58	122							
AT3G10380	Sec8	117	12	37	43	63	155				1.3E+05	1.4E+05	0.0E+00	2.7E+05
AT5G54750	Bet3	21	0	0	5	3	8	0.08		0.08				
AT3G05000	Trs33	20	0	0	2	4	6							
AT5G16280	Trs85	140	0	0	145	74	219		0.18	0.18				
Regulators														
AT3G59770	SAC9	180	74	64	727	576	1,441	5.80	5.25	5.53	6.8E+06	8.0E+06	4.3E+05	1.5E+07
AT1G77140	VPS45	65	32	76	274	200	582		5.25	5.25	5.9E+06	3.2E+06	2.1E+06	1.1E+07
AT5G54310	MTV4	53	1	8	109	78	196				2.9E+06	2.5E+06	4.6E+06	9.9E+06
AT3G60860	BIG2	200	0	0	11	4	15							
AT1G01960	BIG3	195	0	0	7	5	12				4.3E+04	4.4E+04	0.0E+00	8.7E+04
AT5G06970	PATROL1	125	0	3	43	35	81				6.3E+05	1.4E+06	0.0E+00	2.1E+06

Table 2S2: LC/MS-MS data corresponding to discussed proteins.

			Total Spectral Counts					Fold Enrichment (CCV:DFGL)			iBAQ Values			
Accession	Label	MW	Rep 1	Rep 2	Rep 3	Rep 4	Sum	Rep 1	Rep 2	Average	Rep 1	Rep 2	Rep 3	Sum
AT1G71410	SCYL2B	99	43	74	262	219	598		14.94	14.94	1.6E+07	1.7E+07	3.8E+06	3.7E+07
AT3G20290	EHD1	61 kD	0	1	26	45	72				2.2E+06	2.5E+06	0.0E+00	4.7E+06
AT4G05520	EHD2	61 kD	0	3	103	73	179				2.8E+07	3.4E+07	4.6E+04	6.2E+07
AT1G22870	SCYL2A	100	23	57	102	63	245				4.9E+05	1.3E+05	0.0E+00	6.2E+05
AT4G34660	SH3 domain-containing	41 kD	44	18	327	206	595	7.13	9.40	8.27	1.9E+07	2.9E+07	8.5E+06	5.6E+07
AT5G06140	SNX1	47	35	96	233	177	541		3.79	3.79	2.4E+07	2.6E+07	2.5E+06	5.3E+07
AT5G58440	SNX2A	66	24	27	112	123	286				1.7E+06	2.4E+06	4.7E+05	4.6E+06
AT5G07120	SNX2B	64	137	273	249	1115	1,774		4.48	4.48	1.6E+07	2.0E+07	3.2E+06	3.9E+07
AT4G12770	AUXILIN-LIKE2	98	50	45	322	246	663				1.2E+06	1.3E+06	1.3E+06	3.9E+06
AT4G12780	AUXILIN-LIKE1	100	49	126	344	311	830	3.98	3.75	3.86	6.7E+05	1.9E+06	1.4E+06	4.0E+06
AT1G06400	RabA1a	24	0	1	21	7	29				4.8E+06	1.9E+06	0.0E+00	6.7E+06
AT1G16920	RabA1b	24	33	60	120	95	308				6.4E+06	4.3E+06	2.1E+05	1.1E+07
AT5G45750	RabA1c	24	0	12	129	139	280				5.0E+07	2.3E+07	2.2E+06	7.5E+07
AT4G18800	RabA1d	24	8	8	112	84	212		2.86	2.86	4.4E+06	1.7E+06	0.0E+00	6.0E+06
AT3G15060	RabA1g	24	4	11	102	92	209		2.86	2.86	3.5E+06	1.5E+06	0.0E+00	5.0E+06
AT1G09630	RabA2a	24	1	1	38	32	72							
AT1G07410	RabA2b	24	5	26	43	43	117							
AT3G46830	RabA2c	24	13	3	50	14	80	0.15		0.15	5.1E+06	5.5E+06	0.0E+00	1.1E+07
AT5G65270	RabA4a	25	15	14	27	29	85		0.46	0.46	6.6E+05			6.6E+05
AT4G39990	RabA4b	24	2	10	13	7	32				4.2E+06	1.8E+06	3.6E+05	6.4E+06
AT5G47520	RabA5a	24	11	48	74	57	190							
AT3G07410	RabA5b	24	0	1	11	4	16				1.3E+06	1.0E+06	0.0E+00	2.4E+06
AT2G43130	RabA5c	24	0	3	1	1	5							
AT1G73640	RabA6a	26	0	0	29	17	46							
AT4G35860	RabB1b	23	0	2	10	8	20				1.3E+06	9.4E+05	0.0E+00	2.2E+06
AT4G17170	RabB1c	23	0	2	7	3	12							
AT1G43890	RabC1	24	0	2	33	30	65	0.15	0.66	0.41	1.1E+07	6.8E+06	5.5E+05	1.9E+07
AT3G11730	RabD1	23	0	4	25	14	43							
AT1G02130	RabD2a	23	0	30	30	25	85							
AT5G47200	RabD2b	22	120	59	111	86	376				4.8E+07	3.0E+07	1.8E+06	8.0E+07
AT3G53610	RabE1a	24	1	3	57	47	108				1.1E+06	1.4E+06	5.4E+04	2.5E+06
AT4G20360	RabE1b	52	7	1	54	42	104	0.15	0.40	0.27	2.1E+07	1.5E+07	1.1E+07	4.7E+07
AT3G46060	RabE1c	24	62	125	106	157	450	0.58		0.58	9.4E+06	7.8E+06	0.0E+00	1.7E+07
AT5G03520	RabE1d	24	3	3	67	52	125				3.2E+06	2.9E+06	0.0E+00	6.1E+06
AT3G54840	RabF1	22	8	17	14	12	51							
AT4G19640	RabF2b	22	20	0	104	48	172				1.6E+06	1.2E+06	1.4E+06	4.2E+06
AT4G09720	RabG3a	23	0	1	5	11	17		0.99	0.99	4.6E+06	3.3E+06	2.3E+05	8.1E+06
AT3G16100	RabG3c	23	0	1	17	17	35							
AT1G49300	RabG3e	23	0	4	13	19	36	0.27		0.27	4.1E+06	1.2E+06	0.0E+00	5.4E+06
AT3G55020	RABGAP	87	0	0	1	5	6							
AT2G44100	RabGDI1	50	0	1	25	11	37				2.8E+06	1.9E+06	0.0E+00	4.7E+06
AT3G59920	RabGDI2	50	0	2	55	49	106		35.80	35.80	9.0E+06	5.6E+06	0.0E+00	1.5E+07
AT1G08770	PRA1.E	22	0	0	7	6	13	0.83	1.18	1.00				
AT2G40380	PRA1.B2	23	0	0	24	16	40		3.86	3.86				
AT3G56110	PRA1.B1	23	0	2	5	8	15				7.9E+06	1.1E+07	0.0E+00	1.9E+07
AT1G49040	SCD1	132	0	0	10	2	12							
AT3G48860	SCD2	64	2	0	50	37	89				1.0E+06	8.3E+05	0.0E+00	1.8E+06

Table 2S2: LC/MS-MS data corresponding to discussed proteins.

Table 2S2: LC/MS-MS data corresponding to discussed proteins

LC/MS-MS data corresponding to discussed proteins. Data from CCV MS/MS and dimethyl labeling experiments (Supplemental Datasets 1-3) is presented for proteins discussed in the manuscript and categorized by function.

References

Adamowski, M., Narasimhan, M., Kania, U., Glanc, M., De Jaeger, G., and Friml, J. (2018). A Functional Study of AUXILIN-LIKE1 and 2, Two Putative Clathrin Uncoating Factors in Arabidopsis. Plant Cell 30, 700-716.

Ahn, C.S., Han, J.A., and Pai, H.S. (2013). Characterization of in vivo functions of Nicotiana benthamiana RabE1. Planta 237, 161-172.

Antonescu, C.N., Aguet, F., Danuser, G., and Schmid, S.L. (2011). Phosphatidylinositol-(4,5)-bisphosphate regulates clathrin-coated pit initiation, stabilization, and size. Mol Biol Cell 22, 2588-2600.

Antonny, B., Burd, C., De Camilli, P., Chen, E., Daumke, O., Faelber, K., Ford, M., Frolov, V.A., Frost, A., Hinshaw, J.E., Kirchhausen, T., Kozlov, M.M., Lenz, M., Low, H.H., McMahon, H., Merrifield, C., Pollard, T.D., Robinson, P.J., Roux, A., and Schmid, S. (2016). Membrane fission by dynamin: what we know and what we need to know. EMBO J 35, 2270-2284.

Arabidopsis Genome, I. (2000). Analysis of the genome sequence of the flowering plant Arabidopsis thaliana. Nature 408, 796-815.

Arike, L., Valgepea, K., Peil, L., Nahku, R., Adamberg, K., Vilu, R. (2012) Comparison and applications of label-free absolute proteome quantification methods on *Escherichia coli*. Journal of Proteomics. 75, 5437-5448.

Axelos, M., Curie, C., Mazzolini, L., Bardet, C., and Lescure, B. (1992). A Protocol for Transient Gene-Expression in Arabidopsis-Thaliana Protoplasts Isolated from Cell-Suspension Cultures. Plant Physiol Bioch 30, 123-128.

Backues, S.K., Korasick, D.A., Heese, A., and Bednarek, S.Y. (2010). The Arabidopsis dynamin-related protein2 family is essential for gametophyte development. Plant Cell 22, 3218-3231.

Bar, M., Aharon, M., Benjamin, S., Rotblat, B., Horowitz, M., Avni, A. (2008). AtEHDs, novel Arabidopsis EH-domain-containing proteins involved in endocytosis. Plant J 55, 1025-1038.

Bashline, L., Li, S., Zhu, X., and Gu, Y. (2015). The TWD40-2 protein and the AP2 complex cooperate in the clathrin-mediated endocytosis of cellulose synthase to regulate cellulose biosynthesis. Proc Natl Acad Sci U S A 112, 12870-12875.

Bashline, L., Li, S., Anderson, C.T., Lei, L., and Gu, Y. (2013). The endocytosis of cellulose synthase in Arabidopsis is dependent on mu2, a clathrin-mediated endocytosis adaptin. Plant Physiol 163, 150-160.

Bassham, D.C., Brandizzi, F., Otegui, M.S., and Sanderfoot, A.A. (2008). The secretory system of Arabidopsis. Arabidopsis Book 6, e0116.

Bassham, D.C., Sanderfoot, A.A., Kovaleva, V., Zheng, H., and Raikhel, N.V. (2000). AtVPS45 complex formation at the trans-Golgi network. Mol Biol Cell 11, 2251-2265.

Bednarek, S.Y., and Backues, S.K. (2010) Plant dynamin-related protein families DRP1 and DRP2 in plant development. Biochem Soc Trans 38, 797-806.

Berardini, T.Z., Reiser, L., Li, D., Mezheritsky, Y., Muller, R., Strait, E., and Huala, E. (2015). The Arabidopsis information resource: Making and mining the "gold standard" annotated reference plant genome. Genesis 53, 474-485.

Blanc, C., Zufferey, M., and Cosson, P. (2014). Use of in vivo biotinylated GST fusion proteins to select recombinant antibodies. ALTEX 31, 37-42.

Blondeau, F., Ritter, B., Allaire, P.D., Wasiak, S., Girard, M., Hussain, N.K., Angers, A., Legendre-Guillemin, V., Roy, L., Boismenu, D., Kearney, R.E., Bell, A.W., Bergeron, J.J., and McPherson, P.S. (2004). Tandem MS analysis of brain clathrin-coated vesicles reveals their critical involvement in synaptic vesicle recycling. Proc Natl Acad Sci U S A 101, 3833-3838.

Boersema, P.J., Raijmakers, R., Lemeer, S., Mohammed, S., and Heck, A.J. (2009). Multiplex peptide stable isotope dimethyl labeling for quantitative proteomics. Nat Protoc 4, 484-494.

Bolte, S., and Cordelieres, F.P. (2006). A guided tour into subcellular colocalization analysis in light microscopy. J Microsc 224, 213-232.

Bonifacino, J.S. (2004). The GGA proteins: adaptors on the move. Nat Rev Mol Cell Biol 5, 23-32.

Bonifacino, J.S. and Glick, B.S. (2004). The mechanisms of vesicle budding and fusion. Cell. 116, 153-166.

Bonnett, H.T., and Newcomb, E.H. (1966). Coated vesicles and other cytoplasmic components of growing root hairs of radish. Protoplasma 62, 16.

Borner, G.H., Harbour, M., Hester, S., Lilley, K.S., and Robinson, M.S. (2006). Comparative proteomics of clathrin-coated vesicles. J Cell Biol 175, 571-578.

Borner, G.H., Rana, A.A., Forster, R., Harbour, M., Smith, J.C., and Robinson, M.S. (2007). CVAK104 is a novel regulator of clathrin-mediated SNARE sorting. Traffic 8, 893-903.

Borner, G.H., Antrobus, R., Hirst, J., Bhumbra, G.S., Kozik, P., Jackson, L.P., Sahlender, D.A., and Robinson, M.S. (2012). Multivariate proteomic profiling identifies novel accessory proteins of coated vesicles. J Cell Biol 197, 141-160.

Boutte, Y., Frescatada-Rosa, M., Men, S., Chow, C.M., Ebine, K., Gustavsson, A., Johansson, L., Ueda, T., Moore, I., Jurgens, G., and Grebe, M. (2010). Endocytosis restricts Arabidopsis KNOLLE syntaxin to the cell division plane during late cytokinesis. EMBO J 29, 546-558.

Braulke, T. and Bonifacino, J. (2009) Sorting of lysosomal proteins. BBA Molecular Cell Research. 1793, 605-614.

Braun, M., Baluska, F., von Witsch, M., and Menzel, D. (1999). Redistribution of actin, profilin and phosphatidylinositol-4, 5-bisphosphate in growing and maturing root hairs. Planta 209, 435-443.

Burd, C., and Cullen, P.J. (2014). Retromer: a master conductor of endosome sorting. Cold Spring Harb Perspect Biol 6.

Carter, C., Pan, S., Zouhar, J., Avila, E.L., Girke, T., and Raikhel, N.V. (2004). The vegetative vacuole proteome of Arabidopsis thaliana reveals predicted and unexpected proteins. Plant Cell 16, 3285-3303.

Casler, J.C., Papanikou, E., Barrero, J.J., and Glick, B.S. (2019). Maturation-driven transport and AP-1-dependent recycling of a secretory cargo in the Golgi. J Cell Biol.

Chen, H., Fre, S., Slepnev, V., Capua, M., Takei, K., Butler, M., Di Fiore, P., De Camilli, P. (1998) Epsin is an EH-domain-binding protein implicated in clathrin-mediated endocytosis. Nature 394, 793-797.

Cheng, X., Chen, K., Dong, B., Yang, M., Filbrun, S., Myoung, Y., Huang, T., Gu, Y., Wang, G., Fang, N. (2021) Dynamin-dependent vesicle twist at the final stage of clathrin-mediated endocytosis. Nature Cell Biology 23, 859-869.

Clough, S.J., and Bent, A.F. (1998). Floral dip: a simplified method for Agrobacterium-mediated transformation of Arabidopsis thaliana. Plant J 16, 735-743.

Collings, D.A., Gebbie, L.K., Howles, P.A., Hurley, U.A., Birch, R.J., Cork, A.H., Hocart, C.H., Arioli, T., and Williamson, R.E. (2008). Arabidopsis dynamin-like protein DRP1A: a null mutant with widespread defects in endocytosis, cellulose synthesis, cytokinesis, and cell expansion. J Exp Bot 59, 361-376.

Collins, C.A., LaMontagne, E.D., Anderson, J.C., Ekanayake, G., Clarke, A.S., Bond, L.N., Salamango, D.J., Cornish, P.V., Peck, S.C., Heese, A. (2020) EPSIN1 modulates the plasma membrane abundance of FLAGELLIIN SENSING2 for effective immune responses. Plant Physiology. 182:1762-1775.

Conner, S.D., and Schmid, S.L. (2005). CVAK104 is a novel poly-L-lysine-stimulated kinase that targets the beta2-subunit of AP2. J Biol Chem 280, 21539-21544.

Cox, J., and Mann, M. (2008). MaxQuant enables high peptide identification rates, individualized p.p.b.-range mass accuracies and proteome-wide protein quantification. Nat Biotechnol 26, 1367-1372

da Silva Conceicao, A., Marty-Mazars, D., Bassham, D.C., Sanderfoot, A.A., Marty, F., and Raikhel, N.V. (1997). The syntaxin homolog AtPEP12p resides on a late post-Golgi compartment in plants. Plant Cell 9, 571-582.

daSilva, L.L., Taylor, J.P., Hadlington, J.L., Hanton, S.L., Snowden, C.J., Fox, S.J., Foresti, O., Brandizzi, F., and Denecke, J. (2005). Receptor salvage from the prevacuolar compartment is essential for efficient vacuolar protein targeting. Plant Cell 17, 132-148.

Day, K.J., Casler, J.C., and Glick, B.S. (2018). Budding Yeast Has a Minimal Endomembrane System. Dev Cell 44, 56-72 e54.

De Marcos Lousa, C., Gershlick, D.C., and Denecke, J. (2012). Mechanisms and concepts paving the way towards a complete transport cycle of plant vacuolar sorting receptors. Plant Cell 24, 1714-1732.

Dell'Angelica, E.C., Ooi, C.E., and Bonifacino, J.S. (1997). Beta3A-adaptin, (Zwiewka et al., 2011). J Biol Chem 272, 15078-15084.

Dell'Angelica, E.C., Mullins, C., and Bonifacino, J.S. (1999). AP-4, a novel protein complex related to clathrin adaptors. J Biol Chem 274, 7278-7285.

Dettmer, J., Hong-Hermesdorf, A., Stierhof, Y.D., and Schumacher, K. (2006). Vacuolar H+-ATPase activity is required for endocytic and secretory trafficking in Arabidopsis. Plant Cell 18, 715-730.

Dhonukshe, P., Baluska, F., Schlicht, M., Hlavacka, A., Samaj, J., Friml, J., Gadella Jr., T. (2006) Endocytosis of cell surface material mediates cell plate formation during plant cytokinesis. Dev Cell 10: 137 – 150.

Di Rubbo, S., Irani, N.G., Kim, S.Y., Xu, Z.Y., Gadeyne, A., Dejonghe, W., Vanhoutte, I., Persiau, G., Eeckhout, D., Simon, S., Song, K., Kleine-Vehn, J., Friml, J.,

De Jaeger, G., Van Damme, D., Hwang, I., and Russinova, E. (2013). The clathrin adaptor complex AP-2 mediates endocytosis of brassinosteroid insensitive1 in Arabidopsis. Plant Cell 25, 2986-2997.

Doumane, M., Lebecq, A., Colin, L., Fangain, A., Stevens, F., Bareille, J., Hamant, O., Belkhadir, Y., Munnik, T., Jaillais, Y., Caillaud, M. (2021) Inducible depletion of PI(4,5)P_2 by the synthetic iDePP system in *Arabidopsis*. Nature Plants 7, 587-597.

Drakakaki, G., van de Ven, W., Pan, S., Miao, Y., Wang, J., Keinath, N.F., Weatherly, B., Jiang, L., Schumacher, K., Hicks, G., and Raikhel, N. (2012). Isolation and proteomic analysis of the SYP61 compartment reveal its role in exocytic trafficking in Arabidopsis. Cell Res 22, 413-424.

Duwel, M., and Ungewickell, E.J. (2006). Clathrin-dependent association of CVAK104 with endosomes and the trans-Golgi network. Mol Biol Cell 17, 4513-4525.

Ebine, K., Fujimoto, M., Okatani, Y., Nishiyama, T., Goh, T., Ito, E., Dainobu, T., Nishitani, A., Uemura, T., Sato, M.H., Thordal-Christensen, H., Tsutsumi, N., Nakano, A., and Ueda, T. (2011). A membrane trafficking pathway regulated by the plant-specific RAB GTPase ARA6. Nat Cell Biol 13, 853-859.

Ekanayake, G., Smith, J., Jones, K., Stiers, H., Robinson, S., LaMontagne, E., Kostos, P., Cornish, P., Bednarek, S., Heese, A. (2021) DYNAMIN-RELATED PROTEIN DRP1A functions with DRP2B in plant growth, flg22-immune responses, and endocytosis. Plant Phys. 185:1986-2002.

Ekanayake, G., LaMontagne, E., Heese, A. (2019) Never walk alone: clathrin-coated vesicle (CCV) components in plant immunity. Annu Rev Phytopathol. 57: 307-409.

Eisenach, C., Chen, Z.H., Grefen, C., and Blatt, M.R. (2012). The trafficking protein SYP121 of Arabidopsis connects programmed stomatal closure and K(+) channel activity with vegetative growth. Plant J 69, 241-251.

Fan, L., Hao, H., Xue, Y., Zhang, L., Song, K., Ding, Z., Botella, M.A., Wang, H., and Lin, J. (2013). Dynamic analysis of Arabidopsis AP2 sigma subunit reveals a key role in clathrin-mediated endocytosis and plant development. Development 140, 3826-3837.

Fendrych, M., Synek, L., Pecenkova, T., Toupalova, H., Cole, R., Drdova, E., Nebesarova, J., Sedinova, M., Hala, M., Fowler, J.E., and Zarsky, V. (2010). The Arabidopsis Exocyst Complex Is Involved in Cytokinesis and Cell Plate Maturation. Plant Cell 22, 3053-3065.

Feng, Q., Song, S., Yu, S., Wang, J., Li, S., Zhang, Y. (2017). Adaptor protein-3-dependent vacuolar trafficking involves a subpopulation of COPII and HOPS tethering proteins. Plant Physiology 174, 1609-1620.

Feraru, E., Paciorek, T., Feraru, M.I., Zwiewka, M., De Groodt, R., De Rycke, R., Kleine-Vehn, J., and Friml, J. (2010). The AP-3 beta adaptin mediates the biogenesis and function of lytic vacuoles in Arabidopsis. Plant Cell 22, 2812-2824.

Fruholz, S., Fassler, F., Kolukisaoglu, U., and Pimpl, P. (2018). Nanobody-triggered lockdown of VSRs reveals ligand reloading in the Golgi. Nat Commun 9, 643.

Fuji, K., Shirakawa, M., Shimono, Y., Kunieda, T., Fukao, Y., Koumoto, Y., Takahashi, H., Hara-Nishimura, I., and Shimada, T. (2016). The Adaptor

Complex AP-4 Regulates Vacuolar Protein Sorting at the trans-Golgi Network by Interacting with VACUOLAR SORTING RECEPTOR1. Plant Physiol 170, 211-219.

Fujimoto, M., Ebine, K., Nishimura, K., Tsutsumi, N., and Ueda, T. (2020) Longin R-SNARE is retrieved from the plasma membrane by ANTH domain-containing proteins in *Arabidopsis*. PNAS. 117, 25150-25158.

Fujimoto, M., Arimura, S., Ueda, T., Takanashi, H., Hayashi, Y., Nakano, A., and Tsutsumi, N. (2010). Arabidopsis dynamin-related proteins DRP2B and DRP1A participate together in clathrin-coated vesicle formation during endocytosis. Proc Natl Acad Sci U S A 107, 6094-6099.

Gadeyne, A., Sanchez-Rodriguez, C., Vanneste, S., Di Rubbo, S., Zauber, H., Vanneste, K., Van Leene, J., De Winne, N., Eeckhout, D., Persiau, G., Van De Slijke, E., Cannoot, B., Vercruysse, L., Mayers, J.R., Adamowski, M., Kania, U., Ehrlich, M., Schweighofer, A., Ketelaar, T., Maere, S., Bednarek, S.Y., Friml, J., Gevaert, K., Witters, E., Russinova, E., Persson, S., De Jaeger, G., and Van Damme, D. (2014). The TPLATE adaptor complex drives clathrin-mediated endocytosis in plants. Cell 156, 691-704.

Gershlick, D.C., Lousa Cde, M., Foresti, O., Lee, A.J., Pereira, E.A., daSilva, L.L., Bottanelli, F., and Denecke, J. (2014). Golgi-dependent transport of vacuolar sorting receptors is regulated by COPII, AP1, and AP4 protein complexes in tobacco. Plant Cell 26, 1308-1329.

Girard, M., Allaire, P.D., McPherson, P.S., and Blondeau, F. (2005). Non-stoichiometric relationship between clathrin heavy and light chains revealed by quantitative comparative proteomics of clathrin-coated vesicles from brain and liver. Mol Cell Proteomics 4, 1145-1154.

Gray, E.G. (1961). The granule cells, mossy synapses and Purkinje spine synapses of the cerebellum: light and electron microscope observations. J Anat 95, 345-356.

Grefen, C., Donald, N., Hashimoto, K., Kudla, J., Schumacher, K., and Blatt, M.R. (2010). A ubiquitin-10 promoter-based vector set for fluorescent protein tagging facilitates temporal stability and native protein distribution in transient and stable expression studies. Plant J 64, 355-365.

Gu, Y., Zavaliev, R., and Dong, X. (2017). Membrane Trafficking in Plant Immunity. Mol Plant 10, 1026-1034.

Hashimoto-Sugimoto, M., Higaki, T., Yaeno, T., Nagami, A., Irie, M., Fujimi, M., Miyamoto, M., Akita, K., Negi, J., Shirasu, K., Hasezawa, S., and Iba, K. (2013). A Munc13-like protein in Arabidopsis mediates H+-ATPase translocation that is essential for stomatal responses. Nat Commun 4, 2215.

Heinze, L., Freimuth, N., Robling, A., Hahnke, R., Riebschlager, S., Frohlich, A., Sampathkumar, A., McFarlane, H., Sauer, M. (2020) EPSIN1 and MTV1 define functionally overlapping but molecularly distinct *trans*-Golgi network subdomains in *Arabidopsis*. PNAS 117, 25880-25889.

Heucken, N., and Ivanov, R. (2018). The retromer, sorting nexins and the plant endomembrane protein trafficking. J Cell Sci 131.

Higaki, T., Hashimoto-Sugimoto, M., Akita, K., Iba, K., and Hasezawa, S. (2014). Dynamics and environmental responses of PATROL1 in Arabidopsis subsidiary cells. Plant Cell Physiol 55, 773-780.

Hirst, J., Irving, C., and Borner, G.H. (2013). Adaptor protein complexes AP-4 and AP-5: new players in endosomal trafficking and progressive spastic paraplegia. Traffic 14, 153-164.

Hirst, J., Bright, N.A., Rous, B., and Robinson, M.S. (1999). Characterization of a fourth adaptor-related protein complex. Mol Biol Cell 10, 2787-2802.

Hirst, J., Barlow, L.D., Francisco, G.C., Sahlender, D.A., Seaman, M.N., Dacks, J.B., and Robinson, M.S. (2011). The fifth adaptor protein complex. PLoS Biol 9, e1001170.

Hirst, J., Borner, G.H., Antrobus, R., Peden, A.A., Hodson, N.A., Sahlender, D.A., and Robinson, M.S. (2012). Distinct and overlapping roles for AP-1 and GGAs revealed by the "knocksideways" system. Curr Biol 22, 1711-1716.

Hirst, J., Schlacht, A., Norcott, J.P., Traynor, D., Bloomfield, G., Antrobus, R., Kay, R.R., Dacks, J.B., and Robinson, M.S. (2014). Characterization of TSET, an ancient and widespread membrane trafficking complex. Elife 3, e02866

Hirst, J., Itzhak, D., Antrobus, R., Borner, G., Robinson, M. (2018) Role of the AP-5 adaptor protein complex in late endosome-to-Golgi retrieval. PLoS Biology 16, e2004411.

Hooper, C., Tanz, S., Castleden, I., Vacher, M., Small, I., Millar, AH. (2014) SUBAcon: a consensus algorithm for unifying the subcellular localization data of the *Arabidopsis* proteome. Bioinformatics. 30, 3356-3364.

Hulsen, T., de Vlieg, J., Alkema, W. (2008) BioVenn - a web application for the comparison and visualization of biological lists using area-proportional Venn diagrams. BMC Genomics 9,1-6.

Ichikawa, M., Hirano, T., Enami, K., Fuselier, T., Kato, N., Kwon, C., Voigt, B., Schulze-Lefert, P., Baluska, F., and Sato, M.H. (2014). Syntaxin of plant proteins SYP123 and SYP132 mediate root hair tip growth in Arabidopsis thaliana. Plant Cell Physiol 55, 790-800.

Ischebeck, T., Werner, S., Krishnamoorthy, P., Lerche, J., Meijon, M., Stenzel, I., Lofke, C., Wiessner, T., Im, Y.J., Perera, I.Y., Iven, T., Feussner, I., Busch, W., Boss, W.F., Teichmann, T., Hause, B., Persson, S., and Heilmann, I. (2013). Phosphatidylinositol 4,5-bisphosphate influences PIN polarization by controlling clathrin-mediated membrane trafficking in Arabidopsis. Plant Cell 25, 4894-4911.

Itoh, T., Koshiba, S., Kigawa, T., Kikuchi, A., Yokoyama, S., and Takenawa, T. (2001). Role of the ENTH domain in phosphatidylinositol-4,5-bisphosphate binding and endocytosis. Science 291, 1047-1051.

Jackson, L.P., Kelly, B.T., McCoy, A.J., Gaffry, T., James, L.C., Collins, B.M., Honing, S., Evans, P.R., and Owen, D.J. (2010). A large-scale conformational change couples membrane recruitment to cargo binding in the AP2 clathrin adaptor complex. Cell 141, 1220-1229.

Jaillais, Y., Fobis-Loisy, I., Miege, C., and Gaude, T. (2008). Evidence for a sorting endosome in Arabidopsis root cells. Plant J 53, 237-247.

Johnson, A., Dahhan, D., Gnyliukh, N., Kaufmann, W., Zheden, V., Costanzo, T., Mahou, P., Hrtyan, M., Wang, J., Aguilera-Servin, J., van Damme, D., Beaurepaire E., Loose, M., Bednarek, S., Friml, J. (2021) The TPLATE complex

mediates membrane bending during plant clathrin-mediated endocytosis. PNAS 118 (51) e2113046118.

Jolliffe, N.A., Brown, J.C., Neumann, U., Vicre, M., Bachi, A., Hawes, C., Ceriotti, A., Roberts, L.M., and Frigerio, L. (2004). Transport of ricin and 2S albumin precursors to the storage vacuoles of Ricinus communis endosperm involves the Golgi and VSR-like receptors. Plant J 39, 821-833.

Jung, J.Y., Lee, D.W., Ryu, S.B., Hwang, I., and Schachtman, D.P. (2017). SCYL2 Genes Are Involved in Clathrin-Mediated Vesicle Trafficking and Essential for Plant Growth. Plant Physiol 175, 194-209.

Jurgens, G., Park, M., Richter, S., Touihri, S., Krause, C., El Kasmi, F., and Mayer, U. (2015). Plant cytokinesis: a tale of membrane traffic and fusion. Biochem Soc Trans 43, 73-78.

Kaksonen, M., and Roux, A. (2018). Mechanisms of clathrin-mediated endocytosis. Nat Rev Mol Cell Biol. 19, 313-326.

Kang, B.H., Nielsen, E., Preuss, M.L., Mastronarde, D., and Staehelin, L.A. (2011). Electron tomography of RabA4b- and PI-4Kbeta1-labeled trans Golgi network compartments in Arabidopsis. Traffic 12, 313-329.

Kang, H., and Hwang, I. (2014). Vacuolar Sorting Receptor-Mediated Trafficking of Soluble Vacuolar Proteins in Plant Cells. Plants (Basel) 3, 392-408.

Keen, J.H. (1987). Clathrin assembly proteins: affinity purification and a model for coat assembly. J Cell Biol 105, 1989-1998.

Kim, S.Y., Xu, Z.Y., Song, K., Kim, D.H., Kang, H., Reichardt, I., Sohn, E.J., Friml, J., Juergens, G., and Hwang, I. (2013). Adaptor protein complex 2-mediated endocytosis is crucial for male reproductive organ development in Arabidopsis. Plant Cell 25, 2970-2985.

Kirsch, T., Paris, N., Butler, J.M., Beevers, L., and Rogers, J.C. (1994). Purification and initial characterization of a potential plant vacuolar targeting receptor. Proc Natl Acad Sci U S A 91, 3403-3407.

Kitakura, S., Vanneste, S., Robert, S., Lofke, C., Teichmann, T., Tanaka, H., and Friml, J. (2011). Clathrin mediates endocytosis and polar distribution of PIN auxin transporters in Arabidopsis. Plant Cell 23, 1920-1931.

Konopka, C.A., and Bednarek, S.Y. (2008). Comparison of the dynamics and functional redundancy of the Arabidopsis dynamin-related isoforms DRP1A and DRP1C during plant development. Plant Physiol 147, 1590-1602.

Konopka, C.A., Backues, S.K., and Bednarek, S.Y. (2008). Dynamics of Arabidopsis dynamin-related protein 1C and a clathrin light chain at the plasma membrane. Plant Cell 20, 1363-1380.

Kost, B., Lemichez, E., Spielhofer, P., Hong, Y., Tolias, K., Carpenter, C., and Chua, N.H. (1999). Rac homologues and compartmentalized phosphatidylinositol 4, 5-bisphosphate act in a common pathway to regulate polar pollen tube growth. J Cell Biol 145, 317-330.

Kunzl, F., Fruholz, S., Fassler, F., Li, B., and Pimpl, P. (2016). Receptor-mediated sorting of soluble vacuolar proteins ends at the trans-Golgi network/early endosome. Nat Plants 2, 16017.

Lam, B.C., Sage, T.L., Bianchi, F., and Blumwald, E. (2001). Role of SH3 domain-containing proteins in clathrin-mediated vesicle trafficking in Arabidopsis. Plant Cell 13, 2499-2512.

Lauber, M.H., Waizenegger, I., Steinmann, T., Schwarz, H., Mayer, U., Hwang, I., Lukowitz, W., and Jurgens, G. (1997). The Arabidopsis KNOLLE protein is a cytokinesis-specific syntaxin. Journal of Cell Biology 139, 1485-1493.

Lee, G.J., Kim, H., Kang, H., Jang, M., Lee, D.W., Lee, S., and Hwang, I. (2007). EpsinR2 interacts with clathrin, adaptor protein-3, AtVTI12, and phosphatidylinositol-3-phosphate. Implications for EpsinR2 function in protein trafficking in plant cells. Plant Physiol 143, 1561-1575.

Li, R., Rodriguez-Furlan, C., Wang, J., van de Ven, W., Gao, T., Raikhel, N., Hicks, G. (2017). Different endomembrane trafficking pathways establish apical and basal polarities. Plant Cell 29: 90-108.

Lipatova, Z., Hain, A.U., Nazarko, V.Y., and Segev, N. (2015). Ypt/Rab GTPases: principles learned from yeast. Crit Rev Biochem Mol Biol 50, 203-211.

Lundgren, D.H., Hwang, S.I., Wu, L., and Han, D.K. (2010). Role of spectral counting in quantitative proteomics. Expert Rev Proteomics 7, 39-53.

Luo, Y., Scholl, S., Doering, A., Zhang, Y., Irani, N.G., Rubbo, S.D., Neumetzler, L., Krishnamoorthy, P., Van Houtte, I., Mylle, E., Bischoff, V., Vernhettes, S., Winne, J., Friml, J., Stierhof, Y.D., Schumacher, K., Persson, S., and Russinova, E. (2015). V-ATPase activity in the TGN/EE is required for exocytosis and recycling in Arabidopsis. Nat Plants 1, 15094.

Ma, C., Li, W., Xu, Y., and Rizo, J. (2011). Munc13 mediates the transition from the closed syntaxin-Munc18 complex to the SNARE complex. Nat Struct Mol Biol 18, 542-549.

Martins, S., Dohmann, E.M., Cayrel, A., Johnson, A., Fischer, W., Pojer, F., Satiat-Jeunemaitre, B., Jaillais, Y., Chory, J., Geldner, N., and Vert, G. (2015). Internalization and vacuolar targeting of the brassinosteroid hormone receptor BRI1 are regulated by ubiquitination. Nat Commun 6, 6151.

Masclaux, F.G., Galaud, J.P., and Pont-Lezica, R. (2005). The riddle of the plant vacuolar sorting receptors. Protoplasma 226, 103-108.

Mattera, R., Guardia, C.M., Sidhu, S.S., and Bonifacino, J.S. (2015). Bivalent Motif-Ear Interactions Mediate the Association of the Accessory Protein Tepsin with the AP-4 Adaptor Complex. J Biol Chem 290, 30736-30749.

Mayers, J.R., Hu, T., Wang, C., Cardenas, J.J., Tan, Y., Pan, J., and Bednarek, S.Y. (2017). SCD1 and SCD2 Form a Complex That Functions with the Exocyst and RabE1 in Exocytosis and Cytokinesis. Plant Cell 29, 2610-2625.

McGough, I.J., and Cullen, P.J. (2013). Clathrin is not required for SNX-BAR-retromer-mediated carrier formation. J Cell Sci 126, 45-52.

McMichael, C.M., and Bednarek, S.Y. (2013). Cytoskeletal and membrane dynamics during higher plant cytokinesis. New Phytol 197, 1039-1057.

McMichael, C.M., Reynolds, G.D., Koch, L.M., Wang, C., Jiang, N., Nadeau, J., Sack, F.D., Gelderman, M.B., Pan, J., and Bednarek, S.Y. (2013). Mediation of clathrin-dependent trafficking during cytokinesis and cell expansion by Arabidopsis stomatal cytokinesis defective proteins. Plant Cell 25, 3910-3925.

Mosesso, N., Blaske, T., Nagel, M.K., Laumann, M., and Isono, E. (2019). Preparation of Clathrin-Coated Vesicles From Arabidopsis thaliana Seedlings. Front Plant Sci 9, 1972.

Mravec, J., Petrasek, J., Li N., Boeren, S., Karlova, R., Kitakura, S., Parezova, M., Naramoto, S., Nodzynski, T., Dhonukshe, P., Bednarek, S., Zazimalova, E., de Vries, S., Friml, J. (2011) Cell plate restricted association of DRP1A and PIN proteins is required for cell polarity establishment in Arabidopsis. Current Biology. 21, 1055-1060.

Murashige, T., and Skoog, F. (1962). A Revised Medium for Rapid Growth and Bio Assays with Tobacco Tissue Cultures. Physiol Plantarum 15, 473-497.

Nagaraj, N., Wisniewski, J., Geiger, T., Cox, J., Kircher, M., Kelso, J., Paabo, S., Mann, M. (2011) Deep proteome and transcriptome mapping of a human cancer cell line. Molecular Systems Biology 7: 1-8.

Nagel, M., Kalinowska, K., Vogel, K., Reynolds, G.D., Wu, Z., Anzenberger, F., Ichikawa, M., Tsutsumi, C., Sato, M.H., Kuster, B., Bednarek, S.Y., and Isono, E. (2017). Arabidopsis SH3P2 is an ubiquitin-binding protein that functions together with ESCRT-I and the deubiquitylating enzyme AMSH3. Proc Natl Acad Sci U S A.

Narasimhan, M., Johnson, A., Prizak, R., Kaufmann, W., Tan, S., Casillas-Perez, B., Friml, J. (2020). Evolutionarily unique mechanistic framework of clathrin-mediated endocytosis in plants. eLife. 9: 1-30.

Nielsen, E., Cheung, A.Y., and Ueda, T. (2008). The regulatory RAB and ARF GTPases for vesicular trafficking. Plant Physiol 147, 1516-1526.

Niemes, S., Langhans, M., Viotti, C., Scheuring, D., San Wan Yan, M., Jiang, L., Hillmer, S., Robinson, D.G., and Pimpl, P. (2010). Retromer recycles vacuolar sorting receptors from the trans-Golgi network. Plant J 61, 107-121.

Nishimura, K., Matsunami, E., Yoshida, S., Kohata, S., Yamauchi, J., Jisaka, M., Nagaya, T., Yokota, K., and Nakagawa, T. (2016). The tyrosine-sorting motif of the vacuolar sorting receptor VSR4 from Arabidopsis thaliana, which is involved in the interaction between VSR4 and AP1M2, mu1-adaptin type 2 of clathrin adaptor complex 1 subunits, participates in the post-Golgi sorting of VSR4. Biosci Biotechnol Biochem 80, 694-705.

Okekeogbu, I.O., Pattathil, S., Gonzalez Fernandez-Nino, S.M., Aryal, U.K., Penning, B.W., Lao, J., Heazlewood, J., Hahn, M.G., McCann, M.C., Carpita, N.C. (2019) Glycome and proteome components of Golgi membranes are common between two angiosperms with distinct cell-wall structures. Plant Cell 31,1094-1112.

Orci, L., Ravazzola, M., Amherdt, M., Louvard, D., and Perrelet, A. (1985). Clathrin-immunoreactive sites in the Golgi apparatus are concentrated at the trans pole in polypeptide hormone-secreting cells. Proc Natl Acad Sci U S A 82, 5385-5389.

Orr, R., Fury, F., Warner, E., Agar, E., Garbarino, J., Cabral, S., Dubuque, M., Butt, A., Munson, M., Vidali, L. (2021) Rab-E and its interaction with myosin XI are essential for polarised cell growth. New Phytologist 229: 1924-1936.

Papanikou, E., Day, K.J., Austin, J., and Glick, B.S. (2015). COPI selectively drives maturation of the early Golgi. Elife 4.

Park, M., Song, K., Reichardt, I., Kim, H., Mayer, U., Stierhof, Y.D., Hwang, I., and Jurgens, G. (2013). Arabidopsis mu-adaptin subunit AP1M of adaptor protein complex 1 mediates late secretory and vacuolar traffic and is required for growth. Proc Natl Acad Sci U S A 110, 10318-10323.

Parsons, H.T., Stevens, T.J., McFarlane, H.E., Vidal-Melgosa, S., Griss, J., Lawrence, N., Butler, R., Sousa, M.M.L., Salemi, M., Willats, W.G.T., Petzold, C.J., Heazlewood, J., Lilley, K. (2019) Separating Golgi Proteins from *Cis* to *Trans* Reveals Underlying Properties of Cisternal Localization. Plant Cell 31, 2010-2034.

Parsons, H.T., Christiansen, K., Knierim, B., Carroll, A., Ito, J., Batth, T.S., Smith-Moritz, A.M., Morrison, S., McInerney, P., Hadi, M.Z., Auer, M., Mukhopadhyay, A., Petzold, C.J., Scheller, H.V., Loque, D., and Heazlewood, J.L. (2012). Isolation and proteomic characterization of the Arabidopsis Golgi defines functional and novel components involved in plant cell wall biosynthesis. Plant Physiol 159, 12-26.

Pearse, B.M., and Robinson, M.S. (1984). Purification and properties of 100-kd proteins from coated vesicles and their reconstitution with clathrin. EMBO J 3, 1951-1957.

Perkins, D.N., Pappin, D.J., Creasy, D.M., and Cottrell, J.S. (1999). Probability-based protein identification by searching sequence databases using mass spectrometry data. Electrophoresis 20, 3551-3567.

Pinheiro, H., Samalova, M., Geldner, N., Chory, J., Martinez, A., and Moore, I. (2009). Genetic evidence that the higher plant Rab-D1 and Rab-D2 GTPases exhibit distinct but overlapping interactions in the early secretory pathway. J Cell Sci 122, 3749-3758.

Pourcher, M., Santambrogio, M., Thazar, N., Thierry, A.M., Fobis-Loisy, I., Miege, C., Jaillais, Y., and Gaude, T. (2010). Analyses of sorting nexins reveal distinct retromer-subcomplex functions in development and protein sorting in Arabidopsis thaliana. Plant Cell 22, 3980-3991.

Reichardt, I., Stierhof, Y., Mayer, U., Richter, S., Schwarz, H., Schumacher, K., Jurgens, G. (2007) Plant cytokinesis requires do novo secretory trafficking but not endocytosis. Current Biology 17, 2047-2053.

Reynolds, G.D., August, B., and Bednarek, S.Y. (2014). Preparation of enriched plant clathrin-coated vesicles by differential and density gradient centrifugation. Methods Mol Biol 1209, 163-177.

Reynolds, G.D., Wang, C., Pan, J., and Bednarek, S.Y. (2018). Inroads into Internalization: Five Years of Endocytic Exploration. Plant Physiol 176, 208-218.

Robinson, D.G. (2018). Retromer and VSR Recycling: A Red Herring? Plant Physiol 176, 483-484.

Robinson, D.G., and Neuhaus, J.M. (2016). Receptor-mediated sorting of soluble vacuolar proteins: myths, facts, and a new model. J Exp Bot 67, 4435-4449.

Robinson, D.G., and Pimpl, P. (2014) Receptor-mediated transport of vacuolar proteins: a critical analysis and a new model. Protoplasma 251, 247-264.

Robinson, M.S. (2015). Forty Years of Clathrin-coated Vesicles. Traffic 16, 1210-1238.

Rosquete, M.R., Davis, D.J., and Drakakaki, G. (2018). The Plant Trans-Golgi Network: Not Just a Matter of Distinction. Plant Physiol 176, 187-198.

Roth, T.F., and Porter, K.R. (1964). Yolk Protein Uptake in the Oocyte of the Mosquito Aedes Aegypti. L. J Cell Biol 20, 313-332.

Rueden, C.T., Schindelin, J., Hiner, M.C., DeZonia, B.E., Walter, A.E., Arena, E.T., and Eliceiri, K.W. (2017). ImageJ2: ImageJ for the next generation of scientific image data. BMC Bioinformatics 18, 529.

Rutherford, S., and Moore, I. (2002). The Arabidopsis Rab GTPase family: another enigma variation. Curr Opin Plant Biol 5, 518-528.

Sanchez-Rodriguez, C., Shi, Y., Kesten, C., Zhang, D., Sancho-Andres, G., Ivakov, A., Lampugnani, E.R., Sklodowski, K., Fujimoto, M., Nakano, A., Bacic, A., Wallace, I.S., Ueda, T., Van Damme, D., Zhou, Y., and Persson, S. (2018). The Cellulose Synthases Are Cargo of the TPLATE Adaptor Complex. Mol Plant 11, 346-349.

Sanger, A., Hirst, J., Davies, A.K., Robinson, M.S. (2019) Adaptor protein complexes and disease at a glance. Journal of Cell Science. 132, 1-8.

Sauer, M., Delgadillo, M.O., Zouhar, J., Reynolds, G.D., Pennington, J.G., Jiang, L., Liljegren, S.J., Stierhof, Y.D., De Jaeger, G., Otegui, M.S., Bednarek, S.Y., and Rojo, E. (2013). MTV1 and MTV4 encode plant-specific ENTH and ARF GAP proteins that mediate clathrin-dependent trafficking of vacuolar cargo from the trans-Golgi network. Plant Cell 25, 2217-2235.

Schindelin, J., Arganda-Carreras, I., Frise, E., Kaynig, V., Longair, M., Pietzsch, T., Preibisch, S., Rueden, C., Saalfeld, S., Schmid, B., Tinevez, J.Y., White, D.J., Hartenstein, V., Eliceiri, K., Tomancak, P., and Cardona, A. (2012). Fiji: an open-source platform for biological-image analysis. Nat Methods 9, 676-682.

Schwanhausser, B., Busse, D., Li, N., Dittmar, G., Schuchhardt, J., Wolf, J., Chen, W., Selbach, M. (2011) Global quantification of mammalian gene expression control. Nature. 473: 337-342.

Schwihla, M., and Korbei, B. (2020) The beginning of the end: initial steps in the degradation of plasma membrane proteins. Front Plant Sci. 11, 680.

Shevchenko, A., Wilm, M., Vorm, O., and Mann, M. (1996). Mass spectrometric sequencing of proteins silver-stained polyacrylamide gels. Anal Chem 68, 850-858.

Shimada, T., Fuji, K., Tamura, K., Kondo, M., Nishimura, M., Hara-Nishimura, I. (2003) Vacuolar sorting receptor for seed storage proteins in *Arabidopsis thaliana.* PNAS 100, 16095-16100.

Shimizu, Y., Takagi, J., Ito, E., Ito, Y., Ebine, K., Komatsu, Y., Goto Y., Sato, M., Toyooka, K., Ueda, T., Kurokawa, K., Uemura, T., Nakano, A. (2021). Cargo sorting zones in the *trans*-Golgi network visualized by super-resolution confocal live imaging microscopy in plants. Nature Communications. 12, 1-14.

Simpson, F., Peden, A.A., Christopoulou, L., and Robinson, M.S. (1997). Characterization of the adaptor-related protein complex, AP-3. J Cell Biol 137, 835-845.

Smith, J.M., Leslie, M.E., Robinson, S.J., Korasick, D.A., Zhang, T., Backues, S.K., Cornish, P.V., Koo, A.J., Bednarek, S.Y., and Heese, A. (2014). Loss of Arabidopsis thaliana Dynamin-Related Protein 2B reveals separation of innate immune signaling pathways. PLoS Pathog 10, e1004578.

Song, J., Lee, M.H., Lee, G.J., Yoo, C.M., and Hwang, I. (2006). Arabidopsis EPSIN1 plays an important role in vacuolar trafficking of soluble cargo proteins in plant cells via interactions with clathrin, AP-1, VTI11, and VSR1. Plant Cell 18, 2258-2274.

Sosa, R.T., Weber, M.M., Wen, Y., and O'Halloran, T.J. (2012). A single beta adaptin contributes to AP1 and AP2 complexes and clathrin function in Dictyostelium. Traffic 13, 305-316.

Speth, E.B., Imboden, L., Hauck, P., and He, S.Y. (2009). Subcellular localization and functional analysis of the Arabidopsis GTPase RabE. Plant Physiol 149, 1824-1837.

Stolc, V., Samanta, M.P., Tongprasit, W., Sethi, H., Liang, S., Nelson, D.C., Hegeman, A., Nelson, C., Rancour, D., Bednarek, S., Ulrich, E.L., Zhao, Q., Wrobel, R.L., Newman, C.S., Fox, B.G., Phillips, G.N., Jr., Markley, J.L., and Sussman, M.R. (2005). Identification of transcribed sequences in Arabidopsis thaliana by using high-resolution genome tiling arrays. Proc Natl Acad Sci U S A 102, 4453-4458.

Suwastika, I.N., Uemura, T., Shiina, T., Sato, M.H., and Takeyasu, K. (2008). SYP71, a plant-specific Qc-SNARE protein, reveals dual localization to the plasma membrane and the endoplasmic reticulum in Arabidopsis. Cell Struct Funct 33, 185-192.

Takamori, S., Holt, M., Stenius, K., Lemke, E., Gronborg, M., Riedel, D., Urlaub, H., Schenck, S., Brugger, B., Ringler, P., Muller, S., Rammer, B., Grater, F., Hub, J., De Groot, B., Mieskes, G., Moriyama, Y., Klingauf, J., Grubmuller, H., Heuser, J., Wieland, F., Jahn, R. (2006) Molecular anatomy of a trafficking organelle. Cell. 127: 831-846.

Takemoto, K., Ebine, K., Askani, J.C., Kruger, F., Gonzalez, Z.A., Ito, E., Goh, T., Schumacher, K., Nakano, A., and Ueda, T. (2018). Distinct sets of tethering complexes, SNARE complexes, and Rab GTPases mediate membrane fusion at the vacuole in Arabidopsis. Proc Natl Acad Sci U S A 115, E2457-E2466.

Taylor, M., Perraid, D., Merrifield, C. (2011). A high precision survey of the molecular dynamics of mammalian clathrin-mediated endocytosis. PLoS Biology 9: e1000604.

Teh, O.K., Shimono, Y., Shirakawa, M., Fukao, Y., Tamura, K., Shimada, T. (2013) The AP-1 mu adaptin is required for KNOLLE localization at the cell plate to mediate cytokinesis in Arabidopsis. Plant cell Physiology 43, 838-847.

Tong, P., Kornfeld, S. (1989) Ligand interactions of the cation-dependent mannose 6-phosphate receptor: comparison with the cation-independent mannose 6-phosphate receptor. J Biol Chem 264, 7970-7975.

Uemura, T., Sato, M.H., and Takeyasu, K. (2005). The longin domain regulates subcellular targeting of VAMP7 in Arabidopsis thaliana. FEBS Lett 579, 2842-2846.

Uemura, T., Kim, H., Saito, C., Ebine, K., Ueda, T., Schulze-Lefert, P., and Nakano, A. (2012). Qa-SNAREs localized to the trans-Golgi network regulate multiple transport pathways and extracellular disease resistance in plants. Proc Natl Acad Sci U S A 109, 1784-1789.

Vallis, Y., Wigge, P., Marks, B., Evans, P.R., and McMahon, H.T. (1999). Importance of the pleckstrin homology domain of dynamin in clathrin-mediated endocytosis. Curr Biol 9, 257-260.

Van Damme, D., Coutuer, S., De Rycke, R., Bouget, F., Inzé, D., Geelen, D. (2006) Somatic cytokinesis and pollen maturation in *Arabidopsis* depend on TPLATE, which has domains similar to coat proteins. Plant Cell, 18, 3502-3518.

Viotti, C., Bubeck, J., Stierhof, Y.D., Krebs, M., Langhans, M., van den Berg, W., van Dongen, W., Richter, S., Geldner, N., Takano, J., Jurgens, G., de Vries, S.C., Robinson, D.G., and Schumacher, K. (2010). Endocytic and secretory traffic in Arabidopsis merge in the trans-Golgi network/early endosome, an independent and highly dynamic organelle. Plant Cell 22, 1344-1357.

Vollmer, A.H., Youssef, N.N., and DeWald, D.B. (2011). Unique cell wall abnormalities in the putative phosphoinositide phosphatase mutant AtSAC9. Planta 234, 993-1005.

Wang, C., Yan, X., Chen, Q., Jiang, N., Fu, W., Ma, B., Liu, J., Li, C., Bednarek, S.Y., and Pan, J. (2013). Clathrin light chains regulate clathrin-mediated trafficking, auxin signaling, and development in Arabidopsis. Plant Cell 25, 499-516.

Wang, C., Hu, T., Yan, X., Meng, T., Wang, Y., Wang, Q., Zhang, X., Gu, Y., Sanchez-Rodriguez, C., Gadeyne, A., Lin, J., Persson, S., Van Damme, D., Li, C., Bednarek, S.Y., and Pan, J. (2016). Differential Regulation of Clathrin and Its Adaptor Proteins during Membrane Recruitment for Endocytosis. Plant Physiol 171, 215-229.

Wang, X., Cai, Y., Wang, H., Zeng, Y., Zhuang, X., Li, B., and Jiang, L. (2014). Trans-Golgi network-located AP1 gamma adaptins mediate dileucine motif-directed vacuolar targeting in Arabidopsis. Plant Cell 26, 4102-4118.

Wang, J., Mylle, E., Johnson, A., Besbrugge, N., De Jaeger G., Friml, J., Pleskot, R., Van Damme, D. (2020) High temporal resolution reveals simultaneous plasma membrane recruitment of TPLATE complex subunits. Plant Physiology 183, 986-997.

Wang, J., Yperman, K., Grones, P., Jiang, Q., Dragwidge, J., Mylle, E., Mor, E., Nolf, J., Eeckhout, D., De Jaeger, G., De Rybel, B., Pleskot, R., Van Damme, D. (2021) Conditional destabilization of the TPLATE complex impairs endocytic internalization. PNAS 118, 1-

Williams, M.E., Torabinejad, J., Cohick, E., Parker, K., Drake, E.J., Thompson, J.E., Hortter, M., and Dewald, D.B. (2005). Mutations in the Arabidopsis phosphoinositide phosphatase gene SAC9 lead to overaccumulation of PtdIns(4,5)P2 and constitutive expression of the stress-response pathway. Plant Physiol 138, 686-700.

Wolfenstetter, S., Wirsching, P., Dotzauer, D., Schneider, S., Sauer, N. (2012). Routes to the tonoplast: the sorting of tonoplast transporters in *Arabidopsis* mesophyll protoplasts. Plant Cell 24: 215-232.

Wu, B., and Guo, W. (2015). The Exocyst at a Glance. Journal of Cell Science 128, 2957-2964.

Wu, M., and Wu, X. (2021). A kinetic view of clathrin assembly and endocytic cargo sorting. Current Opinion in Cell Biology. 71, 130-138.

Yan, X., Wang, Y., Xu, M., Dahhan, D., Liu, C., Zhang, Y., Lin, J., Bednarek, S., Pan, J. (2021). Cross-talk between clathrin-dependent post-golgi trafficking and clathrin-mediated endocytosis in Arabidopsis root cells. Plant Cell. 10.1093/plcell/koab180.

Yao, L., Janmey, P., Frigeri, L.G., Han, W., Fujita, J., Kawakami, Y., Apgar, J.R., and Kawakami, T. (1999). Pleckstrin homology domains interact with filamentous actin. J Biol Chem 274, 19752-19761

Yperman, K., Papageorgiou, A., Merceron, R., De Munck, S., Bloch, Y., Eeckhout, D., Jiang, Q., Tack, P., Grigoryan, R., Evangelidis, T., Van Leene, J., Vincze, L., Vandenabeele, P., Vanhaecke, F., Potocky, M., De Jaeger, G., Savvides, S., Tripsianes, K., Pleskot, R., Van Damme, D. (2021) Distinct EH domains of the endocytic TPLATE complex confer lipid and protein binding. Nature Communications 12, 1-11.

Yun, H.S., and Kwon, C. (2017). Vesicle trafficking in plant immunity. Curr Opin Plant Biol 40, 34-42.

Zhang, Y., Persson, S., Hirst, J., Robinson, M.S., van Damme, D., and Sanchez-Rodriguez, C. (2015). Change your TPLATE, change your fate: plant CME and beyond. Trends Plant Sci 20, 41-48.

Zhao, Y., Yan, A., Feijo, J.A., Furutani, M., Takenawa, T., Hwang, I., Fu, Y., and Yang, Z. (2010). Phosphoinositides regulate clathrin-dependent endocytosis at the tip of pollen tubes in Arabidopsis and tobacco. Plant Cell 22, 4031-4044.

Zhou, Y., Yang, Y., Niu, Y., Fan, T., Qian, D., Luo, C., Shi, Y., Li, S., An, L., Xiang, Y. (2020) The tip-localized phosphatidylserine established by Arabidopsis ALA3 is crucial for Rab GTPase-mediated vesicle trafficking and pollen tube growth. Plant Cell 32: 3170-3187.

Zhu, X., Li, S., Pan, S., Xin, X., and Gu, Y. (2018). CSI1, PATROL1, and exocyst complex cooperate in delivery of cellulose synthase complexes to the plasma membrane. Proc Natl Acad Sci U S A 115, E3578-E3587.

Zouhar, J., and Sauer, M. (2014). Helping hands for budding prospects: ENTH/ANTH/VHS accessory proteins in endocytosis, vacuolar transport, and secretion. Plant Cell 26, 4232-4244.

Zouhar, J., Rojo, E., and Bassham, D.C. (2009). AtVPS45 is a positive regulator of the SYP41/SYP61/VTI12 SNARE complex involved in trafficking of vacuolar cargo. Plant Physiol 149, 1668-1678.

Zouhar, J., Munoz, A., and Rojo, E. (2010). Functional specialization within the vacuolar sorting receptor family: VSR1, VSR3 and VSR4 sort vacuolar storage cargo in seeds and vegetative tissues. Plant J 64, 577-588.

Zwiewka, M., Feraru, E., Moller, B., Hwang, I., Feraru, M.I., Kleine-Vehn, J., Weijers, D., and Friml, J. (2011). The AP-3 adaptor complex is required for vacuolar function in Arabidopsis. Cell Res 21, 1711-1722.

Chapter Three:

Biochemical analyses of coat and adaptor proteins of plant CCVs

A portion of this chapter is adapted from published work:

Johnson A, Dahhan DA, Gnyliukh N, Kaufmann WA, Zheden V, Costanzo T, Mahou P, Hrtyan M, Wang J, Aguilera-Servin J, Van Damme D, Beaurepaire E, Loose M, Bednarek SY, Friml J (2021) *PNAS* 118 (51) e2113046118

DAD performed experiments and analyzed data relating to Figure 1D and 1E of the publication cited above; these data are included in this chapter.

Abstract

Plants utilize endocytic adaptor complexes to facilitate clathrin-mediated endocytosis, the AP-2 complex, which is evolutionarily conserved across nearly all eukaryotes, and the TPLATE complex, an evolutionarily ancient vesicle adaptor complex which has since been lost from the lineages of yeast and metazoans. In plants, these two complexes function in the initiation of CME and bridge clathrin coat proteins, endocytic cargo, and other CME regulatory proteins. Loss-of-function *ap2* and *tpc* mutants suggest that there is some functional redundancy between these endocytic adaptor complexes. However, the degree to which AP-2 and TPLATE function overlap and under what circumstances, as well as the varying ways in which this function might be regulated, remain unclear. Proteomic data delineating the contents of a mixture of endocytic and post-Golgi trafficking derived plant CCVs also show that TPLATE and AP-2 are differentially represented. Biochemical analyses of purified plant CCV samples shows that TPLATE co-enriches with the CCV less strongly than AP-2 or clathrin coat proteins in the final, critical stage of the CCV purification process and that TPLATE is more accessible to proteolysis than clathrin coat proteins. These data suggest that TPLATE is more transiently associated with the plant CCV than AP-2 and more external or peripheral on the CCV than the clathrin coat proteins.

Introduction

Clathrin-mediated endocytosis (CME) is facilitated by the adaptor protein complexes, AP-2 and TPLATE complex (TPC). Both adaptors interact with endocytic cargo (Sanchez-Rodriguez et al., 2018; Liu et al., 2020), $PI(4,5)P_2$ (Kovtun et al., 2020; Yperman et al., 2021a; Yperman et al., 2021b), clathrin (Gadeyne et al., 2014; Smith et al., 2021), as well as other endocytic trafficking regulators thereby placing AP-2 and TPC in central roles with regards to CME. While clathrin coat proteins and subunits of the AP-2 are evolutionarily conserved across nearly all eukaryotes (Dacks and Robinson, 2017), the hexameric TSET or its expanded octameric plant version, TPLATE, have been lost from several eukaryotic lineages, including yeast and metazoans (Hirst et al., 2014; More et al., 2020). Consequently, land plants have two endocytic adaptor complexes which function in tandem (Bashline et al., 2015) or possibly independently mediate the internalization of an overlapping complement of endocytic cargo (Dahhan and Bednarek, 2022).

Resolving the circumstances in which TPLATE and AP-2 function simultaneously as adaptors mediating internalization of the same endocytic cargo is an active area of investigation. While single *ap-2* mutants are viable (Kim et al., 2013; Yamaoka et al., 2013; Wang et al., 2016), loss of individual TPC subunits result in severe phenotypic defects, including seedling lethality (Bashline et al., 2013; Gadeyne et al., 2014) suggesting that functional differences and a degree of redundancy exist between these two endocytic adaptors. TPC and AP-2 subunit lifetimes at the plasma membrane display similar distributions and interact with the same endocytic trafficking proteins, but TPC and AP-2 subunits do not exclusively co-localize with each other at the plasma membrane

(Gadeyne et al., 2014). Proteomic studies of an enriched mixture of endocytic- and post-Golgi trafficking-derived clathrin-coated vesicles (CCVs) (Chapter Two) revealed an additional difference between these endocytic adaptors. While all subunits of AP-2 were abundant in the proteome and strongly co-enriched with purified CCVs, subunits of the TPLATE complex were comparatively not abundant and displayed a lack of enrichment with purified CCVs (Figure 2.4, Table 2.1, and Supplemental Table 2S2). Since the involvement of the TPLATE complex in CME had been well-established, the discrepancy between the abundance/enrichment behaviors of TPC and AP-2 was striking.

One approach to clarifying any functional differences between AP-2 and TPC in CME is the biochemical study *in vitro* of the association of these complexes with enriched CCVs with the goal of understanding how AP-2 and TPC 'behave' on purified CCVs relative to each other as well as to the clathrin coat proteins. Elucidating these structural details seeks to shed light on the orientation of these endocytic adaptor proteins relative to the clathrin coat and explain why the TPC is less well-represented in the CCV proteome as well as less strongly co-enriching with CCVs than AP-2.

Results

TPLATE complex is associated less strongly than AP2 with enriched CCVs

To assess whether the endocytic adaptor, TPLATE complex (TPC), is as tightly associated with CCVs as the endocytic adaptor, AP-2, quantitative immunoblotting was performed on enriched CCV purifications to compare the relative enrichment of representative TPLATE and AP-2 subunits between the deuterium ficoll gradient load

(DFGL) and clathrin coated vesicle (CCV) fractions (see Chapter 2 and Figure 2S2). These fractions mark the final stage of the differential centrifugation process and the point at which CCV-associated proteins are most greatly enriched (Figure 2S2A) (Reynolds et al., 2014). CCV coat proteins, clathrin heavy chain (CHC) and clathrin light chain (CLC) strongly enriched between DFGL and CCV fractions, as did the AP-2 subunit, AP2μ2, which was reflected by averaged relative enrichments of 8-fold, 8-fold, and 10-fold, respectively (Figure 3.1A and 3.1B). Conversely, neither the transiently associated scissioning factor, DRP1c, or the TPC subunit, TPLATE, enriched as strongly between the DFGL and CCV fractions, as assessed by quantitative immunoblotting (Figure 3.1B). Student's t-test determined no significant difference between the enrichments of CHC and AP2μ2 and a significant difference (p value < 0.001) between CHC and TPLATE (**, p value < 0.001) and between. AP2μ2 and TPLATE (*, p value < 0.05).

The TPLATE complex is more labile *in vitro* than clathrin coat proteins of CCVs

To investigate whether TPC was located on the interior or the exterior of the clathrin coat of a clathrin coated vesicle, enriched CCVs were prepared from T87 suspension cultured Arabidopsis cells as described (Reynolds et al., 2014). Enriched CCVs were subsequently incubated with trypsin, and partially digested CCV samples were analyzed by SDS-PAGE and immunoblotting using anti-CLC and anti-TPLATE primary antibodies to monitor changes in the levels of full-length CLC2 (37 kDa) and TPLATE proteins (130 kDa) over time. Changes in CHC (190 kDa) protein levels over time were assessed by Ponceau staining. The 1176 amino acid TPLATE protein has 132 predicted trypsin

cleavage sites, 1705 amino acid CHC1 isoform has 166 predicted trypsin cleavage sites, and the 338 amino acid CLC1 isoform has 50 predicted trypsin cleavage sites as assessed by PeptideCutter resulting in a ratio of 0.11, 0.10, and 0.15 cleavage sites/amino acid length for TPLATE, CHC1, and CLC1, respectively (Wilkins et al., 1999). Representative Ponceau stain and immunoblots visualizing decreasing CHC, TPLATE, and CLC over time in response to longer incubation of CCVs with trypsin are shown in Figure 3.2A. Following quantitation of the band intensity and area, the amounts of CHC, CLC, and TPLATE over time as a fraction of levels at t = 0 is plotted in Figure 3.2B. One phase decay modeling of each curve resulted in R^2 values of 0.9992 for CHC, 0.9764 for CLC, and 0.9371 for TPLATE. The half-life of TPLATE was predicted to be far shorter (0.2235 hours) in comparison to CHC and CLC (2.783 and 4.993 hours, respectively), suggesting that this TPLATE complex subunit is physically more accessible to trypsin digestion than are the clathrin coat proteins.

CCV adaptor protein complexes are more sensitive to high salt treatment than coat proteins

To identify differences in the associations of CCV adaptor protein complexes such as TPC and AP2 with enriched vesicles relative to CCV coat proteins, CHC and CLC, by biochemical methods, enriched CCV samples were incubated with clathrin isolation buffer (CIB) as previously described (Reynolds et al., 2014) supplemented with increasing salt or Tris pH 11.4 (a pH condition sufficient to strip the clathrin coat (Keen et al., 1979; Allaire et al., 2006) and centrifuged at 200,000 x g to separate vesicles (P, pellet) and proteins released (S, supernatant) from vesicles under these conditions. Both AP2 subunits and

TPLATE subunits were released from CCVs following incubation with CIB supplemented NaCl to a concentration of 250 mM whereas CCV coat proteins remained more tightly associated with the vesicle under these conditions (Figure 3.3). Low salt conditions were insufficient to liberate adaptor or coat proteins from the purified CCVs. Immunoblotting for KNOLLE, an integral membrane protein, served as a control to confirm the total recovery of microsomal membranes within each reaction.

Discussion

The data presented reveal differences in the association and orientation of the TPLATE complex relative to AP-2 and clathrin coat proteins in a heterogenous mixture of endocytic and post-Golgi trafficking derived CCVs enriched from suspension cultured T87 Arabidopsis cells. Both AP-2 and TPC subunits are equally susceptible to high salt treatment and can be partially stripped from the CCV at a concentration of 250 mM (Figure 3.3). In comparison to clathrin coat and AP-2 proteins, TPLATE enrichment between the DFGL and CCV fractions of a CCV purification scheme is significantly decreased and appears to neither enrich nor deplete in the final stage of the purification, while the average fold enrichment of AP-2, CHC, and CLC proteins range from a 8- to 15-fold increase (Figure 3.1). Treatment of enriched CCV fractions with trypsin over a time course also shows that TPLATE is digested at a faster rate than clathrin coat proteins, which suggests that this adaptor protein complex may be oriented on the periphery, or external to, the clathrin coat, and consequently more accessible to proteolysis (Figure 3.2).

The paradigm describing clathrin coat/adaptor orientation in eukaryotes is derived from crystal structures of mammalian CCVs which show that AP-2 is located on the

interior of the clathrin coat, bridging the endocytic cargo with clathrin (Kirchhausen et al., 2014; Smith et al., 2021). While the molecular architecture and relative positions of subunits within the TPLATE complex (Yperman et al., 2021b) and understanding of the protein contacts between TPC, CHC, CLC, AP2, and DRPs have been described (Gadeyne et al., 2014), a more comprehensive structural picture of the endocytic plant CCV to the detail of the metazoan model is in its infancy. Recently, super-resolution microscopy in Arabidopsis plants co-expressing fluorescently tagged TPLATE and CLC2 or TPLATE and AP2α demonstrated that in almost 20% of CME events at the plasma membrane, TPLATE appeared as a ring-shaped fluorescent signal around punctate CLC2 and AP-2 fluorescence, supporting the idea that TPLATE is on the periphery, external to both AP-2 and the clathrin coat (Johnson et al., 2021).

The functional consequence of the TPC being located on the exterior of the endocytic CCV has yet to be fully explored. Arabidopsis protoplasts expressing defective TPC display proportionately more wide, flat clathrin-coated plaques than do protoplasts expressing functional TPC in which more spherical, productive CCVs are formed, and the EH1 subunit of TPC is capable of tubulating membrane *in vitro*, indicating that the TPC functions in membrane bending *in vivo* (Johnson et al., 2021). It is possible that the TPC needs to be positioned on the exterior of the vesicle to aid in membrane invagination during CME, but how this orientation also accommodates the direct interaction of TPC subunits with endocytic cargo, located on the interior of the CCV, which has been demonstrated *in vivo* through bimolecular fluorescence complementation remains to be explained (Sanchez-Rodriguez et al., 2018). Interestingly, the protist *D. discoideum* lacks

orthologs to the EH1 and EH2 subunits of the TPC, but this organism's orthologous TSET complex is not required for viability (Hirst et al., 2014; More et al., 2020).

Together, the biochemical data showing that TPLATE is less strongly associated with the endocytic CCV than AP-2 and the clathrin coat proteins and superresolution microscopy data showing that for some population of CME events TPLATE is external to AP-2 and clathrin validate the observations that subunits of the TPC are less represented in the CCV proteome than clathrin coat and AP-2 proteins (Chapter Two) due to this complex's more external and peripheral association with the CCV.

Materials and Methods

Growth Conditions

Undifferentiated Arabidopsis T87 cells (Axelos et al., 1992) were maintained in MS media supplemented with 0.2 mg/L 2,4-Dichloropphenoxyacetic acid and 1.32 mM KH_2PO_4 under continuous light at 22°C on an orbital shaker at 140 RPM. Cells were passaged weekly at 1:10 dilution.

Purification of CCVs from suspension cultured T87 cells

Clathrin-coated vesicles were isolated from 3.5 day old suspension cultured T87 cells as previously described (Reynolds et al., 2014). Concentrations of protein samples were quantified using Pierce® 660nm Protein Assay (Thermo Scientific).

Quantitative immunoblotting of relative enrichment of CCV-associated proteins

Primary antibodies described in Supplemental Table 1 were used to detect proteins in DFGL and CCV samples separated by SDS-PAGE and transferred to nitrocellulose membranes. Immunoblotting was performed as described (McMichael et al., 2013) Information about antibodies and concentrations used is described in Supplemental Table 1. Immunoblots were visualized using an iBright CL1000 Imaging System (ThermoFisher Scientific). The average pixel intensity and area of protein bands were measured using FIJI. Prism 9 (GraphPad) was used to generate plots of protein enrichment between CCV and DFGL purification steps. Student's t-test was performed to compare between two CCV-associated proteins across three independent CCV purifications.

Trypsin digestion of enriched CCVs and quantitative immunoblotting

75 μL digestion reactions of 40 μg of purified CCVs at a final concentration of 0.5 mg/mL and mass spectrometry grade trypsin (Promega V5280) at a ratio of 10 μg trypsin per 1 mL reaction volume were assembled on ice (He et al., 2021). Aliquots of the digestion reaction were removed at time points 0, 0.5, 1.5, 2.0, 3.0, and 16.5 hours and supplemented immediately with 3x SDS-PAGE Laemmli buffer. Samples were subsequently separated by SDS-PAGE and transferred to nitrocellulose before incubation with Ponceau stain (0.1% (w/v) Ponceau S and 5% (v/v) acetic acid) to visualize CHC followed by immunoblotting using antibodies for TPLATE and CLC (see Supplemental Table 3S1 for information detailing antibodies). Immunoblots were visualized using an iBright CL1000 Imaging System (ThermoFisher Scientific). Each protein band was quantitated by measuring the IntDen values (area x intensity) using FIJI

and normalizing each time point to t = 0. One-phase exponential decay curves were generated using Prism 9 (GraphPad).

CCV Salt Stripping

37.5 μg of purified CCVs prepared from T87 suspension cultured cells as previously described (Reynolds et al., 2014) at a concentration of 0.844 mg/mL were incubated in a reaction volume of 75 μL for 30 minutes with clathrin isolation buffer supplemented with NaCl to a final concentration of 25 mM NaCl or 250 mM NaCl or with 500 mM Tris pH 11.4. After this incubation, CCV samples were centrifuged for 1 hour at 190,000 x g at 4 °C in a TLA 100.3 rotor. Equivalences of S190 and P190 fractions were supplemented with SDS-PAGE Laemmli sample buffer and analyzed by SDS-PAGE and immunoblotting using primary antibodies described in Supplemental Table 3.1. An additional control reaction of CCVs not centrifuged was also included in SDS-PAGE and immunoblotting analysis.

Figures

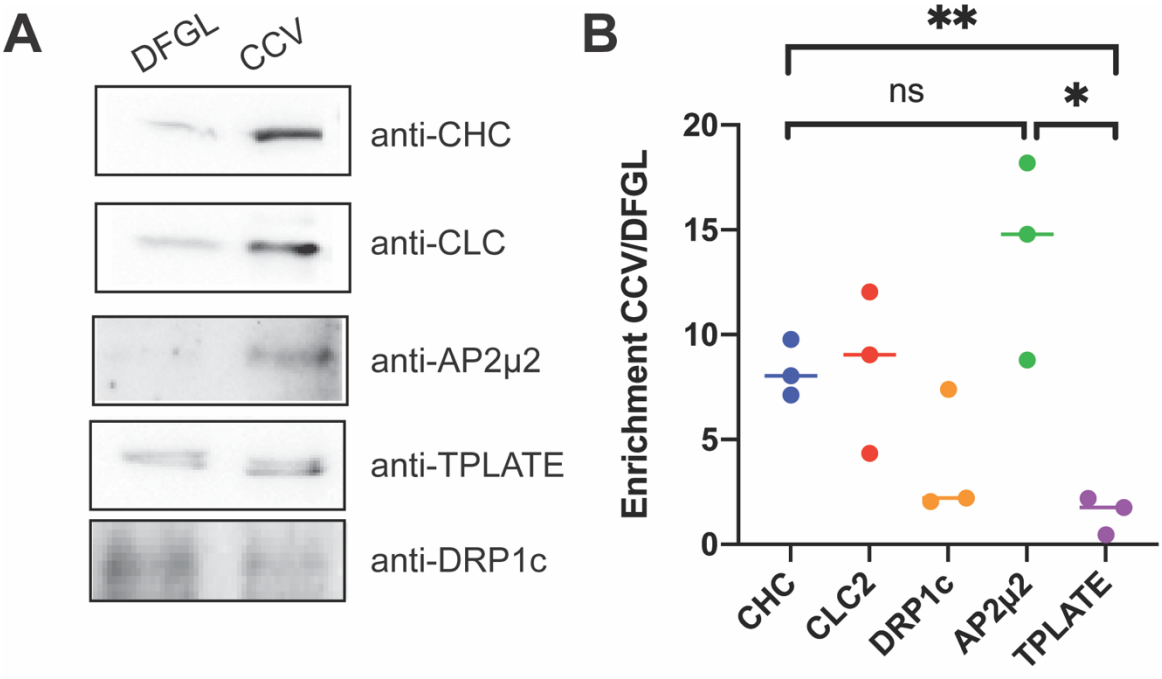

Figure 3.1: TPLATE is associated less strongly than AP-2 with purified CCVs

Figure 3.1: TPLATE is less strongly associated than AP2 with purified CCVs

A) Equal amounts of protein from DFGL and CCV fractions were immunoblotted with antibodies against known CCV associated proteins (CHC, CLC2, AP2μ2, TPLATE, and DRP1c).

B) Quantitation of the enrichment of proteins in (A) between DFGL and CCV purification stages from three independent CCV preparations with error bars indicating standard deviation about the mean. ns = not significant; * = $p < 0.05$; ** = $p < 0.001$.

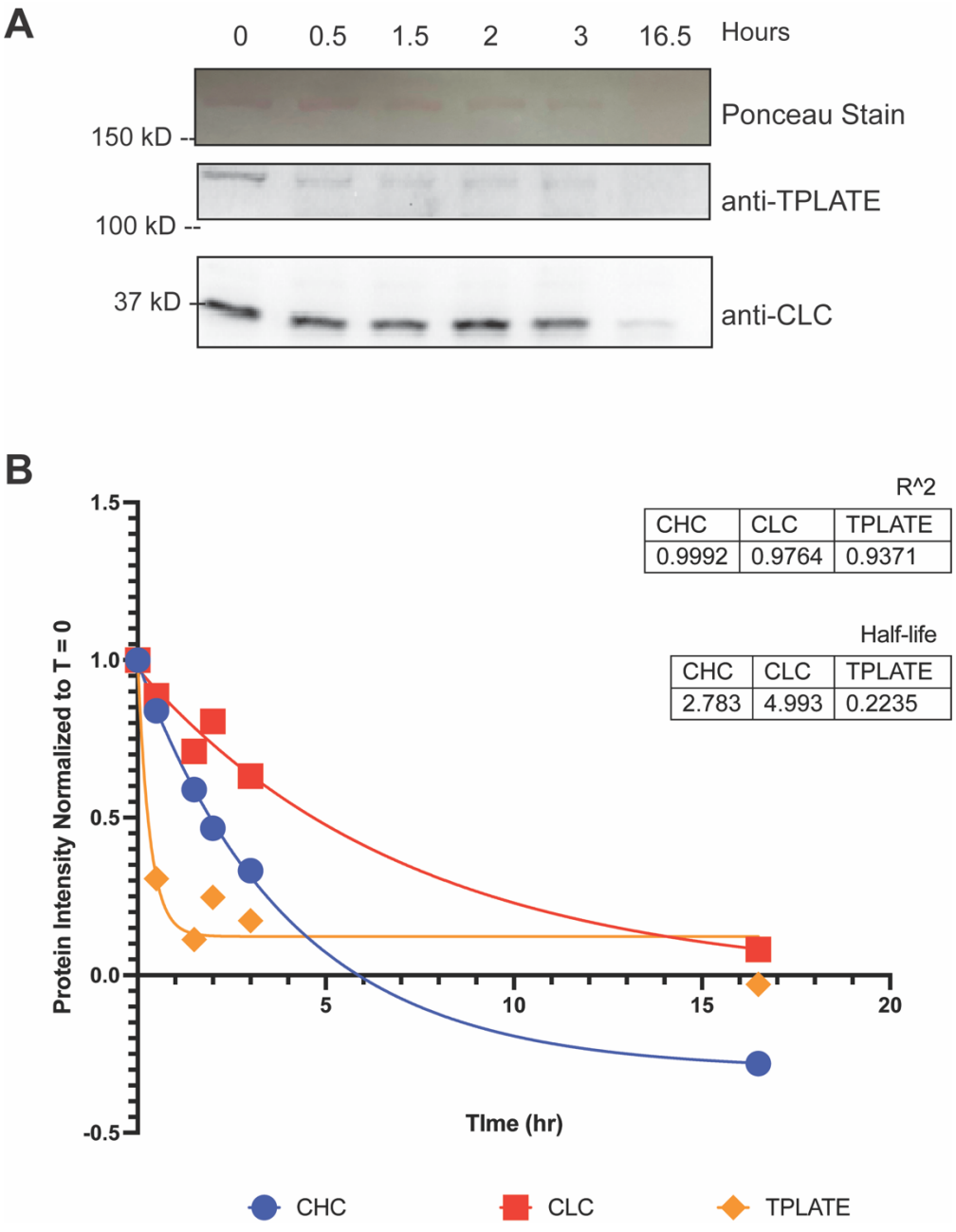

Figure 3.2 The TPLATE complex is more labile *in vitro* than clathrin coat proteins of CCVs

Figure 3.2: The TPLATE complex is more labile *in vitro* than clathrin coat proteins of CCVs

A) Equal volumes of trypsin digestion reactions of purified CCVs at different time points (0, 0.5, 1.5, 2, 3, and 16.5 hours) were analyzed by SDS-PAGE and transferred to nitrocellulose membrane before Ponceau staining to detect CHC protein (190 kDa) levels over time or immunoblotting using anti-TPLATE and anti-CLC antibodies to detect TPLATE (130 kDa) and CLC (37 kDa) protein levels over time.

B) One-phase exponential decay model of CHC, CLC, and TPLATE protein intensities in panel A at each time point normalized to t = 0. R^2 values and half-lives for each curve are indicated at the top right.

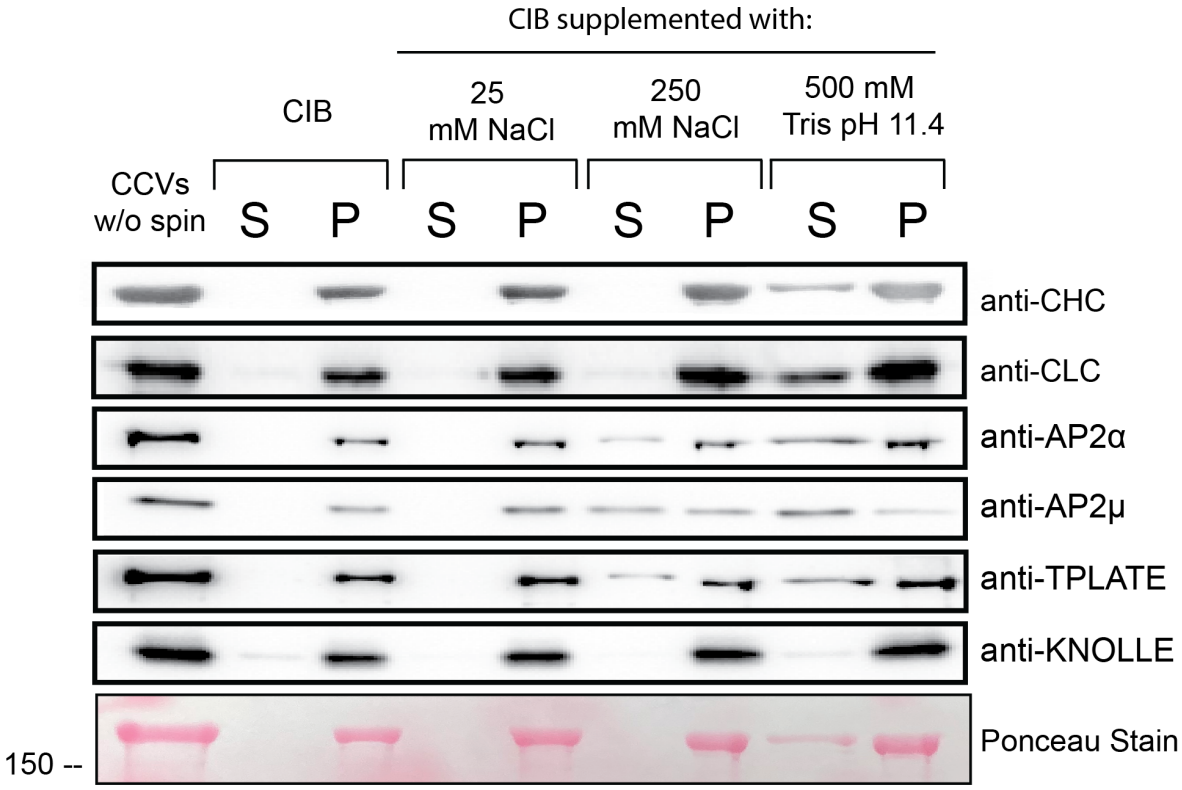

Figure 3.3 CCV-associated adaptor protein complexes are more salt sensitive than CCV coat proteins

Figure 3.3 CCV-associated adaptor protein complexes are more salt sensitive than CCV coat proteins.

CCV samples incubated with clathrin isolation buffer (CIB) supplemented with 25 mM NaCl, 250 mM NaCl, 500 mM Tris pH 11.4, or with no additional reagents were clarified by centrifugation at 190,000 x g for 60 minutes. Equivalent S190 and P190 fractions following this centrifugation, as well as a control CCV sample in CIB not clarified by centrifugation, were analyzed by SDS-PAGE and immunoblotting for known CCV-associated proteins (CHC, CLC, AP2α, AP2μ, and TPLATE) and for integral membrane protein, KNOLLE, as a marker for the presence of microsomal membranes.

Antibodies	Clonality	Primary Dilution for Immunoblot	Secondary	Secondary Dilution	Citation in Work
anti-CLC2	Polyclonal	1:10000	Rabbit	1:5000	Backues, Dissertation, University of Wisconsin-Madison, 2010.
anti-CHC	Monoclonal	1:1000	Mouse	1:5000	Santa Cruz Biotechnology sc-57684
anti-AP2μ2	Polyclonal	1:250	Rabbit	1;:000	Wang et al. *Plant Physiol.* 2016.
anti-TPLATE	Polyclonal	1:1000	Rabbit	1:5000	Dejonghe et al. *Nature Chem Biol.* 2019.
anti-DRP1c	Polyclonal	1:500	Rabbit	1:5000	Kang et al. *Plant Journal.* 2003.
anti-KNOLLE	Polyclonal	1:1000	Rabbit	1:5000	Rancour et al. *Plant Physiol.* 2002.
anti-AP2α	Polyclonal	1:500	Rabbit	1:5000	Song et al. *Plant Physiol.* 2012.

Supplemental Table 3S1 Antibodies used in this study

References

Allaire, P.D., Ritter, B., Thomas, S., Burman, J.L., Denisov, A.Y., Legendre-Guillemin, V., Harper, S.Q., Davidson, B.L., Gehring, K., and McPherson, P.S. (2006). Connecdenn, a novel DENN domain-containing protein of neuronal clathrin-coated vesicles functioning in synaptic vesicle endocytosis. J Neurosci **26,** 13202-13212.

Backues, S.K. (2010). Analysis of Arabidopsis Dynamin-Related Protein 1 and 2 (DRP1 and DRP2) Families. In Biochemistry (Ann Arbor, MI: University of Wiscnsin-Madison), pp. 205.

Bashline, L., Li, S., Zhu, X., and Gu, Y. (2015). The TWD40-2 protein and the AP2 complex cooperate in the clathrin-mediated endocytosis of cellulose synthase to regulate cellulose biosynthesis. Proc Natl Acad Sci U S A **112,** 12870-12875.

Bashline, L., Li, S., Anderson, C.T., Lei, L., and Gu, Y. (2013). The endocytosis of cellulose synthase in Arabidopsis is dependent on mu2, a clathrin-mediated endocytosis adaptin. Plant Physiol **163,** 150-160.

Dacks, J.B., and Robinson, M.S. (2017). Outerwear through the ages: evolutionary cell biology of vesicle coats. Curr Opin Cell Biol **47,** 108-116.

Dahhan, D.A., and Bednarek, S.Y. (2022). Advances in structural, spatial, and temporal mechanics of plant endocytosis. FEBS Lett.

Dejonghe, W., Sharma, I., Denoo, B., De Munck, S., Lu, Q., Mishev, K., Bulut, H., Mylle, E., De Rycke, R., Vasileva, M., Savatin, D.V., Nerinckx, W., Staes, A., Drozdzecki, A., Audenaert, D., Yperman, K., Madder, A., Friml, J., Van Damme, D., Gevaert, K., Haucke, V., Savvides, S.N., Winne, J., and Russinova, E. (2019). Disruption of endocytosis through chemical inhibition of clathrin heavy chain function. Nat Chem Biol **15,** 641-649.

Gadeyne, A., Sanchez-Rodriguez, C., Vanneste, S., Di Rubbo, S., Zauber, H., Vanneste, K., Van Leene, J., De Winne, N., Eeckhout, D., Persiau, G., Van De Slijke, E., Cannoot, B., Vercruysse, L., Mayers, J.R., Adamowski, M., Kania, U., Ehrlich, M., Schweighofer, A., Ketelaar, T., Maere, S., Bednarek, S.Y., Friml, J., Gevaert, K., Witters, E., Russinova, E., Persson, S., De Jaeger, G., and Van Damme, D. (2014). The TPLATE adaptor complex drives clathrin-mediated endocytosis in plants. Cell **156,** 691-704.

He, B., Cai, Q., Qiao, L., Huang, C.Y., Wang, S., Miao, W., Ha, T., Wang, Y., and Jin, H. (2021). RNA-binding proteins contribute to small RNA loading in plant extracellular vesicles. Nat Plants **7,** 342-352.

Hirst, J., Schlacht, A., Norcott, J.P., Traynor, D., Bloomfield, G., Antrobus, R., Kay, R.R., Dacks, J.B., and Robinson, M.S. (2014). Characterization of TSET, an ancient and widespread membrane trafficking complex. Elife **3,** e02866.

Johnson, A., Dahhan, D.A., Gnyliukh, N., Kaufmann, W.A., Zheden, V., Costanzo, T., Mahou, P., Hrtyan, M., Wang, J., Aguilera-Servin, J., van Damme, D., Beaurepaire, E., Loose, M., Bednarek, S.Y., and Friml, J. (2021). The TPLATE complex mediates membrane bending during plant clathrin-mediated endocytosis. Proc Natl Acad Sci U S A **118**.

Kang, B.H., Rancour, D.M., and Bednarek, S.Y. (2003). The dynamin-like protein ADL1C is essential for plasma membrane maintenance during pollen maturation. Plant J **35,** 1-15.

Keen, J.H., Willingham, M.C., and Pastan, I.H. (1979). Clathrin-coated vesicles: isolation, dissociation and factor-dependent reassociation of clathrin baskets. Cell **16,** 303-312.

Kim, S.Y., Xu, Z.Y., Song, K., Kim, D.H., Kang, H., Reichardt, I., Sohn, E.J., Friml, J., Juergens, G., and Hwang, I. (2013). Adaptor protein complex 2-mediated endocytosis is crucial for male reproductive organ development in Arabidopsis. Plant Cell **25,** 2970-2985.

Kirchhausen, T., Owen, D., and Harrison, S.C. (2014). Molecular structure, function, and dynamics of clathrin-mediated membrane traffic. Cold Spring Harb Perspect Biol **6,** a016725.

Kovtun, O., Dickson, V.K., Kelly, B.T., Owen, D.J., and Briggs, J.A.G. (2020). Architecture of the AP2/clathrin coat on the membranes of clathrin-coated vesicles. Sci Adv **6,** eaba8381.

Liu, D., Kumar, R., Claus, L.A.N., Johnson, A.J., Siao, W., Vanhoutte, I., Wang, P., Bender, K.W., Yperman, K., Martins, S., Zhao, X., Vert, G., Van Damme, D., Friml, J., and Russinova, E. (2020). Endocytosis of BRASSINOSTEROID INSENSITIVE1 Is Partly Driven by a Canonical Tyr-Based Motif. Plant Cell **32,** 3598-3612.

More, K., Klinger, C.M., Barlow, L.D., and Dacks, J.B. (2020). Evolution and Natural History of Membrane Trafficking in Eukaryotes. Curr Biol **30,** R553-R564.

Rancour, D.M., Dickey, C.E., Park, S., and Bednarek, S.Y. (2002). Characterization of AtCDC48. Evidence for multiple membrane fusion mechanisms at the plane of cell division in plants. Plant Physiol **130,** 1241-1253.

Reynolds, G.D., August, B., and Bednarek, S.Y. (2014). Preparation of enriched plant clathrin-coated vesicles by differential and density gradient centrifugation. Methods Mol Biol **1209,** 163-177.

Sanchez-Rodriguez, C., Shi, Y., Kesten, C., Zhang, D., Sancho-Andres, G., Ivakov, A., Lampugnani, E.R., Sklodowski, K., Fujimoto, M., Nakano, A., Bacic, A., Wallace, I.S., Ueda, T., Van Damme, D., Zhou, Y., and Persson, S. (2018). The Cellulose Synthases Are Cargo of the TPLATE Adaptor Complex. Mol Plant **11,** 346-349.

Smith, S.M., Larocque, G., Wood, K.M., Morris, K.L., Roseman, A.M., Sessions, R.B., Royle, S.J., and Smith, C.J. (2021). Multi-modal adaptor-clathrin contacts drive coated vesicle assembly. EMBO J **40,** e108795.

Song, K., Jang, M., Kim, S.Y., Lee, G., Lee, G.J., Kim, D.H., Lee, Y., Cho, W., and Hwang, I. (2012). An A/ENTH domain-containing protein functions as an adaptor for clathrin-coated vesicles on the growing cell plate in Arabidopsis root cells. Plant Physiol **159,** 1013-1025.

Wang, C., Hu, T., Yan, X., Meng, T., Wang, Y., Wang, Q., Zhang, X., Gu, Y., Sanchez-Rodriguez, C., Gadeyne, A., Lin, J., Persson, S., Van Damme, D., Li, C., Bednarek, S.Y., and Pan, J. (2016). Differential Regulation of Clathrin and Its Adaptor Proteins during Membrane Recruitment for Endocytosis. Plant Physiol **171,** 215-229.

Wilkins, M.R., Gasteiger, E., Bairoch, A., Sanchez, J.C., Williams, K.L., Appel, R.D., and Hochstrasser, D.F. (1999). Protein identification and analysis tools in the ExPASy server. Methods Mol Biol **112,** 531-552.

Yamaoka, S., Shimono, Y., Shirakawa, M., Fukao, Y., Kawase, T., Hatsugai, N., Tamura, K., Shimada, T., and Hara-Nishimura, I. (2013). Identification and dynamics of Arabidopsis

adaptor protein-2 complex and its involvement in floral organ development. Plant Cell **25,** 2958-2969.

Yperman, K., Wang, J., Eeckhout, D., Winkler, J., Vu, L.D., Vandorpe, M., Grones, P., Mylle, E., Kraus, M., Merceron, R., Nolf, J., Mor, E., De Bruyn, P., Loris, R., Potocky, M., Savvides, S.N., De Rybel, B., De Jaeger, G., Van Damme, D., and Pleskot, R. (2021a). Molecular architecture of the endocytic TPLATE complex. Sci Adv **7**.

Yperman, K., Papageorgiou, A.C., Merceron, R., De Munck, S., Bloch, Y., Eeckhout, D., Jiang, Q., Tack, P., Grigoryan, R., Evangelidis, T., Van Leene, J., Vincze, L., Vandenabeele, P., Vanhaecke, F., Potocky, M., De Jaeger, G., Savvides, S.N., Tripsianes, K., Pleskot, R., and Van Damme, D. (2021b). Distinct EH domains of the endocytic TPLATE complex confer lipid and protein binding. Nat Commun **12,** 3050.

Chapter 4: Regulation of SCD Complex Assembly and Localization

This chapter is unpublished early-stage manuscript and contains cited intellectual and experimental contributions from Jonathan Mayers and Fang Hao.

DAD performed the experiments and analyzed data relating to all figures shown and wrote the chapter.

Abstract

Proteins of the Stomatal Cytokinesis Defective (SCD) complex are essential for multiple stages of plant growth and development, mediate exocytic trafficking, and are both associated with purified CCVs and required for efficient endocytosis. Tandem affinity purification followed by mass spectrometry and colocalization experiments recently identified two SCD2-like proteins, SCD2b and SCD2c, and a pleckstrin homology domain containing protein, MyTH1, as interactors of the SCD complex. The functions of these proteins in SCD complex-mediated post-Golgi trafficking remain to be established, as well as the degree to which they are required for plant growth and development. *In vitro* lipid-overlay assays demonstrate that recombinant AtMyTH1 interacts broadly with multiple phosphoinositide phosphate species, but not with other anionic phospholipids, and directly with AtSCD1. *scd2c*-3 T-DNA insertion mutants display seedling growth defects statistically indistinguishable from those of *scd2-1* loss-of-function mutants, while *scd2b-2* plants appear wild-type. SCD1 total protein levels are decreased in *scd2c* and *myth1*, but not *scd2b*, backgrounds when compared to wild-type, recapitulating this phenotype of *scd2* loss-of-function mutants and suggesting that the function and/or regulation of SCD1 is related to SCD2c and MyTH1, as well as SCD2. In turn, the assembly of SCD1 into a high molecular weight complex is dependent on the presence of SCD2. Together, these data provide information about the protein- and lipid-based factors putatively regulating SCD complex function and localization underlying post-Golgi trafficking.

Introduction

Nearly one fifth of proteins encoded by the Arabidopsis genome are predicted to be synthesized and traffic within the endomembrane system, and approximately 3,000 proteins contribute to the plasma membrane proteome in rice (Arabidopsis Genome, 2000; Cao et al., 2016). The transport of an abundance of cargos through the endomembrane system, including to and from the plasma membrane (illustrated in Figure 1.1), is finely spatially and temporally coordinated to ensure that soluble and membrane proteins are specifically delivered to the appropriate destination. The trans-Golgi network compartment, which in plants serves as the early endosome (Dettmer et al., 2006) (TGN/EE), is the central hub for these diverse transport pathways and both collects internalized protein and membrane cargo and facilitates the distribution of newly synthesized, recycled, and vacuolar protein cargo, as well as lipids and cell wall polysaccharides (Uemura, 2016; Rosquete et al., 2018). The exocytic transport of proteins and membrane away from the TGN/EE fulfills basic cellular functions such as shuttling newly synthesized proteins to their sites of function (e.g. the plasma membrane and cell plate); cell plate formation; and transport of proteins to the vacuole for storage and degradation (Aniento et al., 2021; Kang et al., 2022).

In addition to enabling cellular homeostasis and cell division, polarized, exocytic trafficking is critical to the tip growth of multiple structures or cell types of several model land plant species, such as the tips of root hairs and pollen tubes of the weed, *Arabidopsis thaliana*, as well as the caulonemal cells emerging in the early growth stages of the moss plant, *Physcomitrium (Physcomitrella) patens* (Orr et al., 2020a). In these structures, tip growth is facilitated by a balance between exocytic transport delivering membrane, cell

wall components, and proteins to the apical region of the growing structure and endocytic transport at the subapical, lateral region of the growing structure.

A unique combination of lipids and proteins enriched variously through the endomembrane system is the foundation of the directionality of transport pathways of eukaryotic cells (Stenmark, 2009; Nielsen, 2020; Posor et al., 2022). The accumulations of lipids and proteins at a specific compartment result in 1) a molecular 'signature' characterizing each endomembrane compartment and 2) protein and lipid gradients across the endomembrane system of the plant cell. These specific, protein- and lipid-based endomembrane compartment signatures are recognized through protein- and lipid-binding motifs of proteins that may function in vesicular transport by organizing transport at the donor membrane compartment or recruiting downstream effector proteins that facilitate contact with the acceptor membrane. Consequently, the protein and lipid signature gradients stretching across the endomembrane system promote the associations and dissociations of trafficking machinery in a regulated manner and form the basis of directional transport.

The lipid-based features identifying an endomembrane compartment (and potential donor or acceptor membranes of vesicular transport) include the packing, curvature, and electrostatic potential of the membrane bilayer (Bigay and Antonny, 2012). The electrostatic potential of the membrane reflects the cytosol-oriented charges of the head groups of anionic phospholipid species (phosphatidylinositol (PI), phosphatidic acid (PA), phosphatidylserine (PS), and phosphatidylinositol phosphates (PIP)) that comprise 10% of the total phospholipid content of the plant cell (Noack and Jaillais, 2020). The membrane surface charge associated with a particular endomembrane compartment is

subject to the number of accessible (i.e. not bound by protein) anionic phospholipid head groups, the local pK_a, and the number of charges on a single head group (e.g. PI vs its more electronegative, phosphorylated isoform, $PI(4,5)P_2$) (Simon et al., 2016). The orientation of the anionic headgroups of these phospholipids in the cytosol enables these molecules to serve as anchors or recognition sites for proteins capable of interacting with the anionic head groups through polybasic patches or lipid binding domains or by the coordinate recognition of a second protein localized to the membrane containing the phospholipid of interest (Jean and Kiger, 2012; Noack and Jaillais, 2020). These lipid-based factors may be additive, as the simultaneous recognition of electrostatic membranes and curvature is critical for protein recognition at the TGN/EE (Platre et al., 2018).

The plasma membrane and cell plate are the most electronegative membrane surfaces of the plant cell, relative to other endomembrane compartments (Simon et al., 2016). The electronegative character of the plant plasma membrane surface charges relies on PI(4)P, PA, and PS but not to a significant degree on $PI(4,5)P_2$, though this phospholipid recruits endocytic trafficking machinery to the plasma membrane. This is in contrast to the model in animal cells, where $PI(4,5)P_2$ is critical to the membrane surface charges of the plasma membrane (Simon et al., 2016). An electronegative gradient formed by the decreasing levels of PI(4)P and PS occurs across the plant endomembrane system, with the plasma membrane as the most negatively charged platform, the TGN/EE intermediate, and the late endosomes/multivesicular bodies as the least negatively charged of these endomembrane compartments (Platre et al., 2018).

Proteins functioning in vesicular trafficking are recruited to specific endomembrane compartments through affinities for the cytosolic head groups of anionic phospholipids. These affinities, conferred by lipid binding domains (which also recognize lipid packing and membrane curvature) or linear motifs (e.g. cationic domains or polybasic clusters), may be specific for a particular anionic phospholipid species or capable of broadly interacting with multiple species (Noack and Jaillais, 2020). Consequently, independent of any other recruitment factors, a trafficking protein of interest may in theory localize to multiple endomembrane compartments. In one scenario, a protein predicted to interact specifically with PI(4)P *in vitro* may label multiple compartments *in vivo*, as PI(4)P is found in great abundance at both the TGN/EE and plasma membrane of plants. In another scenario, a protein predicted to interact promiscuously with multiple PIP species *in vitro* may have a narrower localization *in vivo*.

What additional features contribute to a greater specificity in the localization of a trafficking protein *in vivo*? Coincident detection, which is the simultaneous recognition of a phospholipid and protein localized to the same endomembrane compartment, is one mechanism to recruit a trafficking protein containing lipid binding domains or cationic/polybasic motifs to a specific endomembrane compartment when 1) its anionic phospholipid binding partner is present in multiple locations throughout the cell or 2) its affinity for phospholipids is weak and/or promiscuous (Jean and Kiger, 2012) (Figure 4.1A). Regulation of the secretory trafficking regulator, FAPP1, a pleckstrin homology (PH) domain containing protein, is a notable example of coincident detection, as simultaneous interaction with both PI(4)P and the TGN-localized GTPase, Arf1, recruits FAPP1 to the TGN despite the presence of PI(4)P at the plasma membrane and

endosomal compartments, as well as at the TGN and Golgi apparatus (He et al., 2011; Posor et al., 2022). These interactions are mediated through the PH domain of FAPP1, a predominantly phosphatidylinositol-binding protein domain present in regulators of protein trafficking and PI kinases and phosphatases. 80-90% of all PH domains interact weakly and broadly with multiple PI species, with the remainder of known PH domains interacting strongly and specifically with PIs, specifically $PI(4,5)P_2$ (Kutateladze, 2010). Experimental data are consequently required to validate the affinity of PH-domain containing proteins for various PI species on a case-by-case basis *in vivo* and *in vitro.*

In plants, the enrichment of PI(4)P at the PM, as well as TGN/EE, and strong electronegative character of the PM result in the preferential localization of a PI(4)P binding protein in the absence of any concomitant endosome-localized interaction partner (Simon et al., 2016). Careful dissection of the affinities for various endomembrane compartments of plants using a diverse array of lipid binding probes subsequently revealed that proteins with highly cationic motifs (six positive charges or more in a close sequence) are preferentially localized to the plant plasma membrane in the absence of any coincident detection interactions (Platre et al., 2018; Platre et al., 2019).

In addition to the PI-based code distinguishing endomembrane compartments, protein hallmarks also contribute to the identities of various endomembrane compartments. These include the Rab GTPase family, which has greatly expanded in plants to encompass 57 members localized differentially across the endomembrane pathway, and soluble *N*-ethylmaleimide-sensitive factor attachment protein receptor (SNARE) proteins, which are integral membrane proteins that mediate homotypic and heterotypic membrane fusion (Rutherford and Moore, 2002; Nielsen, 2020; Ito and

Uemura, 2022). Subfamilies of Rab GTPases and specific SNARE proteins localize to different endomembrane compartments, and interaction of vesicle trafficking components with specific Rab GTPases and SNARE proteins confer directionality to a trafficking pathway.

Rab GTPases toggle between GTP-bound ‘active’ state promoting membrane trafficking functions through interaction with diverse effector proteins and GDP-bound ‘inactive’ states (Borchers et al., 2021). The activation of Rab GTPases occurs through the action of Rab guanine nucleotide exchange factor proteins (Rab GEFs) which interact with the GDP-bound Rab GTPase and stimulate the exchange of GDP for GTP (Nielsen, 2020). The membrane association, functions, and subsequent activations of downstream factors by both Rab GTPases and phosphoinositide species occur in cascades to ultimately facilitate trafficking pathways (Jean and Kiger, 2012). One such notable example is the activation of the yeast Rab GTPase, Sec4p, which mediates association of the exocytic vesicle with the exocyst complex, an evolutionarily conserved tethering factor for exocytic vesicles at the plasma membrane (Ravikumar et al., 2017). In this model, the association of the yeast Rab GTPase, Ypt32p, with the TGN recruits the GEF of Sec4p, Sec2p, to the TGN. In turn, Sec2p binds and activates its cognate GTPase, Sec4p, which is subsequently able to interact with the exocyst complex (Wu and Guo, 2015).

The orthologous plant Rab GTPase for yeast Sec4p functioning in post-Golgi, exocytic trafficking is the AtRabE1 subfamily of proteins, of which five members (RabE1a-E1e) are found in Arabidopsis (Rutherford and Moore, 2002; Zheng et al., 2005). The expression in plants of a RabE1 isoform variant which is predicted to be GTP-bound (and

therefore constitutively active) results in the constitutive secretion of extracellular proteins, while the induction of a dominant-negative, GDP-bound form suppresses secretion of the marker, secGFP, data which together support a role for RabE1 in exocytic trafficking (Zheng et al., 2005; Speth et al., 2009). This same constitutively GTP-bound RabE1 variant also results in stabilized interaction with a phosphatidylinositol phosphate kinase that produces PI(4,5)P_2, a product located at the PM and cell plate, suggesting that modulating phosphoinositide levels may also be a downstream function of this exocytic Rab GTPase (Camacho et al., 2009). While RabE1 GTPases are clear orthologs to mammalian/yeast Rab8/Sec4p, the cognate GEFs for these Rab GTPases appear to be evolutionarily divergent.

The putative candidate for the GEF of AtRabE1 is the Differentially Expressed in Normal and Neoplastic cells (DENN)-domain containing protein, STOMATAL CYTOKINESIS DEFECTIVE 1. AtSCD1 interacts specifically with TGN/EE-localized RabE1 GTPase isoforms and has an affinity for the putatively inactive, GDP-locked RabE1c variant, in comparison to the constitutively active, GTP-locked variant, supporting a role for SCD1 as an activating factor for this GTPase (Mayers et al., 2017). Velocity sedimentation, confocal microscopy, and affinity purification coupled with mass spectrometry have expanded the interaction network of AtSCD1. AtSCD1 forms a stable, high molecular weight complex with a second evolutionarily divergent (in comparison to yeast and animals) protein, STOMATAL CYTOKINESIS DEFECTIVE 2 (AtSCD2) and interacts with RabE1c, the exocyst complex, as well as two SCD2-like orthologs, AtSCD2b and AtSCD2c. Disruption of the gene expression of *RabE1*, *SCD1*, and *SCD2* in Arabidopsis, *N. benthamiana,* and *O. sativa* result in stomatal guard cell defects and

aberrant cell division (Falbel et al., 2003; Ahn et al., 2013; McMichael et al., 2013; Wang et al., 2022). Proteomic data also identify an evolutionarily divergent protein in Arabidopsis named for its structural homology to C-terminus (tail) region of Myosin I (MyTH1) as a reciprocal interactor of AtSCD1, AtSCD2, and the SCD2-like proteins (Jonathan Mayers, data unpublished). The reciprocal identifications of SCD1, SCD2, SCD2b, SCD2c, and MyTH1 in tandem affinity purifications coupled to mass spectrometry suggest that these proteins function together as the core SCD complex, and fluorescence microscopy confirms that SCD2b, SCD2c, and MyTH1 colocalize strongly with SCD1 at the cell plate of dividing Arabidopsis cells (Jonathan Mayers, data unpublished). However, whether SCD2b, SCD2c, and MyTH1 participate exocytosis and clathrin-mediated endocytosis, two trafficking pathways converging on the TGN/EE in which SCD1 and SCD2 function, are not yet established (Falbel et al., 2003; McMichael et al., 2013; Mayers et al., 2017).

Considering the recent expansion of the interaction network of SCD1 and SCD2 and the regulation of the yeast ortholog of RabE1 by an interaction network utilizing coincident detection (Mizuno-Yamasaki et al., 2010), a number of intriguing questions remain to be answered: What is the composition of the SCD complex, and what intermolecular protein contacts mediate this assembly? Which protein and phospholipid factors are required for the association of the putative GEF, SCD1, with the TGN/EE and therefore bear on its activation of its cognate GTPase, RabE1c? Are the recently identified SCD2-like orthologs and MyTH1 protein involved in the same trafficking pathways as SCD1 and SCD2 in plants, and to what degree are they essential for plant growth and development? The answers to these questions will clarify whether a model of coincident

detection involving the SCD complex regulates RabE1 function at the TGN/EE and to what extent the divergent regulation of the GTPase, RabE1, is conserved among land plants.

Results

Identification of SCD complex accessory proteins and conservation among land plants

Previous characterization of *AtSCD1* and *AtSCD2* demonstrated that the protein products encoded by these genes associated in a high molecular weight complex and functioned in both exocytic and endocytic trafficking, though the specific enzymatic or scaffolding functions of these proteins remain to be firmly established (McMichael et al., 2013; Mayers et al., 2017). Two of four predicted paralogs of ASCD2, AtSCD2b and AtSCD2c, were identified as interactors of both AtSCD1 and AtSCD2 based on tandem affinity purification coupled to mass spectrometry (Mayers et al., 2017) (Table 4S1 and Figure 4.2). Unpublished work further shows that SCD2b and SCD2c colocalize with SCD1 at the cell plate, a central target for both endocytic and exocytic trafficking within the cell (data not shown, J. Mayers). Together, the colocalization and proteomic data suggest that SCD2b and SCD2c associate and possibly function with SCD1 and SCD2, but whether these SCD2-like proteins are essential for plant growth and development to the extent of SCD2 or under what circumstances they function with the SCD complex in mediating protein trafficking remain to be established.

SCD2b (At5g13260) and *SCD2c* (At5g23700) encode one and three transcripts, respectively, depending on splice variations (Figure 4S1). The corresponding Arabidopsis

protein products have a domain organization similar to that of AtSCD2 as assessed by Paircoil2 and InterPro with C-terminal “SCD2 domains” of unknown function, N-terminal intrinsically disordered regions, and two intermediate coiled coil (CC) domains (Figure 4.2) (McMichael et al., 2013; Blum et al., 2021). The latter domain can act as scaffolds for the stable homo- or heterooligomerization of coiled coil domain-containing proteins (Meyer et al., 2021; Simm et al., 2021).

In addition to the identifications of the SCD2-like proteins, SCD2b and SCD2c, a TH1-domain containing protein not conserved among Opisthokonts was also identified as an interactor of AtSCD1, AtSCD2, AtSCD2b, and AtSCD2c (data not shown, J. Mayers). This protein, Myosin Tail Homology I (MyTH1), is named for its structural homology to the tail region of Myosin I, an unconventional, short-necked class of myosin proteins not found in land plants. The TH1 domain in turn is largely composed of a pleckstrin homology (PH) domain, which interacts broadly with multiple phosphatidylinositol phosphate (PIP) species display specificity for particular PIPs (Jean and Kiger, 2012; Lu et al., 2015). Interaction with phospholipids signatures of various endomembrane compartments can also be mediated through basic-hydrophobic motifs, peptide sequences enriched for basic and hydrophobic amino acids (Brzeska et al., 2020; Posor et al., 2022). The bioinformatics tool, HelixWeb, which calculates an arbitrary index assessing the basic-hydrophobic quality of overlapping 20 amino acid windows of a polypeptide sequence, identifies two basic-hydrophobic motifs within AtMyTH1 (residues 87-96 and 46-57, the former of which, located in the pleckstrin homology domain, has the greater basic-hydrophobic quality) enriched in lysine and arginine residues which may mediate interaction with anionic phospholipids (Figure 4.2). Within the expanded HsMyo1c protein,

the tail of which is structurally homologous to AtMyTH1, positively charged residues within the pleckstrin homology domain mediate interaction with negatively charged phospholipids (Lu et al., 2015).

Protein and lipid factors organizing SCD complex assembly and membrane recruitment

The putative activation of the RabE1 GTPase by SCD1 at the TGN/EE is likely dependent upon the recruitment of the SCD1 protein to the TGN/EE and may involve the interaction and complexing with SCD2, which indirectly interacts with RabE1 proteins and is required alongside SCD1 for efficient post-Golgi trafficking (Mayers et al., 2017). The expansion of the interaction network of SCD1 and SCD2 (and potentially the SCD complex) raises questions about whether these newly identified proteins (SCD2b, SCD2c, and MyTH1) contribute to the protein and lipid-based molecular determinants specifically regulating SCD complex assembly and membrane recruitment, as well as SCD1 enzymatic activity and exocytic trafficking, broadly.

Critical to understanding SCD complex assembly is the mapping of intermolecular interactions between SCD1, SCD2 and orthologs, and AtMyTH1. To that end, a heterologous, mammalian cell culture based system was used to express full-length and truncated AtSCD1 with two alternative N-terminal epitope tags to circumvent the difficulty in obtaining soluble AtSCD1 from *E. coli* (Figure 4S2). To demonstrate proof of principle, twinStrepII-AtSCD1^{FULL} with an intermediate flexible linker of 15 amino acids was expressed in HEK293-FT cells following transient transfection. Clarified lysate (S190) of HEK293-FT cells expressing twinStrepII-AtSCD1^{FULL} and clarified lysate (S190) of PSB-

d plant cell culture expressing tandem affinity tag (TAP)-AtSCD1 were subsequently incubated with recombinant GST-AtMyTH1, GST-AtRabE1c^{WT}, GST-control protein immobilized on glutathione sepharose beads. Compared to the negative control (GST bait), twinStrepII-AtSCD1^{FULL} interacted specifically with purified GST-MyTH1 and GST-AtRabE1c^{WT}, demonstrating direct interaction between AtSCD1 and AtMyTH1 and the utility of HEK293-FT expressed AtSCD1 in recapitulating the direct binding previously shown between SCD1 and RabE1c (Figure 4.3) (Figure 4S3) (Mayers et al., 2017). Due to the extremely strong affinity of the recombinant twinStrepII-tagged AtSCD1 constructs for the Strep-Tactin Sepharose resin used to purify these proteins which ultimately hampered their ability to be eluted under tested conditions, a second set of recbominant AtSCD1 constructs were generated for heterologous expression using a N-terminal FLAG epitope tag, Factor Xa cleavage site, and 15 amino acid flexible linker region (Figure 4S2).

The demonstration of direct binding between SCD1 and MyTH1 and the domain prediction of AtMyTH1 raise the question of whether MyTH1 could function in recruitment of SCD1 to membranes relative to post-Golgi trafficking (e.g. the TGN/EE or plasma membrane). As an initial test of the lipid-binding capacity of MyTH1, recombinant, His_6-MyTH1 was expressed in and purified from bacterial cells before incubation with a membrane on which various phospholipids, including diverse anionic phospholipids and multiple species of PIP species were immobilized. Immunoblotting of this membrane using an antibody raised against N-terminally His_6-tagged, full-length AtMyTH1 (Fig 4S3) showed that MyTH1 was able to interact strongly *in vitro* with multiple PIP lipid species (including two not found in plants, PI(3,4,5)P_3 and PI(3,4)P_2) but with weak affinity for the anionic phospholipid, phosphatidic acid, and with no affinity for the anionic phospholipid,

phosphatidylserine, which largely conveys to the plasma membrane its strong electronegative character (Figure 4.4). These data suggest that AtMyTH1 may function to recruit SCD1 (and thereby the SCD complex) to membranes enriched in PIP molecules, but this *in vitro* lipid binding assay does not reflect the complexity of endomembrane phospholipid compositions *in vivo* or the potential for other interacting proteins, e.g. SCD1, to simultaneously and/or independently interact with the membrane of interest. *In vitro* lipid binding assays using recombinant AtSCD1 and liposomes with biological mimetic phospholipid compositions across a range of diameters will more accurately assess the ability of AtMyTH1, as well as SCD1 and SCD2, to interact with membranes of interest. Combining these liposome binding assays *in vivo* with single and combinatorial point mutants targeting the basic-hydrophobic motifs of AtMyTH1 will also probe whether the lysines and arginine residues enriched in these motifs also contribute to the ability of AtMyTH1 to bind membranes of interest.

The recruitment of AtSCD1 to the TGN/EE or the plasma membrane may also be affected by its association with other proteins localized to these membranes. The organization of AtSCD1 and AtSCD2 into a high molecular weight complex of 430 – 720 kDa and the post-Golgi and endocytic trafficking defects associated with either *scd1* or *scd2* mutants indicates that assembly of these proteins into the SCD complex may regulate the function of SCD1 and/or SCD2 (Mayers et al., 2017) (Jonathan Mayers, data not shown). The identification of SCD2b and SCD2c as interactors of SCD1 and SCD2 based on proteomic and colocalization experiments expands the list of proteins which are putatively incorporated into the SCD complex.

To clarify the involvement of SCD2 and its orthologs in assembly of the SCD complex, detergent-solubilized, post-nuclear protein extracts were prepared from wild-type (WT) and *scd2* homozygous loss-of-function mutant seedlings followed by immunoblotting with antibodies for AtSCD1 (anti-SCD1) or antibodies for AtSCD2 which also recognize AtSCD2b and AtSCD2c (henceforth termed anti-SCD2^{BROAD}) (Figure 4.5A). The resulting data confirmed the presence of the high molecular weight (~720 kDa) species labeled by both anti-SCD1 and anti-SCD2^{BROAD}, as well as an intermediate weight (~240-480 kDa) species labeled by anti-SCD2^{BROAD}. The latter species suggests that SCD2 and/or SCD2b and SCD2c may homo- or heteroligomerize into a complex which excludes SCD1. In addition, low molecular weight species below 250 kDa labeled by both anti-SCD1 and anti-SCD2^{BROAD} indicate that SCD1 and SCD2- or SCD2-like proteins may homo- or hetero-oligomerize. Notably, in the *scd2* background, the high, ~720 kDa protein species is absent, indicating that SCD2 is required for assembly of this highest molecular weight species and that the presence of SCD2b and SCD2c are not redundant with SCD2 in this aspect.

Previous analysis of microsomal membranes prepared from suspension cultured plant cells through denaturing SDS-PAGE indicated that SCD1 and SCD2 are peripheral membrane proteins but did not differentiate between the oligomeric status of these proteins associated with microsomal membranes (McMichael et al., 2013). To interrogate a model wherein the ‘complete’, high molecular weight SCD complex (SCD1 + SCD2) is assembled only on membranes and monomeric SCD1 and SCD2 proteins are cytosolic, cytosolic and microsomal membrane fractions were analyzed by native PAGE and immunoblotted using anti-SCD1 and anti-SCD2^{BROAD} antibodies (Figure 4.5B). High

molecular weight SCD1- and SCD2-containing native protein complexes were associated only the microsomal membranes, and neither SCD1 or SCD2 in any oligomeric status were associated with the cytosol. Immunoblotting for the cytosolic AAA+ ATPase chaperone CDC48 and integral membrane marker KNOLLE was used to confirm the integrity of the S150 and P150 fractions (Figure 4.5B).

Phenotypic characterization of *scd2*-like and *myth1* mutants

Similar to the promoter expression pattern of *SCD2*, $MyTH1_{pro}$-*GUS* expression in wild-type Arabidopsis lines transformed with a GUS reporter protein under the control of a 1.9 kb MyTH1 promoter region is observed in cotyledon stomatal guard cells (Figure 4S4A and 4S4B), but whereas $SCD2_{pro}$-*GUS* expression is not observed in the primary root tip, GUS staining driven by $MyTH1_{pro}$ is also observed in the primary root tip of seedlings (Figure 4S4C). Homozygous *myth1-1* and *myth1-2* plants of ecotype backgrounds WS and Col-0, respectively, confirmed to be loss-of-function plants due to T-DNA insertions in the first and second exons (Figure 4S1 and 4S5A) do not display the aberrant stomatal guard cell morphology exhibited by *scd1* and *scd2* plants as assayed by propidium iodide staining (Figure 4S5B) (Falbel et al., 2003; McMichael et al., 2013). Neither *myth1-1* nor *myth1-2* heterozygous progeny segregate at the seedling stage along any observable phenotypes when grown horizontally or vertically on ½ MS + 0.6% or 1.0% (w/v) agar plates without sucrose.

After four weeks after germination, the appearance of rosettes of homozygous *myth1-1* (WS) begin to vary from wild-type (WS) and can be characterized as having smaller (shorter and rounder) leaves and irregular organization about the inflorescence

(Figure 4S5C and 4S5D). About 5 weeks after germination and 1 week after bolting, the inflorescences of homozygous *myth1-1* demonstrate drooping and instability and subsequently collapse under their own weight, as compared to wild-type (WS) plants of equivalent inflorescence height (Figure 4S5D). *myth1-2* plants of the Col-0 ecotype do not display the same weak inflorescence phenotypes after bolting.

Loss-of-function *scd2b-2* and *scd2c-3* alleles derived from T-DNA insertions in the 15th intron and 3rd exon, respectively, have been verified by RT-PCR to show that *SCD2b* and *SCD2c* transcripts are not expressed (Figures 4S2, 4.6A, and 4.6B). Heterozygous populations of *scd2b-2* do not segregate along any observable phenotypes when grown horizontally or vertically on ½ MS + 0.6% or 1.0% (w/v) agar plates without sucrose, and homozygous *scd2b-2* plants do not display any observable phenotypes in tissue development at the seedling or plant stages including a lack of defects in reproductive structures, key phenotypic defects associated with *scd2* plants (McMichael et al., 2013).

Conversely, homozygous *scd2c-3* seedlings are smaller compared to wild-type (Col-0) when grown on ½ MS + 0.6% (w/v) agar without sucrose (Figure 4.6C). Measurements of cotyledon area 6 DAG of Col-0 and *scd2c-3* lines show a two-fold approximate decrease for cotyledon size of *scd2c* (n = 18, mean area 0.016 cm^2) compared to wild-type (n = 13 seedlings, mean area 0.032 cm^2) (Fig 4.6D). No statistically significant difference in cotyledon area at the same age and under the same growth conditions is observed between wild-type (n = 13, mean area 0.032 cm^2) and *myth1* (n = 20, mean area 0.039 cm^2) or *scd2b* mutants (n = 31, mean area 0.029 cm^2) (46D). No statistically significant difference in cotyledon area of 6 DAG seedlings is apparent between *scd2* (n = 12 seedlings, mean area 0.010 cm^2) and *scd2c* (n = 18 seedlings,

mean area of 0.016 cm^2) seedlings at this early stage (Fig 4.6E), though *scd2c-3* plants subsequently grow and develop normally and exhibit none of the plant growth and reproductive structure defects associated with *scd2* plants (McMichael et al., 2013).

Preparation of lysates of WT, *scd2b, scd2c*, and *myth1* mutant seedlings prepared in the presence of 1% Triton X-100 (v/v) and 0.05% NP-40 (v/v) followed by denaturing PAGE and quantitative immunoblotting demonstrates that disruptions of *MyTH1* and *SCD2c,* but not *SCD2b* resulting in loss of MyTH1, SCD2c, and SCD2b protein result in a reduction of SCD1 protein levels in comparison to wild-type (Figures 4S5A and 4.6F-G), a phenotype shared by *scd2* mutants (McMichael et al., 2013).

Preparation of detergent-solubilized, post-nuclear protein extracts from wild-type (WT) and homozygous loss-of-function *scd2b* and *scd2c* seedlings followed by immunoblotting show that anti-SCD1 antibody consistently labels a high molecular weight species (> 480 kDa) in the absence of SCD2b and SCD2c (Figure 4.6H) suggesting that that SCD2b and SCD2c do not contribute to the ~720 kDa protein species containing SCD1 and SCD2.

Discussion

Phenotypic data demonstrating the degree to which the losses of newly identified SCD complex-associated proteins, MyTH1 and SCD2 orthologs, SCD2b and SCD2c, recapitulate *scd1* and *scd2* growth and development and biochemical data describing the contexts in which SCD2b, SCD2c, and MyTH1 may support SCD complex function *in vivo* are presented.

MyTH1, a putative membrane-association promoting factor?

Here, AtMyTH1 has been shown *in vitro* to interact directly with recombinant, full-length AtSCD1 (Figure 4.3) and with phosphatidylinositol phospholipid (PIP) species (Figure 4.4) but exhibit reduced affinity for other anionic or net neutrally charged phospholipids. Together, these data suggest that the pleckstrin homology domain-containing MyTH1 may mediate the recruitment of SCD1, and in turn, other proteins associated with SCD1 to membranes of interest (such as the TGN/EE or plasma membrane) which are enriched in PIPs. However, further experiments will need to clarify 1) whether SCD1 and SCD2 are themselves capable of interaction with phospholipids and 2) the affinities of SCD1, SCD2, and MyTH1 for phospholipids in a biologically relevant context, e.g. using *in vitro* binding assays with TGN/EE or plasma membrane-mimetic liposomes or observing the membrane-enrichments or -depletions of SCD complex associated proteins in plant lines with markers for specific phospholipids or inducible perturbation of phospholipid levels (Doumane et al., 2021). The broad affinity MyTH1 displays for multiple PIPs which are themselves differentially enriched throughout the plant endomembrane system suggests that a combination of lipid- and protein-based factors may be required to recruit the SCD complex to specific donor membranes. Experiments to assess the microsomal membrane association of SCD1 and SCD2, previously shown to be peripheral proteins (McMichael et al., 2013), in the absence of MyTH1 will also be informative in clarifying whether MyTH1 is required for enhancing the membrane association of these proteins and consequently, regulating SCD complex-mediated exocytic trafficking.

The viability of *myth1* mutants and absence of severe phenotypic defects (Figures 4S5) observed in *scd1* and *scd2* loss-of-function lines casts doubt on whether MyTH1 is required for exocytic and endocytic trafficking to the degree of SCD1 and SCD2. This is surprising considering the co-localization between MyTH1 and SCD1 at the cell plate of dividing Arabidopsis cells (Jonathan Mayers, data not shown), an exocytic trafficking acceptor membrane; the reciprocal interactions between MyTH1 and the SCD complex shown by *in vitro* binding assays and mass spectrometry; the $MyTH1_{PRO}$ activity in the stomatal guard cells (Figure 4S4), a tissue-specific observation mirroring $SCD2_{PRO}$ activity (McMichael et al., 2013); and perhaps most importantly, a decrease in total SCD1 protein levels in multiple *myth1* alleles (Figure 4S5A). Decreases in SCD1 protein levels have also been observed in *scd2* loss-of-function mutants (McMichael et al., 2013), but whether the origin of this phenotype is due to decreased stability of SCD1 protein in the absence of interaction partners such as SCD2 or MyTH1 or changes in the transcription and translation of *SCD1* remains to be firmly established. Likewise, whether the inflorescence stability and aberrant rosette morphology of mid- and late-stage *myth1-1* are due to disruption of *AtMyTH1* will need to be validated through a rescue of Ws/*myth1-1* with native or over-expression promoter driven *MyTH1*.

Functional differences between SCD2 and SCD2-like orthologs in SCD complex assembly

The identification of two SCD2-like proteins as associated proteins of both SCD1 and SCD2 from PSB-d suspension cultured cell lines over-expressing TAP-SCD1 and -SCD2 introduced two new potentially functionally redundant candidates of SCD2 which, though

essential for plant growth and development and both endocytic and exocytic transport, remains obscured in its function in these trafficking pathways (Mayers et al., 2017). Though both coiled-coil and SCD2-domains are conserved between SCD2, SCD2b, and SCD2c, the sequence identity and similarities are higher between SCD2 and SCD2c than between SCD2 and SCD2b (Figure 4.2) (McMichael et al., 2013). Identification, validation, and characterization of *scd2b* and *scd2c* loss-of-function mutants here has helped to clarify any functional distinctions between SCD2b and SCD2c. Analysis of the size of *scd2-like* seedlings 6 DAG demonstrates that *scd2c* and *scd2* loss-of-function mutants are indistinguishable at this growth stage, but that *scd2b* mutant seedlings do not differ significantly from wild-type seedlings in terms of size (Figure 4.6C-E). However, *scd2c-3* plants do not display defects in plant growth at 14 weeks after germination or in the development of reproductive structure as previously observed in *scd2* plants (McMichael et al., 2013). It is possible that the presence of SCD2 functionally compensates for loss of SCD2c in the *scd2c-3* background. Rescue of this phenotype remains to be performed, as does an investigation of stomatal guard cell development in both *scd2b* and *scd2c* backgrounds. Similar to *scd2* and *myth1* mutants, SCD1 protein levels are also reduced in *scd2c*, but not *scd2b* backgrounds compared to wild-type (Figure 4.6F and 4.6G), suggesting that the function and/or regulation of SCD1 is linked to *SCD2c.*

The functional equivalences between SCD2 and its paralogs, SCD2b and SCD2c, have also been investigated at the subcellular level. Published (Mayers et al., 2017) and unpublished (Jonathan Mayers, data not shown) work have indicated that the upper limit size of the SCD complex is 480 kDa (as measured by glycerol gradient sedimentation)

and 720 kDa (as measured by native PAGE), respectively, and is formed of both SCD1 and SCD2, which are each capable of homooligomerization into species smaller than the upper limit SCD complex. The degree to which other proteins associated with the SCD complex are present in this upper limit SCD complex remains an open question.

Native PAGE analyses of wild-type, *scd2*, and wild-type plants over-expressing RFP-SCD2b or -SCD2c indicate that SCD2 contributes to the high molecular weight complex (approximately 720 kDa) and that this complex is associated only with the microsomal membranes of plant cells (Figure 4.5). In turn, in the absence of SCD2, SCD1 does not migrate in a 720 kDa sized complex, suggesting that SCD2 is required for assembly of the high molecular weight complex. No change is observed in the sizes of SCD1-containing protein complexes between wild-type and loss-of-function *scd2b* and *scd2c* seedlings (Figure 4.6G).

Clarifying any functional differences between SCD1-containing complexes of varying sizes is key to establishing whether regulation of SCD complex size is a mechanism by which SCD complex-mediated exocytic and endocytic transport is regulated. If, for example, the high molecular weight species of 480 – 720 kDa containing SCD1 and SCD2, but not SCD2b and SCD2c, contains putative GEF activity towards a small GTPase, such as RabE1, then the determination of the intermolecular interactions and proteins involved in assembly of this complex are critical. A complementary path to assessing the potential for SCD complex assembly as a means to regulate SCD1 function is understanding whether the various hetero- and homo-oligomeric complexes containing SCD1 and SCD2 are cytosolic or microsomal membrane associated, e.g. associated with the TGN/EE or PM.

SCD complex membrane association mediated by coincident detection

Two hypotheses by which SCD1 and consequently, the SCD complex, are recruited and retained at endomembrane compartments of interest, such as the TGN/EE and PM, incorporate the model of coincident detection (Figure 4.7). In yeast, the membrane association of the pleckstrin homology domain containing- trafficking regulator, FAPP1, is mediated by simultaneous interaction with the anionic phospholipid PI(4)P and with the small GTPase, Arf1 (He et al., 2011; Posor et al., 2022). Analogously, SCD1 may be recruited to the TGN/EE via simultaneous interaction with MyTH1, which in turn recognizes a PIP enriched at the TGN/EE such as PI(4)P, and with a small GTPase (Figure 4.7 top). Alternatively, MyTH1 may not be required for SCD1 association with the TGN/EE, and any transient or weak affinity between SCD1 and a small GTPase at the TGN/EE is compensated for by oligomerization of SCD2 (not SCD2b or SCD2c) which simultaneously mediates interaction with other SCD1-containing complexes at the TGN/EE.

Materials and Methods

Plant Materials and Growth Conditions

Arabidopsis thaliana lines are sourced as follows: WS and Col-0 seed from Arabidopsis Biological Resource Center (ABRC); *scd2-1* as previously described (McMichael et al., 2013); T-DNA insertion mutant *myth1-1* (WS) FLAG_207A11, INRA; T-DNA insertion mutant *myth1-2* (Col-0) SAIL 828 G09, ABRC; T-DNA insertion mutant *scd2c-3* (Col-0) SALK 048684C, ABRC; T-DNA insertion mutant *scd2b-2* (Col-0) SALK 015405C, ABRC; transgenic *SCD2b* and *SCD2c* over-expression lines as previously described (Fang Hao); *MyTH1*$_{Pro}$*-GUS* generated by J. Mayers (unpublished, Bednarek Lab). Seeds were sterilized in 70% (v/v) ethanol with 0.1% (v/v) Triton X-10 for 5 minutes and in 90% (v/v) ethanol for 1 minute prior to plating on ½ strength MS media (Murashige and Skoog, 1962) containing 0.6% (w/v) agar. Seeds were stratified without light at 4°C for 3 days prior to growing under continuous light at 22°C. Plants grown on soil were transferred from plates after 7 to 14 days to Metro-Mix 360 (SunGro Horticulture) and grown at 22°C long days (16 hours of light exposure). *myth1-1*, *myth1-2*, *scd2c-3*, and *scd2b-2* mutants were genotyped using primers DD1/DD4 and DD4/DD5; DD3/DD7 and DD6/DD7; DD2/9 and DD8/DD9; DD2/DD11 and DD10/DD11 respectively (Supplemental Table 4S3).

RT-PCR

30 – 50 microliters of RNA was purified from 30 – 100 mg of 7-14 DAG WT, *scd2b*, or *scd2c* plants using the RNEasy Plant Kit (Qiagen 74904). RNA samples from each background were treated with 1 microliter ezDNase (Invitrogen 11766051) for 5 minutes at 37°C. cDNA was generated from each DNase treated RNA sample using SuperScript

IV VILO Master Mix (Invitrogen 11756050) with and without (negative control) reverse transcriptase following manufacturer's instructions. cDNA was amplified using EconoTaq master mix (Lucigen, 30035) in a reaction volume of 25 microliters and 1 microliter of cDNA template diluted 1:10. 100 bp of actin was amplified from cDNA sample obtained as a positive control using primers DD12 and DD13 (Supplemental Table 4S3), annealing temperature of 55 °C, and 15 seconds elongation time. 1614 bp of *SCD2b* was amplified using primers DD14 and DD15 (Supplemental Table 4S3), an annealing temperature of 59 °C, and elongation time of 60 seconds. Approximately 1700 bp of *SCD2c* was amplified using primers DD16 and DD17 (Supplemental Table 4S3), an annealing temperature of 62 °C, and an elongation time of 60 seconds.

Plasmid Construction

Mammalian codon optimized *AtSCD1* CDS (3710) with N-terminal twinStrep tag and flexible linker (Supplemental Figure 4S2) was inserted into pFLAG CMV 5.1 mammalian expression vector by Synbio Technologies (Monmouth Junction, New Jersey) between EcoRI and BamHI cut sites. Constructs of twinStrep and flexible linker-tagged truncated AtSCD1 (Supplemental Figure 4S2) were generated by digestion of pFLAG CMV 5.1 with SacI and BamHI restriction enzymes, amplification of *AtSCD1* CDS fragments encoding truncations of interest using Phusion Polymerase in a 25 microliter reaction volume and indicated primers, subsequent purification of PCR products by gel DNA recovery kit (Zymoclean D4001), and 2- or 3-part Gibson recombination reactions with 1:1 equimolar ratio unless the *AtSCD1* CDS fragment was approximately 1 kb or less. Primers used to

amplify twinStrep-tagged AtSCD1 truncations are as follows: uDENN + DENN + 9 amino acid (DD18 + DD19); tripartite DENN domain (DD18 + DD20); tripartite DENN + linker (DD18 + DD21); linker + WD-40 repeats (DD18 + DD22 and DD23 and DD24); and WD-40 repeats (DD18 + DD25 and DD26 + DD24).

Constructs of FLAG-, FactorXa-, and flexible linker-tagged full-length and truncated AtSCD1 (Supplemental Figure 4S2) were generated similarly using Gibson cloning and digestion of pFLAG CMV 5.1 with NotI and BamHI restriction enzymes and amplification of linear insert with a forward primer sequence (DD27) encoding start codon, FLAG tag, FactorXa cleavage site, flexible linker region and reverse primer sequence as indicated: full-length AtSCD1 (DD28), tripartite DENN domain (DD20), tripartite DENN + linker (DD21), linker + WD-40 repeats (DD24) and WD-40 repeats (DD24). Constructs were verified by diagnostic digest and sequencing using primer DD29.

633 bp of *AtMyTH1* CDS was amplified from pRSF Duet Vector with open reading frame encoding His_6-AtMyTH1 using Gateway compatible primers DD30 and DD31, Phusion polymerase, annealing temperature of 53 °C, and elongation time of 1 minute. PCR product was subcloned into pDONR221 (P1P2) vector before recombination with pDEST15 Gateway vector to introduce N-terminal GST tag.

Histochemistry & Light Microscopy

Histochemical staining to visualize GUS reporter activity in 5 DAG seedlings from three independent T2 Col-0:*MyTH1*$_{Pro}$*-GUS* lines was performed as described (McMichael et al., 2013). 10x, 20x, and 40x objectives on an Olympus light microscope and Leiza MZ6 stereoscope were used to visualize the stomatal guard cells, primary root tips, and other

tissues. 8 bit images were collected with an ISO 400 and automatic exposure at a resolution of 1600x1200 pixels.

Propidium iodide staining was performed to visualize the cell walls of pavement and stomatal guard cells of 6 DAG Col-0, WS, *myth1-1*, and *myth1-2* seedlings. Briefly, seedlings were incubated in 1 mg/mL (w/v) propidium iodide in ddH_20 for 90 seconds, briefly rinsed in ddH_20, and mounted in ddH_20 before visualization with Nikon ECLIPSE Ti2 using a laser power source with 488 nm excitation wavelength and 40x objective. Numerical aperture was set to 1.2 microns and 1024 pixel area images collected with 6.2 pixel dwell time.

Generation and purification of anti-MyTH1 antibodies

LOBSTR *E. coli* cells transformed with pRSF-Duet vector containing His_6-AtMyTH1 were grown at 37 °C in Luria broth supplemented with 50 mg/L kanamycin and 34 mg/L chloramphenicol until OD_{600} reached 0.6 before induction with 0.1 mM isopropyl b-D-1-thiogalactopyranoside and expression of protein for 16 hours at 18 °C. Cells were concentrated by centrifugation at 6,000 x g, washed with 1x Tris buffered saline, pH 7.4, and re-suspended in a lysis buffer of 500 mM KCl, 100 mM Tris-HCl pH 7.4, 5 mM $MgCl_2$, 20 mM imidazole, 2 mM β-mercaptoethanol, 1x protease inhibitor cocktails and supplemented with 20 mg benzamidine-HCl and 20 mg lysozyme before sonication to lyse *E. coli* cells. Soluble protein was collected and incubated with HisPur Co^{2+} resin (Invitrogen, 89964) according to manufacturer's instructions. Following elution, His_6-AtMyTH1 was dialyzed against 1x phosphate buffered saline pH 7.4, 150 mM NaCl, 5%

glycerol, and 2 mM β-mercaptoethanol. Concentration of dialyzed protein was determined by Pierce BCA protein assay (ThermoScientific 23225) against a bovine serum albumin standard curve.

GST-AtMyTH1 was purified from Rosetta *E. coli* cells transformed with pDEST15 expression vector after an expression period of 1.5 hours at 37 °C induced with 0.1 mM isopropyl b-D-1-thiogalactopyranoside when the OD_{600} of the culture reached 0.45. Following lysis in a buffer of 1x phosphate buffered saline pH 7.4, 500 mM NaCl, 10 mM EDTA, 0.1% Tween-20, and 1 mM PMSF and purification using glutathione Sepharose (Cytiva17075604) following manufacturer's instructions, GST-AtMyTH1 was covalently crosslinked to beads using dimethyl pimelimidate dihydrochloride (Sigma 8388-1G).

Rabbit antibodies generated against His_6-AtMyTH1 (Covance Research Products) were purified against GST-AtMyTH1 covalently linked to glutathione Sepharose beads (Cytiva17075604) and eluted using 100 mM glycine pH 2.5 into a buffer of 1 M Tris pH 8.0 before concentration and buffer exchange using 10 kDa MWCO filter into 1x TBS, pH 7.3 supplemented with bovine serum albumin to a concentration of 1.0 mg/mL.

Expression and purification of AtSCD1 in HEK293-FT Cell Culture

20 μg of pFLAG CMV 5.1 vector containing N-terminally twinStrep-tagged full-length or truncated AtSCD1 encoding ORFs (Supplemental Figure 4S2) purified using the PureLink™ HiPure Plasmid Midiprep Kit (Invitrogen K210004) were introduced using calcium phosphate transfection into 70-90% confluent HEK293-FT cells cultured in DMEM + 10% fetal bovine serum. Following expression for 48 hours, cells were collected

and re-suspended in Buffer W (100 mM Tris-HCl pH 8.0, 150 mM NaCl, 1 mM EDTA, 1% Triton X-100 (v/v), 1 mM DTT, 1x cOmplete EDTA-free protease inhibitor cocktail (Roche, 11386170001)). Cells were lysed by passage through a 23 gauge needle 20x and the lysate subsequently clarified by centrifugation at 190,000 x g in a TLA 100.3 rotor at 4 °C. The S190 fraction was then incubated with Strep-Tactin Sepharose (IBA 2-1201-002) for 1 hour at 4 °C and washed 3x with Buffer W. Immobilized twin-Strep tagged proteins and Strep-Tactin Sepharose were supplemented with SDS-PAGE sample buffer and analyzed by SDS-PAGE and quantitative immunoblotting using anti-SCD1 antibody.

Protein and Lipid Binding Assays

2.5 μg each of His_6-AtMyTH1 and commercial GST-PLC_{δ}^{PH} (Echelon Biosciences G-4501) were incubated with PIP strips (Echelon Biosciences P-6001) following manufacturer's instructions before immunoblotting using anti-GST or anti-AtMyTH1 primary antibodies in a primary antibody solution of 1x Tris buffered saline, 0.1% (v/v) Tween-20, and 4% fat-free milk and a secondary antibody solution of 1x phosphate buffered saline, 0.1% (v/v) Tween-20, and 3% (w/v) bovine serum albumin. Chemiluminescent detection was performed using SuperSignal™ West Femto Maximum Sensitivity Substrate (ThermoFisher Scientific 34094) and an iBright CL1000 imaging system (ThermoFisher Scientific).

TAP-SCD1 was co-immunoprecipitated from PSB-d suspension cell culture soluble protein extracts prepared in the presence of Triton X-100 as described (Mayers et al., 2017) against purified GST or GST-MyTH1 as bait proteins immobilized on glutathione

Sepharose or His_6-AtMyTH1 immobilized on Co^{2+} HisPur resin or Co^{2+} resin alone as bait. Following washes, glutathione Sepharose and Co^{2+} resin were supplemented with SDS-PAGE sample buffer and the identities of proteins bound determined by SDS-PAGE and immunoblotting using anti-SCD1 or anti-MyTH1 antibodies.

Aliquots of S190 fractions of HEK293-FT cells expressing twinStrep-AtSCD1^{FULL} prepared as described above (*Expression and purification of AtSCD1 in HEK293-FT Cell Culture*) were incubated with GST, GST-AtMyTH1, or GST-RabE1c^{WT} purified as described above or as previously described (Mayers et al., 2017) and immobilized on glutathione Sepharose. 1% of the input (GST or GST-tagged proteins and S190 of twinStrep-AtSCD1^{FULL} expressing HEK293-FT orTAP-SCD1 expressing PSB-d soluble protein fraction) was removed and supplemented with SDS-PAGE sample buffer for analysis. Following washes with a buffer of 1x phosphate buffered saline pH 7.4, 500 mM NaCl, 0.1% Tween-20, 1 mM β-mercaptoethanol, SDS-PAGE sample buffer was added directly to the glutathione Sepharose beads and the bound proteins analyzed by SDS-PAGE and immunoblotting using anti-GST or anti-SCD1 antibodies.

Preparation of microsomal membrane fractions

Undifferentiated suspension cultured PSB-d Arabidopsis cells grown in MSMO growth media under constant darkness on an orbital shaker were collected 6 days after passaging through centrifugation at 50 x g. Pelleted cells were re-suspended in microsomal isolation buffer (MIB: 20 mM HEPES/NaOH pH 7.2, 50 mM KOAc, 1 mM $Mg(OAc)_2$, 250 mM sorbitol, 1 mM DTT) and lysed twice using a nitrogen bomb protocol. Cellular debris was fractionated using a 1,000 x g spin for 10 minutes at 4 °C, and the S1

fraction centrifuged at 150,000 x g for 30 minutes at 4 °C. P150 resuspended in MIB and re-centrifuged at 150,000 x g for 30 minutes at 4 °C to ensure no S150 was retained. Pellet re-suspended in volume of MIB equivalent to original S150 volume. S1, S150, and P150 fractions were subsequently analyzed through SDS-PAGE or native PAGE.

Protein extract preparation, SDS-PAGE, and native PAGE of scd *and wild-type seedlings*

6 DAG Col-0, *scd2b-2*, *scd2c-3*, and *myth1-2* seedlings germinated on ½ MS + 0.6% agar (w/v) were ground under N_2 (l) in an extraction buffer of 50 mM HEPES/NaOH pH 7.6, 100 mM KCl, 0.5 mM EDTA, 0.5 mM MgCl2, 0.05% NP-40 (v/v), 10% glycerol, 1x PICD, 1x PICW, 1x PhosSTOP™ phosphatase inhibitor (Roche 4906845001), and Triton X-100 at a final concentration of 0.5% (v/v). The lysate was clarified with a 16,000 x g spin for 10 minutes at 4 °C to pellet, and S16 fraction centrifuged at 150,000 x g in Beckman polyallomer tubes in a TLA 100.3 rotor for 20 minutes at 4 °C to yield the S150 fraction. S150 fractions were quantitated using Pierce BCA protein assay (ThermoScientific 23225) against a bovine serum albumin standard curve.

For SDS-PAGE, S150 samples were supplemented with 3x SDS-PAGE Laemmli sample buffer and heated for 5 minutes at 65 °C. Equal amounts of protein by mass across each condition were loaded alongside Precision Plus Protein All Blue prestained protein standards (Bio-Rad 1610373) in a 4-12.5% acrylamide gel before transferring to nitrocellulose membrane and immunoblotting using anti-SCD1 and anti-cFBPase primary antibodies at 1:1000 in 1x Tris buffered saline + 0.1% Tween-20 (v/v) + 4% (w/v) milk. To

account for changes in SCD1 protein abundance between *scd* and accessory mutants in comparison to wild-type, cFBPase levels were used as a loading control, and the amount of SCD1 protein relative to cFBPase protein was determined for each genetic background. This ratio in mutant backgrounds was subsequently normalized to the ratio for wild-type. Three independent SDS-PAGE and quantitative immunoblots were performed using S150 purified from pooled homozygous *scd2b*, *scd2c*, and *myth1-2* seedlings, and one-way ANOVA with multiple comparison statistical analysis was performed using Prism 9 (GraphPad) to assess whether the ratio of SCD1:cFBPase was significantly different between wild-type and *scd2b*, *scd2c*, and *myth1-2* backgrounds.

For native PAGE analysis, S150 samples were prepared in the same manner as described above without phosphatase inhibitors and supplemented with native PAGE buffer and NativePAGE 5% G-250 sample additive to a concentration one-quarter of the detergent present in the protein samples. Equal amounts of S150 from wild-type, *scd2-1*, Col-0/*SCD2b*::*RFP-SCD2b*, and Col-0/*Ubq*$_{10}$*::RFP-SCD2c* were separated by 4-16% NativePAGE^{TM} 4 to 16%, Bis-Tris, 1.0 mm protein gel (Invitrogen BN1002BOX) alongside NativeMARK^{TM} unstained protein standards (Invitrogen LC0725). Resolved proteins were transferred to PVDF membrane before fixation with 8% (v/v) acetic acid and incubation of membrane with Ponceau stain (0.1% (w/v) Ponceau S and 5% (v/v) acetic acid) to stain protein standards and assess equal loading across conditions. Following Ponceau staining, PVDF membranes were blocked using the same procedure as nitrocellulose membranes and incubated with primary antibodies: anti-SCD1 (1:1000), anti-SCD2^{BROAD} (1:1000), or anti-RFP (1:000).

Primary antibodies used are detailed in Supplemental Table 4S2.

Semiautomated measurement of cotyledon area

High resolution images were taken of Col-0, *scd2c-3*, *scd2b-2*, *scd2-1*, and *myth1-2* seedlings germinated on ½ MS + 0.6% (w/v) agar plates and grown for 6 days after germination under constant light. FIJI was used to process raw image files by first setting the scale to 1.0 cm and cropping the image to exclude the border of the plate but include as many seedlings as possible. The color image of seedlings was then converted to 8 bit and the threshold adjusted so “default” and “red” settings selected. The analyze particles feature was then selected and threshholded such that an area of 0.005 pixels^2 was the minimum size of object to be measured (practically, only seeds were excluded at this threshold). Circularity was set to 0.00 – 1.00. The following parameters were selected: show outlines, display results (area), summarize, add to manager, exclude on edges, and include holes. Manual annotation was performed to ensure that all counted structures were true individual seedlings (thus, any clumped seedlings were excluded). The resulting table of sizes (area) of seedlings observed was analyzed by Prism 9 (GraphPad). Between 12 and 31 seedlings were measured from each background, and one-way ANOVA with multiple comparison statistical analysis was performed.

Bioinformatic Analyses

Protein domain predictions were obtained using InterPro (EBI, European Molecular Biology Laboratory) (Madeira et al., 2022), ProSite (Expasy, Swiss Institute of Bioinformatics), PFAM (EBI, European Molecular Biology Laboratory) (Madeira et al., 2022), and UniProt (UniProt, 2021). Protein sequence identities and alignments across

more than two sequences were determined using Clustal Omega (Sievers et al., 2011). Pairwise sequence identity and similarity were calculated using EMBOSS Needle (Rice et al., 2000). Peptide sequences enriched in basic hydrophobic character were identified using BH-search (Brzeska et al., 2010).

Figures

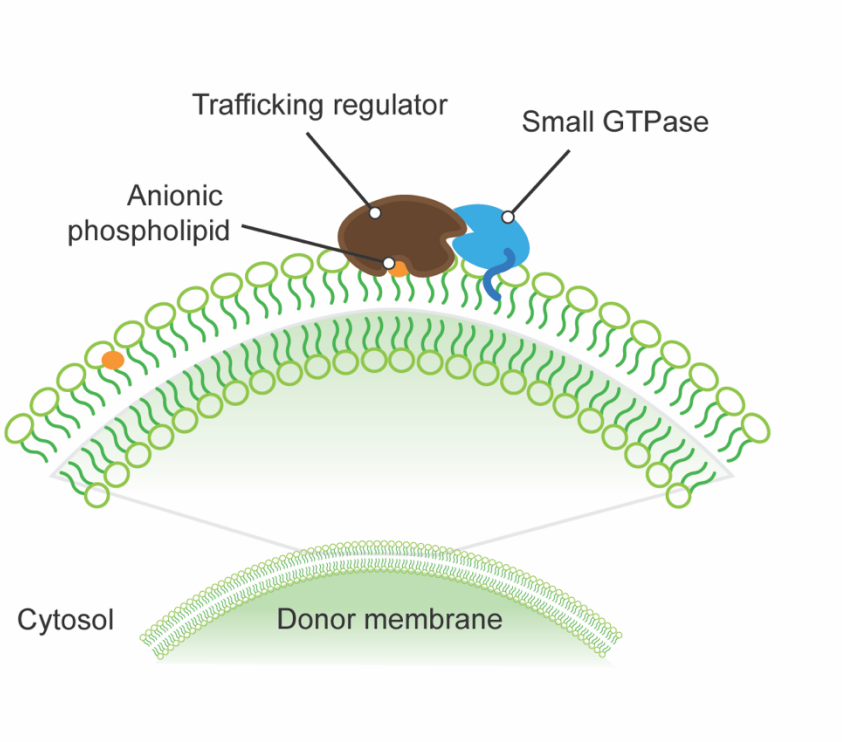

Figure 4.1 Generic model of coincident detection

Figure 4.1 Generic model of coincident detection

Stylized illustration depicting the principle of coincident detection, in which a trafficking regulator protein is recruited to a specific membrane due to simultaneous interaction with both an anionic phospholipid and small GTPase present at that membrane.

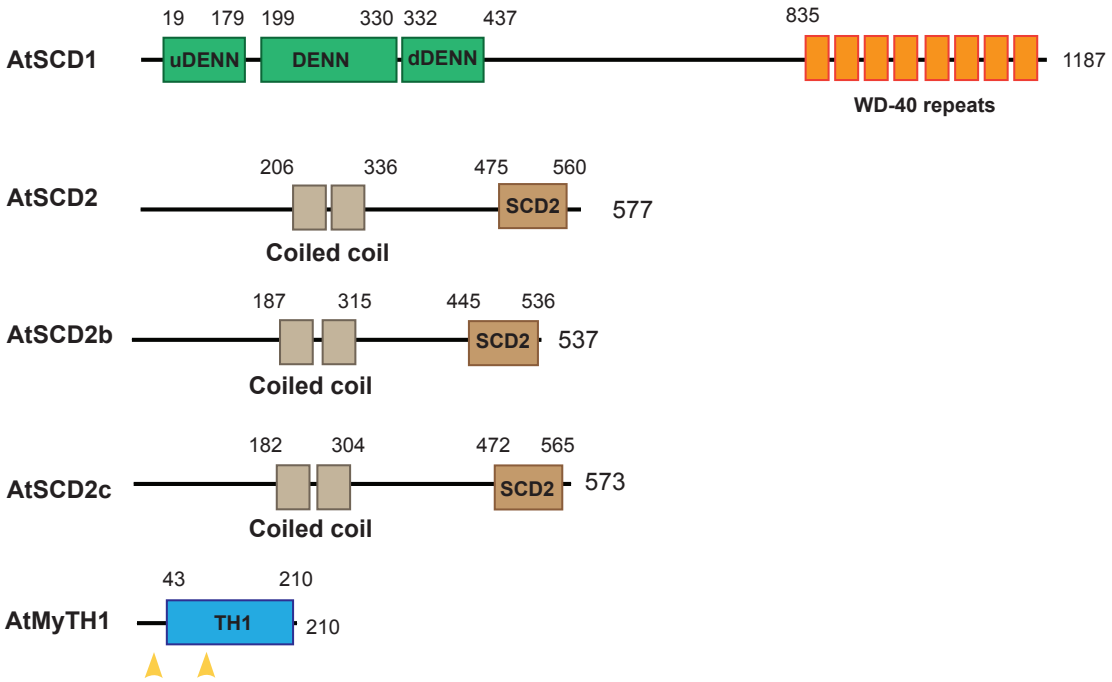

Figure 4.2: Domain organization of SCD complex & associated proteins

Figure 4.2 Domain organization of SCD complex and accessory proteins

Schematic illustrating the domains and their relative positions corresponding to the *Arabidopsis thaliana* SCD1; SCD2 and its paralogs, SCD2b and SCD2c; and MyTH1 proteins containing 1187, 577, 537, 573, and 210 amino acids respectively. The relative positions and sizes of the domains within each protein are demarcated by the residue numbers above each respective domain. SCD1 contains a tripartite DENN domain, intermediate linker region, and eight C-terminal WD-40 motifs. SCD2, SCD2b, and SCD2c contain two coiled-coil domains and a C-terminal domain of unknown function characterized as the "SCD2 domain" (IPR040321). MyTH1 contains a short unstructured N-terminus of about 40 amino acids and a Tail Homology I (TH1) domain named for homology to the tail region of Myosin I. In turn, the TH1 domain contains a pleckstrin homology domain. Yellow triangles indicate regions of relatively high basic-hydrophobic character potentially mediating interaction with anionic phospholipids.

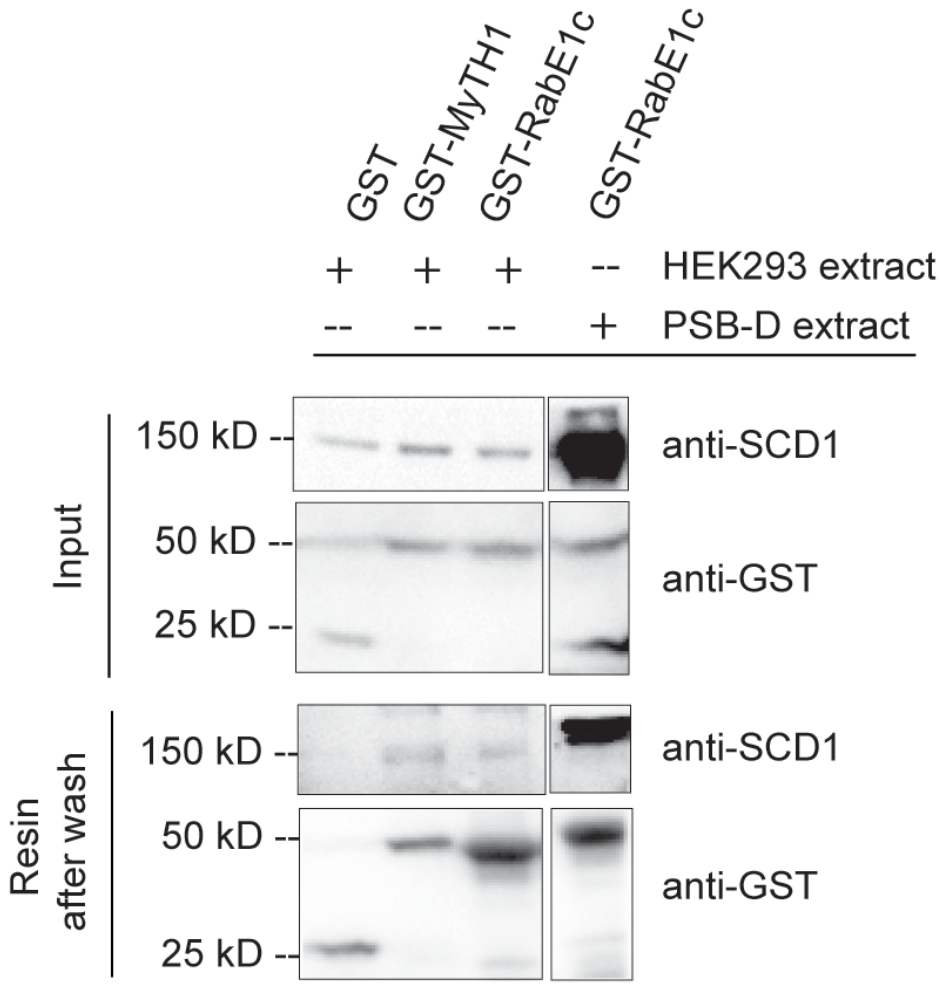

Figure 4.3 HEK293-FT expressed twinStrep-linker-AtSCD1^{FULL} interacts directly with AtMyTH1

Figure 4.3 HEK293-FT expressed twinStrep-linker-AtSCD1^{FULL} interacts directly with AtMyTH1.

Soluble protein extract prepared from Arabidopsis suspension cultured PSB-d cells expressing TAP-SCD1 or HEK293-FT cultured cells expressing full-length twinStrep-linker-AtSCD1^{FULL} was incubated with recombinant GST, GST-MyTH1, or GST-RabE1c. Binding of bait and soluble extract proteins was assessed through immunoblotting of binding assay inputs (top panels) and proteins retained to glutathione Sepharose resin after washing unbound proteins (bottom panel) using antibodies for SCD1 and GST. Anti-SCD1 antibody detects SCD1 protein on the glutathione Sepharose resin when baits GST-MyTH1 or -RabE1c are used to pull-down twinStrep-linker-AtSCD1^{FULL} (150 kDa) or TAP-SCD1 (150 kDa).

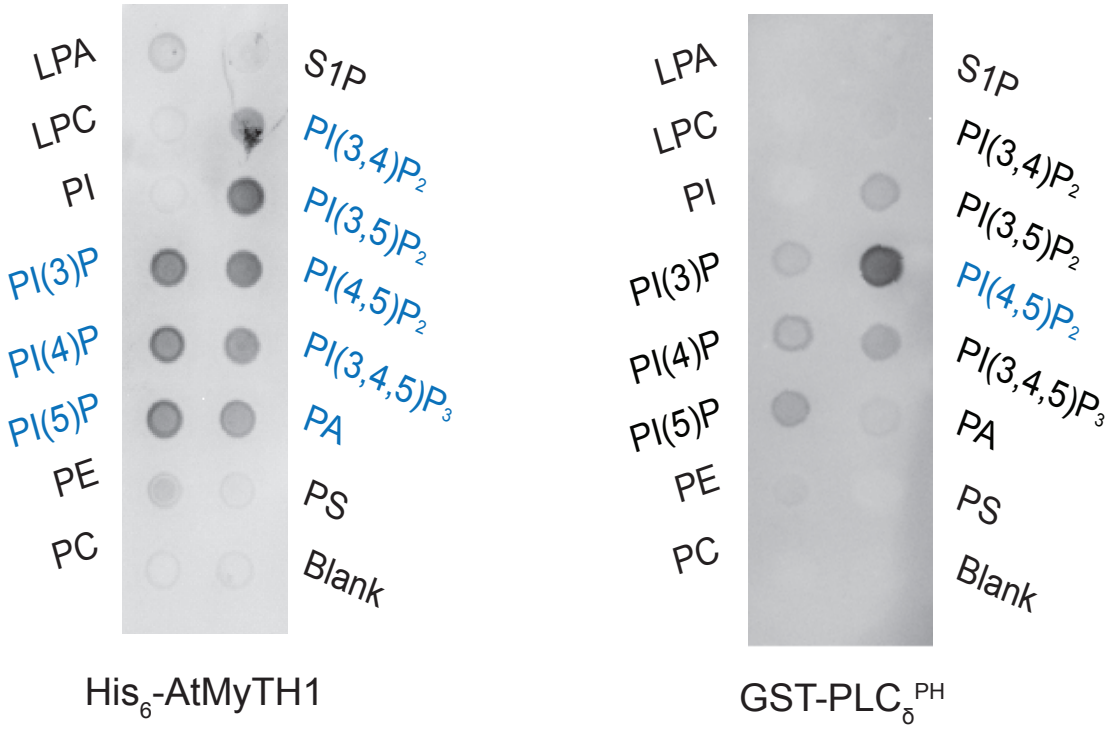

Figure 4.4 AtMyTH1 interacts broadly *in vitro* with phosphatidylinositol phospholipids

Figure 4.4 AtMyTH1 interacts broadly *in vitro* with phosphatidylinositol phospholipids.

The presence of 2.4 μg and 2.5 μg of recombinant His_6-AtMyTH1 or GST-PLC_{δ}^{PH} incubated with PIP strips (Echelon Biosciences P-6001) on which various species of phospholipids are immobilized were detected by immunoblotting using anti-MyTH1 or anti-GST antibodies. Phospholipid species labeled in blue indicate positive reaction between the lipid and the protein of interest incubated with that membrane. Recombinant AtMyTH1 has affinity for multiple phosphatidylinositol phosphate species (PI(3)P, PI(4)P, PI(5)P, PI(3,4)P_2, PI(3,5)P_2, PI(4,5)P_2, PI(3,4,5)P_3) and phosphatidic acid but not for phosphatidylethanolamine (PE), phosphatidylserine (PS), phosphatidylcholine (PC), or phosphoinositide (PI). Commercial GST-PLC_{δ}^{PH} (G-4501) interacted specifically with PI(4,5)P_2.

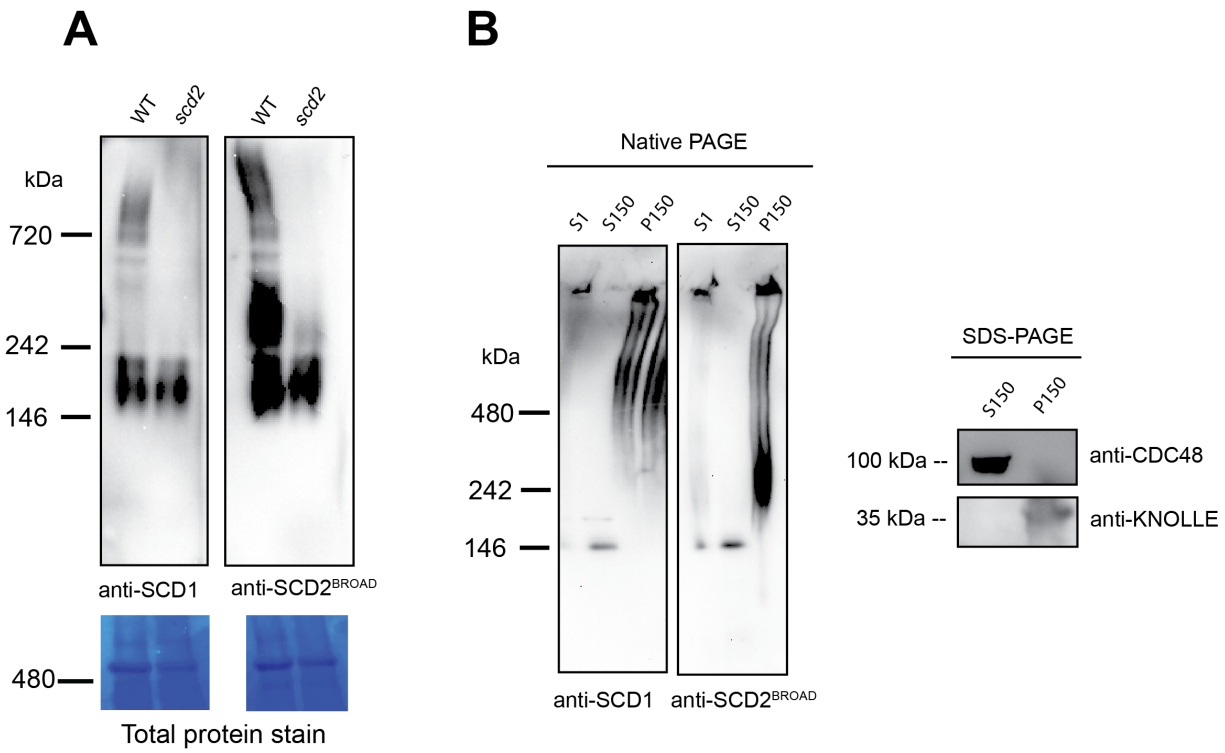

Figure 4.5 SCD2 is required for assembly of high molecular weight SCD complex

Figure 4.5 SCD2 is required for assembly of high molecular weight SCD complex.

A. 22.5 μg of detergent solubilized protein extract prepared from pooled WT or *scd2-1* Arabidopsis seedlings in the presence of TX-100 and NP-40 were analyzed by 4-16% native PAGE and immunoblotting using antibodies for SCD1 (anti-SCD1) or SCD2 and its orthologs, SCD2b and SCD2c (anti-SCD2^{BROAD}). Visualization of equal protein loading obtained by Ponceau staining is indicated below each corresponding immunoblot.

B. Equivalent volumes of S1, S150, and P150 prepared in the absence of detergent from suspension cultured Arabidopsis PSB-d cells were analyzed by (left) 4-16% native PAGE and immunoblotting using antibodies for SCD1 (anti-SCD1) or SCD2 and its orthologs, SCD2b and SCD2c (anti-SCD2^{BROAD}); or (right) 4-12% SDS-PAGE and immunoblotting using antibodies for CDC48 (anti-CDC48; cytosolic protein marker) and KNOLLE (anti-KNOLLE; integral membrane protein marker). Numbers to the left of immunoblots indicate the molecular weight of the native or denatured proteins visualized.

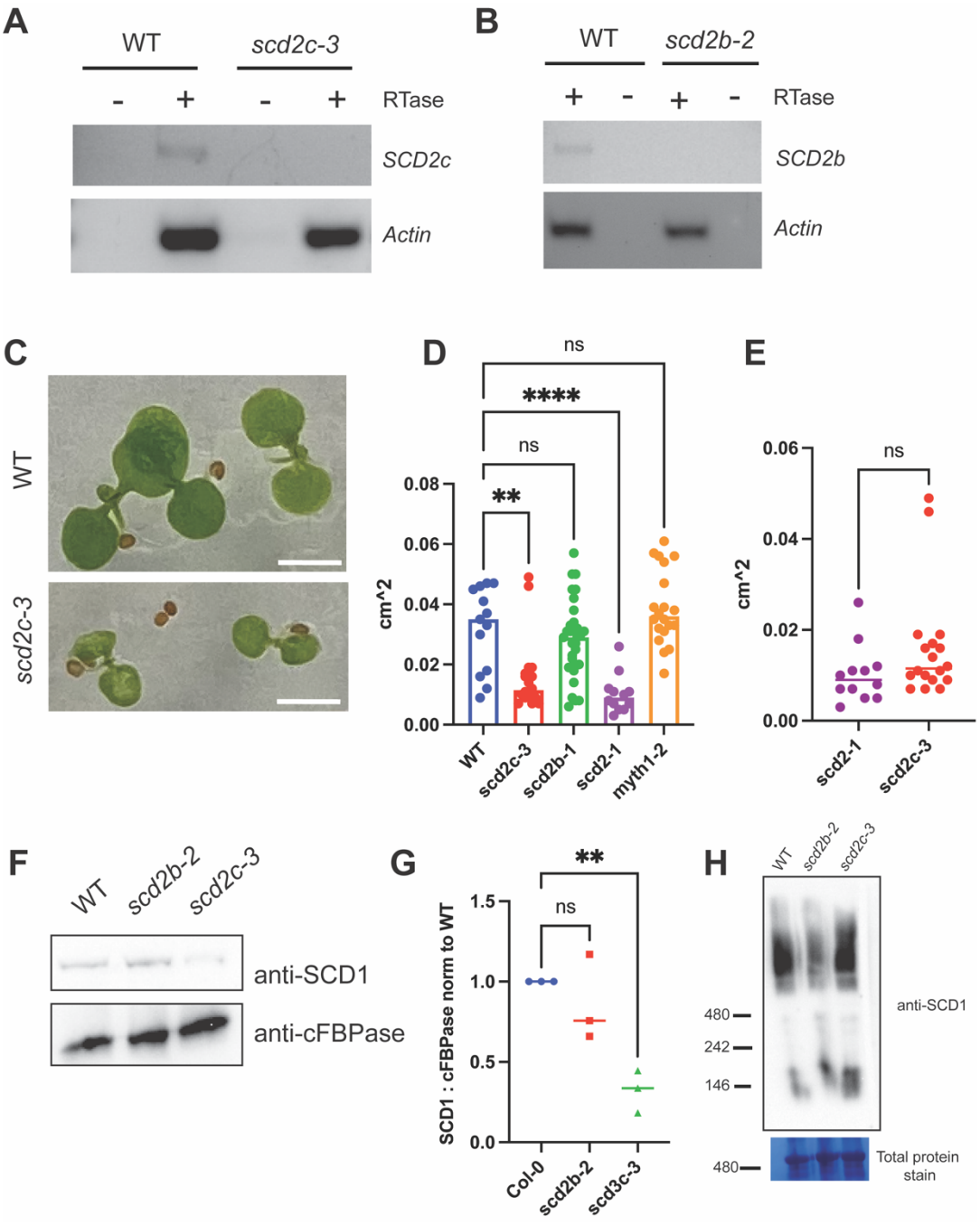

Figure 4.6 Validation and characterization of *scd2-like* mutants

Figure 4.6 Validation and characterization of *scd2-like* mutants.

A. Amplification of 100 bp *Actin* and ~1700 bp *SCD2c* cDNA from cDNA library prepared from WT and *scd2c-3* Arabidopsis seedlings in the presence or absence of reverse transcriptase (RTase) as indicated.

B. Amplification of 100 bp *Actin* and ~1700 bp *SCD2b* cDNA from cDNA library prepared from WT and *scd2b-2* Arabidopsis seedlings in the presence or absence of reverse transcriptase (RTase) as indicated.

C. WT and *scd2c-3* Arabidopsis seedlings 6 days after germination on ½ MS + 0.6% (w/v) agar without sucrose. Scale bar = 200 μm.

D. Area (cm^2) of cotyledons of individual seedlings of WT (Col-0), *scd2c-3*, *scd2b-1*, *scd2-1*, and *myth1-2* backgrounds 6 days after germination on ½ MS + 0.6% agar (w/v) without sucrose (n = 12 – 21 seedlings). Statistical significance provided by one-way ANOVA with multiple comparisons. ** p value < 0.0019. *** p value < 0.0001.

E. Area (cm^2) of cotyledons of individual seedlings of *scd2-1* and *scd2c-3* seedlings 6 days after germination ½ MS + 0.6% agar (w/v) without sucrose. Statistical significance provided by two-tailed t-test. ns, no statistical significant difference.

F. Immunoblot of 22.5 μg of detergent solubilized protein extract prepared from pooled WT, *scd2b-2*, or *scd2c-3* Arabidopsis seedlings in the presence of TX-100 and NP-40 analyzed by SDS-PAGE. Immunoblotting using antibodies for SCD1 (anti-SCD1) control cytosolic protein marker, cFBPase (anti-cFBPase) was performed to normalize equal protein amounts in each lane.

G. Quantitation of immunoblots in **(F)** using densitometry scanning. Size and mean intensity of bands detected by anti-SCD1 antibody were normalized to size and mean intensity of bands detected by anti-cFBPase for each background. Three biological replicates (three separate SDS-PAGE and immunoblots from pooled WT, *scd2b*, or *scd2c* seedlings) were performed and statistical significance derived from one-way ANOVA with multiple comparisons. ** p value < 0.0055.

H. 25 μg of detergent solubilized protein extract prepared from pooled WT, *scd2b-2,* or *scd2c-3* Arabidopsis seedlings in the presence of TX-100 and NP-40 were analyzed by 4-16% native PAGE and immunoblotting using antibodies for SCD1 (anti-SCD1). Visualization of equal protein loading obtained by Ponceau staining is indicated below each corresponding immunoblot.

Model #1:
Coincident detection
with SCD1, SCD2, and MyTH1

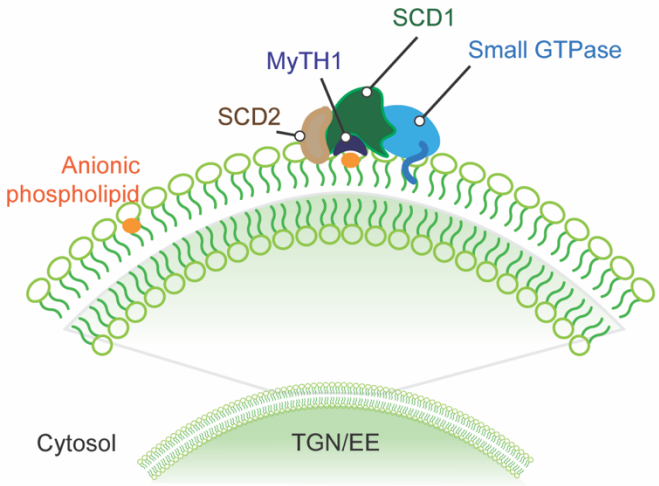

Model #2:
Coincident detection
with SCD1 and SCD2

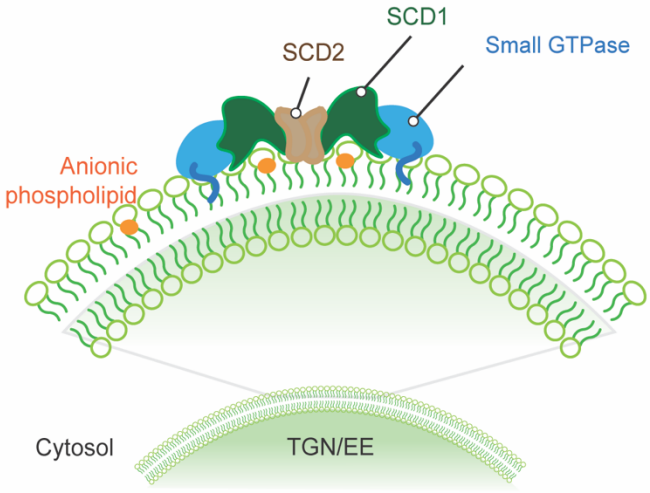

Figure 4.7 Models of SCD complex recruitment to the TGN/EE via coincident detection

Figure 4.7 Models of SCD complex recruitment to the TGN/EE via coincident detection

Stylized illustrations depicting hypothetical models by which coincidence detection regulates the recruitment to and retention of the SCD complex at the TGN/EE to facilitate exocytic trafficking. In the top model, SCD1 is recruited to the TGN/EE through simultaneous interaction with 1) MyTH1 which in turn interacts with anionic phospholipids enriched at the TGN/EE and 2) a small GTPase localized to the TGN/EE. In the second model, SCD1 does not depend on MyTH1 for recruitment to the TGN/EE and instead is recruited to or retained at the TGN/EE via simultaneous interaction with 1) a small GTPase localized to the TGN/EE and 2) interaction with SCD2 which oligomerizes with SCD2 of another SCD complex localized to the TGN/EE via interaction with a small GTPase.

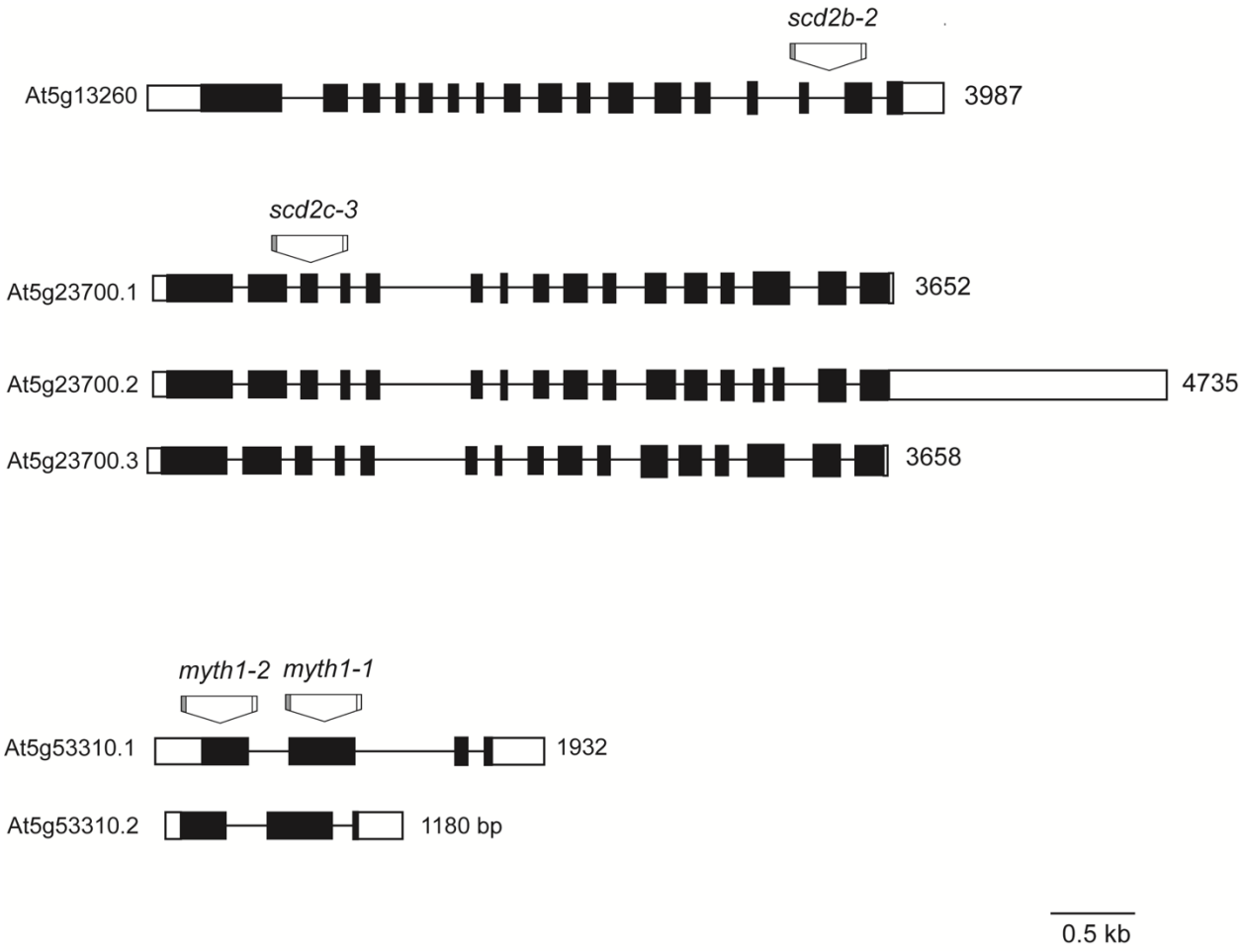

Figure 4S1 Gene organization of *AtSCD2b, AtSCD2c,* and *MyTH1*

Figure 4S1 Gene organization of *AtSCD2b, AtSCD2c,* and *AtMyTH1*

Schematics of the gene organizations of the predicted variants of the genes encoding AtSCD2b, AtSCD2c, and AtMyTH1 with the positions of the T-DNA insertions of the *scd2b-2*, *scd2c-3*, *myth1-2*, and *myth1-1* alleles. Unfilled boxes represent untranslated regions (UTRs), filled boxes represent exons, and unboxed lines represent introns. T-DNA insertions are not drawn to scale. Scale bar = 0.5 kb.

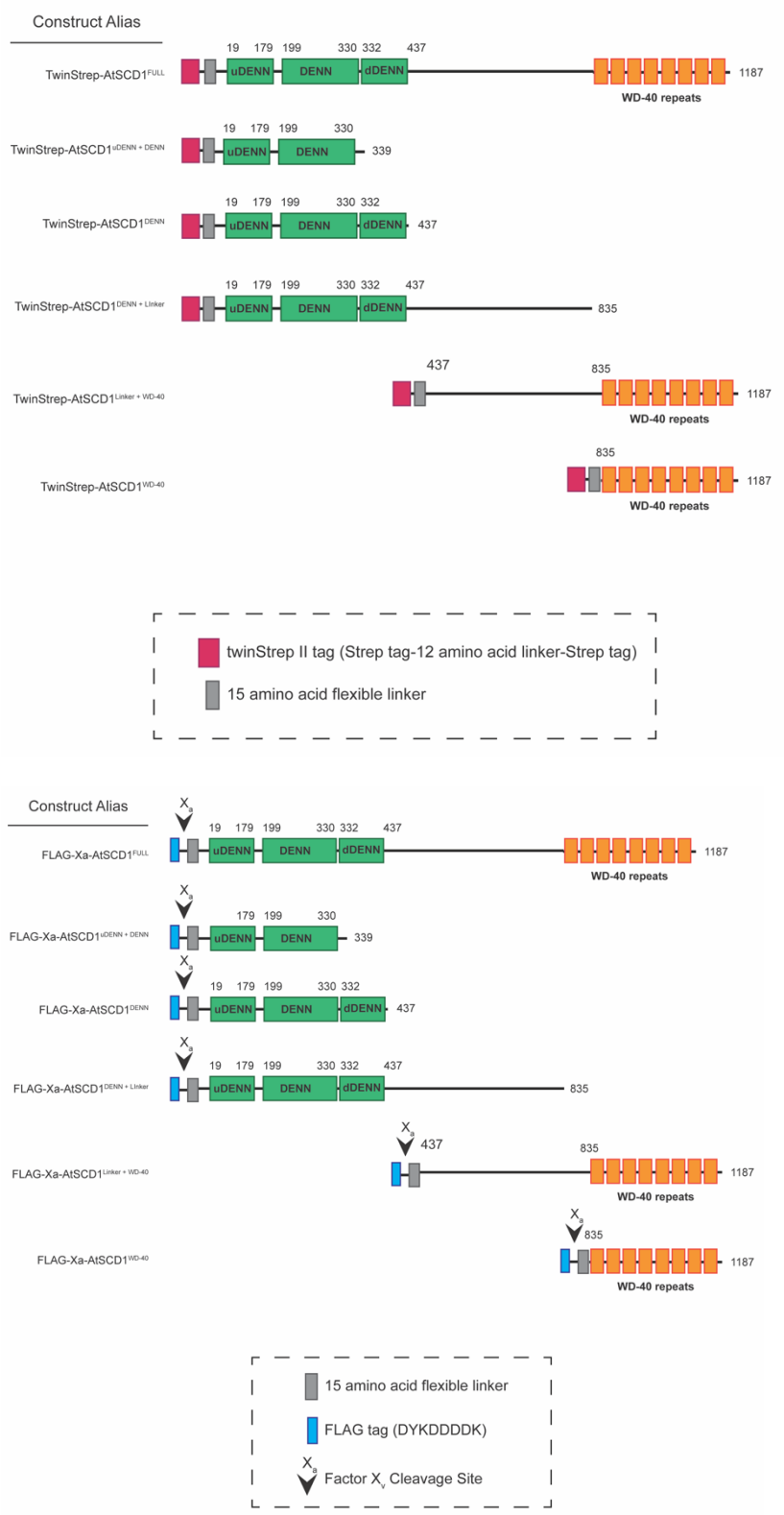

Figure 4S2 Scheme of recombinant full-length and truncated AtSCD1 constructs

Figure 4S2: Scheme of recombinant full-length and truncated AtSCD1 constructs

Schematics illustrating the recombinant AtSCD1 reagents generated for expression in mammalian cell culture. Full-length or truncated AtSCD1 were tagged at the N-terminus with an epitope tag and linker region as well as possible cleavage site to facilitate purification of AtSCD1 using the mammalian expression vector, pFLAG CMV 5.1.

(Top) A twinStrep tag consisting of two Strep tags separated by a 12 amino acid flexible linker (WSHPQFEK-GGGSGGGSGGSA-WSHPQFEK) followed by a 15 amino acid flexible linker (GGGGSGGGGSGGGGS) was cloned at the N-terminus of the full-length AtSCD1 protein sequence (1-1187 amino acids) or truncations consisting of the uDENN + DENN segments of the tripartite DENN domain (1-339 aa); the complete tripartite DENN domain (1-437 aa); the tripartite DENN domain + intermediate linker region (1-835 aa); the intermediate linker region + WD-40 repeats (437-1187); or the WD-40 repeats (835-1187 aa). The mammalian codon optimized open reading frames encoding these proteins were inserted into pFLAG CMV 5.1 by way of Gibson cloning at the SacI and BamHI restriction enzyme sites.

(Bottom) A FLAG epitope tag (DYKDDDDK) followed by a Factor Xa cleavage site (IEGR) and 15 amino acid flexible linker (GGGGSGGGGSGGGGS) was cloned at the N-terminus of the full-length AtSCD1 protein sequence (1-1187 amino acids) or truncations consisting of the uDENN + DENN segments of the tripartite DENN domain (1-339 aa); the complete tripartite DENN domain (1-437 aa); the tripartite DENN domain + intermediate linker

region (1-835 aa); the intermediate linker region + WD-40 repeats (437-1187); or the WD-40 repeats (835-1187 aa). The mammalian codon optimized open reading frames encoding these proteins were inserted into pFLAG CMV 5.1 by way of Gibson cloning at the NotI and BamHI restriction enzyme sites.

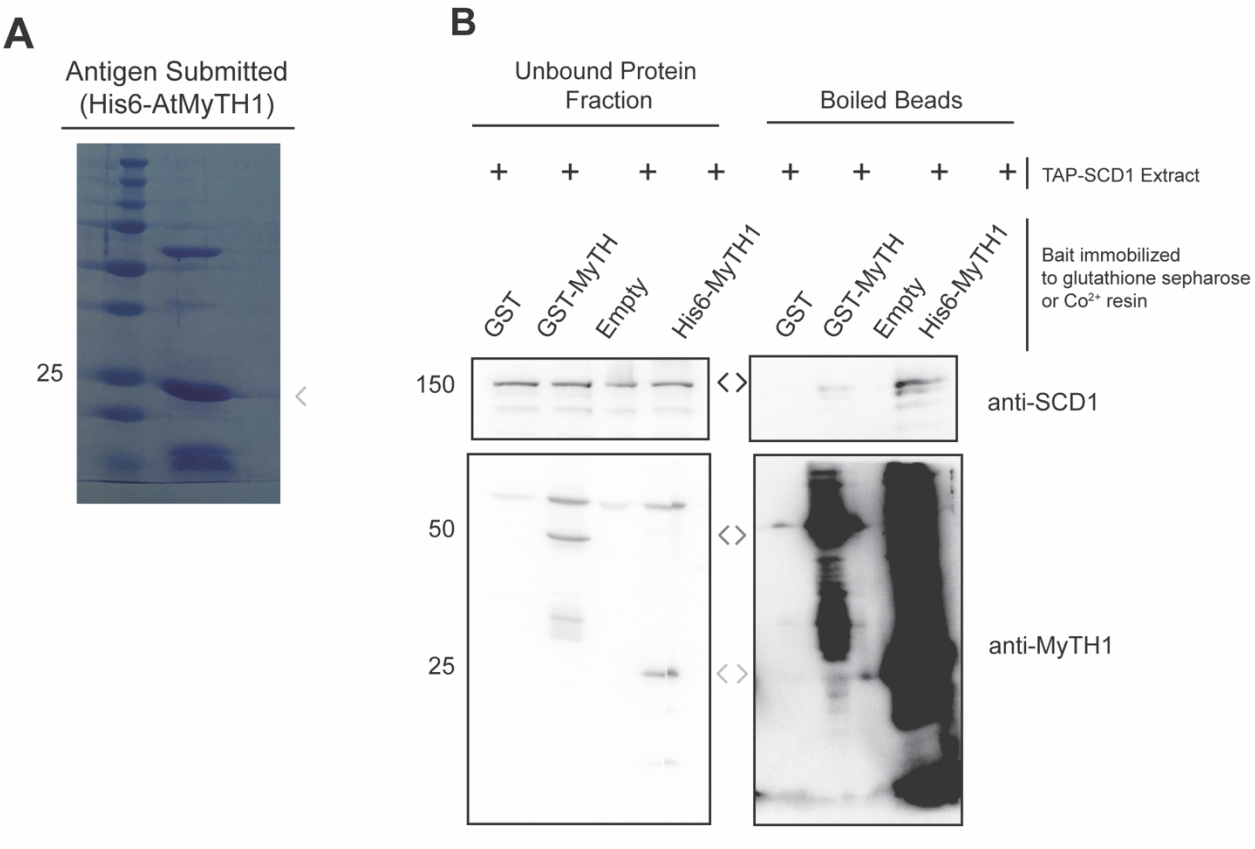

Figure 4S3: Generation and validation of anti-AtMyTH1 antibody

Figure 4S3: Generation and validation of anti-MyTH1 antibody

A) Coomassie stain of SDS-PAGE of recombinant His6-AtMyTH1 (25 kDa) submitted for polyclonal antibody production. The “25” kDa marker to the left of the SDS-PAGE indicates the His_6-AtMyTH1 protein.

B) Pull-down assay between recombinant GST-AtMyTH1 (50 kDa) and His_6-AtMyTH1 (25 kDa) and soluble protein extract of PSB-d cells expressing tandem affinity purification (TAP)-tagged AtSCD1 (TAP-SCD1, 150 kDa). TAP-SCD1 containing protein extract was incubated with GST (negative control) or GST-AtMyTH1 and glutathione Sepharose beads or His_6-AtMyTH1 and Co^{2+} resin or Co^{2+} resin alone (negative control). SDS-PAGE and immunoblotting using anti-SCD1 or anti-MyTH1 antibodies of unbound protein fractions (left) and resin with bound proteins (right) show association of TAP-SCD1 with recombinant, tagged AtMyTH1 constructs as well as recognition of 50 kDa (GST-AtMyTH1) and 25 kDa His_6-AtMyTH1 protein bands by anti-MyTH1 antibody.

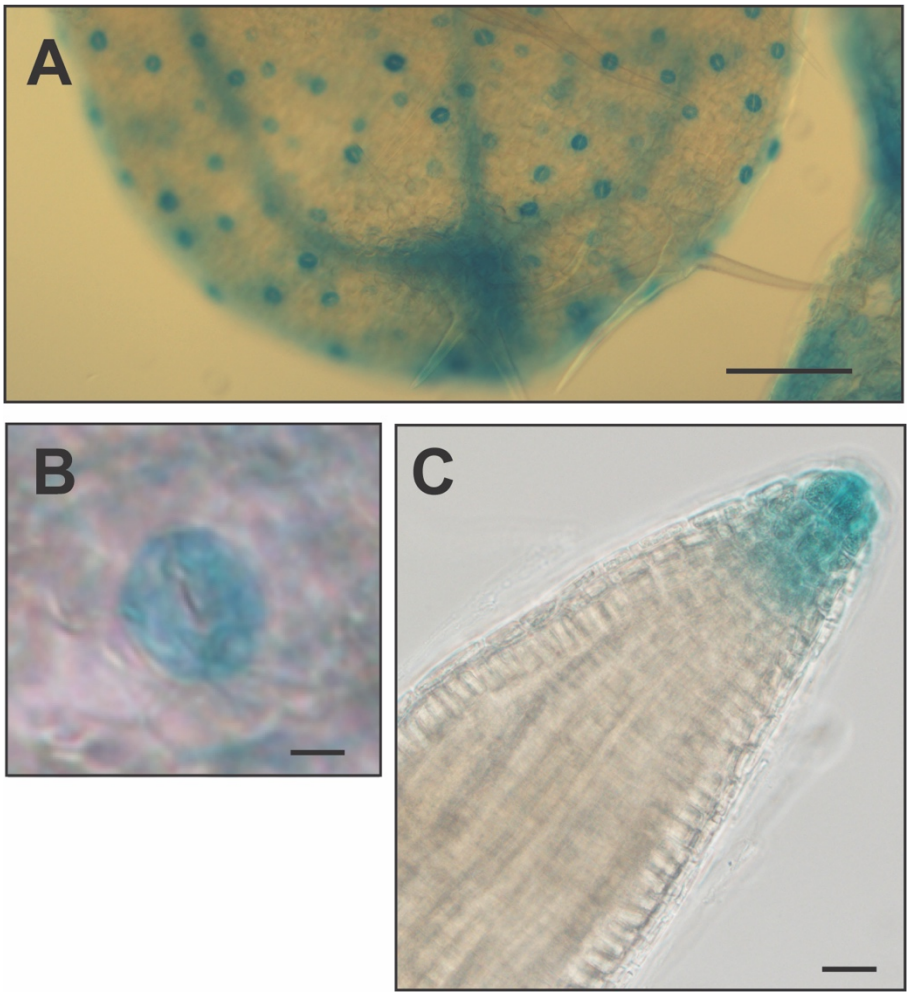

Figure 4S4: *MyTH1*$_{pro}$*-GUS* histochemical staining

Figure 4S4 *MyTH1$_{pro}$-GUS* histochemical staining

(A) *MyTH1$_{pro}$-GUS/*Col-0 cotyledon 5 days after germination. Strong blue staining of the stomatal guard cells indicates *MyTH1$_{pro}$* activity. Bar = 100 µm.

(B) *MyTH1$_{pro}$-GUS/*Col-0 stomatal guard cell 5 days after germination. Bar = 10 µm.

(C) Primary root tip of *MyTH1$_{pro}$-GUS/*Col-0 5 days after germination. Bar = 100 µm.

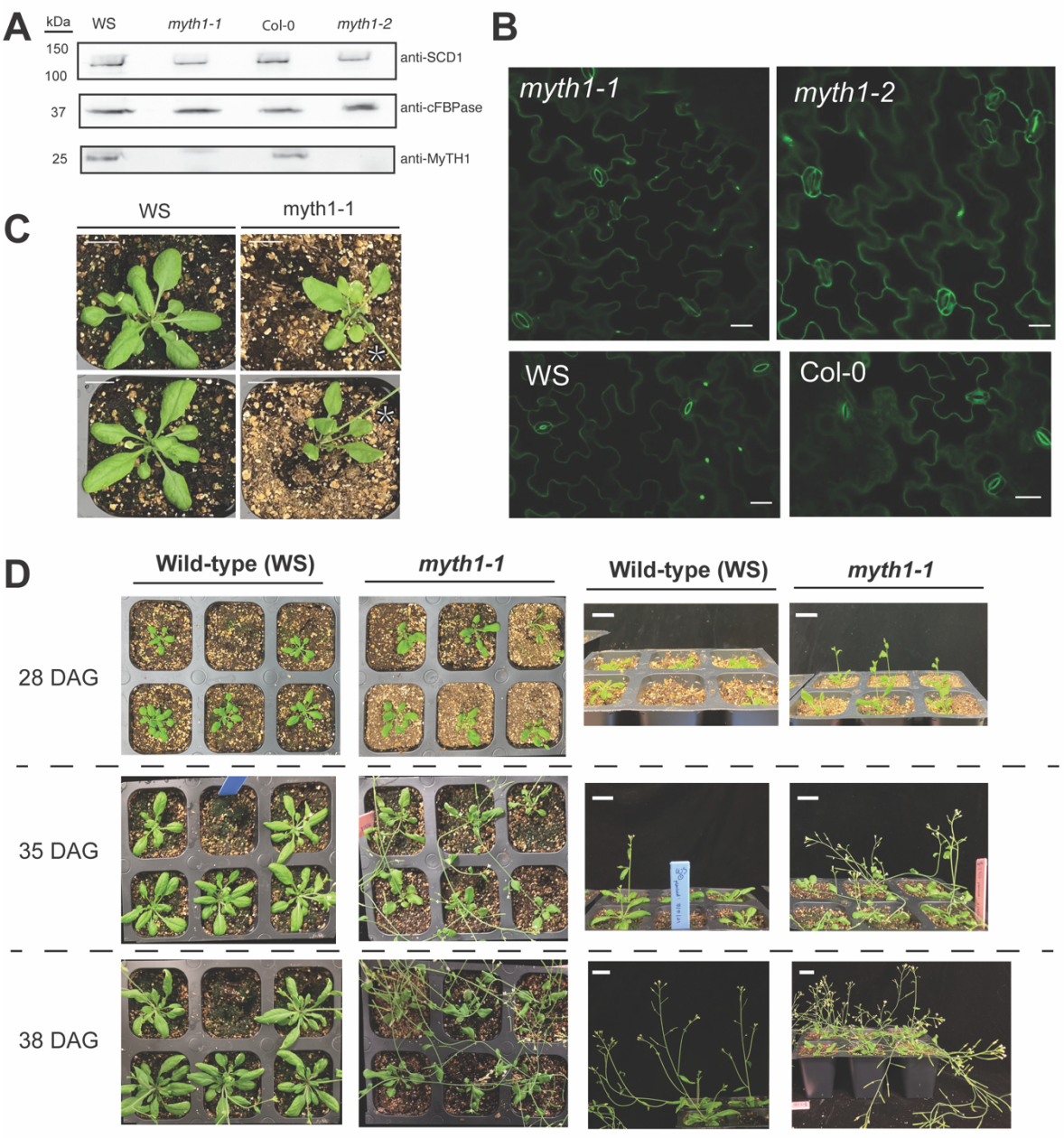

Figure 4S5: Validation and characterization of *myth1* mutants

Figure 4S5: Validation and characterization of *myth1* mutants

A) SDS-PAGE and immunoblot of total protein extracts prepared from WT (WS and Col-0), *myth1-1,* and *myth1-2* seedlings using antibodies for SCD1 (130 kDa), cFBPase (37 kDa), and MyTH1 (25 kDa).

B) Cell walls of pavement and stomatal guard cells of WT and *myth1* seedlings visualized using propidium iodide 6 days after germination. Scale bar = 10 μm.

C) Rosettes of WT (WS) and *myth1-1* plants 30 days after germination. White stars indicate presence inflorescence. Scale bar = 1.0 cm.

D) Aerial and side views following WT (WS) and *myth1-1* plants 28, 35, and 38 days after germination. Scale bar = 2.5 cm.

Arabidopsis thaliana			
Product	Accession Number	UniProtKB ID	Features of Interest
SCD1	At1g49040.1	Q8RXA7	Tripartite DENN domain 8x WD-40 motifs[1]
SCD2	At3g48860.2	Q8RWD5	Intrinsically disordered region 2x Coiled-coil domain SCD2 domain Clathrin binding motif APμ binding motif[2]
SCD2b	At5g13260	Q8VZL1	Intrinsically disordered region 2x Coiled-coil domain SCD2 domain APμ binding motif[2]
SCD2c	At5g23700	F4KE93	Intrinsically disordered region 2x Coiled-coil domains SCD2 domain Clathrin binding motif APμ binding motif[2]
MyTH1	At5g53310	Q9ASY2	Pleckstrin homology domain Basic hydrophobic motifs

Table 4S1 Accession numbers and features of *Arabidopsis thaliana* SCD complex and accessory proteins

Table 4S1 Accession numbers and features of *Arabidopsis thaliana* SCD complex and accessory proteins

Accession numbers and UniProtKB identification numbers corresponding to the protein product listed in the first column. Features of interest such as domains or motifs identified in earlier publications or predicted by bioinformatic tools such as UniProt, InterPro, ProSite, and BH-search are indicated in the column at the right.

Citations:

1. Falbel et al. *Development.* 2003.
2. McMichael et al. *Plant Cell.* 2013.

Antibodies	Clonality	Primary Dilution for Immunoblot	Secondary	Secondary Dilution	Citation in Work
anti-SCD1	Polyclonal	1:1000	Rabbit	1:5000	Korasick et al. 2010
anti-SCD2^{BROAD}	Polyclonal	1:1000	Rabbit	1:5000	McMichael et al. 2013
anti-MyTH1	Polyclonal	1:250	Rabbit	1:5000	This work
anti-cFBPase	Polyclonal	1:5000	Rabbit	1:5000	Agrisera AS04043
anti-GST	Polyclonal	1:1000	Rabbit	1:5000	
anti-RFP	Polyclonal	1:1000	Rabbit	1:5000	Applied Biological Materials G093
anti-CDC48	Polyclonal	1:1000	Chicken	1:5000	Rancour et al. 2002
anti-KNOLLE	Polyclonal	1:1000	Rabbit	1:1000	Rancour et al. 2002

Table 4S2 Antibodies used in this study

Table 4S2: Antibodies used in this study

Information describing the antibodies used in this study are presented (clonality, dilution factor of the primary antibody, secondary antibody information, and citation).

Name	Sequence (5' → 3')	Purpose/ Comments
DD 1	CGTGTGCCAGGTGCCCACGGAATAGT	FLAG Left Border (LB), Genotyping
DD 2	ATTTTGCCGATTTCGGAAC	SALK LB, Genotyping
DD 3	TAGCATCTGAATTTCATAACCAATCTCGATACAC	SAIL LB, Genotyping
DD 4	ATGAAGATCGAAGTGTGGGTG	FLAG 207A11 LP, Genotyping
DD 5	CGGACTATTATCGTGATTGCC	FLAG 207A11 RP, Genotyping
DD 6	CATCAAAAACCAAAAATTGCG	SAIL 828 G09 LP, Genotyping
DD 7	GCGGCGCTTCTTAATTAAAAC	SAIL 828 G09 RP, Genotyping
DD 8	AGCCTCCAGAGACACTCCTTC	SALK 048684C LP, Genotyping
DD 9	GGACCTATCAACGGTTCCTTC	SALK 048684C RP, Genotyping
DD 10	TGAAATCGTCATCCGAGATTC	SALK 015405C LP, Genotyping
DD 11	AGCCAGGCTTCTAATTTCACC	SALK 015405C RP, Genotyping
DD 12	CCCTCCAGAGAGGAAATACT	Actin RT PCR FW
DD 13	CTCGTCATACTCTGCCTTTG	Actin RT PCR REV
DD 14	ATGGAGCGAGCACGAACC	SCD2b RT PCR FW
DD 15	TTACTGGCTGGACCTGGAGG	SCD2c RT PCR REV
DD 16	ATGGATCTCAGGAGACCGAG	SCD2c RT PCR FW
DD 17	TTAAGAGTCAAGGTTGTGATTTGAAAG	SCD2c RT PCR REV
DD 18	GGCGTGTACGGTGGGAGGTCTATATAAGCAGAGCTATGTGGAGCCACCCCCAGTTC	twinStrep-AtSCD1 FW, Gibson
DD 19	CATCGTCGTCCTTGTAATCAGCCCGGGATCCTAAGGGATCTCCTCGCTGGTGGTGATC	twinStrep-uDENN+DENN+ 9 aa REV, Gibson
DD 20	TTGTCATCGTCGTCCTTGTAATCAGCCCGGGATCTTATCTCCTCTCCAGGTAGTCC	twinStrep-tripartite DENN REV, Gibson
DD 21	ACTTGTCATCGTCGTCCTTGTAATCAGCCCGGGATCTTAGATCTTCTTCTGGGCTGCG	twinStrep-tripartite DENN + linker REV, Gibson
DD 22	AGGTTGGTGCTCTTCTCGTCGCTGCTCAGAGAGCCGCCTCCTCCGCTT	twinStrep + tag-linker REV, Gibson
DD 23	AGGAGGAGGAAGCGGAGGAGGCGGCTCTCTGAGCAGCGACGAGAAGAGC	SCD1 linker + WD-40 FW, Gibson
DD 24	ACTTGTCATCGTCGTCCTTGTAATCAGCCCGGGATCCTAGATGTTGATGGTAGCGTCC	SCD1 REV, Gibson
DD 25	GCTCCTCCGTGTCCTTTCAGCACCCTGACGTTGGTCTGAGAGCCGCCTCCTCC	twinStrep + tag-linker REV, Gibson
DD 26	GGAGGAGGAAGCGGAGGAGGCGGCTCTCAGACCAACGTCAGGGTGC	WD-40 repeats FW, Gibson
DD 27	ATATAAGCAGAGCTCGTTTAGTGAACCGTCAGAATTAAGCTTGCATGGATTATAAAGATGATGATGATAAAATTGAGGGTCGGGGCGGAGGAGGAAGCGGAGG	FLAG-Xa-Linker FW, Gibson

DD 28	CTACTTGTCATCGTCGTCCTTGTAATCAGCCCGGGATCCTAGATGTTGATG GTAGCGTC	FLAG-Xa-SCD1 REV, Gibson
DD 29	CCAAAATGTCGTAATAACCC	pFLAG CMV 5.1 Sequencing Primer FW
DD 30	GGGGACAAGTTTGTACAAAAAAGCAGGCTTCATGAACCGGTTGAAGGAGC AAAAGGG	AtMyTH1 GST pDEST15 FW
DD 31	GGGGACCACTTTGTACAAGAAAGCTGGGTCTTCACTTCCACACAAATTTGG TC	AtMyTH1 GST pDEST15 REV
DD 32	ATCCCACAAATTGATAAGTAC	pDEST15 Sequencing Primer
DD 33	GTAAAACGACGGCCAGT	pDONR221 Sequencing Primer

Table 4S3: Primers used in this study

Table 4S3 Primers used in this study

The alias (first column), sequence from 5’ to 3’ (second column), and name, orientation, and purpose (third column) of oligonucleotides used in this study are detailed.

References

Adamowski, M., Narasimhan, M., Kania, U., Glanc, M., De Jaeger, G., and Friml, J. (2018). A Functional Study of AUXILIN-LIKE1 and 2, Two Putative Clathrin Uncoating Factors in Arabidopsis. Plant Cell **30,** 700-716.

Ahn, C.S., Han, J.A., and Pai, H.S. (2013). Characterization of in vivo functions of Nicotiana benthamiana RabE1. Planta **237,** 161-172.

Aniento, F., de Medina Hernandez, V.S., Dagdas, Y., Rojas-Pierce, M., and Russinova, E. (2021). Molecular mechanisms of endomembrane trafficking in plants. Plant Cell.

Arabidopsis Genome, I. (2000). Analysis of the genome sequence of the flowering plant Arabidopsis thaliana. Nature **408,** 796-815.

Arora, D., and Damme, D.V. (2021). Motif-based endomembrane trafficking. Plant Physiol **186,** 221-238.

Backues, S.K. (2010). Analysis of Arabidopsis Dynamin-Related Protein 1 and 2 (DRP1 and DRP2) Families. In Biochemistry (Ann Arbor, MI: University of Wiscnsin-Madison), pp. 205.

Backues, S.K., and Bednarek, S.Y. (2010). Arabidopsis dynamin-related protein 1A polymers bind, but do not tubulate, liposomes. Biochem Biophys Res Commun **393,** 734-739.

Backues, S.K., Korasick, D.A., Heese, A., and Bednarek, S.Y. (2010). The Arabidopsis dynamin-related protein2 family is essential for gametophyte development. Plant Cell **22,** 3218-3231.

Bandmann, V., and Homann, U. (2012). Clathrin-independent endocytosis contributes to uptake of glucose into BY-2 protoplasts. Plant J **70,** 578-584.

Bandmann, V., Muller, J.D., Kohler, T., and Homann, U. (2012). Uptake of fluorescent nano beads into BY2-cells involves clathrin-dependent and clathrin-independent endocytosis. FEBS Lett **586,** 3626-3632.

Baral, A., Irani, N.G., Fujimoto, M., Nakano, A., Mayor, S., and Mathew, M.K. (2015). Salt-induced remodeling of spatially restricted clathrin-independent endocytic pathways in Arabidopsis root. Plant Cell **27,** 1297-1315.

Barberon, M., Dubeaux, G., Kolb, C., Isono, E., Zelazny, E., and Vert, G. (2014). Polarization of IRON-REGULATED TRANSPORTER 1 (IRT1) to the plant-soil interface plays crucial role in metal homeostasis. Proc Natl Acad Sci U S A **111,** 8293-8298.

Barberon, M., Zelazny, E., Robert, S., Conejero, G., Curie, C., Friml, J., and Vert, G. (2011). Monoubiquitin-dependent endocytosis of the iron-regulated transporter 1 (IRT1) transporter controls iron uptake in plants. Proc Natl Acad Sci U S A **108,** E450-458.

Barth, M., and Holstein, S.E. (2004). Identification and functional characterization of Arabidopsis AP180, a binding partner of plant alphaC-adaptin. J Cell Sci **117,** 2051-2062.

Bashline, L., Li, S., Zhu, X., and Gu, Y. (2015). The TWD40-2 protein and the AP2 complex cooperate in the clathrin-mediated endocytosis of cellulose synthase to regulate cellulose biosynthesis. Proc Natl Acad Sci U S A **112,** 12870-12875.

Bashline, L., Li, S., Anderson, C.T., Lei, L., and Gu, Y. (2013). The endocytosis of cellulose synthase in Arabidopsis is dependent on mu2, a clathrin-mediated endocytosis adaptin. Plant Physiol **163,** 150-160.

Bednarek, S.Y., and Backues, S.K. (2010). Plant dynamin-related protein families DRP1 and DRP2 in plant development. Biochem Soc Trans **38,** 797-806.

Bigay, J., and Antonny, B. (2012). Curvature, lipid packing, and electrostatics of membrane organelles: defining cellular territories in determining specificity. Dev Cell **23,** 886-895.

Blum, M., Chang, H.Y., Chuguransky, S., Grego, T., Kandasaamy, S., Mitchell, A., Nuka, G., Paysan-Lafosse, T., Qureshi, M., Raj, S., Richardson, L., Salazar, G.A., Williams, L., Bork, P., Bridge, A., Gough, J., Haft, D.H., Letunic, I., Marchler-Bauer, A., Mi, H., Natale, D.A., Necci, M., Orengo, C.A., Pandurangan, A.P., Rivoire, C., Sigrist, C.J.A., Sillitoe, I., Thanki, N., Thomas, P.D., Tosatto, S.C.E., Wu, C.H., Bateman, A., and Finn, R.D. (2021). The InterPro protein families and domains database: 20 years on. Nucleic Acids Res **49,** D344-D354.

Boehm, C.M., Obado, S., Gadelha, C., Kaupisch, A., Manna, P.T., Gould, G.W., Munson, M., Chait, B.T., Rout, M.P., and Field, M.C. (2017). The Trypanosome Exocyst: A Conserved Structure Revealing a New Role in Endocytosis. PLoS Pathog **13,** e1006063.

Bonnett Jr., H.T., and Newcomb, E.H. (1966). Coated Vesicles and Other Cytoplasmic Components of Growing Root Hairs of Radish. Protoplasma **62,** 59-75.

Borchers, A.C., Langemeyer, L., and Ungermann, C. (2021). Who's in control? Principles of Rab GTPase activation in endolysosomal membrane trafficking and beyond. J Cell Biol **220**.

Borner, G.H., Sherrier, D.J., Weimar, T., Michaelson, L.V., Hawkins, N.D., Macaskill, A., Napier, J.A., Beale, M.H., Lilley, K.S., and Dupree, P. (2005). Analysis of detergent-resistant membranes in Arabidopsis. Evidence for plasma membrane lipid rafts. Plant Physiol **137,** 104-116.

Boutte, Y., Frescatada-Rosa, M., Men, S., Chow, C.M., Ebine, K., Gustavsson, A., Johansson, L., Ueda, T., Moore, I., Jurgens, G., and Grebe, M. (2010). Endocytosis restricts Arabidopsis KNOLLE syntaxin to the cell division plane during late cytokinesis. EMBO J **29,** 546-558.

Brzeska, H., Gonzalez, J., Korn, E.D., and Titus, M.A. (2020). Basic-hydrophobic sites are localized in conserved positions inside and outside of PH domains and affect localization of Dictyostelium myosin 1s. Mol Biol Cell **31,** 101-117.

Brzeska, H., Guag, J., Remmert, K., Chacko, S., and Korn, E.D. (2010). An experimentally based computer search identifies unstructured membrane-binding sites in proteins: application to class I myosins, PAKS, and CARMIL. J Biol Chem **285,** 5738-5747.

Camacho, L., Smertenko, A.P., Perez-Gomez, J., Hussey, P.J., and Moore, I. (2009). Arabidopsis Rab-E GTPases exhibit a novel interaction with a plasma-membrane phosphatidylinositol-4-phosphate 5-kinase. J Cell Sci **122,** 4383-4392.

Cao, J., Yang, C., Li, L., Jiang, L., Wu, Y., Wu, C., Bu, Q., Xia, G., Liu, X., Luo, Y., and Liu, J. (2016). Rice Plasma Membrane Proteomics Reveals Magnaporthe oryzae Promotes Susceptibility by Sequential Activation of Host Hormone Signaling Pathways. Mol Plant Microbe Interact **29,** 902-913.

Chaparro-Garcia, A., Schwizer, S., Sklenar, J., Yoshida, K., Petre, B., Bos, J.I., Schornack, S., Jones, A.M., Bozkurt, T.O., and Kamoun, S. (2015). Phytophthora infestans RXLR-WY Effector AVR3a Associates with Dynamin-Related Protein 2 Required for Endocytosis of the Plant Pattern Recognition Receptor FLS2. PLoS One **10,** e0137071.

Cocucci, E., Aguet, F., Boulant, S., and Kirchhausen, T. (2012). The first five seconds in the life of a clathrin-coated pit. Cell **150,** 495-507.

Collings, D.A., Gebbie, L.K., Howles, P.A., Hurley, U.A., Birch, R.J., Cork, A.H., Hocart, C.H., Arioli, T., and Williamson, R.E. (2008). Arabidopsis dynamin-like protein DRP1A: a null mutant with widespread defects in endocytosis, cellulose synthesis, cytokinesis, and cell expansion. J Exp Bot **59,** 361-376.

Cui, Y., Li, X., Yu, M., Li, R., Fan, L., Zhu, Y., and Lin, J. (2018). Sterols regulate endocytic pathways during flg22-induced defense responses in Arabidopsis. Development **145**.

Dacks, J.B., and Robinson, M.S. (2017). Outerwear through the ages: evolutionary cell biology of vesicle coats. Curr Opin Cell Biol **47,** 108-116.

Dahhan, D.A., and Bednarek, S.Y. (2022). Advances in structural, spatial, and temporal mechanics of plant endocytosis. FEBS Lett.

Dahhan, D.A., Reynolds, G.D., Cardenas, J.J., Eeckhout, D., Johnson, A., Yperman, K., Kaufmann, W.A., Vang, N., Yan, X., Hwang, I., Heese, A., De Jaeger, G., Friml, J., Van Damme, D., Pan, J., and Bednarek, S.Y. (2022). Proteomic characterization of isolated Arabidopsis clathrin-coated vesicles reveals evolutionarily conserved and plant-specific components. Plant Cell.

de Jong, F., and Munnik, T. (2021). Attracted to membranes: lipid-binding domains in plants. Plant Physiol **185,** 707-723.

Dejonghe, W., Sharma, I., Denoo, B., De Munck, S., Lu, Q., Mishev, K., Bulut, H., Mylle, E., De Rycke, R., Vasileva, M., Savatin, D.V., Nerinckx, W., Staes, A., Drozdzecki, A., Audenaert, D., Yperman, K., Madder, A., Friml, J., Van Damme, D., Gevaert, K., Haucke, V., Savvides, S.N., Winne, J., and Russinova, E. (2019). Disruption of endocytosis through chemical inhibition of clathrin heavy chain function. Nat Chem Biol **15,** 641-649.

Depta, H., and Robinson, D.G. (1986). The isolation and enrichment of coated vesicles from suspension-cultured carrot cells. Protoplasma **130,** 162-170.

Dettmer, J., Hong-Hermesdorf, A., Stierhof, Y.D., and Schumacher, K. (2006). Vacuolar H+-ATPase activity is required for endocytic and secretory trafficking in Arabidopsis. Plant Cell **18,** 715-730.

Dhonukshe, P., Aniento, F., Hwang, I., Robinson, D.G., Mravec, J., Stierhof, Y.D., and Friml, J. (2007). Clathrin-mediated constitutive endocytosis of PIN auxin efflux carriers in Arabidopsis. Curr Biol **17,** 520-527.

Di Rubbo, S., Irani, N.G., Kim, S.Y., Xu, Z.Y., Gadeyne, A., Dejonghe, W., Vanhoutte, I., Persiau, G., Eeckhout, D., Simon, S., Song, K., Kleine-Vehn, J., Friml, J., De Jaeger, G., Van Damme, D., Hwang, I., and Russinova, E. (2013). The clathrin adaptor complex AP-2 mediates endocytosis of brassinosteroid insensitive1 in Arabidopsis. Plant Cell **25,** 2986-2997.

Doumane, M., Lebecq, A., Colin, L., Fangain, A., Stevens, F.D., Bareille, J., Hamant, O., Belkhadir, Y., Munnik, T., Jaillais, Y., and Caillaud, M.C. (2021). Inducible depletion of PI(4,5)P2 by the synthetic iDePP system in Arabidopsis. Nat Plants **7,** 587-597.

Eisenberg, E., and Greene, L.E. (2007). Multiple roles of auxilin and hsc70 in clathrin-mediated endocytosis. Traffic **8,** 640-646.

Ekanayake, G., LaMontagne, E.D., and Heese, A. (2019). Never Walk Alone: Clathrin-Coated Vesicle (CCV) Components in Plant Immunity. Annu Rev Phytopathol **57,** 387-409.

Ekanayake, G., Smith, J.M., Jones, K.B., Stiers, H.M., Robinson, S.J., LaMontagne, E.D., Kostos, P.H., Cornish, P.V., Bednarek, S.Y., and Heese, A. (2021). DYNAMIN-RELATED PROTEIN DRP1A functions with DRP2B in plant growth, flg22-immune responses, and endocytosis. Plant Physiol **185,** 1986-2002.

Falbel, T.G., Koch, L.M., Nadeau, J.A., Segui-Simarro, J.M., Sack, F.D., and Bednarek, S.Y. (2003). SCD1 is required for cytokinesis and polarized cell expansion in Arabidopsis thaliana [corrected]. Development **130,** 4011-4024.

Feng, Y., Hiwatashi, T., Minamino, N., Ebine, K., and Ueda, T. (2022). Membrane trafficking functions of the ANTH/ENTH/VHS domain-containing proteins in plants. FEBS Lett.

Ford, M.G., Mills, I.G., Peter, B.J., Vallis, Y., Praefcke, G.J., Evans, P.R., and McMahon, H.T. (2002). Curvature of clathrin-coated pits driven by epsin. Nature **419,** 361-366.

Frick, M., Bright, N.A., Riento, K., Bray, A., Merrified, C., and Nichols, B.J. (2007). Coassembly of flotillins induces formation of membrane microdomains, membrane curvature, and vesicle budding. Curr Biol **17,** 1151-1156.

Fujimoto, M., and Tsutsumi, N. (2014). Dynamin-related proteins in plant post-Golgi traffic. Front Plant Sci **5,** 408.

Fujimoto, M., Arimura, S., Nakazono, M., and Tsutsumi, N. (2008). Arabidopsis dynamin-related protein DRP2B is co-localized with DRP1A on the leading edge of the forming cell plate. Plant Cell Rep **27,** 1581-1586.

Fujimoto, M., Ebine, K., Nishimura, K., Tsutsumi, N., and Ueda, T. (2020). Longin R-SNARE is retrieved from the plasma membrane by ANTH domain-containing proteins in Arabidopsis. Proc Natl Acad Sci U S A **117,** 25150-25158.

Fujimoto, M., Arimura, S., Ueda, T., Takanashi, H., Hayashi, Y., Nakano, A., and Tsutsumi, N. (2010). Arabidopsis dynamin-related proteins DRP2B and DRP1A participate together in clathrin-coated vesicle formation during endocytosis. Proc Natl Acad Sci U S A **107,** 6094-6099.

Gadeyne, A., Sanchez-Rodriguez, C., Vanneste, S., Di Rubbo, S., Zauber, H., Vanneste, K., Van Leene, J., De Winne, N., Eeckhout, D., Persiau, G., Van De Slijke, E., Cannoot, B., Vercruysse, L., Mayers, J.R., Adamowski, M., Kania, U., Ehrlich, M., Schweighofer, A., Ketelaar, T., Maere, S., Bednarek, S.Y., Friml, J., Gevaert, K., Witters, E., Russinova, E., Persson, S., De Jaeger, G., and Van Damme, D. (2014). The TPLATE adaptor complex drives clathrin-mediated endocytosis in plants. Cell **156,** 691-704.

Gall, L., Stan, R.C., Kress, A., Hertel, B., Thiel, G., and Meckel, T. (2010). Fluorescent detection of fluid phase endocytosis allows for in vivo estimation of endocytic vesicle sizes in plant cells with sub-diffraction accuracy. Traffic **11,** 548-559.

Goode, B.L., Eskin, J.A., and Wendland, B. (2015). Actin and endocytosis in budding yeast. Genetics **199,** 315-358.

Gu, M., Liu, Q., Watanabe, S., Sun, L., Hollopeter, G., Grant, B.D., and Jorgensen, E.M. (2013). AP2 hemicomplexes contribute independently to synaptic vesicle endocytosis. Elife **2,** e00190.

Gurunathan, S., Chapman-Shimshoni, D., Trajkovic, S., and Gerst, J.E. (2000). Yeast exocytic v-SNAREs confer endocytosis. Mol Biol Cell **11,** 3629-3643.

Hao, H., Fan, L., Chen, T., Li, R., Li, X., He, Q., Botella, M.A., and Lin, J. (2014). Clathrin and Membrane Microdomains Cooperatively Regulate RbohD Dynamics and Activity in Arabidopsis. Plant Cell **26,** 1729-1745.

Harley, S.M., and Beevers, L. (1989). Isolation and partial characterization of clathrin-coated vesicles from pea (Pisum sativum L.) cotyledons. Protoplasma **150,** 103-109.

Hawes, C. (2005). Cell biology of the plant Golgi apparatus. New Phytol **165,** 29-44.

He, B., Cai, Q., Qiao, L., Huang, C.Y., Wang, S., Miao, W., Ha, T., Wang, Y., and Jin, H. (2021). RNA-binding proteins contribute to small RNA loading in plant extracellular vesicles. Nat Plants **7,** 342-352.

He, J., Scott, J.L., Heroux, A., Roy, S., Lenoir, M., Overduin, M., Stahelin, R.V., and Kutateladze, T.G. (2011). Molecular basis of phosphatidylinositol 4-phosphate and ARF1 GTPase recognition by the FAPP1 pleckstrin homology (PH) domain. J Biol Chem **286,** 18650-18657.

Hirst, J., Schlacht, A., Norcott, J.P., Traynor, D., Bloomfield, G., Antrobus, R., Kay, R.R., Dacks, J.B., and Robinson, M.S. (2014). Characterization of TSET, an ancient and widespread membrane trafficking complex. Elife **3,** e02866.

Huang, S., Konishi, N., Yamaji, N., Shao, J.F., Mitani-Ueno, N., and Ma, J.F. (2021). Boron uptake in rice is regulated posttranslationally via a clathrin-independent pathway. Plant Physiology.

Irani, N.G., Di Rubbo, S., Mylle, E., Van den Begin, J., Schneider-Pizon, J., Hnilikova, J., Sisa, M., Buyst, D., Vilarrasa-Blasi, J., Szatmari, A.M., Van Damme, D., Mishev, K., Codreanu, M.C., Kohout, L., Strnad, M., Cano-Delgado, A.I., Friml, J., Madder, A., and Russinova, E. (2012). Fluorescent castasterone reveals BRI1 signaling from the plasma membrane. Nat Chem Biol **8,** 583-589.

Ischebeck, T., Werner, S., Krishnamoorthy, P., Lerche, J., Meijon, M., Stenzel, I., Lofke, C., Wiessner, T., Im, Y.J., Perera, I.Y., Iven, T., Feussner, I., Busch, W., Boss, W.F., Teichmann, T., Hause, B., Persson, S., and Heilmann, I. (2013). Phosphatidylinositol 4,5-bisphosphate influences PIN polarization by controlling clathrin-mediated membrane trafficking in Arabidopsis. Plant Cell **25,** 4894-4911.

Ito, E., and Uemura, T. (2022). RAB GTPases and SNAREs at the trans-Golgi network in plants. J Plant Res **135,** 389-403.

Jean, S., and Kiger, A.A. (2012). Coordination between RAB GTPase and phosphoinositide regulation and functions. Nat Rev Mol Cell Biol **13,** 463-470.

Johnson, A., and Vert, G. (2017). Single Event Resolution of Plant Plasma Membrane Protein Endocytosis by TIRF Microscopy. Front Plant Sci **8,** 612.

Johnson, A., Gnyliukh, N., Kaufmann, W.A., Narasimhan, M., Vert, G., Bednarek, S.Y., and Friml, J. (2020). Experimental toolbox for quantitative evaluation of clathrin-mediated endocytosis in the plant model Arabidopsis. J Cell Sci **133**.

Johnson, A., Dahhan, D.A., Gnyliukh, N., Kaufmann, W.A., Zheden, V., Costanzo, T., Mahou, P., Hrtyan, M., Wang, J., Aguilera-Servin, J., van Damme, D., Beaurepaire, E., Loose, M.,

Bednarek, S.Y., and Friml, J. (2021). The TPLATE complex mediates membrane bending during plant clathrin-mediated endocytosis. Proc Natl Acad Sci U S A **118**.

Jose, M., Tollis, S., Nair, D., Mitteau, R., Velours, C., Massoni-Laporte, A., Royou, A., Sibarita, J.B., and McCusker, D. (2015). A quantitative imaging-based screen reveals the exocyst as a network hub connecting endocytosis and exocytosis. Mol Biol Cell **26,** 2519-2534.

Kaneda, M., van Oostende-Triplet, C., Chebli, Y., Testerink, C., Bednarek, S.Y., and Geitmann, A. (2019). Plant AP180 N-Terminal Homolog Proteins Are Involved in Clathrin-Dependent Endocytosis during Pollen Tube Growth in Arabidopsis thaliana. Plant Cell Physiol **60,** 1316-1330.

Kang, B.H., Rancour, D.M., and Bednarek, S.Y. (2003a). The dynamin-like protein ADL1C is essential for plasma membrane maintenance during pollen maturation. Plant J **35,** 1-15.

Kang, B.H., Busse, J.S., and Bednarek, S.Y. (2003b). Members of the Arabidopsis dynamin-like gene family, ADL1, are essential for plant cytokinesis and polarized cell growth. Plant Cell **15,** 899-913.

Kang, B.H., Anderson, C.T., Arimura, S.I., Bayer, E., Bezanilla, M., Botella, M.A., Brandizzi, F., Burch-Smith, T.M., Chapman, K.D., Dunser, K., Gu, Y., Jaillais, Y., Kirchhoff, H., Otegui, M.S., Rosado, A., Tang, Y., Kleine-Vehn, J., Wang, P., and Zolman, B.K. (2022). A glossary of plant cell structures: Current insights and future questions. Plant Cell **34,** 10-52.

Kelly, B.T., McCoy, A.J., Spate, K., Miller, S.E., Evans, P.R., Honing, S., and Owen, D.J. (2008). A structural explanation for the binding of endocytic dileucine motifs by the AP2 complex. Nature **456,** 976-979.

Kelly, B.T., Graham, S.C., Liska, N., Dannhauser, P.N., Honing, S., Ungewickell, E.J., and Owen, D.J. (2014). Clathrin adaptors. AP2 controls clathrin polymerization with a membrane-activated switch. Science **345,** 459-463.

Kim, S.Y., Xu, Z.Y., Song, K., Kim, D.H., Kang, H., Reichardt, I., Sohn, E.J., Friml, J., Juergens, G., and Hwang, I. (2013). Adaptor protein complex 2-mediated endocytosis is crucial for male reproductive organ development in Arabidopsis. Plant Cell **25,** 2970-2985.

Kirchhausen, T., Owen, D., and Harrison, S.C. (2014). Molecular structure, function, and dynamics of clathrin-mediated membrane traffic. Cold Spring Harb Perspect Biol **6,** a016725.

Kitakura, S., Vanneste, S., Robert, S., Lofke, C., Teichmann, T., Tanaka, H., and Friml, J. (2011). Clathrin mediates endocytosis and polar distribution of PIN auxin transporters in Arabidopsis. Plant Cell **23,** 1920-1931.

Konopka, C.A., and Bednarek, S.Y. (2008). Comparison of the dynamics and functional redundancy of the Arabidopsis dynamin-related isoforms DRP1A and DRP1C during plant development. Plant Physiol **147,** 1590-1602.

Konopka, C.A., Backues, S.K., and Bednarek, S.Y. (2008). Dynamics of Arabidopsis dynamin-related protein 1C and a clathrin light chain at the plasma membrane. Plant Cell **20,** 1363-1380.

Kovtun, O., Dickson, V.K., Kelly, B.T., Owen, D.J., and Briggs, J.A.G. (2020). Architecture of the AP2/clathrin coat on the membranes of clathrin-coated vesicles. Sci Adv **6,** eaba8381.

Kurzchalia, T.V., and Parton, R.G. (1999). Membrane microdomains and caveolae. Curr Opin Cell Biol **11,** 424-431.

Kutateladze, T.G. (2010). Translation of the phosphoinositide code by PI effectors. Nat Chem Biol **6,** 507-513.

Lam, B.C., Sage, T.L., Bianchi, F., and Blumwald, E. (2001). Role of SH3 domain-containing proteins in clathrin-mediated vesicle trafficking in Arabidopsis. Plant Cell **13,** 2499-2512.

Larson, E.R., Van Zelm, E., Roux, C., Marion-Poll, A., and Blatt, M.R. (2017). Clathrin Heavy Chain Subunits Coordinate Endo- and Exocytic Traffic and Affect Stomatal Movement. Plant Physiol **175,** 708-720.

Lee, J., Hanh Nguyen, H., Park, Y., Lin, J., and Hwang, I. (2022). Spatial regulation of RBOHD via AtECA4-mediated recycling and clathrin-mediated endocytosis contributes to ROS accumulation during salt stress response but not flg22-induced immune response. Plant J **109,** 816-830.

Leslie, M.E., Rogers, S.W., and Heese, A. (2016). Increased callose deposition in plants lacking DYNAMIN-RELATED PROTEIN 2B is dependent upon POWDERY MILDEW RESISTANT 4. Plant Signal Behav **11,** e1244594.

Li, H., von Wangenheim, D., Zhang, X., Tan, S., Darwish-Miranda, N., Naramoto, S., Wabnik, K., De Rycke, R., Kaufmann, W.A., Gutl, D., Tejos, R., Grones, P., Ke, M., Chen, X., Dettmer, J., and Friml, J. (2021). Cellular requirements for PIN polar cargo clustering in Arabidopsis thaliana. New Phytol **229,** 351-369.

Li, R., Liu, P., Wan, Y., Chen, T., Wang, Q., Mettbach, U., Baluska, F., Samaj, J., Fang, X., Lucas, W.J., and Lin, J. (2012). A membrane microdomain-associated protein, Arabidopsis Flot1, is involved in a clathrin-independent endocytic pathway and is required for seedling development. Plant Cell **24,** 2105-2122.

Li, X., and Pan, S.Q. (2017). Agrobacterium delivers VirE2 protein into host cells via clathrin-mediated endocytosis. Sci Adv **3,** e1601528.

Li, X., Wang, X., Yang, Y., Li, R., He, Q., Fang, X., Luu, D.T., Maurel, C., and Lin, J. (2011). Single-molecule analysis of PIP2;1 dynamics and partitioning reveals multiple modes of Arabidopsis plasma membrane aquaporin regulation. Plant Cell **23,** 3780-3797.

Lin, F., Krishnamoorthy, P., Schubert, V., Hause, G., Heilmann, M., and Heilmann, I. (2019). A dual role for cell plate-associated PI4Kbeta in endocytosis and phragmoplast dynamics during plant somatic cytokinesis. EMBO J **38**.

Liu, D., Kumar, R., Claus, L.A.N., Johnson, A.J., Siao, W., Vanhoutte, I., Wang, P., Bender, K.W., Yperman, K., Martins, S., Zhao, X., Vert, G., Van Damme, D., Friml, J., and Russinova, E. (2020). Endocytosis of BRASSINOSTEROID INSENSITIVE1 Is Partly Driven by a Canonical Tyr-Based Motif. Plant Cell **32,** 3598-3612.

Lo Presti, L., and Kahmann, R. (2017). How filamentous plant pathogen effectors are translocated to host cells. Curr Opin Plant Biol **38,** 19-24.

Lopez-Hernandez, T., Haucke, V., and Maritzen, T. (2020). Endocytosis in the adaptation to cellular stress. Cell Stress **4,** 230-247.

Lu, D., Lin, W., Gao, X., Wu, S., Cheng, C., Avila, J., Heese, A., Devarenne, T.P., He, P., and Shan, L. (2011). Direct ubiquitination of pattern recognition receptor FLS2 attenuates plant innate immunity. Science **332,** 1439-1442.

Lu, Q., Li, J., Ye, F., and Zhang, M. (2015). Structure of myosin-1c tail bound to calmodulin provides insights into calcium-mediated conformational coupling. Nat Struct Mol Biol **22,** 81-88.

Luu, D.T., Martiniere, A., Sorieul, M., Runions, J., and Maurel, C. (2012). Fluorescence recovery after photobleaching reveals high cycling dynamics of plasma membrane aquaporins in Arabidopsis roots under salt stress. Plant J **69,** 894-905.

Madeira, F., Pearce, M., Tivey, A.R.N., Basutkar, P., Lee, J., Edbali, O., Madhusoodanan, N., Kolesnikov, A., and Lopez, R. (2022). Search and sequence analysis tools services from EMBL-EBI in 2022. Nucleic Acids Res.

Marhava, P. (2021). Recent developments in the understanding of PIN polarity. New Phytol.

Martiniere, A., Fiche, J.B., Smokvarska, M., Mari, S., Alcon, C., Dumont, X., Hematy, K., Jaillais, Y., Nollmann, M., and Maurel, C. (2019). Osmotic Stress Activates Two Reactive Oxygen Species Pathways with Distinct Effects on Protein Nanodomains and Diffusion. Plant Physiol **179,** 1581-1593.

Massol, R.H., Boll, W., Griffin, A.M., and Kirchhausen, T. (2006). A burst of auxilin recruitment determines the onset of clathrin-coated vesicle uncoating. Proc Natl Acad Sci U S A **103,** 10265-10270.

Mayers, J.R., Hu, T., Wang, C., Cardenas, J.J., Tan, Y., Pan, J., and Bednarek, S.Y. (2017). SCD1 and SCD2 Form a Complex That Functions with the Exocyst and RabE1 in Exocytosis and Cytokinesis. Plant Cell **29,** 2610-2625.

McMichael, C.M., and Bednarek, S.Y. (2013). Cytoskeletal and membrane dynamics during higher plant cytokinesis. New Phytol **197,** 1039-1057.

McMichael, C.M., Reynolds, G.D., Koch, L.M., Wang, C., Jiang, N., Nadeau, J., Sack, F.D., Gelderman, M.B., Pan, J., and Bednarek, S.Y. (2013). Mediation of clathrin-dependent trafficking during cytokinesis and cell expansion by Arabidopsis stomatal cytokinesis defective proteins. Plant Cell **25,** 3910-3925.

Men, S., Boutte, Y., Ikeda, Y., Li, X., Palme, K., Stierhof, Y.D., Hartmann, M.A., Moritz, T., and Grebe, M. (2008). Sterol-dependent endocytosis mediates post-cytokinetic acquisition of PIN2 auxin efflux carrier polarity. Nat Cell Biol **10,** 237-244.

Meyer, M.D., Winzeler, J., Taylor, S.M., Kilgore, A., Edicha, K., Chitwood, C., Spearin, Z., Silvia, S., Chakraborty, R., Smith, J.E., Kennedy, B., Zois, C., Cawthon, H., Gilruth, M., and Backues, S.K. (2021). Mapping Critical Residues in ATG11's Coiled-Coil 2 Domain that Block Multiple Interactions and Disrupt Selective Autophagy. Front Cell Dev Biol **9,** 775364.

Mizuno-Yamasaki, E., Medkova, M., Coleman, J., and Novick, P. (2010). Phosphatidylinositol 4-phosphate controls both membrane recruitment and a regulatory switch of the Rab GEF Sec2p. Dev Cell **18,** 828-840.

More, K., Klinger, C.M., Barlow, L.D., and Dacks, J.B. (2020). Evolution and Natural History of Membrane Trafficking in Eukaryotes. Curr Biol **30,** R553-R564.

Morrow, I.C., Rea, S., Martin, S., Prior, I.A., Prohaska, R., Hancock, J.F., James, D.E., and Parton, R.G. (2002). Flotillin-1/reggie-2 traffics to surface raft domains via a novel golgi-independent pathway. Identification of a novel membrane targeting domain and a role for palmitoylation. J Biol Chem **277,** 48834-48841.

Moscatelli, A., Ciampolini, F., Rodighiero, S., Onelli, E., Cresti, M., Santo, N., and Idilli, A. (2007). Distinct endocytic pathways identified in tobacco pollen tubes using charged nanogold. J Cell Sci **120,** 3804-3819.

Motley, A.M., Berg, N., Taylor, M.J., Sahlender, D.A., Hirst, J., Owen, D.J., and Robinson, M.S. (2006). Functional analysis of AP-2 alpha and mu2 subunits. Mol Biol Cell **17,** 5298-5308.

Narasimhan, M., Johnson, A., Prizak, R., Kaufmann, W.A., Tan, S., Casillas-Perez, B., and Friml, J. (2020). Evolutionarily unique mechanistic framework of clathrin-mediated endocytosis in plants. Elife **9**.

Nguyen, H.H., Lee, M.H., Song, K., Ahn, G., Lee, J., and Hwang, I. (2018). The A/ENTH Domain-Containing Protein AtECA4 Is an Adaptor Protein Involved in Cargo Recycling from the trans-Golgi Network/Early Endosome to the Plasma Membrane. Mol Plant **11,** 568-583.

Nielsen, E. (2020). The Small GTPase Superfamily in Plants: A Conserved Regulatory Module with Novel Functions. Annu Rev Plant Biol **71,** 247-272.

Noack, L.C., and Jaillais, Y. (2020). Functions of Anionic Lipids in Plants. Annu Rev Plant Biol **71,** 71-102.

Onelli, E., Prescianotto-Baschong, C., Caccianiga, M., and Moscatelli, A. (2008). Clathrin-dependent and independent endocytic pathways in tobacco protoplasts revealed by labelling with charged nanogold. J Exp Bot **59,** 3051-3068.

Orr, R.G., Cheng, X., Vidali, L., and Bezanilla, M. (2020). Orchestrating cell morphology from the inside out - using polarized cell expansion in plants as a model. Curr Opin Cell Biol **62,** 46-53.

Otegui, M.S., Mastronarde, D.N., Kang, B.H., Bednarek, S.Y., and Staehelin, L.A. (2001). Three-dimensional analysis of syncytial-type cell plates during endosperm cellularization visualized by high resolution electron tomography. Plant Cell **13,** 2033-2051.

Ott, T. (2017). Membrane nanodomains and microdomains in plant-microbe interactions. Curr Opin Plant Biol **40,** 82-88.

Paez Valencia, J., Goodman, K., and Otegui, M.S. (2016). Endocytosis and Endosomal Trafficking in Plants. Annu Rev Plant Biol **67,** 309-335.

Pearse, B.M. (1976). Clathrin: a unique protein associated with intracellular transfer of membrane by coated vesicles. Proc Natl Acad Sci U S A **73,** 1255-1259.

Pizarro, L., Leibman-Markus, M., Schuster, S., Bar, M., and Avni, A. (2019). Tomato Dynamin Related Protein 2A Associates With LeEIX2 and Enhances PRR Mediated Defense by Modulating Receptor Trafficking. Front Plant Sci **10,** 936.

Platre, M.P., Bayle, V., Armengot, L., Bareille, J., Marques-Bueno, M.D.M., Creff, A., Maneta-Peyret, L., Fiche, J.B., Nollmann, M., Miege, C., Moreau, P., Martiniere, A., and Jaillais, Y. (2019). Developmental control of plant Rho GTPase nano-organization by the lipid phosphatidylserine. Science **364,** 57-62.

Platre, M.P., Noack, L.C., Doumane, M., Bayle, V., Simon, M.L.A., Maneta-Peyret, L., Fouillen, L., Stanislas, T., Armengot, L., Pejchar, P., Caillaud, M.C., Potocky, M., Copic, A., Moreau, P., and Jaillais, Y. (2018). A Combinatorial Lipid Code Shapes the Electrostatic Landscape of Plant Endomembranes. Dev Cell **45,** 465-480 e411.

Posor, Y., Jang, W., and Haucke, V. (2022). Phosphoinositides as membrane organizers. Nat Rev Mol Cell Biol.

Putta, P., Creque, E., Piontkivska, H., and Kooijman, E.E. (2020). Lipid-protein interactions for ECA1 an N-ANTH domain protein involved in stress signaling in plants. Chem Phys Lipids **231,** 104919.

Rancour, D.M., Dickey, C.E., Park, S., and Bednarek, S.Y. (2002). Characterization of AtCDC48. Evidence for multiple membrane fusion mechanisms at the plane of cell division in plants. Plant Physiol **130,** 1241-1253.

Ravikumar, R., Steiner, A., and Assaad, F.F. (2017). Multisubunit tethering complexes in higher plants. Curr Opin Plant Biol **40,** 97-105.

Reynolds, G.D., August, B., and Bednarek, S.Y. (2014). Preparation of enriched plant clathrin-coated vesicles by differential and density gradient centrifugation. Methods Mol Biol **1209,** 163-177.

Reynolds, G.D., Wang, C., Pan, J., and Bednarek, S.Y. (2018). Inroads into Internalization: Five Years of Endocytic Exploration. Plant Physiol **176,** 208-218.

Rice, P., Longden, I., and Bleasby, A. (2000). EMBOSS: the European Molecular Biology Open Software Suite. Trends Genet **16,** 276-277.

Robatzek, S., Chinchilla, D., and Boller, T. (2006). Ligand-induced endocytosis of the pattern recognition receptor FLS2 in Arabidopsis. Genes Dev **20,** 537-542.

Robinson, M.S. (2015). Forty Years of Clathrin-coated Vesicles. Traffic **16,** 1210-1238.

Rodal, S.K., Skretting, G., Garred, Ø., Vilhardt, F., Deurs, B.v., and Sandvig, K. (1999). Extraction of Cholesterol with Methyl-β-Cyclodextrin Perturbs Formation of Clathrin-coated Endocytic Vesicles. Molecular Biology of the Cell **10,** 961-974.

Rosquete, M.R., Davis, D.J., and Drakakaki, G. (2018). The Plant Trans-Golgi Network: Not Just a Matter of Distinction. Plant Physiol **176,** 187-198.

Rutherford, S., and Moore, I. (2002). The Arabidopsis Rab GTPase family: another enigma variation. Curr Opin Plant Biol **5,** 518-528.

Sanchez-Rodriguez, C., Shi, Y., Kesten, C., Zhang, D., Sancho-Andres, G., Ivakov, A., Lampugnani, E.R., Sklodowski, K., Fujimoto, M., Nakano, A., Bacic, A., Wallace, I.S., Ueda, T., Van Damme, D., Zhou, Y., and Persson, S. (2018). The Cellulose Synthases Are Cargo of the TPLATE Adaptor Complex. Mol Plant **11,** 346-349.

Scheele, U., Kalthoff, C., and Ungewickell, E. (2001). Multiple interactions of auxilin 1 with clathrin and the AP-2 adaptor complex. J Biol Chem **276,** 36131-36138.

Schmid, E.M., and McMahon, H.T. (2007). Integrating molecular and network biology to decode endocytosis. Nature **448,** 883-888.

Schmid, S.L., and Frolov, V.A. (2011). Dynamin: functional design of a membrane fission catalyst. Annu Rev Cell Dev Biol **27,** 79-105.

Schwihla, M., and Korbei, B. (2020). The Beginning of the End: Initial Steps in the Degradation of Plasma Membrane Proteins. Front Plant Sci **11,** 680.

Sharma, P., Sabharanjak, S., and Mayor, S. (2002). Endocytosis of lipid rafts: an identity crisis. Semin Cell Dev Biol **13,** 205-214.

Sievers, F., Wilm, A., Dineen, D., Gibson, T.J., Karplus, K., Li, W., Lopez, R., McWilliam, H., Remmert, M., Soding, J., Thompson, J.D., and Higgins, D.G. (2011). Fast, scalable generation of high-quality protein multiple sequence alignments using Clustal Omega. Mol Syst Biol **7,** 539.

Simm, D., Hatje, K., Waack, S., and Kollmar, M. (2021). Critical assessment of coiled-coil predictions based on protein structure data. Sci Rep **11,** 12439.

Simon, M.L., Platre, M.P., Marques-Bueno, M.M., Armengot, L., Stanislas, T., Bayle, V., Caillaud, M.C., and Jaillais, Y. (2016). A PtdIns(4)P-driven electrostatic field controls cell membrane identity and signalling in plants. Nat Plants **2,** 16089.

Slupianek, A., Kasprowicz-Maluski, A., Myskow, E., Turzanska, M., and Sokolowska, K. (2019). Endocytosis acts as transport pathway in wood. New Phytol **222,** 1846-1861.

Smith, J.M., Leslie, M.E., Robinson, S.J., Korasick, D.A., Zhang, T., Backues, S.K., Cornish, P.V., Koo, A.J., Bednarek, S.Y., and Heese, A. (2014). Loss of Arabidopsis thaliana Dynamin-Related Protein 2B reveals separation of innate immune signaling pathways. PLoS Pathog **10,** e1004578.

Smith, S.M., Larocque, G., Wood, K.M., Morris, K.L., Roseman, A.M., Sessions, R.B., Royle, S.J., and Smith, C.J. (2021). Multi-modal adaptor-clathrin contacts drive coated vesicle assembly. EMBO J **40,** e108795.

Sommer, B., Oprins, A., Rabouille, C., and Munro, S. (2005). The exocyst component Sec5 is present on endocytic vesicles in the oocyte of Drosophila melanogaster. J Cell Biol **169,** 953-963.

Song, K., Jang, M., Kim, S.Y., Lee, G., Lee, G.J., Kim, D.H., Lee, Y., Cho, W., and Hwang, I. (2012). An A/ENTH domain-containing protein functions as an adaptor for clathrin-coated vesicles on the growing cell plate in Arabidopsis root cells. Plant Physiol **159,** 1013-1025.

Speth, E.B., Imboden, L., Hauck, P., and He, S.Y. (2009). Subcellular localization and functional analysis of the Arabidopsis GTPase RabE. Plant Physiol **149,** 1824-1837.

Stefano, G., Renna, L., Wormsbaecher, C., Gamble, J., Zienkiewicz, K., and Brandizzi, F. (2018). Plant Endocytosis Requires the ER Membrane-Anchored Proteins VAP27-1 and VAP27-3. Cell Rep **23,** 2299-2307.

Stefano, G., Renna, L., Lai, Y., Slabaugh, E., Mannino, N., Buono, R.A., Otegui, M.S., and Brandizzi, F. (2015). ER network homeostasis is critical for plant endosome streaming and endocytosis. Cell Discov **1,** 15033.

Stenmark, H. (2009). Rab GTPases as coordinators of vesicle traffic. Nat Rev Mol Cell Biol **10,** 513-525.

Tahara, H., Yokota, E., Igarashi, H., Orii, H., Yao, M., Sonobe, S., Hashimoto, T., Hussey, P.J., and Shimmen, T. (2007). Clathrin is involved in organization of mitotic spindle and phragmoplast as well as in endocytosis in tobacco cell cultures. Protoplasma **230,** 1-11.

Tejos, R., Sauer, M., Vanneste, S., Palacios-Gomez, M., Li, H., Heilmann, M., van Wijk, R., Vermeer, J.E., Heilmann, I., Munnik, T., and Friml, J. (2014). Bipolar Plasma Membrane Distribution of Phosphoinositides and Their Requirement for Auxin-Mediated Cell Polarity and Patterning in Arabidopsis. Plant Cell **26,** 2114-2128.

Tran, T.M., Ma, Z., Triebl, A., Nath, S., Cheng, Y., Gong, B.Q., Han, X., Wang, J., Li, J.F., Wenk, M.R., Torta, F., Mayor, S., Yang, L., and Miao, Y. (2020). The bacterial quorum sensing signal DSF hijacks Arabidopsis thaliana sterol biosynthesis to suppress plant innate immunity. Life Sci Alliance **3**.

Uemura, T. (2016). Physiological Roles of Plant Post-Golgi Transport Pathways in Membrane Trafficking. Plant Cell Physiol **57,** 2013-2019.

Ungewickell, E., Ungewickell, H., Holstein, S.E., Lindner, R., Prasad, K., Barouch, W., Martin, B., Greene, L.E., and Eisenberg, E. (1995). Role of auxilin in uncoating clathrin-coated vesicles. Nature **378,** 632-635.

UniProt, C. (2021). UniProt: the universal protein knowledgebase in 2021. Nucleic Acids Res **49,** D480-D489.

Van Damme, D., Coutuer, S., De Rycke, R., Bouget, F.Y., Inze, D., and Geelen, D. (2006). Somatic cytokinesis and pollen maturation in Arabidopsis depend on TPLATE, which has domains similar to coat proteins. Plant Cell **18,** 3502-3518.

Van Damme, D., Gadeyne, A., Vanstraelen, M., Inze, D., Van Montagu, M.C., De Jaeger, G., Russinova, E., and Geelen, D. (2011). Adaptin-like protein TPLATE and clathrin recruitment during plant somatic cytokinesis occurs via two distinct pathways. Proc Natl Acad Sci U S A **108,** 615-620.

Wang, C., Yan, X., Chen, Q., Jiang, N., Fu, W., Ma, B., Liu, J., Li, C., Bednarek, S.Y., and Pan, J. (2013a). Clathrin light chains regulate clathrin-mediated trafficking, auxin signaling, and development in Arabidopsis. Plant Cell **25,** 499-516.

Wang, C., Hu, T., Yan, X., Meng, T., Wang, Y., Wang, Q., Zhang, X., Gu, Y., Sanchez-Rodriguez, C., Gadeyne, A., Lin, J., Persson, S., Van Damme, D., Li, C., Bednarek, S.Y., and Pan, J. (2016). Differential Regulation of Clathrin and Its Adaptor Proteins during Membrane Recruitment for Endocytosis. Plant Physiol **171,** 215-229.

Wang, F., Cheng, Z., Wang, J., Zhang, F., Zhang, B., Luo, S., Lei, C., Pan, T., Wang, Y., Zhu, Y., Wang, M., Chen, W., Lin, Q., Zhu, S., Zhou, Y., Zhao, Z., Wang, J., Guo, X., Zhang, X., Jiang, L., Bao, Y., Ren, Y., and Wan, J. (2022). Rice STOMATAL CYTOKINESIS DEFECTIVE2 regulates cell expansion by affecting vesicular trafficking in rice. Plant Physiol.

Wang, J., Mylle, E., Johnson, A., Besbrugge, N., De Jaeger, G., Friml, J., Pleskot, R., and Van Damme, D. (2020). High Temporal Resolution Reveals Simultaneous Plasma Membrane Recruitment of TPLATE Complex Subunits. Plant Physiol **183,** 986-997.

Wang, J., Yperman, K., Grones, P., Jiang, Q., Dragwidge, J., Mylle, E., Mor, E., Nolf, J., Eeckhout, D., De Jaeger, G., De Rybel, B., Pleskot, R., and Van Damme, D. (2021). Conditional destabilization of the TPLATE complex impairs endocytic internalization. Proc Natl Acad Sci U S A **118**.

Wang, L., Cheng, M., Yang, Q., Li, J., Wang, X., Zhou, Q., Nagawa, S., Xia, B., Xu, T., Huang, R., He, J., Li, C., Fu, Y., Liu, Y., Bao, J., Wei, H., Li, H., Tan, L., Gu, Z., Xia, A., Huang, X., Yang,

Z., and Deng, X.W. (2019a). Arabinogalactan protein-rare earth element complexes activate plant endocytosis. Proc Natl Acad Sci U S A **116,** 14349-14357.

Wang, P., and Hussey, P.J. (2019). Plant ER-PM Contact Sites in Endocytosis and Autophagy: Does the Local Composition of Membrane Phospholipid Play a Role? Front Plant Sci **10,** 23.

Wang, P., Hawes, C., and Hussey, P.J. (2017a). Plant Endoplasmic Reticulum-Plasma Membrane Contact Sites. Trends Plant Sci **22,** 289-297.

Wang, P., Pleskot, R., Zang, J., Winkler, J., Wang, J., Yperman, K., Zhang, T., Wang, K., Gong, J., Guan, Y., Richardson, C., Duckney, P., Vandorpe, M., Mylle, E., Fiserova, J., Van Damme, D., and Hussey, P.J. (2019b). Plant AtEH/Pan1 proteins drive autophagosome formation at ER-PM contact sites with actin and endocytic machinery. Nat Commun **10,** 5132.

Wang, Q., Zhao, Y., Luo, W., Li, R., He, Q., Fang, X., Michele, R.D., Ast, C., von Wiren, N., and Lin, J. (2013b). Single-particle analysis reveals shutoff control of the Arabidopsis ammonium transporter AMT1;3 by clustering and internalization. Proc Natl Acad Sci U S A **110,** 13204-13209.

Wang, S., Yoshinari, A., Shimada, T., Hara-Nishimura, I., Mitani-Ueno, N., Feng Ma, J., Naito, S., and Takano, J. (2017b). Polar Localization of the NIP5;1 Boric Acid Channel Is Maintained by Endocytosis and Facilitates Boron Transport in Arabidopsis Roots. Plant Cell **29,** 824-842.

Waszczak, C., Carmody, M., and Kangasjarvi, J. (2018). Reactive Oxygen Species in Plant Signaling. Annu Rev Plant Biol **69,** 209-236.

Wilkins, M.R., Gasteiger, E., Bairoch, A., Sanchez, J.C., Williams, K.L., Appel, R.D., and Hochstrasser, D.F. (1999). Protein identification and analysis tools in the ExPASy server. Methods Mol Biol **112,** 531-552.

Winkler, J., De Meyer, A., Mylle, E., Storme, V., Grones, P., and Van Damme, D. (2021). Nanobody-Dependent Delocalization of Endocytic Machinery in Arabidopsis Root Cells Dampens Their Internalization Capacity. Front Plant Sci **12,** 538580.

Wu, B., and Guo, W. (2015). The Exocyst at a Glance. J Cell Sci **128,** 2957-2964.

Yamaoka, S., Shimono, Y., Shirakawa, M., Fukao, Y., Kawase, T., Hatsugai, N., Tamura, K., Shimada, T., and Hara-Nishimura, I. (2013). Identification and dynamics of Arabidopsis adaptor protein-2 complex and its involvement in floral organ development. Plant Cell **25,** 2958-2969.

Yan, X., Wang, Y., Xu, M., Dahhan, D.A., Liu, C., Zhang, Y., Lin, J., Bednarek, S.Y., and Pan, J. (2021). Cross-talk between clathrin-dependent post-Golgi trafficking and clathrin-mediated endocytosis in Arabidopsis root cells. Plant Cell **33,** 3057-3075.

Yoshinari, A., Fujimoto, M., Ueda, T., Inada, N., Naito, S., and Takano, J. (2016). DRP1-Dependent Endocytosis is Essential for Polar Localization and Boron-Induced Degradation of the Borate Transporter BOR1 in Arabidopsis thaliana. Plant Cell Physiol **57,** 1985-2000.

Yoshinari, A., Hosokawa, T., Amano, T., Beier, M.P., Kunieda, T., Shimada, T., Hara-Nishimura, I., Naito, S., and Takano, J. (2019). Polar Localization of the Borate Exporter BOR1 Requires AP2-Dependent Endocytosis. Plant Physiol **179,** 1569-1580.

Yperman, K., Wang, J., Eeckhout, D., Winkler, J., Vu, L.D., Vandorpe, M., Grones, P., Mylle, E., Kraus, M., Merceron, R., Nolf, J., Mor, E., De Bruyn, P., Loris, R., Potocky, M., Savvides,

S.N., De Rybel, B., De Jaeger, G., Van Damme, D., and Pleskot, R. (2021a). Molecular architecture of the endocytic TPLATE complex. Sci Adv **7**.

Yperman, K., Papageorgiou, A.C., Merceron, R., De Munck, S., Bloch, Y., Eeckhout, D., Jiang, Q., Tack, P., Grigoryan, R., Evangelidis, T., Van Leene, J., Vincze, L., Vandenabeele, P., Vanhaecke, F., Potocky, M., De Jaeger, G., Savvides, S.N., Tripsianes, K., Pleskot, R., and Van Damme, D. (2021b). Distinct EH domains of the endocytic TPLATE complex confer lipid and protein binding. Nat Commun **12,** 3050.

Yu, M., Li, R., Cui, Y., Chen, W., Li, B., Zhang, X., Bu, Y., Cao, Y., Xing, J., Jewaria, P.K., Li, X., Bhalerao, R.P., Yu, F., and Lin, J. (2020). The RALF1-FERONIA interaction modulates endocytosis to mediate control of root growth in Arabidopsis. Development **147**.

Zaman, M.F., Nenadic, A., Radojicic, A., Rosado, A., and Beh, C.T. (2020). Sticking With It: ER-PM Membrane Contact Sites as a Coordinating Nexus for Regulating Lipids and Proteins at the Cell Cortex. Front Cell Dev Biol **8,** 675.

Zhang, Y., Persson, S., Hirst, J., Robinson, M.S., van Damme, D., and Sanchez-Rodriguez, C. (2015). Change your TPLATE, change your fate: plant CME and beyond. Trends Plant Sci **20,** 41-48.

Zhao, Y., Yan, A., Feijo, J.A., Furutani, M., Takenawa, T., Hwang, I., Fu, Y., and Yang, Z. (2010). Phosphoinositides regulate clathrin-dependent endocytosis at the tip of pollen tubes in Arabidopsis and tobacco. Plant Cell **22,** 4031-4044.

Zheng, H., Camacho, L., Wee, E., Batoko, H., Legen, J., Leaver, C.J., Malho, R., Hussey, P.J., and Moore, I. (2005). A Rab-E GTPase mutant acts downstream of the Rab-D subclass in biosynthetic membrane traffic to the plasma membrane in tobacco leaf epidermis. Plant Cell **17,** 2020-2036.

Zouhar, J., and Sauer, M. (2014). Helping hands for budding prospects: ENTH/ANTH/VHS accessory proteins in endocytosis, vacuolar transport, and secretion. Plant Cell **26,** 4232-4244.

Chapter 5: Conclusions and Future Directions

Common themes of membrane trafficking systems

The movements of proteins and membranes within the subcellular compartments of the eukaryotic cell as well as to and from the perimeter of the cell enable not only the housekeeping functions of the cell, but also facilitate the cellular responses to abiotic or biotic stresses, cell division and cytokinesis, and cell growth and expansion. Universal, but not exhaustive, themes of trafficking in eukaryotes include the recognition of protein and membrane cargos, deformation of donor membrane, movement of the transport compartment (vesicle), activating and effector proteins, and recognition of and tethering to acceptor membrane. In addition to vesicle coat proteins (including clathrin); adaptor protein complexes bridging membrane, cargo, and vesicle coat (including AP-1-5 and TSET/TPLATE); and regulatory GTPases and tethering complexes retained from the last eukaryotic common ancestor (LECA), duplications, expansions, and losses of genes encoding membrane-trafficking factors during 1.5 billion years of evolution have contributed to increased complexity of trafficking pathways and their regulation in modern eukaryotes (Schlacht et al., 2014; Dacks and Field, 2018). The subcellular space of plants is generally organized similar to other eukaryotes including an elaborate endomembrane pathway composed of ER, Golgi, TGN, and endosomes (Aniento et al., 2021) but also include specialized characteristics such as a merged TGN/EE compartment and cell plate to partition the cell during cytokinesis (Barlow and Dacks, 2018) among which the plant cell's complement of evolutionarily conserved and divergent trafficking proteins function.

The TGN/EE serves as the central hub for multiple transport pathways of the plant cell, from which newly synthesized or recycled proteins are distributed (or re-distributed) to the plasma membrane, vacuole, or cell plate through exocytic or post-Golgi trafficking

and to which plasma membrane-localized kinases, receptors, transporters, and cellulose synthases are internalized prior to their recycling or degradation via CME or CIE (Rosquete et al., 2018; Dahhan and Bednarek, 2022). A comprehensive review of the mechanisms underlying endocytosis in plants and recent technologies enabling greater temporal and structural resolution is detailed in Chapter 1.

Clathrin-coated vesicles converge on the TGN/EE in different fashions enabled by their associations with different oligomeric protein complexes which recognize cargo at specific subcellular compartments. A combination of proteomic, biochemical, and microscopy-based analyses presented in Chapter 2 delineate the complement of proteins associated with a heterogenous mixture of post-Golgi and endocytic derived CCVs purified from plant cells, yielding new insights about the functions of CCVs and associated proteins in plants and establishing a key resource for the comparative study of CCV-mediated trafficking between plants and Opisthokonts using protein abundance and fold enrichment as key metrics (Figure 2S2). A core CCV proteome of 781 proteins was identified across three complementary proteomic workflows, 213 of which were more than two-fold abundant in the final purification step, where the most significant enrichment of CCV-associated proteins occurs as assessed by immunoblotting (Figure 2.3) (Reynolds et al., 2014). This category of CCV-coenriching proteins include the expected clathrin coat proteins, auxilin-like putative vesicle uncoating factors, and all subunits of the AP-1 and AP-2 adaptor complexes which direct CCV trafficking at the TGN/EE and plasma membrane, respectively (Figure 2.5). Curiously, subunits of the adaptor, AP-4 were also identified in the CCV proteome as both highly abundant and significantly co-enriching with the purified vesicles as opposed to transiently associated factors or cytsosolic and

endomembrane compartment contaminants (Figure 2.4 and Table 2.1). AP-4 was subsequently localized at the TGN/EE and shown to interact with clathrin to varying degrees (Figure 2.6) (Shimizu et al., 2021). These observations suggest that unlike in mammalian cells, where AP-4 functions independently of clathrin to mediate post-Golgi trafficking and disruption of AP-4 function results in defects in autophagy, this adaptor complex mediates CCV trafficking in plants (Robinson, 2015; Sanger et al., 2019).

TPLATE and SCD – evolutionarily divergent trafficking complexes regulating conserved trafficking pathways

An additional significant outcome from establishment of the CCV proteome was that while unlabeled and dimethyl labeled proteomic datasets supported by quantitative immunoblotting confirmed the high abundance and co-enrichment of all subunits of the endocytic adaptor AP-2, subunits of the endocytic adaptor TPLATE complex (TPC) were notably of low abundance and actively depleting from the purified CCV (Figures 2.4 and 2.5 and Table 2.1). Plant CME is known to be dependent on the TPC, and subunits of the TPC colocalize with clathrin at the plasma membrane, exhibit similar lifetime distributions and kinetics, and associate with endocytic cargo (Zhang et al., 2015; Dahhan and Bednarek, 2022). The TPLATE complex is a key example of a ‘jotnarlog,’ a recently established term describing proteins which are broadly distributed among a wide variety of lineages and were originally present in the LECA but have since been lost in metazoan or yeast model systems, hindering their study and obscuring these proteins from view (More et al., 2020). Initially thought to be a plant-specific mediator of endocytosis, TPLATE emerged to be the embryophyte version of the more widespread hexameric

TSET complex. However, the degree to which TPLATE/TSET is required for viability and functions in endocytosis varies between plant and Dictyostelium (Hirst et al., 2014; Dacks and Robinson, 2017).

A rationale for the low abundance and weak enrichment of TPC observed in the CCV proteome emerged with biochemical studies of a heterogenous mixture of post-Golgi and endocytic-derived CCVs and superresolution microscopy of CCVs at the plasma membrane (Chapter 3) (Johnson et al., 2021). Biochemical data showed that compared to AP-2, TPLATE is more weakly associated with the CCV and may be more accessible to environmental stresses than the clathrin coat proteins (Figures 3.1 and 3.2). TPLATE was subsequently observed to be located on the exterior of the endocytic vesicle, peripheral to both AP-2 and clathrin coat proteins, in approximately 20% of CME events at the plasma membrane (Johnson et al., 2021).

The Stomatal Cytokinesis Defective (SCD) complex is a second notable example of evolutionary divergence between the complexes regulating membrane trafficking of plants and the Opisthokonts. Work presented in Chapter Four describes the early characterization of recently identified proteins associated with the SCD complex, which is critical to plant growth and development, post-Golgi trafficking, and clathrin-mediated endocytosis (Falbel et al., 2003; McMichael et al., 2013; Mayers et al., 2017). The SCD1 protein of this complex is a putative activator of RabE1 GTPase, which is localized to the TGN/EE of plant cells and mediates exocytic transport (Mayers et al., 2017). While RabE1 is an evolutionarily conserved GTPase mediating exocytic trafficking (Borchers et al., 2021; Ito and Uemura, 2022), a functional equivalent to the SCD complex has not yet been identified in Opisthokonts. Therefore, the regulation of this essential trafficking

factor, the SCD complex, remains to be established in plants using the model plant organisms *Physcomitrium patens* or *Arabidopsis thaliana*. Reagents for the study of the SCD complex in Physcomitrium are presented in Appendix A.

The extents to which the SCD complex-associated proteins SCD2b, SCD2c, and MyTH1 are critical to post-Golgi and endocytic trafficking remain to be fully elucidated. The phenotypes of *myth1*, *scd2b*, and *scd2c* T-DNA insertion alleles are milder than those observed for *scd1* and *scd2* under the conditions tested, suggesting that whatever their function alongside the SCD complex, they may not play as critical a role as the SCD complex in post-Golgi trafficking and CME. Despite the activity of the $MyTH1_{PRO}$ in stomatal guard cells, *myth1* plants do not show the same defects in stomatal guard cells observed in *scd1* and *scd2* plants (Figures 4S3 and 4S4). However, *scd2c* seedlings display a reduction in cotyledon size and are indistinguishable at this age from *scd2-1* plants, though ultimately these plants continually to develop without the growth or reproductive defects of *scd2-1* homozygotes (Figure 4.6).

Proteomic, biochemical, and microscopy data support a functional relationship between the SCD complex and SCD2b, SCD2c, and MyTH1. All three colocalize with SCD1 at the cell plate, a hub for membrane trafficking in plant cells undergoing division, and tandem affinity purification coupled to mass spectrometry using SCD2b, SCD2c, and MyTH1 as baits reciprocally identify SCD1 and SCD2 as interactors (unpublished work, J. Mayers). Recombinant SCD1 expressed in HEK293-FT cells interacts directly with MyTH1 (Figure 4.3), and the levels of SCD1 *in vivo* are dependent on the presence of *SCD2c* and *MyTH1*, but not *SCD2b* (Figures 4S4 and 4S6). However, whereas SCD2 is essential for the formation of the high molecular weight SCD complex (> 720 kDa), the

SCD2-like proteins, SCD2b and SCD2c, do not appear to be incorporated into this protein complex despite a conservation of domains and sequence identity greater than 75% in the case of SCD2 and SCD2c (Figure 4.5 and 4.6). As the function of SCD2 is unknown, predictions of SCD2b and SCD2c function *in vivo* are similarly limited. All three orthologs share two centrally located coiled-coil domains which in other proteins have been shown to trigger protein oligomerization and increase the potential for scaffolding of associated proteins on membrane (Martinez et al., 2019). It is possible that the oligomerization of SCD2 facilitates the associations of multiple SCD1-containing complexes on membrane.

The SCD complex associated protein, MyTH1, contains a pleckstrin homology domain and was found to interact with anionic phospholipids *in vitro* (specifically PIPs, though with a broad affinity for multiple species), but significance *in vivo* of this data remains to be established. The recruitment and retention of TGN-localized trafficking regulators has been shown to be regulated by a model of coincidence detection (Figure 4.1) and multiple models incorporating SCD2 and/or MyTH1 oligomerization and membrane interaction can be postulated to regulate SCD1 recruitment to plasma membrane and consequently, its interaction with and activation of a small GTPase, such as RabE1 (Figure 4.7).

The plant TGN/EE & the intersection of post-Golgi and endocytic trafficking

Chapter Four has focused on the putative functions of the SCD complex in post-Golgi trafficking due to specific interaction between SCD1 and RabE1 family of GTPases and defects in recycling of the plasma membrane localized protein, PIN2, in *scd1* and *scd2* mutants (Mayers et al., 2017). Yet the concurrent involvement of the SCD complex in

CME is supported by multiple lines of evidence, such as the co-enrichment of SCD1 and SCD2 with purified CCVs, reduced internalization of the membrane marker, FM4-64, in *scd1* and *scd2* backgrounds, and the colocalization of SCD1 and SCD2 proteins with CLC at or near the plasma membrane (McMichael et al., 2013).

Despite these observations, the direct involvement of SCD1 and SCD2 (and consequently of SCD2b, SCD2c, and MyTH1) in mediating CME is not certain, and caution is warranted when interpreting implied function related to defects observed simultaneously in post-Golgi trafficking and CME in *scd* mutant background. Recent work detailed by Yan et al. has shown that clathrin-mediated post-Golgi trafficking and endocytosis are coupled such that genetic or pharmacological disruption of one pathway results in impairment of the other trafficking pathway (Yan et al., 2021). The precise origin of this cross-talk is not fully elucidated but may be related to the integrity of the TGN/EE on which both trafficking pathways converge. The convergence of the TGN and EE in plant cells into one subcellular compartment limits the avenues in which the origin of this phenomenon may be addressed, as separation of the TGN and early endosomes into discrete compartments in metazoan species may mitigate the cross-talk between CME into the early endosomes and post-Golgi trafficking from the TGN.

Future directions

Several critical questions remain regarding the functions and regulation of the SCD complex and associated SCD2-like and MyTH1 proteins. First, as SCD1 and SCD2 organize into a heterogenous high molecular weight complex and homoligomerize into smaller complexes, which species is the ‘functional’ complex, i.e. acts as a putative GEF

for RabE1? Does the interaction between SCD1 and SCD2 positively regulate the putative enzymatic activity of SCD1? This may be resolved *in vitro* by utilizing recombinant mammalian cell expressed SCD1 for assays of GEF activity towards RabE1c and titrating in increasing amounts of SCD2 and 2-like proteins, as well as MyTH1, or by enrichments of SCD1 and SCD2 containing complexes of various sizes from suspension cultured or plant tissue by size exclusion chromatography and performing GEF activity assays with various fractions.

Future experiments will need to establish the contexts in which MyTH1 is essential for the recruitment of SCD1 (and the SCD complex) to membranes of interest. Answering these questions in addition to establishing whether SCD1 and SCD2 have the capacity to associate with membranes in the absence of MyTH1 is essential to gauging whether a model of coincidence detection which regulates the activity of other small GTPases is appropriate to describe SCD complex recruitment to the membrane. The preliminary *in vitro* lipid overlay assay shows that the PH domain of MyTH1 confers broad PIP-association and precludes the simple assignment of MyTH1 function to a single endomembrane compartment characterized by a specific PIP species. Probing the associations of the full (high molecular weight) SCD complex and hemicomplexes of individual subunits with liposomes mimicking biological membrane compositions (e.g. of the plant plasma membrane or TGN/EE) is essential to understanding how protein- and lipid-based properties regulate SCD complex membrane association and putative GEF activation of RabE1.

Any functional redundancies among SCD2 and its related proteins, SCD2b and SCD2c, will need to be established by generating *scd2b/scd2c*, *scd2/scd2c, scd2/scd2b,*

and *scd2/scd2b/scd2c* plant crosses. An alternative approach may be aided by silencing *SCD2* expression in Physcomitrium and assessing whether over-expression of related *PpSCD2-like* genes is sufficient to rescue any observed defects. The shorter timeline of gene disruption and morphological analysis of Physcomitrium (detailed in Appendix A) compared to Arabidopsis is greatly advantageous. Complementary comparative studies of SCD1 and MyTH1 function in Physcomitrium will help establish whether SCD complex function is required for growth and development of representatives of the earliest land plant lineages.

Perspectives

The results described in this thesis have greatly advanced our understanding of multiple membrane trafficking pathways in plants and the ways in which plants diverge in their regulation of conserved membrane trafficking pathways and machinery in comparison to other Eukaryotes. Firstly, I have written a review of the literature detailing endocytic mechanisms of plants, including what we know about both clathrin-independent as well as clathrin-mediated pathways (Dahhan and Bednarek, 2022). My review incorporates data gathered from metazoan and yeast model organisms in instances where data collected from plants is not present and also indicates points of divergence among plant species and between plants and other Eukaryotes. In addition, I describe relationships between endocytic transport and trafficking converging on the endoplasmic reticulum and trans-Golgi network. This comprehensive review provides context for recent experimental data showing multiple opportunities for interplay between the endocytic and exocytic

pathways of the plant cell, a project which I also helped to complete (Yan et al. Plant Cell, 2021).

Previously, there was no comprehensive picture of the contents of clathrin coated vesicles in plants, while the contents of animal CCVs had already been elucidated by proteomic means. The proteomic and biochemical data I have collected have established and validated a significant resource for the plant biology and eukaryotic membrane trafficking communities (Dahhan et al. 2022). This resource has already helped researchers to understand whether their proteins of interest are involved in CCV-mediated transport or are themselves trafficked by CCVs and consequently serves as a springboard for the generation of new hypotheses. It is also an essential control for future experiments seeking to broadly perturb CCV mediated transport. I am excited for the next stage, in which future researchers will begin to parse the contents and regulation of smaller subpopulations of plant vesicles such as endocytic versus post-Golgi transport derived CCVs or AP-1 versus AP-4 positive CCVs.

Prompted by proteomic data detailing the contents of the Arabidopsis CCVs, I gathered biochemical data investigating the association of the TPLATE complex with enriched plant CCV samples in comparison to other CME machinery. These data validated the external localization of the TPLATE complex on the endocytic vesicle in comparison to AP-2 which in turn supported the additional function of the TPLATE complex as a membrane bending factor (Johnson et al. 2021). In addition, I have contributed purifications of suspension culture derived plant CCVs used by collaborators to develop new automated, high-throughput tools for analysis of the morphology of plant CCVs *in situ* (Johnson et al. 2022, under review).

Previous work by Jon Mayers, Colleen McMichael, and Greg Reynolds established the composition of the Jotnarlog, the Stomatal Cytokinesis Defective complex, in plants, and identified new proteins associated with this complex and implicated the SCD complex in both clathrin-mediated endocytosis and exocytic trafficking. How both pathways are facilitated by the same complex is a major open question, as is the regulation of SCD complex assembly. I have validated and partially characterized multiple plants which are defective in SCD complex-associated proteins; identified phenotypic differences and similarities compared to those of the hallmark proteins of the SCD complex, SCD1 and SCD2; and begun to tease apart the composition of the SCD complex. Future work will establish whether these SCD1 and SCD2 associated proteins facilitate SCD complex function in one trafficking pathway compared to another and in what developmental or cellular contexts they function at all. The biochemical data I have gathered is the foundation of understanding whether the coincidence detection model appropriately describes the localization of the SCD complex at the TGN/EE or plasma membrane. The biological function of the 'high molecular weight SCD complex' is particularly curious, as loss of this protein species in the absence of the SCD2 protein is likely critical to causing the severe developmental defects of *scd1* and *scd2* plants.

The genetic and biochemical tools for study of SCD complex function in Arabidopsis are complemented by the resources I have generated and described for the comparative analysis of SCD complex function using the moss, *Physcomitrium patens*. These tools are essential to future experiments aiming to understand whether the SCD complex functions similarly in other land plants and for the generation of *scd* mutants more quickly than can be created in Arabidopsis backgrounds.

References

Aniento, F., de Medina Hernandez, V.S., Dagdas, Y., Rojas-Pierce, M., and Russinova, E. (2021). Molecular mechanisms of endomembrane trafficking in plants. Plant Cell.

Barlow, L.D., and Dacks, J.B. (2018). Seeing the endomembrane system for the trees: Evolutionary analysis highlights the importance of plants as models for eukaryotic membrane-trafficking. Semin Cell Dev Biol **80,** 142-152.

Borchers, A.C., Langemeyer, L., and Ungermann, C. (2021). Who's in control? Principles of Rab GTPase activation in endolysosomal membrane trafficking and beyond. J Cell Biol **220**.

Dacks, J.B., and Robinson, M.S. (2017). Outerwear through the ages: evolutionary cell biology of vesicle coats. Curr Opin Cell Biol **47,** 108-116.

Dacks, J.B., and Field, M.C. (2018). Evolutionary origins and specialisation of membrane transport. Curr Opin Cell Biol **53,** 70-76.

Dahhan, D.A., and Bednarek, S.Y. (2022). Advances in structural, spatial, and temporal mechanics of plant endocytosis. FEBS Lett.

Falbel, T.G., Koch, L.M., Nadeau, J.A., Segui-Simarro, J.M., Sack, F.D., and Bednarek, S.Y. (2003). SCD1 is required for cytokinesis and polarized cell expansion in Arabidopsis thaliana [corrected]. Development **130,** 4011-4024.

Hirst, J., Schlacht, A., Norcott, J.P., Traynor, D., Bloomfield, G., Antrobus, R., Kay, R.R., Dacks, J.B., and Robinson, M.S. (2014). Characterization of TSET, an ancient and widespread membrane trafficking complex. Elife **3,** e02866.

Ito, E., and Uemura, T. (2022). RAB GTPases and SNAREs at the trans-Golgi network in plants. J Plant Res **135,** 389-403.

Johnson, A., Dahhan, D.A., Gnyliukh, N., Kaufmann, W.A., Zheden, V., Costanzo, T., Mahou, P., Hrtyan, M., Wang, J., Aguilera-Servin, J., van Damme, D., Beaurepaire, E., Loose, M., Bednarek, S.Y., and Friml, J. (2021). The TPLATE complex mediates membrane bending during plant clathrin-mediated endocytosis. Proc Natl Acad Sci U S A **118**.

Martinez, D., Legrand, A., Gronnier, J., Decossas, M., Gouguet, P., Lambert, O., Berbon, M., Verron, L., Grelard, A., Germain, V., Loquet, A., Mongrand, S., and Habenstein, B. (2019). Coiled-coil oligomerization controls localization of the plasma membrane REMORINs. J Struct Biol **206,** 12-19.

Mayers, J.R., Hu, T., Wang, C., Cardenas, J.J., Tan, Y., Pan, J., and Bednarek, S.Y. (2017). SCD1 and SCD2 Form a Complex That Functions with the Exocyst and RabE1 in Exocytosis and Cytokinesis. Plant Cell **29,** 2610-2625.

McMichael, C.M., Reynolds, G.D., Koch, L.M., Wang, C., Jiang, N., Nadeau, J., Sack, F.D., Gelderman, M.B., Pan, J., and Bednarek, S.Y. (2013). Mediation of clathrin-dependent trafficking during cytokinesis and cell expansion by Arabidopsis stomatal cytokinesis defective proteins. Plant Cell **25,** 3910-3925.

More, K., Klinger, C.M., Barlow, L.D., and Dacks, J.B. (2020). Evolution and Natural History of Membrane Trafficking in Eukaryotes. Curr Biol **30,** R553-R564.

Reynolds, G.D., August, B., and Bednarek, S.Y. (2014). Preparation of enriched plant clathrin-coated vesicles by differential and density gradient centrifugation. Methods Mol Biol **1209,** 163-177.

Robinson, M.S. (2015). Forty Years of Clathrin-coated Vesicles. Traffic **16,** 1210-1238.

Rosquete, M.R., Davis, D.J., and Drakakaki, G. (2018). The Plant Trans-Golgi Network: Not Just a Matter of Distinction. Plant Physiol **176,** 187-198.

Sanger, A., Hirst, J., Davies, A.K., and Robinson, M.S. (2019). Adaptor protein complexes and disease at a glance. J Cell Sci **132**.

Schlacht, A., Herman, E.K., Klute, M.J., Field, M.C., and Dacks, J.B. (2014). Missing pieces of an ancient puzzle: evolution of the eukaryotic membrane-trafficking system. Cold Spring Harb Perspect Biol **6,** a016048.

Shimizu, Y., Takagi, J., Ito, E., Ito, Y., Ebine, K., Komatsu, Y., Goto, Y., Sato, M., Toyooka, K., Ueda, T., Kurokawa, K., Uemura, T., and Nakano, A. (2021). Cargo sorting zones in the trans-Golgi network visualized by super-resolution confocal live imaging microscopy in plants. Nat Commun **12,** 1901.

Yan, X., Wang, Y., Xu, M., Dahhan, D.A., Liu, C., Zhang, Y., Lin, J., Bednarek, S.Y., and Pan, J. (2021). Cross-talk between clathrin-dependent post-Golgi trafficking and clathrin-mediated endocytosis in Arabidopsis root cells. Plant Cell **33,** 3057-3075.

Zhang, Y., Persson, S., Hirst, J., Robinson, M.S., van Damme, D., and Sanchez-Rodriguez, C. (2015). Change your TPLATE, change your fate: plant CME and beyond. Trends Plant Sci **20,** 41-48.

Appendix A: Reagents for the study of SCD function in *Physcomitrium patens*

Statement of contribution: I generated all the constructs and data presented in this appendix under the supervisions of the Bednarek Lab (University of Wisconsin-Madison) and the Vidali Lab (Worcester Polytechnic Institute). MyoUTi, pAPi, and pUGi constructs were freely given by the Vidali lab.

Introduction

While the exocytic trafficking components RabE1c and exocyst are evolutionarily conserved across eukaryotes (Zhen and Stenmark, 2015; Minamino, 2019; Zarsky, 2022), orthologs of the *Arabidopsis thaliana* protein SCD1, which serves as the putative activator of RabE1 GTPase and interactor of the exocytic vesicle tethering factor, exocyst, and its associated proteins, SCD2 and MyTH1, appear to be absent or divergent in structure in yeast and metazoan lineages. Key to understanding whether the degree to which the function of the SCD complex (SCD1, SCD2, and possibly MyTH1) as a regulator of evolutionarily conserved post-Golgi trafficking components is evolutionarily divergent is the identification and comparative study of the SCD complex subunits in other plant species.

The early emergence of primarily tip-growing chloronemal and caulonemal tissues of the moss, *Physcomitrium (Physcomitrella) patens*, which rely on complex and highly regulated polarized cell expansion has established this species as a key organism for the study of membrane and protein trafficking pathways (Orr et al., 2020a). Because Physcomitrella is a representative of the mosses within the bryophyte group, the earliest lineages of land plants to evolve, it is also a critical model organism in the study of the traits which have established the evolutionary fitness of the embryophytes and their abilities to adapt to terrestrial environments (Lang et al., 2008; Rensing et al., 2008). A sequenced haploid genome, short life cycle and ease of culturing and growth, tools for semi-automated morphological analysis, and plethora of well-established gene editing protocols have facilitated experiments utilizing Physcomitrium (Prigge and Bezanilla, 2010; Galotto et al., 2019).

The requirement of RabE GTPaes in Physcomitrium for polarized cell growth and exocytosis has been established, as well as the functional equivalency between AtRabE1c and PpRabE1 proteins, as expression of *AtRabE1c* is able to rescue Physcomitrium plants with RNAi-mediated silenced *RabE1* expression (Orr et al., 2020c). The conservation of the involvement of RabE GTPases in polarized cellular growth between Arabidopsis and Physcomitrium and close relationship of PpRabE1 and AtRabE1 proteins suggest that the regulation of RabE1 function in Physcomitrium may function similarly to that in Arabidopsis (Speth et al., 2009; Orr et al., 2020c). To address this gap in our knowledge, several reagents and protocols have been developed for the comparative study of SCD complex and MyTH1 function in Physcomitrium.

Results

Identification of SCD complex and accessory proteins in Physcomitrium patens

Protein BLAST of AtSCD1 (At1g49040.1) protein sequence against the predicted protein sequences of the model organism, *Physcomitrium (Physcomitrella) patens*, which relies on exocytic and endocytic trafficking for tip growth identified a putative ortholog, PpSCD1, with 52.8% identical /71.0% similar sequence across the full length amino acid sequence to AtSCD1 (Supplemental Table AS1). Characteristic tripartite DENN domain and WD-40 motifs are conserved in PpSCD1, as well as a predicted SBF1/SBF2 domain IPR022096) located in the intermediate linker region (Figure A.1).

Protein BLAST of the AtSCD2 protein sequence identified four putative candidates encoding coiled coil domain-containing proteins orthologous to AtSCD2, two of which share identical amino acid sequences (Supplemental Tables AS1 and AS2). Table AS2

plots the percent identity between Arabidopsis SCD2 and SCD2-like proteins and the three unique protein sequences orthologous to SCD2 in Physcomitrella. The similar percent identities between the different permutations of the Physcomitrella amino acid sequences and those of Arabidopsis SCD2 and SCD2-like orthologs and the lack of unique protein domains and motifs between the paralogs of either species preclude the identification of equivalences between the Physcomitrella SCD2 paralogs and the Arabidopsis SCD2 paralogs on the basis of these features.

Physcomitrella also contains a predicted protein, PpMyTH1, orthologous to AtMyTH1, with a conserved PH domain but shortened N-terminal region and overall 42.5% identical/74.5% similar amino acid identity. The presence of a basic-hydrophobic motif which putatively regulates membrane association of this SCD complex-associated factor (and thereby potentially the SCD complex) is also conserved in Physcomitrella and is predicted to occur at residues 59-66 (Figure A.1).

Investigation of SCD complex function using *Physcomitrium patens*

A pilot experiment to assess the requirement of SCD1 function for plant growth and development outside of Arabidopsis was performed using RNAi-based silencing of *PpSCD1* expression. Briefly, the 5’ UTR region of *PpSCD1* was cloned into a Gateway-based RNAi vector (pGAPi) which induces silencing of the gene of interest alongside silencing of the gene encoding adenine phosphoribosyltransferase following transformation of protoplasted Physcomitrella cells (Orr et al., 2020b). Subsequently, plants can be screened on growth media containing the selective agent, 2-fluoroadenine, which is lethal to plants continuing to express adenine phosphoribosyltransferase.

Morphological phenotypic data such as plant area gathered through automated epifluorescence microscopy following screening and recovery are obtained by visualization of both cell walls and chlorophyll autofluorescence and inform whether the RNAi-silenced gene of interest is required for growth and development (Galotto et al., 2019).

A 386 bp region of the 5' UTR of PpSCD1 (Pp3c26_9700V3.1) was cloned into pGAPi. Physcomitrella protoplasts were transformed with positive control pAPi vector silencing only adenine phosphoribosyltransferase, negative control pUGi silencing no gene, MyoUTi vector silencing both the 5' of both isoforms of Physcomitrella Myosin XI, and pGAPi RNAi-silencing vectors targeting the 5' UTRs of *PpSCD1.* Plant growth (area) phenotypes induced by silencing of *PpSCD1* were observed through epifluorescence microscopy of chlorophyll autofluorescence (red channel) and calcofluor staining (blue channel) of *PpSCD1*-silenced and control-treated plants (Figure A.2A). Compared to control Physcomitrium plants silencing only adenine phosphoribosyltransferase (pAPi condition), viable *PpSCD1* plants were significantly smaller (p-value < 0.05, $n = 52 – 322$ plants) and were not significantly different in size from plants with silenced *Myosin XI* (MyoUTi condition) (ns, $n = 45 – 52$ plants). Statistical significance was assessed by one-way ANOVA with multiple comparisons across pAPi, pUGi, MyoUTi, and 5'UTR *PpSCD1* conditions, while individual paired conditions were assessed with two tailed student's t-test.

Discussion

Comparative studies of SCD complex function using the predominantly tip growing developmental stage of the model organism, Physcomitrium (Physcomitrella) patens is

essential to understanding whether the SCD complex functions in growth and development and membrane trafficking outside of *Arabidopsis thaliana* and serves as a plant-specific regulator of evolutionarily conserved trafficking pathways and proteins. Protein sequence homology has identified orthologs of SCD1, SCD2-like proteins, and MyTH1 between Arabidopsis and Physcomitrium with conserved protein domains and motifs, as well as minor variations, suggesting conserved protein function (Figure A.1, Table AS1). More stringent phylogenetic analysis of the SCD2-like protein sequences in Physcomitrium, Arabidopsis, and other species of representative various plant lineages is critical to the identification of clear orthologs of AtSCD2b and AtSCD2c, the functions of which appear to be less essential to plant growth and development than AtSCD2, outside of Arabidopsis.

To facilitate the analysis of *PpSCD1* and *PpMyTH1* function, several RNAi-based tools have been developed to silence the expression of these genes and assess various morphological features in response (Figure A.2, Table AS3), as well as conduct biochemical analyses of PpSD1 protein function (Figure A.3). Preliminary RNAi experiments support the hypothesis that the function of SCD1 in polarized growth and requirement for growth and development is conserved outside of Arabidopsis (Figure A.2).

Materials and Methods

Growth conditions

Wild-type Grandsen strain (Ashton et al., 1979) of *Physcomitrium patens* was propagated weekly by plating homogenized plant tissue on $PpNH_4$ plates ($PpNO_3$ moss medium, Cassion Labs PMP02-1LT; 0.5 g/L di-ammonium tartrate, 0.8% (w/v) agar (Sigma A1296)). Plated moss was grown at 25 °C under long-day (16 hour light, 8 hour dark) light conditions (90 $\mu mol/m^{-2}s^{-1}$).

Plasmid construction

PpSCD1 and *PpMyTH1* RNAi constructs were generated using the Gateway cloning system (Invitrogen) by subcloning linear fragments (5' UTR, 3'UTR and 5'UTR and 3'UTR in tandem) into pDONR221-P1P2 entry vector and recombination of the entry vector with pGAPi, an RNAi expression vector simultaneously targeting the UTR of interest and adenine phosphoribosyltransferase, (Orr et al., 2020b). *PpSCD1* and *PpMyTH1* CDS were subcloned into pDONR221-P1P2 entry vector and recombined with pTH-Ubi, a Gateway compatible vector for complementation in moss using the ubiquitin promoter of maize (Vidali et al., 2007).

Linear 5' (386 bp) and 3' (430 bp) UTR regions of *PpSCD1* (Pp3c26_9700) were amplified from genomic DNA using Gateway compatible primers DD34/DD35 and DD36/DD37, respectively. Linear 5' (376 bp) and 3' (727 bp) UTR regions of *PpMyTH1* (Pp3c8_900) were amplified from genomic DNA using Gateway compatible primers DD42/DD43 and DD44/DD45, respectively. Crude genomic DNA prepared from 100 mg

of Grandsen strain *Physcomtrium patens* chloronemal tissue 6 days after passaging was used as the template for amplification of linear 5' and 3' UTR amplicons.

Linear 5' and 3' UTRs of *PpSCD1* were cloned in tandem to generate a single linear 5'3'UTR fragment targeting both UTRs of *PpSCD1* simultaneously. This linear 5'3'UTR fragment targeting *PpSCD1* was generated using a combination of PCR, restriction digest, and ligation by amplifying the 5' UTR using primer pairs DD34/DD38 and the 3' UTR DD39/DD37, PCR clean up and digestion with HindIII restriction enzyme, and phosphorylation and ligation of digested PCR reactions.

Due to difficulties amplifying an internal region of *PpSCD1* CDS, an open reading frame encoding *PpSCD1* inserted into pDONR221-P1P2 was synthesized by SynBio Technologies using the available sequence information for the splice variant Pp3c26_9700V3.1. The first 400 bp of *PpSCD1* CDS can successfully be amplified using primer pairs DD40 and DD41. *PpMyTH1* CDS (561 bp) sequence was amplified from cDNA (see "RT-PCR", below) prepared from Grandsen strain of moss using primer pairs DD46/DD47.

All linear RNAi and CDS fragments contained attB1 and attB2 Gateway recombination sites at the 5' and 3' ends, respectively, and were recombined with pDONR221-P1P2 vector prior to recombination with pGAPi or pTH-Ubi. Final constructs were verified by sequencing.

All PCR was performed using Phusion high-fidelity DNA polymerase (New England BioLabs, M0530). All oligonucleotides were ordered from Integrated DNA Technologies.

RT-PCR

RNA was prepared from 90 mg of Grandsen strain Physcomitrella seven days after passaging by grinding tissue under liquid nitrogen and following manufacturer's instructions in the RNeasy Plant Mini Kit (Qiagen 74904). Reverse transcription to generate cDNA was performed according to manufacturer's instructions using + RT and – RT reactions using the SuperScript IV VILO master mix with ezDNAse treatment (ThermoFisher Scientific 11766050). *PpMyTH1* CDS was amplified from cDNA using 2 μL of a 1:10 dilution of template cDNA in a 20 μL PCR reaction.

Physcomitrella protoplasting, transformation, and RNAi

Briefly, RNAi of Physcomitrium was accomplished by PEG/Ca transformation of 30 μg of RNAi plasmids into protoplasted Physcomitrium before recovery, selection, and imaging and morphological analysis as previously described (Cove et al., 2009; Galotto et al., 2019; Orr et al., 2020b).

Densely grown plates of Grandsen strain *P. patens* 8 days after passaging were protoplasted under sterile conditions: moss was transferred to a Petri dish with 12 mL of 8% (w/v) mannitol and cellulase and pectinase to 0.5% (w/v) and rocked very slowly for 1 hour at room temperature. Protoplasts were harvested by collection against sterile nylon filters (BD Falcon 1243444) and concentrated by 200 x g spin for 5 minutes. Protoplasts were then washed twice with 8% (w/v) mannitol and adjusted to a cell density of 1.6 x 10^6 cells/mL in MMg buffer (0.4 M mannitol, 150 mM $MgCl_2$, and 20 mM MES pH 5.7). Individual transformations were assembled and incubated for 30 minutes at room temperature: 30 μg of Maxiprep purified plasmid, 300 μL protoplasts, and 350 μL

PEG4000/Ca (40% (w/v) PEG 4000, 200 mM mannitol, and 1 M $CaCl_2$). After 30 minutes, transformed protoplasts were diluted 1:10 with W5 buffer (154 mM NaCl, 125 mM $CaCl_2$, 5 mM KCL, and 2 mM MES pH 5.7) and concentrated with 200 x g spin for 5 minutes before resuspension in $PpNH_4$ liquid media, 8.5% (w/v) mannitol, and 10 mM $CaCl_2$ and transfer to PRM-B plates ($PpNH_4$, 6% (w/v) mannitol, 0.8% (w/v) agar). Following 4 days of recovery under light and temperature growth conditions described above, protoplasts were transferred to selection plates ($PpNH_4$, 1.25 μg/mL 2-fluoroadenine (Oakwood Chemicals CAS 700-49-2), and 0.8% (w/v) agar) for an additional two days under light and temperature growth conditions described above.

To collect images of transformed Physcomitrium plants for morphological analysis, moss were transferred from selection plates to solid $PpNH_4$ plates supplemented with 10 μg/mL Calcofluor White (Sigma Aldrich 18909). Images were collected across two channels (chlorophyll channel, 150 ms exposure; calcofluor channel, 90 ms exposure) on a Zeiss inverted epifluorescence microscope. 13 x 13 grids (each tile 1421.05 μm x 1064.75 μm) at 100 magnification were collected across each plate and stitched together in FIJI using 15% margins generating 12 bit images with an entire area of 210.681 mm^2.

Generation and purification of GST-PpSCD1^{DENN}

An open reading frame encoding PpSCD1^{DENN} (amino acids 1-605) was cloned into the BamHI and NotI sites of the bacterial expression vector pGEX-4T-1 by SynBio Technologies to introduce a glutathione S transferase (GST) tag and thrombin cleavage site at the N-terminus of PpSCD1^{DENN}.

The purification of GST-PpSCD1^{DENN} from inclusion bodies was adapted from protocols describing purification of proteins from inclusion bodies (Frangioni and Neel, 1993; Tao et al., 2010). GST-PpSCD1^{DENN} was expressed in Rosetta *E. coli* cells at 28 °C for 2.5 hours at an OD_{600} between 0.4 and 0.6 before concentration of cells in STE buffer (10 mM Tris pH 8.0, 150 mM NaCl, 1 mM EDTA, 1 mM DTT, 0.5 mM PMSF, 1x PICD, 1x PICW) at a concentration of 500 mL cell culture per 30 mL STE buffer. Following lysis by sonication, the lysate was supplemented with Triton X-100 to a concentration of 10% (v/v), incubated on ice for 15 minutes, and centrifuged at 12,000 x g for 10 minutes at 4 °C. The P30 fraction was successively washed with 250 mL STE buffer supplemented with the following reagents and centrifugation at 12,000 x g for 10 minutes at 4 °C: STE + 10% (v/v) Triton X-100; STE + 1% (v/v) Triton X-100; STE + 2 M NaCl; and STE + 1 M NaCl. After the last wash, the pellet was resuspended in cold deionized water and subjected to one flash freeze/thaw cycle and centrifuged at 12,000 x g for 10 minutes at 4 °C. GST-PpSCD1^{DENN} contained in the pelleted inclusion bodies was solubilized by re-suspension in STE + 0.3% (w/v) Sarkosyl (N-laurylsarcosine, Sigma L9150) and rotation at room temperature for 30 minutes. Triton X-100 and CHAPS were added to solubilized protein mixture at concentrations of 2% (v/v) and 40 mM, respectively, before incubation on ice for 30 minutes followed by centrifugation at 18,000 x g for 20 minutes at 4 °C. The resulting supernatant was supplemented with 5% (v/v) glycerol and supplemented with SDS-PAGE Laemmli buffer for analysis.

Figures

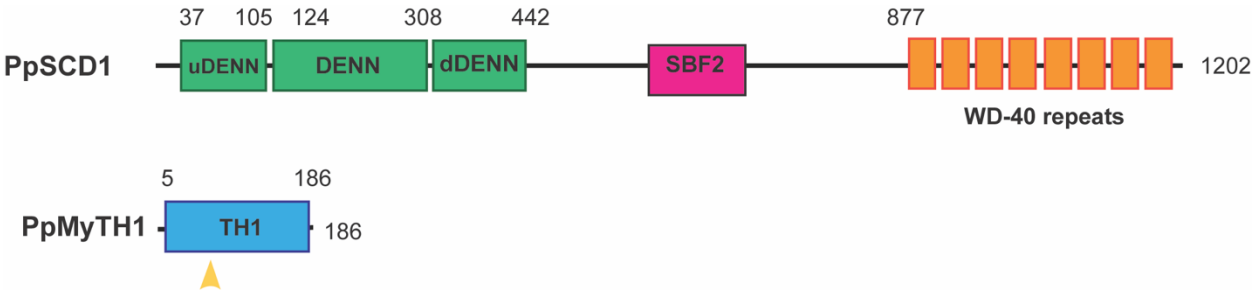

Figure A.1 Domain organization of PpSCD1 and PpMyTH1

Figure A.1 Domain organization of PpSCD1 and PpMyTH1

Schematic illustrating the domains and their relative positions corresponding to the *Physcomitrium patens* SCD1 and MyTH1 proteins containing 1202 and 186 amino acids respectively. The relative positions and sizes of the domains within each protein are demarcated by the residue numbers above each respective domain. PpSCD1 contains a tripartite DENN domain, intermediate linker region, and eight C-terminal WD-40 motifs. PpMyTH1 contains only a Tail Homology I (TH1) domain named for homology to the tail region of Myosin I. In turn, the TH1 domain contains a pleckstrin homology domain. A yellow triangle indicates a region of relatively high basic-hydrophobic character potentially mediating interaction with anionic phospholipids.

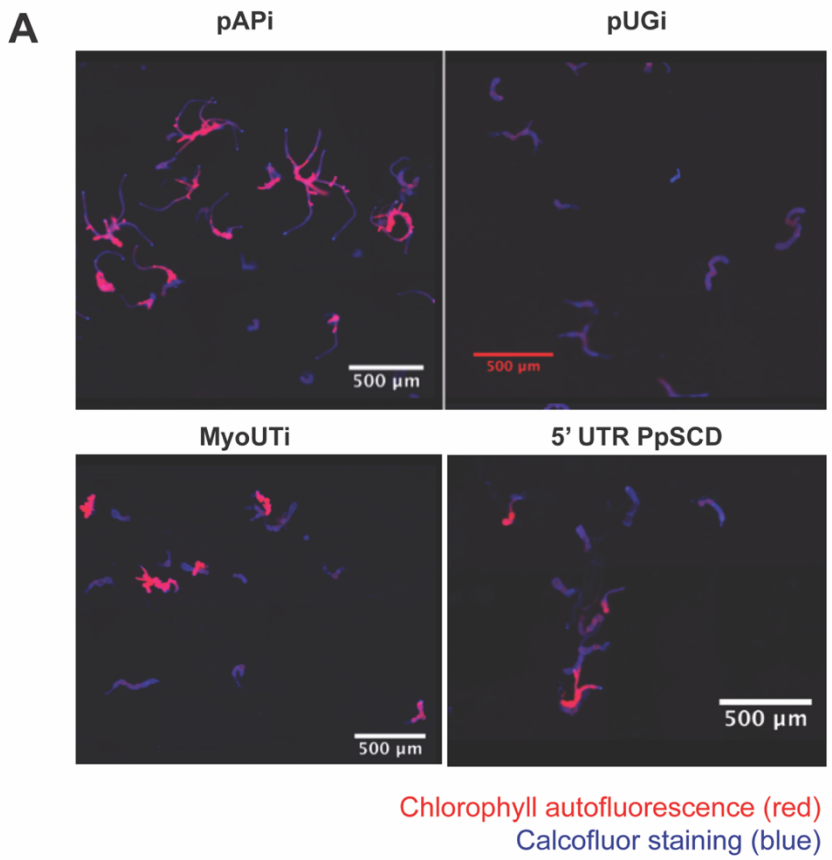

Figure A.2: RNAi targeting the 5' UTR of *PpSCD1* results in Physcomitrium plants of reduced size

Figure A.2 RNAi targeting the 5' UTR of *PpSCD1* results in Physcomitrium plants of reduced size

(A) Regenerated Physcomitrium plants transformed with RNAi constructs pAPi (positive control), pUGi (negative control), MyoUTi (silencing of *MyoXI*), and 5' UTR *PpSCD1* (silencing of *PpSCD1*). Calcofluor staining visualized in blue denotes the cell walls of Physcomitrium plants, while chlorophyll autofluorescence visualizes living plants. Scale bar = 500 μm.

(B) Scatter plot of the mean area of plants in panel (A) ± standard error about the mean. Number of plants analyzed from each condition: pAPi (322), pUGi (48), MyoUTi (45), and 5' UTR *PpSCD1* (52). Statistical analysis derived from one-way ANOVA followed by multiple comparisons. * p-value < 0.05.

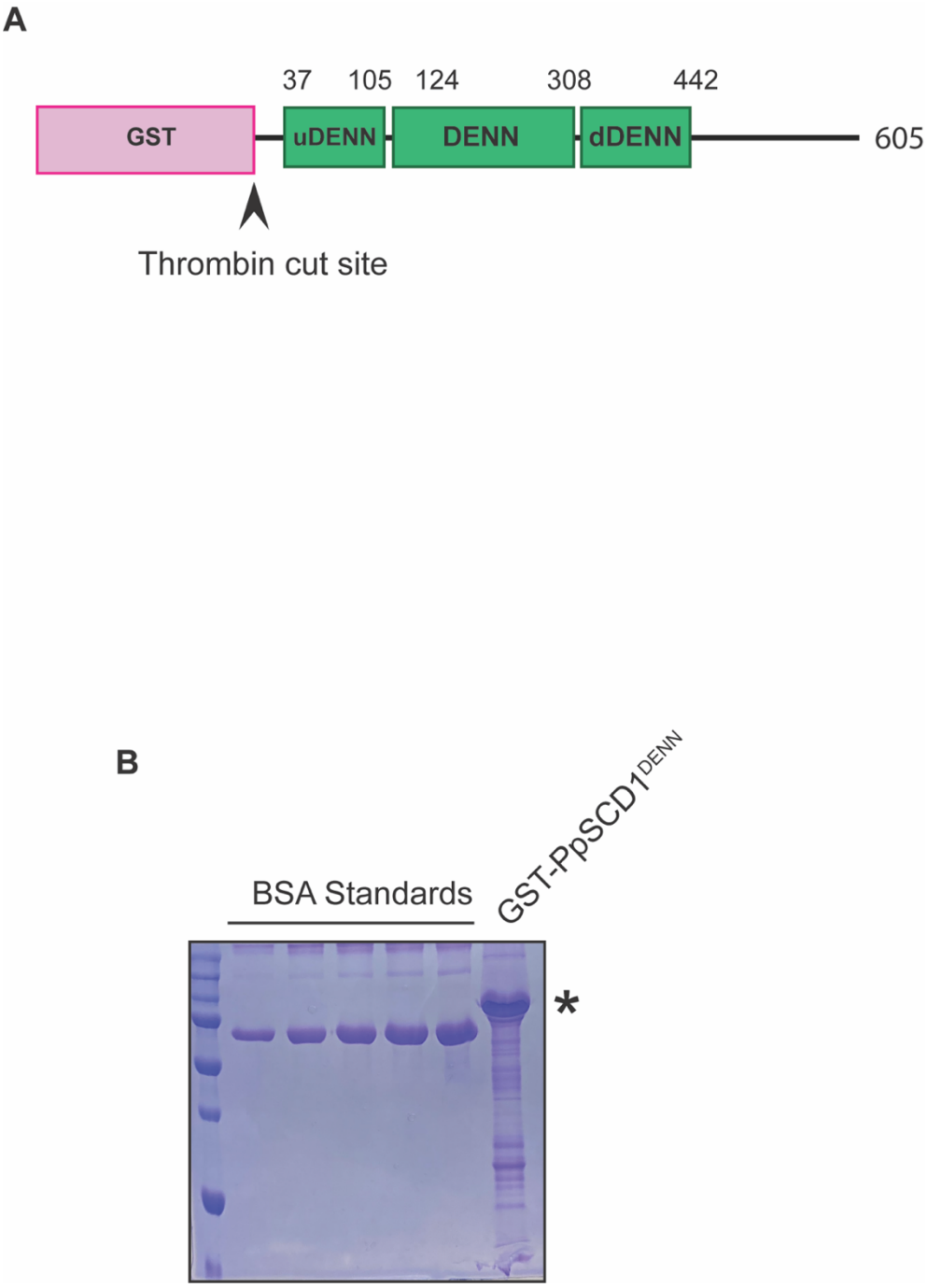

Figure A.3 Generation of GST-PpSCD1^{DENN} antigen

Figure A.3 Generation of GST-PpSCD1^{DENN} antigen

A. Schematic illustrating location of GST tag and thrombin cleavage site relative to the region of PpSCD1 (amino acids 1-605) against which an antibody was raised. The relative positions and sizes of the domains within each protein are demarcated by the residue numbers above each respective domain.
B. Coomassie stained SDS-PAGE of GST-PpSCD1^{DENN} purified from inclusion bodies. The asterisk indicates the correct band corresponding to GST-PpSCD1^{DENN}.

Physcomitrium patens			
Product	Accession Number	UniProtKB ID	Features of Interest
SCD1	Pp3c26_9700	A0A2K1ICE7	Tripartite DENN domain SBF2 domain 8x WD-uniprot40 motifs
SCD2-like 1	Pp3c19_10380V3.1	A9T6M7	Intrinsically disordered region Coiled-coil domains
SCD2-like 2	Pp3c22_21290V3.1	N/A	Intrinsically disordered region Coiled-coil domains
SCD2-like 2	Pp3c22_21255V3.1	N/A	Intrinsically disordered region Coiled-coil domains
SCD2-like 3	Pp3c19_9680V3.1	A9T6R9	Intrinsically disordered region Coiled-coil domains
MyTH1	Pp3c8_900	N/A	Pleckstrin homology domain Basic hydrophobic motif

Table AS1 Accession numbers, domains, and motifs of *Physcomitrium patens* SCD complex and accessory proteins

Table AS1 Accession numbers, domains, and motifs of *Physcomitrium patens* SCD complex and accessory proteins

Accession numbers and UniProtKB identification numbers corresponding to the protein product listed in the first column. Features of interest such as domains or motifs identified in earlier publications or predicted by bioinformatic tools such as UniProt, InterPro, ProSite, and BH-search are indicated in the column at the right.

	Pp3c19_10380V3.1	Pp3c22_21290V3.1	Pp3c22_21255V3.1	Pp3c19_9680V3.1	AtSCD2b	AtSCD2	AtSCD2c
Pp3c19_10380V3.1	100	61.73	61.73	62.93	42.26	43.65	41.19
Pp3c22_21290V3.1	61.73	100	100	84.89	46.05	48.67	46.64
Pp3c22_21255V3.1	61.73	100	100	84.89	46.05	48.67	46.64
Pp3c19_9680V3.1	62.93	84.89	84.89	100	46.93	50.19	46.81
AtSCD2b	42.26	46.05	46.05	46.93	100	55.03	52.51
AtSCD2	43.65	48.67	48.67	50.19	55.03	100	75
AtSCD2c	41.19	46.64	46.64	46.81	52.51	75	100

Table AS2 Percent identity matrix between SCD2-like proteins of Arabidopsis and Physcomitrium

Table AS2 Percent identity matrix between SCD2-like proteins of Arabidopsis and Physcomitrium

Protein sequence identity of the four predicted Physcomitrella SCD2 homologs and Arabidopsis SCD2 and SCD2-like proteins, AtSCD2b and AtSCD2c, compared pair-wise across the length of the entire protein.

Name	Sequence (5' → 3')	Purpose/ Comments
DD 34	GGGGACAAGTTTGTACAAAAAAGCAGGCTTAGACCATTGTGCTCCGTCTC	PpSCD1 5' UTR FW, Gateway
DD 35	GGGGACCACTTTGTACAAGAAAGCTGGGTGGATTGATTTTTATGTTTGTGACGCGATC	PpSCD1 5' UTR REV, Gateway
DD 36	GGGGACAAGTTTGTACAAAAAAGCAGGCTTAGTATTTAATTACAAGCTGTCAGCAGATC	PpSCD1 3' UTR FW, Gateway
DD 37	GGGGACCACTTTGTACAAGAAAGCTGGGTGGCTGATAAATCAGGTTTACGAATAAAC	PpSCD1 3' UTR REV, Gateway
DD 38	AAAAAAAAGCTTGATTGATTTTTATGTTTGTGACGCGATC	PpSCD1 5' UTR Tandem REV, Gateway
DD 39	AAAAAAAAGCTTGTATTTAATTACAAGCTGTCAGCAGATC	PpSCD1 3' UTR Tandem FW, Gateway
DD 40	ATGGGCCGGTTACTGGAGTATTTTC	PpSCD1 CDS Control Amplicon (bp 1-400) FW
DD 41	GAGAAAGAAAACAGATACACTTGTCAACATAATAATTC	PpSCD1 CDS Control Amplicon (bp 1-400) REV
DD 42	GGGGACAAGTTTGTACAAAAAAGCAGGCTTAGTAGTGACAAGTGCTCCTCGTC	PpMyTH1 5' UTR FW, Gateway
DD 43	GGGGACCACTTTGTACAAGAAAGCTGGGTGGGTCAGGGAGGAGACCAGAG	PpMyTH1 5' UTR REV, Gateway
DD 44	GGGGACAAGTTTGTACAAAAAAGCAGGCTTATTGCTTATCCAAGTGCTCGGGAG	PpMyTH1 3' UTR FW, Gateway
DD 45	GGGGACCACTTTGTACAAGAAAGCTGGGTGAAGATGGTAGCAGCAGCAGATAC	PpMyTH1 3' UTR REV, Gateway
DD 46	5'GGGGACAAGTTTGTACAAAAAAGCAGGCTTAATGTTGGGTGAGGACGGCATG	PpMyTH1 CDS FW
DD 47	GGGGACCACTTTGTACAAGAAAGCTGGGTGTCACTTATCCACAAACTTCGTTTTAGTTCC	PpMyTH1 CDS REV

Table AS3 Primers used in this study

Table AS3 Primers used in this study

The alias (first column), sequence from 5’ to 3’ (second column), and name, orientation, and purpose (third column) of oligonucleotides used in this study are detailed.

References

Ashton, N.W., Grimsley, N.H., and Cove, D.J. (1979). Analysis of gametophytic development in the moss, Physcomitrella patens, using auxin and cytokinin resistant mutants. Planta **144,** 427-435.

Cove, D.J., Perroud, P.F., Charron, A.J., McDaniel, S.F., Khandelwal, A., and Quatrano, R.S. (2009). Transformation of moss Physcomitrella patens gametophytes using a biolistic projectile delivery system. Cold Spring Harb Protoc **2009,** pdb prot5145.

Frangioni, J.V., and Neel, B.G. (1993). Solubilization and purification of enzymatically active glutathione S-transferase (pGEX) fusion proteins. Anal Biochem **210,** 179-187.

Galotto, G., Bibeau, J.P., and Vidali, L. (2019). Automated Image Acquisition and Morphological Analysis of Cell Growth Mutants in Physcomitrella patens. Methods Mol Biol **1992,** 307-322.

Lang, D., Zimmer, A.D., Rensing, S.A., and Reski, R. (2008). Exploring plant biodiversity: the Physcomitrella genome and beyond. Trends Plant Sci **13,** 542-549.

Minamino, N.U., T. (2019). RAB GTPases and their effectors in plant endosomal transport. Current Opinion in Plant Biology **52,** 61-68.

Orr, R.G., Cheng, X., Vidali, L., and Bezanilla, M. (2020a). Orchestrating cell morphology from the inside out - using polarized cell expansion in plants as a model. Curr Opin Cell Biol **62,** 46-53.

Orr, R.G., Foley, S.J., Sherman, C., Abreu, I., Galotto, G., Liu, B., Gonzalez-Guerrero, M., and Vidali, L. (2020b). Robust Survival-Based RNA Interference of Gene Families Using in Tandem Silencing of Adenine Phosphoribosyltransferase. Plant Physiol **184,** 607-619.

Orr, R.G., Furt, F., Warner, E.L., Agar, E.M., Garbarino, J.M., Cabral, S.E., Dubuke, M.L., Butt, A.M., Munson, M., and Vidali, L. (2020c). Rab-E and its interaction with myosin XI are essential for polarized cell growth. New Phytol.

Prigge, M.J., and Bezanilla, M. (2010). Evolutionary crossroads in developmental biology: Physcomitrella patens. Development **137,** 3535-3543.

Rensing, S.A., Lang, D., Zimmer, A.D., Terry, A., Salamov, A., Shapiro, H., Nishiyama, T., Perroud, P.F., Lindquist, E.A., Kamisugi, Y., Tanahashi, T., Sakakibara, K., Fujita, T., Oishi, K., Shin, I.T., Kuroki, Y., Toyoda, A., Suzuki, Y., Hashimoto, S., Yamaguchi, K., Sugano, S., Kohara, Y., Fujiyama, A., Anterola, A., Aoki, S., Ashton, N., Barbazuk, W.B., Barker, E., Bennetzen, J.L., Blankenship, R., Cho, S.H., Dutcher, S.K., Estelle, M., Fawcett, J.A., Gundlach, H., Hanada, K., Heyl, A., Hicks, K.A., Hughes, J., Lohr, M., Mayer, K., Melkozernov, A., Murata, T., Nelson, D.R., Pils, B., Prigge, M., Reiss, B., Renner, T., Rombauts, S., Rushton, P.J., Sanderfoot, A., Schween, G., Shiu, S.H., Stueber, K., Theodoulou, F.L., Tu, H., Van de Peer, Y., Verrier, P.J., Waters, E., Wood, A., Yang, L., Cove, D., Cuming, A.C., Hasebe, M., Lucas, S., Mishler, B.D., Reski, R., Grigoriev, I.V., Quatrano, R.S., and Boore, J.L. (2008). The Physcomitrella genome reveals evolutionary insights into the conquest of land by plants. Science **319,** 64-69.

Speth, E.B., Imboden, L., Hauck, P., and He, S.Y. (2009). Subcellular localization and functional analysis of the Arabidopsis GTPase RabE. Plant Physiol **149,** 1824-1837.

Tao, H., Liu, W., Simmons, B.N., Harris, H.K., Cox, T.C., and Massiah, M.A. (2010). Purifying natively folded proteins from inclusion bodies using sarkosyl, Triton X-100, and CHAPS. Biotechniques **48,** 61-64.

Vidali, L., Augustine, R.C., Kleinman, K.P., and Bezanilla, M. (2007). Profilin is essential for tip growth in the moss Physcomitrella patens. Plant Cell **19,** 3705-3722.

Zarsky, V. (2022). Exocyst functions in plants: secretion and autophagy. FEBS Lett.

Zhen, Y., and Stenmark, H. (2015). Cellular functions of Rab GTPases at a glance. J Cell Sci **128,** 3171-3176.